



**HAL**  
open science

# Fabrication of nanofibrous mats by "green" electrospinning for liquid microfiltration applications

Domitille Mailley

► **To cite this version:**

Domitille Mailley. Fabrication of nanofibrous mats by "green" electrospinning for liquid microfiltration applications. Physics [physics]. Université de Strasbourg, 2018. English. NNT : 2018STRAE019 . tel-02100975

**HAL Id: tel-02100975**

**<https://theses.hal.science/tel-02100975>**

Submitted on 16 Apr 2019

**HAL** is a multi-disciplinary open access archive for the deposit and dissemination of scientific research documents, whether they are published or not. The documents may come from teaching and research institutions in France or abroad, or from public or private research centers.

L'archive ouverte pluridisciplinaire **HAL**, est destinée au dépôt et à la diffusion de documents scientifiques de niveau recherche, publiés ou non, émanant des établissements d'enseignement et de recherche français ou étrangers, des laboratoires publics ou privés.

*ÉCOLE DOCTORALE Physique – Chimie Physique*  
ICPEES - UMR 7515

**THÈSE** présentée par :

**Domitille Mailley**

Soutenue le : **3 octobre 2018**

pour obtenir le grade de : **Docteur de l'Université de Strasbourg**

Discipline/ Spécialité : Physique des Polymères

**Fabrication of nanofibrous mats by “green”  
electrospinning for liquid microfiltration  
applications.**

**THÈSE dirigée par :**

**M. Guy SCHLATTER**

PR., Université de Strasbourg

**RAPPORTEURS :**

**Mme Karen DE CLERCK**

PR., Université de Gand

**M. Dominique HOURDET**

PR., UPMC – Sorbonne Université

**AUTRES MEMBRES DU JURY :**

**M. Marc AUDENAERT**

Responsable partenariats R&D chez Arkéma

**Mme Nadia BAHLOULI**

PR., Université de Strasbourg

**Mme Anne HEBRAUD**

MCF, Université de Strasbourg



## REMERCIEMENTS

*Il paraît que la seule partie que les gens lisent d'une thèse est la partie « remerciements ». J'espère de tout cœur que mes « remerciements » combleront vos attentes.*

*A Guy Schlatter et à Anne Hébraud qui m'ont encadré durant ces trois années. Pour leurs conseils précieux qui m'ont permis de mûrir en tant que chercheuse, en m'aidant à fournir un travail scientifique sérieux, carré et rigoureux.*

*Aux membres de mon jury de thèse qui ont accepté d'évaluer mon travail.*

*Aux partenaires du projet CLARIFIL dans lequel s'inscrit la thèse.*

*Aux membres permanents de l'ICPEES : Nicolas Leclerc, Luc Avérous, et Eric Pollet et à l'ensemble du personnel technique de l'ICPEES: Christophe Mélart, Christophe Sutter, Thierry Djekkriff, Sabine Siegwald et Romain Bernard pour toute l'aide qu'ils m'ont apportée. A Catherine Kientz pour son accueil chaleureux le matin qui augure une bonne journée. A Céline pour sa joie de vivre.*

*A tous ceux que j'ai pu rencontrer au cours de ces trois années à L'ICPEES, doctorants, post-doctorants, ingénieurs-recherche, techniciens et stagiaires. Pour les rires et les moments formidables que nous avons passé ensemble. A Morgane, Manon, Florence, Théodore, Stéphanie, Matthieu, Thibault, Thibault, Pierre, Caroline, Meng, Wassim, Ouassim Kim, Audrey, Sophie, Julien, Mohammad, Ozgün, Chenzhang, Rodolphe, Martin, Sam, Sébastien, Lucie et Zion.*

*A mes meilleures amies de toujours. A Valentine, Camille, Marguerite, Lucie, Jeanne, Cléa, Clémence et Claire pour leur soutien, leur appui et leur sincère amitié.*

*A toute ma grande famille, en particulier ma sœur Ombeline et mes trois frères Jean, Antoine et Charles. A ceux qui sont et qui ont été. A mes parents également. Pour ce qu'ils m'ont enseigné et pour ce qu'ils m'ont permis d'apprendre.*

*A Clément qui m'a inconditionnellement soutenu.*

*A ceux qui liront ma thèse jusqu'au bout avec l'espoir de les avoir agréablement intéressés.*



# NOTA BENE

Titre français:

« Green » électrospinning de membranes nanofibreuses pour des applications de filtration liquide.

Titre anglais:

Fabrication of nanofibrous mats by “green” electrospinning for liquid microfiltration applications.

Cette thèse de doctorat a été rédigée en anglais conformément à l’autorisation délivrée par Monsieur le Professeur Aziz DINIA, professeur des universités à l’Université de Strasbourg et directeur de l’Ecole Doctorale de Physique et Chimie-physique (ED 182).

# TABLE OF CONTENT

<b>Introduction .....</b>	<b>8</b>
<b>Communications</b>	<b>9</b>
<b>List of symbols and abbreviations</b>	<b>10</b>
<b>1. Bibliography .....</b>	<b>11</b>
1.1 Electrospinning of nanofibers	12
1.1.1 Principle	12
1.1.2 Fiber formation	13
1.1.3 Relative humidity	14
<i>1.1.3.1 Role of humidity during the electrospinning process on solvent evaporation</i>	15
<i>1.1.3.2 Role of humidity during the electrospinning process on fiber solidification</i>	17
<i>1.1.3.3 Effects of humidity on electrospun fibers</i>	18
<i>1.1.3.4 Effects of humidity on the nonwoven mat structure</i>	24
1.2 Liquid filtration	31
1.2.1 Principle	31
1.2.2 Parameters	32
1.3 Electrospun membranes for liquid filtration	35
Abbreviations	40
References	40
<b>2. Electrospinning of bio-based polyamide 11 mats .....</b>	<b>49</b>
2.1 Introduction	50
2.2 Materials and methods	53
2.3 Fabrication of thin fibers by electrospinning	54
2.3.1 Effect of solvent proportions	54
2.3.2 Role of humidity	56
2.3.3 Effect of PA11 concentration	56
2.3.4 Effect of the distribution of the molar mass	59
2.4 Characterization of electrospun PA11 mats	64
2.4.1 Hydrophilic properties	65
2.4.2 Mechanical properties	66
2.4.3 Pore size, thickness and fiber diameter	67
2.5 Conclusion	68
References	69

<b>3. Electrospinning in aqueous solvents .....</b>	<b>73</b>
3A Electrospinning of aqueous suspensions of water insoluble polymers	74
3A.1 Introduction	74
3A.2 Materials and methods	75
3A.3 Fabrication of continuous fibers	77
3A.3.1 Particles and template polymer concentrations	78
3A.3.2 Effect of curing temperature	80
3A.3.3 Washing	80
3A.4 Fabrication of liquid filtration mats	81
3A.4.1 Fabrication of mats	81
3A.4.2 Mechanical properties	84
3A.4.3 Hydrophilic properties	86
3A.4.4 Filtration properties	87
3A.5 Conclusion	90
3B Electrospinning of pure polymer-free tannic acid solutions	91
3B.1 Introduction	91
3B.2 Materials and methods	92
3B.3 Polymer-free electrospinning of tannic acid	95
3B.4 Aggregation and self-assembling properties of tannic acid in water-ethanol : fiber formation mechanisms	97
3B.5 Cross-linking of tannic acid fibers	103
3B.6 Electrospinning of a blend composed of TA and $\text{Fe}(\text{NO}_3)_3$	107
3B.7 Conclusion	107
References	109
<b>4. Development of a multi-jet spinneret .....</b>	<b>115</b>
4.1 Introduction	116
4.2 Materials and methods	117
4.3 Drawbacks linked to the electrospinning with a needle	119
4.4 Development of a multi-jet spinneret	121
4.4.1 Electrospinning with multi-jet spinnerets	121
4.4.2 Fabrication of mats with a constant thickness	122
4.4.3 Productivity of multi-jet spinnerets	128
4.4.3.1 <i>Productivity in the case of a solution of 6 wt% of PA11 in FA/DCM 50/50 v/v</i>	128
4.4.3.2 <i>Productivity in the case of a solution of 5 wt% of PVA - 0.5 wt% of Pluronic 127 in water</i>	132
4.5 Conclusion	132
References	134
<b>Concluding remarks and outlook .....</b>	<b>137</b>

<b>Appendix 1 :</b>	<b>Rheology of PA11 at 200°C</b>	<b>143</b>
<b>Appendix 2 :</b>	<b>Characterization of the spunbonded support layer</b>	<b>147</b>
<b>Appendix 3 :</b>	<b>Water uptake in PA11</b>	<b>149</b>
<b>Appendix 4 :</b>	<b>Coaxial electrospinning of aqueous polymer suspensions</b>	<b>150</b>
<b>Appendix 5 :</b>	<b>Characterization of aqueous polymer suspensions and water soluble polymers</b>	<b>156</b>
<b>Appendix 6 :</b>	<b>Electrospinning of coPA suspensions with other template polymers</b>	<b>161</b>
<b>Appendix 7 :</b>	<b>Electrospinning, curing and washing of MAPP/PVA, PVDF-PMMA/PVA and PVDF/PVA mats</b>	<b>162</b>
<b>Appendix 8 :</b>	<b>Polymer removal after washing</b>	<b>168</b>
<b>Appendix 9 :</b>	<b>Stress-strain curves</b>	<b>173</b>
<b>Appendix 10 :</b>	<b>Characterization of filtering suspensions and permeability of mats</b>	<b>174</b>
<b>Appendix 11 :</b>	<b>Estimation of hydrodynamic diameters <math>D_{TA}</math> of TA aggregates from DLS measurements</b>	<b>179</b>
<b>Appendix 12 :</b>	<b>Summary in French</b>	<b>181</b>

# INTRODUCTION

The fabrication of nano-fibrous membranes for the filtration of liquids via more environmentally friendly strategies, or in other words via "greener" strategies, is today a major concern both from an ecological point of view and for the safety of the personnel of production plants. The work consisted, thus, in developing nanofibrous mats by a "green" electrospinning process for liquid microfiltration. To be used for liquid microfiltration applications, membranes must be composed of fine and regular fibers inducing small, regular and interconnected pores (pore size between 0.1  $\mu\text{m}$  and 10  $\mu\text{m}$ ). The electrospinning process allows the fabrication of mats answering to these criteria. Electrospinning is a process allowing the fabrication, generally from a polymer solution, of nonwoven mats composed of fibers having diameters between 50 nm and a few micrometers depending on processing conditions and material properties. Thanks to the fineness and the regularity of electrospun fibers, electrospinning mats present small pores (pore size in the same range than the fiber diameter), and porosities greater than 80% unlike commercial liquid microfiltration membranes whose porosities do not exceed 40%. Consequently, the production of liquid filtration membranes by a « green » electrospinning process could even increase production rates while respecting the environment more.

In order to carry out the project, two ways have been explored: the electrospinning of a bio-sourced material and the electrospinning of aqueous solutions. Thus, a first part of the thesis, which is part of the CLARIFIL project (funded by the « fond unique interministériel » (FUI)) focuses on the electrospinning of polyamide 11, a bio-based polymer already used in food-related applications (**Chapter 2**). A second part of the thesis focuses on fabricating mats from aqueous solutions to get rid of toxic vapors coming from the evaporation of solvents often used during the process (**Chapter 3**). In this context, two ways were investigated: (i) the electrospinning of aqueous suspensions of hydrophobic polymers and (ii) the electrospinning of a bio-based molecule, tannic acid, by exploiting the supramolecular interactions present in the solution. Finally, a multi-jet spinneret was developed to produce mats large enough to be used in standard membrane filtration devices (**Chapter 4**). Indeed, electrospinning has few industrial applications because of low production rates and due to the fact that toxic solvents are often required. By developing new electrospinning environmentally friendly strategies that allow avoiding the use of toxic solvents, the industrialization of the electrospinning process becomes economically viable.

# COMMUNICATIONS

## Articles

### Published:

Domitille Mailley, Manon Allais, Pascal Hébraud, Dris Ihiawakrim, Vincent Ball, Florent Meyer, Anne Hébraud, and Guy Schlatter. “Polymer-Free Electrospinning of Tannic Acid and Cross-Linking in Water for Hybrid Supramolecular Nanofibres.” *Nanoscale* 10, no. 19 (2018): 9164–73. <https://doi.org/10.1039/C8NR01067F>.

### To be published:

Domitille Mailley, Anne Hébraud, Guy Schlatter. “Fabrication by electrospinning of liquid filtration mats from aqueous polypropylene suspensions.”

Domitille Mailley, Anne Hébraud, Guy Schlatter. “Fabrication by green electrospinning of liquid filtration mats from aqueous PVDF based suspensions.”

Marie Blackford, Domitille Mailley, Rémy Ghidossi, Anne Hébraud, Guy Schlatter, Martine Mietton-Peuchot. “Nonwoven filter media applied to liquid microfiltration: A review.”

Domitille Mailley, Anne Hébraud, Guy Schlatter. “The role of humidity in electrospinning: a Review.”

## Conferences

Oral presentation in international conference:

D. Mailley, M. Allais, P. Hébraud, V. Ball, F. Meyer, A. Hébraud and G. Schlatter, *Tannic acid nanofibers from polymer free solution*, Electrospin 2018, Stellenbosch, South Africa, January 2018

# LIST OF SYMBOLS AND ABBREVIATIONS

coPA	Copolyamide
DCM	Dichloromethane
DLS	Dynamic light scattering
DSC	Differential scanning calorimetry
EtOH	Ethanol
FA	Formic acid
Fe <sup>3+</sup>	Iron (III) cation
Fe(NO <sub>3</sub> ) <sub>3</sub>	Iron (III) nitrate
H <sub>2</sub> O	Water
IR	Infrared
MAPP	Maleic anhydride grafted polypropylene
NaIO <sub>4</sub>	Sodium periodate
PA	Polyamide
PA6	Polyamide 6
PA11	Polyamide 11
PA11(47.4)	Rilsan® 11 (M <sub>w</sub> = 47 400 g/mol)
PA11(36)	Rilsan® 11 (M <sub>w</sub> = 36 000 g/mol)
PA11(5.6)	Rilsan® 11 (M <sub>w</sub> = 5 600 g/mol)
PMMA	Poly(methyl methacrylate)
PP	Polypropylene
PVA	Polyvinyl alcohol
PVDF	Polyvinylidene fluoride
RH	Relative humidity
SEM	Scanning Electron Microscopy
T	Temperature
T <sub>g</sub>	Glass transition temperature
TA	Tannic acid
TGA	Thermogravimetric analysis

# 1

## BIBLIOGRAPHY

*This chapter introduces the basics necessary to the comprehension of the thesis. A focus is given on the electrospinning process (and especially on one process parameter: humidity), on liquid microfiltration and on electrospun filtering membranes.*



## 1.1 Electrospinning of nanofibers

### 1.1.1 Principle

Electrospinning [1–4] is a process allowing the production of a nanofibrous nonwoven mat from a polymer solution subjected to the action of a high difference of electric potential established between a metallic needle and a conductive collector (Figure 1.1a). The polymer solution is placed in a syringe, pushed out of the syringe at constant rate towards a metallic needle. When the difference of electric potential is high enough, the droplet of polymer solution exiting the needle takes the shape of the so-called Taylor cone from which a charged jet is propelled (Figure 1.1b). During its flight travel in the air, the charged jet is subjected to whipping movements and the solvent evaporates. Thereby the jet elongates and solidifies. Eventually a dry fiber with an average diameter ranging from tens of nm to few microns is deposited on the collector in the form of a nonwoven mat (Figure 1.1c).

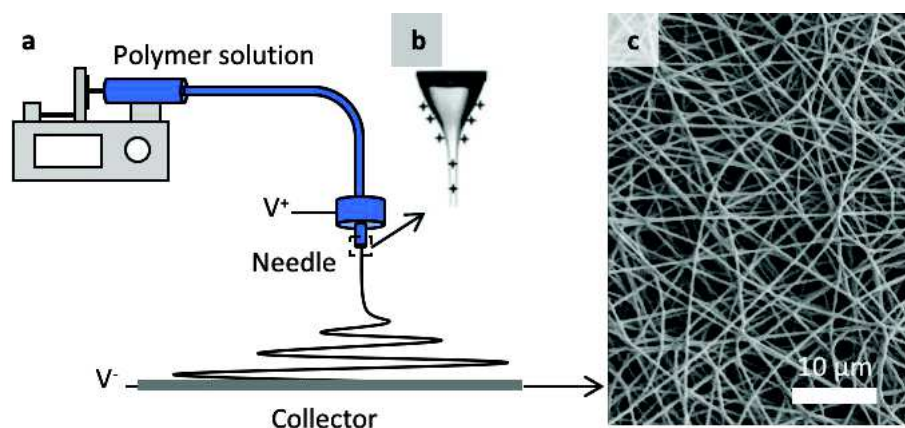


**Figure 1.1.** Single needle electrospinning setup: a) Schematic graph, b) Taylor Cone (Taken from Li et Xia, 2004 [4]), c) Electrospinning mat.

The structure of the electrospun mat depends on the processing parameters (setup geometry, flow rate, applied voltage distance between the needle and the collector), the polymer solution properties (nature of the solution, viscosity, surface tension, conductivity) and the ambient parameters (temperature, humidity) [5–8]. Contrary to all the other parameters, the effect of the humidity of the ambient air on the nonwoven mat properties has scarcely been studied. It is thus deeply described in part 1.1.3. Depending on the chosen electrospinning parameters, different type of structures can be formed such as beads, bead-on-string fibers, uniform fibers, rough fibers, rubans, surface pores, bulk pores, nano-nets and core/shell fibers (Figure 1.2). Electrospinning parameters are chosen according to the application [4,9]. For liquid filtration applications, homogenous mats of equal thickness composed of thin and regular fibers are promoted so that filtration takes place similarly in each point of the electrospun mat.

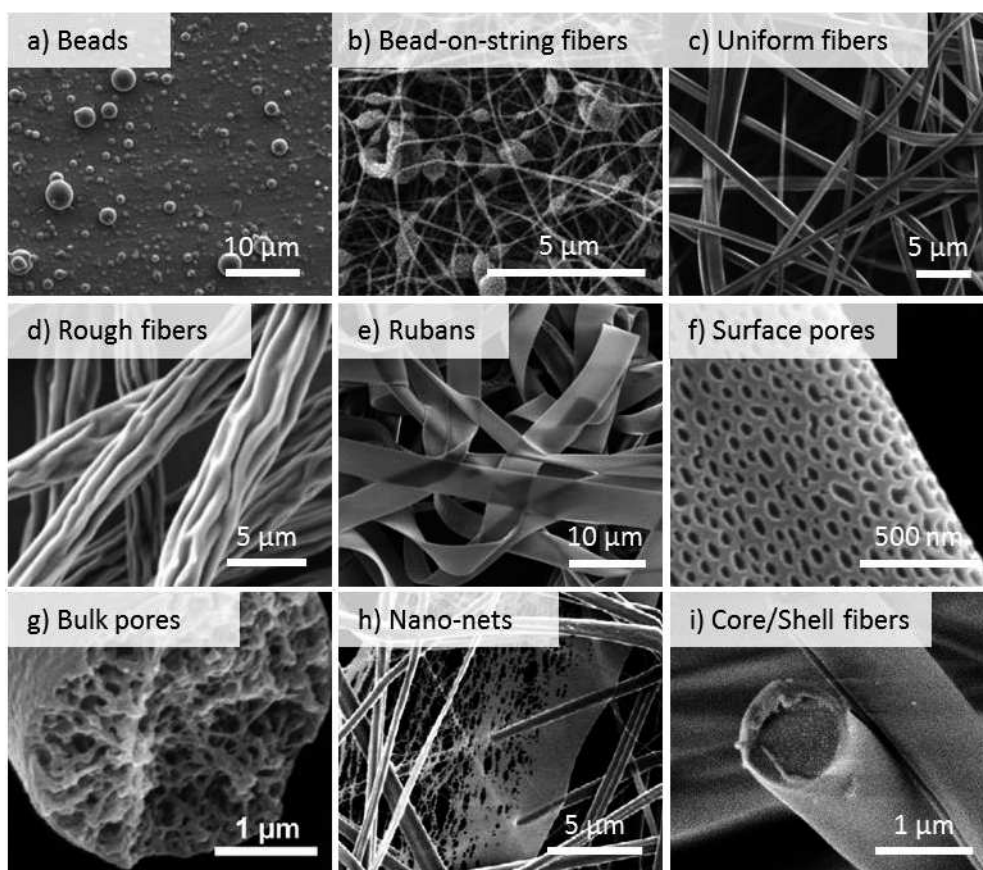


**Figure 1.2.** Different type of nanofibers that can be obtained by electrospinning. d) Pai et al. (2009) [10], f) Kim et al. (2005) [11], h) Fashandi and Karimi (2012) [12], i) Ding et al. (2006) [13].

### 1.1.2 Fiber formation

The formation of fibers from a polymer solution depends on the number of polymer chain entanglements in the solution. It is consequently linked to the solution concentration, to the polymer molar mass and thus to the solution viscosity (Figure 1.3). In the dilute regime, polymer chains are isolated. Above the “chain overlap concentration” ( $C^*$ ), in the semidilute unentangled regime, polymer chains begin interacting but are too small to entangle. Above the entanglement concentration ( $C_e$ ), in the semidilute entangled regime, polymer chains entangle. Below the entanglement concentration ( $C_e$ ), only bead-on-string fibers or beads can be electrospun as interactions between polymer chains are few or inexistent. Above  $C_e$ , regular, continuous and beaded-free fibers can be electrospun as the number of entanglements between polymer chains is sufficient to form a continuous nanofiber during the process without rupture of the jet [14–16]. More precisely, the electrospinning of fibers is generally possible above  $2-2.5C_e$  for neutral solutions composed of linear polymer chains [14,15] and above approximately  $7-8C_e$  [17] for polyelectrolytes.

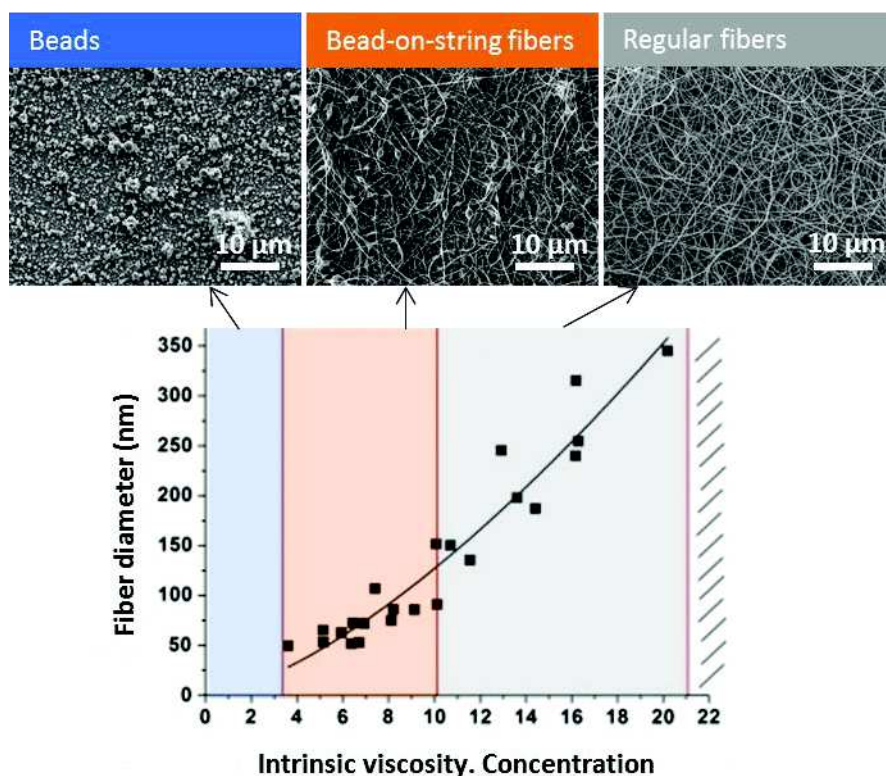


**Figure 1.3.** Concentration regimes related to the ability to electrospin fibers as a function of the fiber diameter. Adapted from Lavielle et al. (2013) [18].

### 1.1.3 Relative humidity

In a practical point of view, the humidity of the ambient air is assessed with the absolute humidity (AH) which corresponds to the mass of water for a given mass of air, as it is a thermodynamic parameter independent of any other physical parameters. Unfortunately, the direct measurement of AH is not possible. The humidity of the ambient air is, instead, evaluated through the relative humidity (RH) which depends on the temperature and the pressure of air. The link between AH, RH and the temperature is clarified in Figure 1.4 (taken from Fashandi et al. [12]). RH represents, in percent, the ratio between the partial pressure of water vapor and the equilibrium vapor pressure of water at the same temperature.

Understanding the effect of humidity on the structure of electrospun mats enables to tailor structures for targeted applications [19–21]. Cotton-like structures can improve cell adhesion [22] and cell penetration inside electrospun scaffolds for biomedical applications [23,24]. Oriented fibers have been used to enhance liquid filtration efficiencies [25] and for tendon and ligament tissue engineering [26]. The reduction of the fiber diameter was found to be highly interesting for electrospun grafts [27] and liquid filtration [28]. Beaded fibers have been studied for photonic applications [29], controlled release applications [30,31] and fog harvesting applications [32]. Porous fibers of  $\gamma$ -Fe<sub>2</sub>O<sub>3</sub>/PVA showed good degradation rates and cytocompatibility for biomedical applications [33]. Porous fibers could also be of great interest for absorption applications such as oil [34], phenol and iodine [35] and for microfiltration applications [36]. Finally, mats containing nano-nets are being developed for state-of-the-art sensing applications [37].

Several authors observed that humidity can affect the process of electrospinning leading eventually to different fiber structures and properties. In the present review, we propose to clarify the role of humidity on

solvent evaporation and on fiber solidification rates during the electrospinning process. Then, we aim at indexing and explaining all the impacts that humidity can have on the structure of nonwovens identified in the literature.

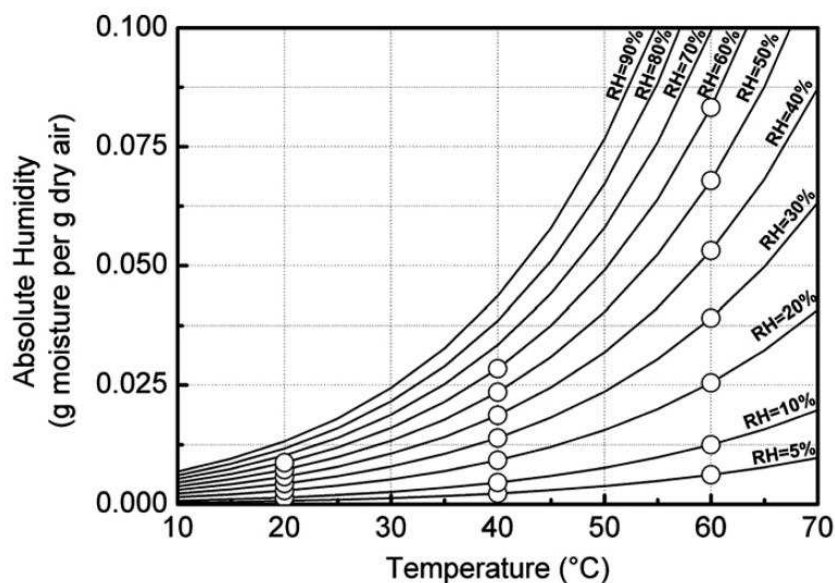


**Figure 1.4.** Absolute humidity at sea-level atmospheric pressure as a function of relative humidity and temperature. Reprinted with permission from Fashandi et al. [12].

### *1.1.3.1 Role of humidity during the electrospinning process on solvent evaporation*

During the electrospinning process, solvent evaporation occurs at the tip of the needle and during the jet flight until it reaches the collector. At the tip of the needle, a droplet of polymer solution is formed with a residence time in the order of few seconds leading to solvent evaporation by a diffusion mechanism. Then, evaporation happens along the electrospinning jet in few tens of milliseconds [1]. This second evaporation is favored by a convection mechanism due to the whipping movements of the jet. These whipping movements elongate the jet, generate more surfaces and lead to high air velocities both tangentially and transversally to the jet axis promoting thus an efficient solvent evaporation from the surface of the jet. This second step of evaporation is the most important because it leads to the deposition of a dry nanofiber on the collector.

The direct link between evaporation rate and humidity during the electrospinning process has been physically clarified in Equation 1 by Yarin et al. [38]. It depends on the type of solvent (i.e. non-aqueous, water or aqueous solvents).



$$\frac{\partial M_s}{\partial t} = -\rho h_m [c_{s,eq}(T) - c_{s\infty}] 2\pi a \lambda ds \quad \text{Equation 1.1}$$

With:  $M_s$ : Mass of solvent

$\rho$ : Solvent density

$h_m$ : Mass transfer coefficient for the evaporation

$c_{s,eq}(T)$ : Saturation vapor concentration of solvent at temperature T

$c_{s\infty}$ : Vapor concentration in the atmosphere far from the jet

$a$ : Cross-sectional radius

$\lambda$ : Geometrical stretching ratio

$ds$ : Surface element

When the solvent is not aqueous, then  $c_{s\infty}$  is equal to 0 leading to an efficient evaporation which only depends on the saturated vapor pressure of the solvent. However, in the case of aqueous solvents (Figure 1.5), at a given temperature, the water contained into the jet of polymer tends to evaporate due to the condition of equilibrium. If the water vapor pressure of the working place is close to the saturation vapor pressure determined by the ambient parameters (i.e. when the difference  $c_{s,eq}(T) - c_{s\infty}$  in eq. 1 is close to 0), only little water can be evaporated in order to fulfill the equilibrium condition. In that case, the evaporation of the jet is slow. On the contrary, when the water vapor pressure is far below the saturated vapor pressure, a high evaporation from the jet is necessary to fulfill the equilibrium condition. In this situation, the evaporation of the water contained in the electrospun jet is facilitated [39,40]. In the case of a hydrophilic solvent (Figure 1.5), depending on the capacity of the solvent to absorb water, the evaporation rate of the jet is susceptible to change in the same way as when water is used as solvent [41,42].

Humidity also affects indirectly the evaporation rate as water vapor molecules get ionized under a high electric potential and partially discharge the electrospinning jet [43]. Although air is commonly considered as an insulating gas, under high electric potentials, it becomes able to conduct a leakage current thanks to the creation of ions in the air [44]. As a result, for any kind of solvent (Figure 1.5), the electrospinning jet gets partially discharged through recombination with the surrounding ionized air. With an increase in humidity, the ionization of the air is enhanced due to the higher amount of water vapor molecules in the air. Water vapor molecules can be easily ionized thanks to their low ionization energy compared to other species present in the air such as nitrogen [45,46]. As a result, at high humidity, the electrospinning jet is discharged even more [47]. As the charge density on the jet is lowered at high humidity, the amplitude of the whipping movements is reduced. The reduction of the amplitude of the whipping movements slows down the evaporation rate of the solvent at high humidity [11,48–50].

When the evaporation of the solvent is very fast, humidity can have a last indirect effect due to water condensation at the jet surface. Evaporation induces a decrease of the temperature at the interface where it takes place. The decrease of the temperature comes from the evaporation itself, which is endothermic, as liquid water is transformed into water vapor. This means, in electrospinning that the temperature at the surface of the fibers is reduced during the process. Fast evaporation leading to fast cooling of the fibers is believed to enable the condensation of water vapor molecules present in the air on the surface of the fibers. Condensed water droplets, which are eliminated from the dried electrospun fibers, may leave imprints on the surface of the fibers giving birth to textured fibers. This mechanism is called the breath figure mechanism and will be

discussed further in part 1.1.3.3 [12,51,52]. This phenomenon has only been noticed for hydrophobic polymers, as their precipitation is accelerated at high humidity.

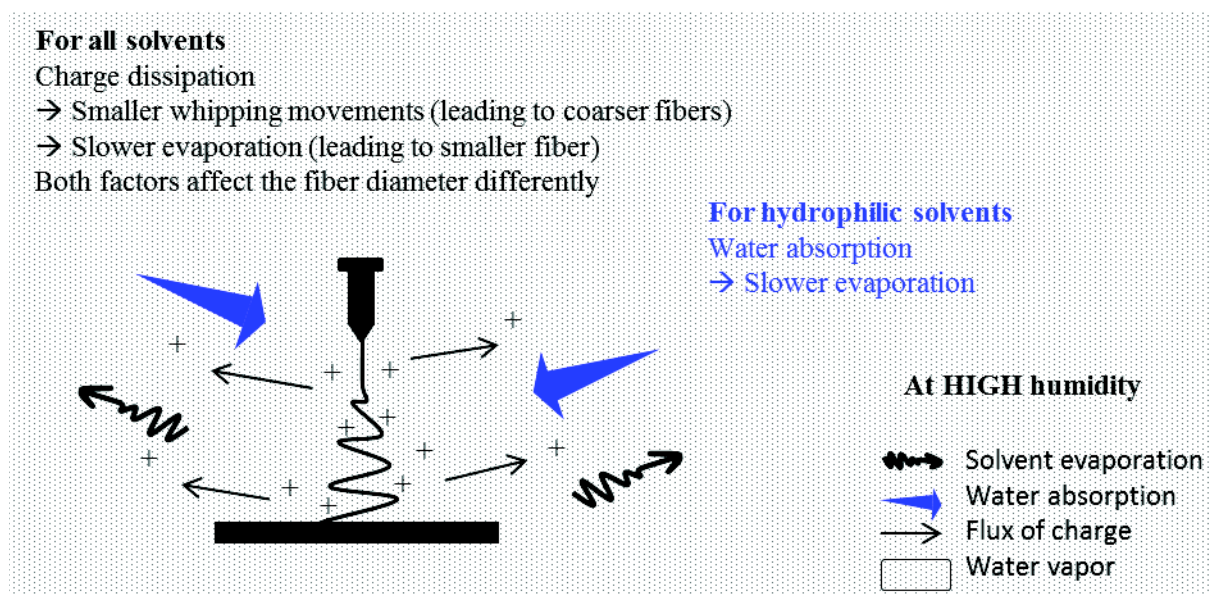


**Figure 1.5.** At high humidity, effects of humidity on the evaporation rate of the electrospinning jet as a function of the solvents.

In conclusion, in electrospinning, evaporation is achieved thanks to convection mechanisms due to the whipping movements of the jet. Humidity disturbs the evaporation rate of the solvent differently regarding the solvent type. It has a direct impact in the case of hydrophilic solvents as it delays solvent evaporation. It has also an indirect impact on any solvent as it reduces the whipping movements of the electrospinning jet and the evaporation rate by boosting the discharge of the jet. Last but not least, fast evaporating solvents at high humidity occurring for non-aqueous solvents, can promote water vapor condensation on the surface of the electrospun jet. Ultimately, the evaporation of the solvent from the jet leads to different ways of drying and fiber solidification and finally different kinds of fiber morphologies and non-woven mat structures which will be discussed in the next parts.

### ***1.1.3.2 Role of humidity during the electrospinning process on fiber solidification***

Electrospun fibers can solidify thanks to phase separations during the electrospinning process. Phase separation happens when the solution composition crosses the miscibility limit which generates polymer and solvent rich regions [53]. Phase diagrams can be used to predict the miscibility limit of a solution and consequently phase separation [12,54,55]. Different mechanisms can equally take place during phase separation: evaporation induced phase separation (EIPS) [56], thermal induced phase separation (TIPS) and vapor induced phase separation (VIPS) [52,57]. EIPS is a consequence of evaporation. The solution precipitates as too much solvent has been evaporated and the polymer is no longer soluble into the solution. TIPS happens when, because of the evaporation of the solvent, the surface of the fibers cools down. In that case the limit of solubility is lowered and the solution may precipitate. During VIPS, the vapor acts as a non-

solvent. This leads to the precipitation of the polymer out of the solution. After fiber solidification, dried fibers are deposited on the collector and form the nonwoven mat. Humidity can influence the solidification rate of the fibers and favor one of the phase separations mechanisms. Its effect varies along with the nature of the polymer and of the solvent.

It has been previously seen that humidity postpones the evaporation of the solvent if the solvent is water or if the solvent is hydrophilic. Thus, it delays the solidification of fibers (Figure 1.6a) [39,40,42]. Hygroscopic polymers can also absorb a small amount of water present in the air. As a result, a tremendous reduction of the glass transition due to a plasticizing effect is observed favoring the elongation of the jet during longer time before final solidification [58,59]. As a result, fibers can elongate during longer times before solidifying. So, high humidity, which promotes the absorption of water, postpones solidification and enables electrospun jets to stretch more out [60–62] (Figure 1.6b). When a hydrophobic polymer is used, water vapor acts as a non-solvent for the polymer. Consequently, the increase of humidity leads to a faster solidification rate of the fibers [42,48,63] (Figure 1.6c).

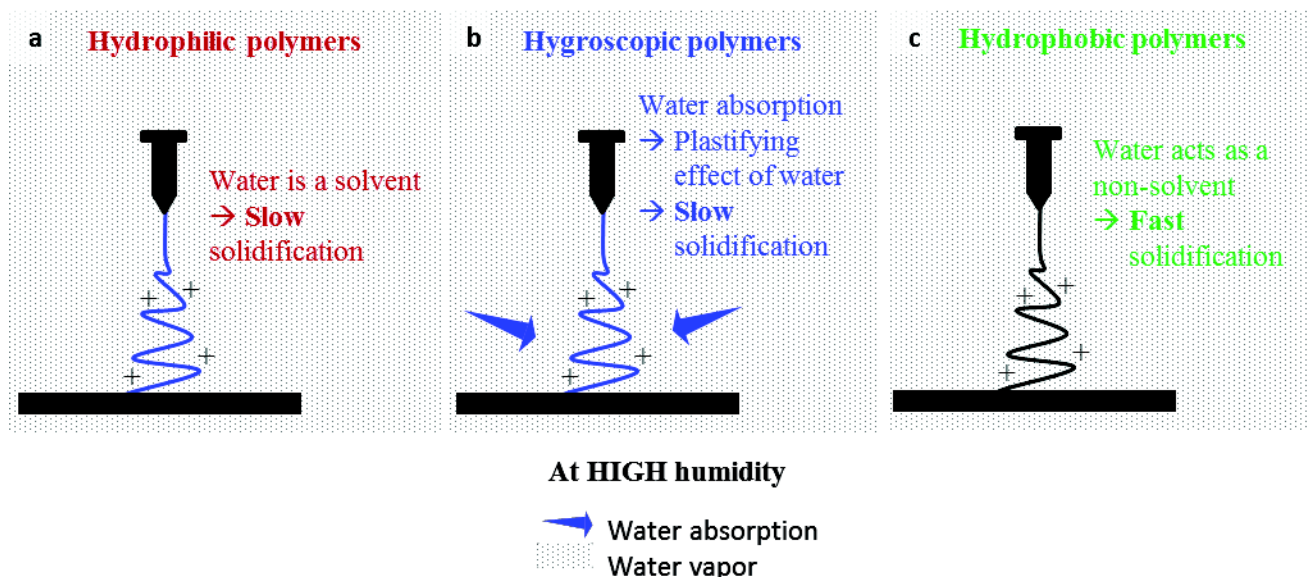


**Figure 1.6.** At high humidity, effects of humidity on the solidification rate of the electrospinning jet as a function of polymers: a) hydrophilic polymers, b) hygroscopic polymers and c) hydrophobic polymers.

In conclusion, the solidification rate of the fibers depends greatly by many ways on the humidity. Furthermore, the relations between humidity and solidification rate vary differently regarding the solvent and the used polymer. Finally, it is worth noting that according to the solidification rate, fibers have more or less time to stretch out and instabilities have also more or less time to appear. Therefore, the solidification rate determines the morphology and the structure of the resulting electrospun mat.

### 1.1.3.3 Effects of humidity on electrospun fibers

As a consequence of the effect of the humidity on the electrospinning process (amount of charges, evaporation, solidification) the final morphology of fibers is affected. Experiments have shown that the average diameter of the fibers may be influenced by humidity as well as the external shape of the fibers (beads-on-string fibers, beads) and the internal morphology of the fiber (surface roughness, pores located in

the fiber shell or in the whole volume of the fiber) depending on whether a hydrophilic or a hydrophobic polymer is used.

### FIBER SHAPE AND DIAMETER

The first effect of humidity that acts on the final fiber diameter is the discharge of the electrospinning jet at high humidity due to the increased amount of water molecules in the air. The jet is consequently less vigorously subjected to whipping instabilities and less elongated [64]. Then, humidity affects the solidification rate in different ways depending on the polymer-solvent systems, thus influencing the final diameter.

On one hand, for a system composed of a hydrophobic polymer, the absorption of water in the jet would lead to VIPS and early solidification. This results in thicker diameters and the suppression of bead-on-string morphologies that could be observed at low humidity (Figure 1.7 from E to A with increasing humidity). On the other hand, for a hydrophilic or hygroscopic polymer, water absorption in the jet would lead to delayed solidification either due to slower evaporation or to plasticizing of the polymer. In this case the jet thins until it is subjected to the development of a capillary instability leading to the formation of beaded fibers (Figure 1.7 from A to E with increasing humidity).

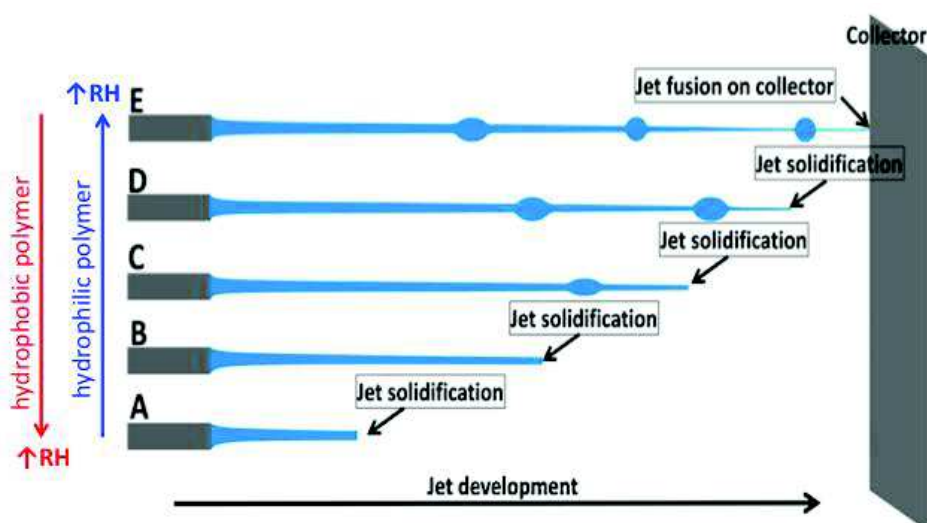


**Figure 1.7.** Schematic representation of electrospun jets as a function of the RH. Adapted from [39].

Table 1.1 gives the evolution of the fiber diameters when increasing the relative humidity for the various polymer/solvent systems given in the literature. For hydrophobic polymers, fibers become thicker at high humidity [11,48,49,63,65,66]. As an example, Kim et al. [11] electrospun PS in THF/DMF and noted that the mean fiber diameter increased by 300 % between 10% and 70% RH at 20°C. The increase of the fiber diameter has been reported for hydrophilic solvents such as DMF as well as hydrophobic solvents such as chloroform. The VIPS depends on the phase diagram of the solvent/polymer/water system. Pai et al. [67] and Fashandi et al. [12] have shown that increasing the humidity could advantageously suppress the bead-on-string structure of PS fibers obtained from DMF solutions at RH averaging 5%-10%. At higher humidity, the solidification of the jet occurred before the development of the capillary instability.



Ref	Polymer	Solvent	Temperature (°C)	RH gap (%)	Diameter variation (%)
[39]	PVA	Water	24	4-60	-76
[62]	PA4.6	Acetic acid/Formic acid	21	10-70	-64
[60]	PA6	Acetic acid/Formic acid	20	15-63	-57
[39]	PEO	3% acetic acid in water	24	4-40	-48
[40]	PEO	Water	21-22	5-49	-43
[62]	PA6.9	Acetic acid/Formic acid	21	10-70	-21
[68]	HA	DMF/Water	25	8-18	-14
[66]	SAN	THF/DMF	23	30-45	+6
[49]	CA	Acetone/DMF/Ethanol	25	20-70	+17
[63]	PEI	NMP	25	30-70	+124
[65]	PLLA	Chloroform	25	30-80	+129
[11]	PS	THF/DMF 6/4	20	10-70	+192
[48]	PSU	DMF	22	0-60	+211
[48]	PAN	DMF	22	0-60	+320

**Table 1.1.** Evolution of the fiber diameter of various polymer/solvent electrospinning systems with RH.

On the contrary, when a hydrophilic polymer is dissolved in water or in a hydrophilic solvent [40,68], the fiber diameter is thinner at high humidity. For instance, the diameter of PVA fibers was decreased by four when Pelipenko et al. [39] increased the relative humidity from 4% to 60% at 24°C due to slower evaporation of the water. As discussed previously, bead-on-string fibers were obtained at high humidity for PVA in water [39] or PEO in water [40]. Tripatanasuwan et al. [40] even described the evolution of the bead-on-string morphology of PEO fibers with increasing RH after their apparition at 52% RH (Figure 1.8).

Hygroscopic polymers, such as polyamides in acetic acid/formic acid, follow the same tendency [60,62]. In this case, the absorption of water in the jet plasticizes the polymer and lowers the solidification rate of the fibers enabling a higher stretching of the fibers.

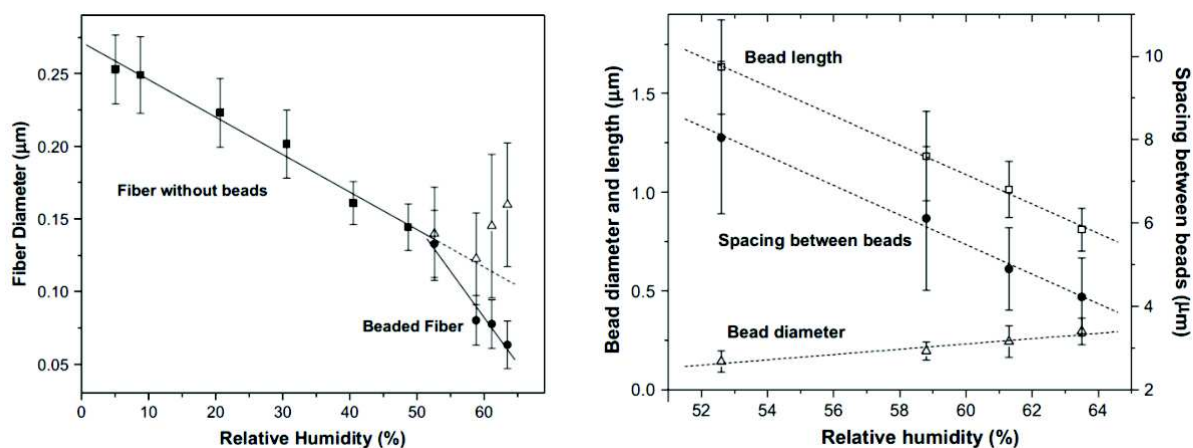


**Figure 1.8.** POE nanofibers electrospun from water solutions at different relative humidity. Left: average diameter of the fibers, right: average bead diameters, bead length and distances between beads. Reprinted with permission from [40].

#### SURFACE ROUGHNESS AND POROSITY

For hydrophobic polymers in various solvents, depending on humidity, electrospinning can lead to wrinkled or rough fibers [67], as well as fibers having pores at their surface [52,56,69] or in their core [12] (Table 1.2). For instance, Figure 1.9 shows different kind of porous fibers. Indeed, the surface and internal morphology of the fibers is formed at the moment of the fiber solidification, which is due to the combined effect of the evaporation of the solvent and the absorption of water vapor into the fiber. The mass transfers of the solvent towards the outside of fibers and of water towards the core of fibers lead to solvent/non-solvent gradients inside the fiber and a change of solubility of the polymer inducing phase separation via TIPS, EIPS or VIPS mechanisms.

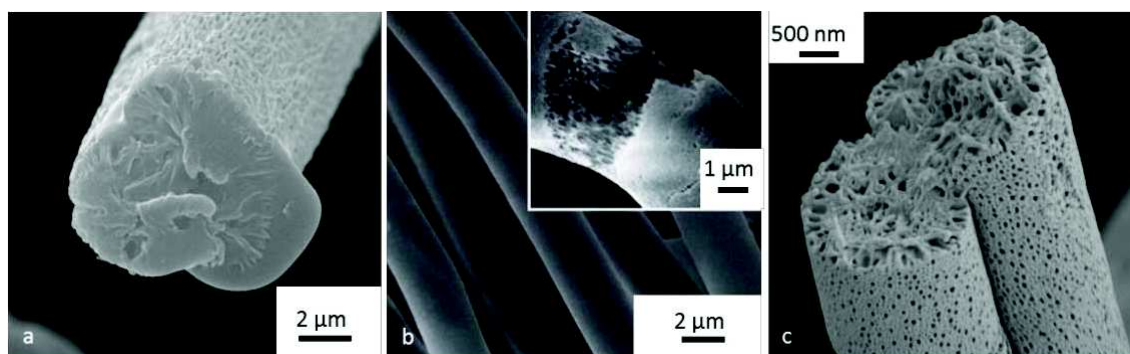


**Figure 1.9.** (a) PS fibers composed of a porous surface and a solid inside electrospun in THF at 40°C and 60% RH. Reprinted with permission from [12]. (b) PS fibers composed of a smooth surface and internal pores electrospun in THF and DMF at 24°C and 45% RH. Reprinted with permission from [70]. (c) Fibers containing PS, sorbitan monooleate and fluorescein sodium salt composed of a porous surface and internal pores electrospun in DMF and chloroform at 20°C and 60% RH. Reprinted with permission from [53].

VIPS is directly related with the diffusion of water inside the fibers, which is a non-solvent for hydrophobic polymers. At high humidity and for solvents that are miscible with water, such as THF or DMF, the mass transfer of water inside the fiber will lead to a change of composition of the polymer solution that can be described by composition paths on the solvent/non solvent/polymer phase diagram (Figure 1.10). If the solvent evaporation rate is faster than water absorption, the composition path I will be followed and no phase separation occurs in the solution. Fashandi et al. have shown that this was the case of PS electrospun from THF solutions because THF evaporation is rapid but also because the homogeneous region was larger for PS-THF-water solutions with up to 5% water. Therefore for PS electrospun from THF solution, the core of the fibers is compact [11,12,57]. If the composition path followed during electrospinning crosses the binodal curve to end in the metastable region (path II), phase separation will occur via nucleation and growth mechanism, leading to a porous core with isolated cellular pores. Finally, if the composition path crosses the spinodal curve and ends up in the unstable region, phase separation will occur via spinodal decomposition, leading to co-continuous interconnected networks of pore in the core of the fibers. This has been observed for PS solutions in DMF [54,57,67,70]. In this case, evaporation of DMF is slower and the homogeneous region of the phase diagram is small, precipitation occurring with less than 0.2% of water in a PS/DMF solution. Lu et al. [57] observed fibrils inside the core of PS fibers electrospun from DMF. This is probably due to the bicontinuous phase separation undergone during electrospinning, combined with the elongation of the structure. Porous fibrous core have also been observed for poly(ether imide) in DMF [55], or styrene/acrylonitrile copolymers in ethanol/DMF 2/3 [66].

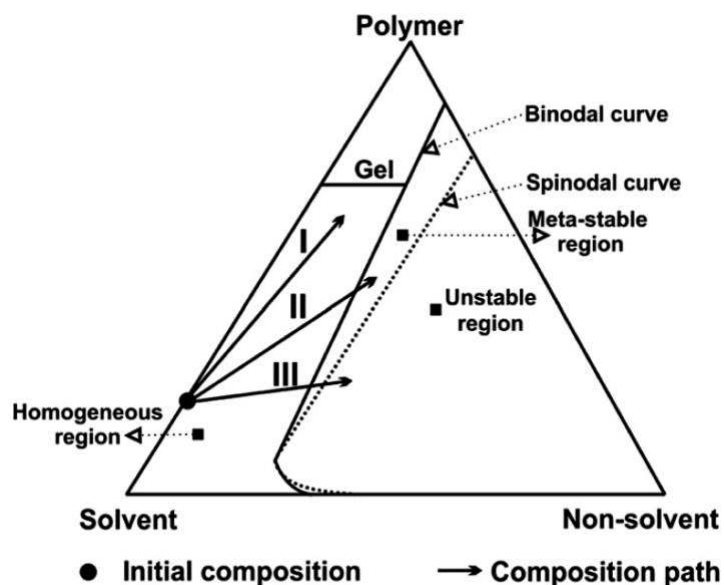


**Figure 1.10.** Schematic representation of polymer-solvent-non solvent phase diagram and the possible composition paths that can undergo fibers during electrospinning Reprinted with permission from [12].

The rate of solvent evaporation depends on the vapor pressure of the solvent. Evaporation of the solvent combined to slow diffusion may lead to the formation of polymer concentration gradients with a high concentration near the surface, leading to thin solid skin around the jet. This skin is then subjected to compressive radial stresses that cause buckling instabilities, leading to wrinkled or rough fibers. Pai et al. [67]

have linked the appearance of rough fibers (Figure 1.11) with the drying time and the buckling time first described by Pauchard et al. [71] for polymer solution droplets. The drying time ( $t_D$ ) is the time needed for the fiber to dry completely. It is proportional to the diameter of the fibers inversely proportional to the evaporation rate. The buckling time ( $t_B$ ) depends on the mutual diffusion coefficient of the polymer-solvent system, the solution concentration and is inversely proportional to the square of evaporation rate. Smooth fibers are obtained when  $t_B > t_D$ , whereas rough fibers are formed if  $t_B$  is comparable to  $t_D$ . For example, in the case of PS solution in THF, the appearance of wrinkled fibers depends on the diameter of the fibers, or the molecular weight of the polymer. Thicker fibers tend to collapse because the time needed for complete drying of the fiber is larger while fibers made from higher molecular weight collapse because, the diffusion coefficient of the polymer-solvent system is low, which result in lower  $t_B$ . In the case of PS fibers electrospun from DMF solutions, wrinkled fibers were also observed at low relative humidity. However, when the relative humidity is high enough, the phase separation inside the fibers due to absorption of water is faster than both buckling and drying, leading to porous fibers with circular cross-sections [12,67].

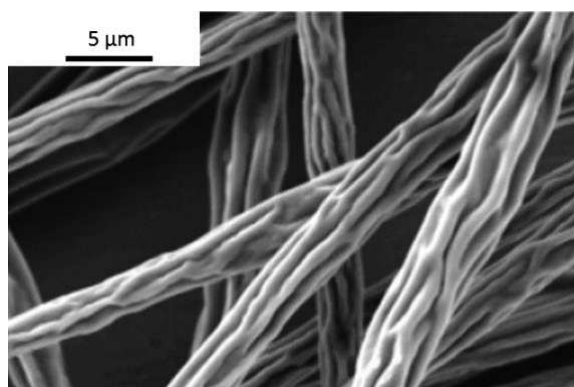


**Figure 1.11.** PS rough fibers electrospun in DMF at 15% RH at room temperature. Reprinted with permission from [67].

Finally, rapid evaporation of the solvent also leads to an important temperature decrease due to the latent heat loss, leading to the condensation of water vapor at the surface of the fibers. After complete evaporation, pores at the surface of the fibers left by the water droplets and also called breath figures [72] can be observed. Yazgan et al. [73] correlated the transition from smooth fibers to rough fibers with other physical values namely the dew point ( $T_{dp}$ ) and the wet-bulb temperature ( $T_{wb}$ ). The dew point ( $T_{dp}$ ) is an absolute parameter which is related to AH. It corresponds to the temperature at which water vapor starts to condensate and forms the first liquid droplet. The wet-bulb temperature refers to the minimum temperature that the polymer solution reaches during evaporation due to latent heat loss. Water condensation on the fiber occurs when  $T_{dp} - T_{wb} > 0$ . They observed this phenomenon for PCL fibers electrospun from dichloromethane or chloroform (Figure 1.12). It was also observed for PS, PMMA or PLA fibers electrospun from fast evaporating solvent such as THF, acetone, dichloromethane or chloroform [11,51,52,56,74]. Casper et al. [51] showed that the size of the pores created on the surface of PS fibers, electrospun from THF, increased with the relative humidity, but surprisingly, also with the molecular weight of the polymer. It was concluded that in this case, both the condensation of water and phase separation on the surface of the fibers, due to the decrease of temperature probably occurs at the same time.

Finally, the mechanisms leading to structured morphology of the fibers can also be complicated by the mixture of two different solvents with different boiling temperature, or affinity with the polymer, as suggested by Yazgan et al. [73].

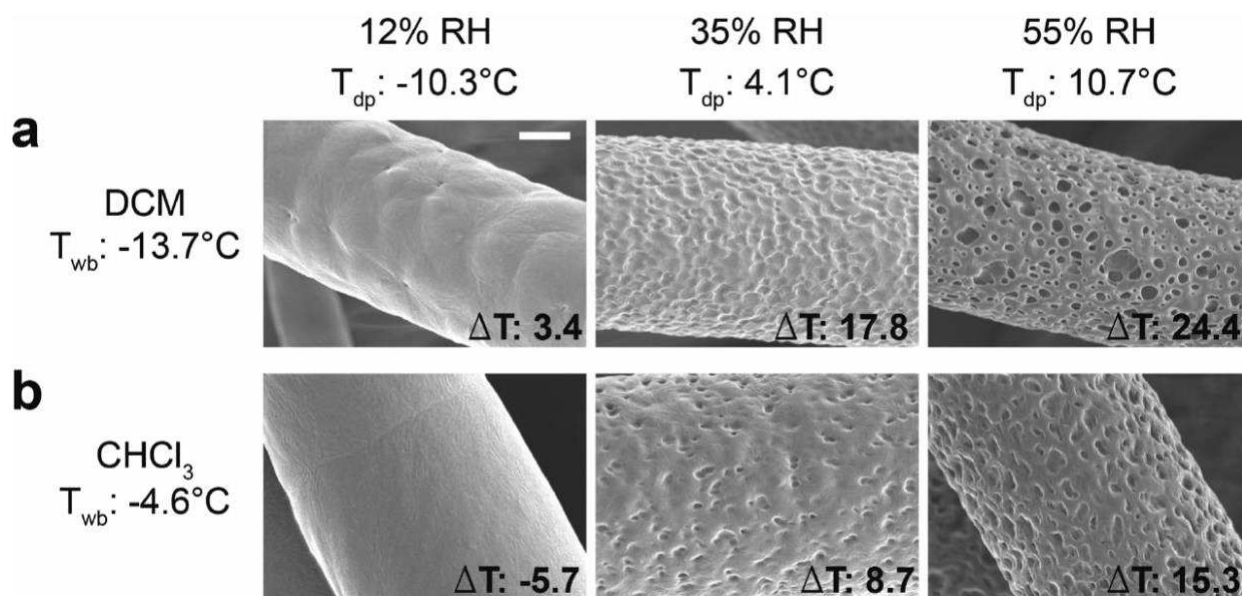


**Figure 1.12.** Morphologies of electrospun PCL fibers spun with dichloromethane (DCM) and chloroform (CHCl<sub>3</sub>): SEM micrographs and corresponding  $\Delta T (T_{dp} - T_{wb})$  of (a) DCM (upper row) and (b) CHCl<sub>3</sub> (lower row) solution spun PCL fibers at 12%, 35% and 55% RH, respectively (scale bar: 2  $\mu\text{m}$ ). Reprinted with permission from [73].

In conclusion variations in fibers morphologies must be differentiated according to whether the polymer is hydrophilic or hydrophobic. For hydrophobic polymers, the fiber diameter increases as humidity increases due to fast polymer precipitation contrary to hydrophilic polymers. In this case, water acts as a non-solvent. In addition, the competition between solvent evaporation and polymer precipitation at high humidity may lead to the creation of rough fibers and of pores on the surface or in the bulk of fibers. On the contrary, if the polymer is hydrophilic, then the fiber diameter decreases as humidity increases due to water absorption. Water absorption in hydrophilic polymers delays the solidification of fibers mainly because of polymer plasticizing leading to a longer stretching of the electrospinning jet. The deferment of the solidification of the jet enables the appearance of bead-on-string fibers at high humidity and can also lead to fiber sticking and to the fabrication of films as it will be seen in the next part.

#### 1.1.3.4 Effects of humidity on the nonwoven mat structure

Variations in humidity can also have consequences on the structure at the scale of the electrospun nonwoven mats. With a variation of RH, fibers can stick together or be differently oriented. Mats can turn into films or differently gain a cotton-like structure. Finally, nano-nets may be found in the structure of mats between the fibers.



## FIBER-STICKING AND FILM FORMATION

This phenomenon happens when the solvent is not completely evaporated leading to the deposition of fibers which are not completely solidified before reaching the collector. As previously discussed, the cases for which humidity postpones the solvent evaporation correspond to the cases when the solvent is water or when it is hydrophilic. Consequently, the small amount of residual solvent that remains on the fibers enables them to stick together. Fibers-sticking conveys electrospun mats better mechanical properties [13,68]. For example, Ding et al. [13] observed this behavior at 75% RH with PAA fibers electrospun in a mixture of water and ethanol at 25 °C. When the solidification of the fibers is even slower, they cannot solidify any more, fuse together and turn into a film (Table 1.2) [39,42,68,75,76]. This behavior happens above all in the case of water or hydrophilic solvents at high RH. De Vrieze et al. [42] reported a film formation for the electrospinning of PVP in ethanol starting from 60% RH for a distance between the syringe and the collector of 12 cm at 10°C (Figure 1.13). Yao et al. [68] noted that fibers were prone to fuse together when RH was increased until a film was formed for HA in DMF and deionized water system starting at 38% RH at 25°C. Liang et al. [76] electrospun in water a PEO film when RH was raised between 83% and 93% at 25°C. Thus controlling the humidity can help the tuning of the overall mechanical properties of the final nonwoven mat as well as its porous structure (i.e. the porosity and the pore size between the fibers).

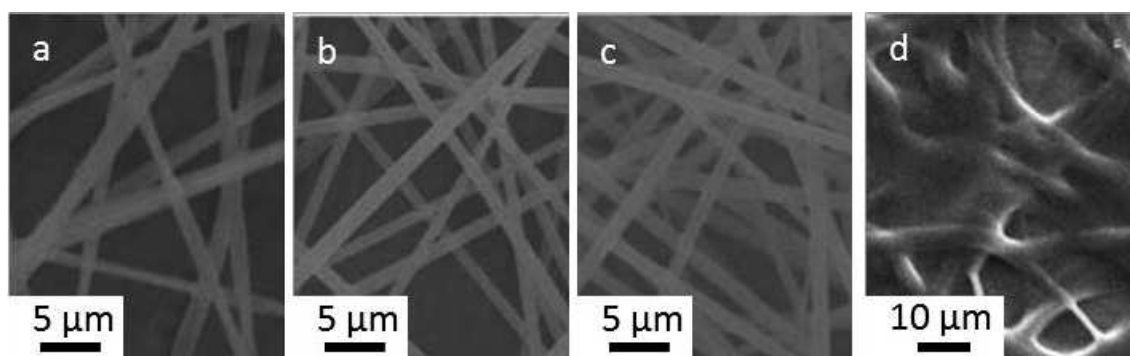


**Figure 1.13.** PVP fibers and film electrospun in ethanol at (a) 20% RH, (b) 30% RH, (c) 45% RH and (d) 60% RH at 20°C. Reprinted with permission from [42].

## COTTON-LIKE 3D STRUCTURES

Electrospinning is a process that generally allows only the fabrication of thin nanofibrous membranes having a thickness lower than few hundreds of microns. However, it has been reported that under specific conditions cotton-like structures can be obtained with thickness as high as few cm. Such 3D structures can be obtained only when the electrostatic charges cannot efficiently dissipate from the surface of the deposited fiber to the collector. A fluffy cotton-like structure of several cm height were obtained by Li and Long [77] for the electrospinning of PS and PVP/nitrate and by Bonino et al. [78] for the electrospinning of alginate-based systems (Figure 1.14). Huang et al. [48] suggested a mechanism leading to the formation of such structures in the cases of PAN and PSU nonwovens electrospun from DMF solutions. Fast solidification induces rare fiber-fiber bounding in nonwovens limiting thus the whole charge dissipation and finally yielding a cotton-like structure. More precisely, residual solvent is needed to allow fiber-fiber adhesion, and as because of fast solidification the amount of residual solvent on the surface of the fibers is reduced, very few fibers can bound together increasing thus fiber-fiber charge repulsions. For aqueous polyelectrolyte solutions, as observed for

alginate [78], the mechanism leading to the formation of the cotton-like structures is more complex because the humidity plays an important role on the evaporation rate, on one hand, and on the amount of charges carried by deposited fiber, on the other hand (Figure 1.14). Indeed, an increase of RH allows keeping the charged groups (R-COO<sup>-</sup> and Na<sup>+</sup>) of the polyelectrolyte in their dissociated forms favoring thus the fiber-fiber repulsions necessary for the formation of the cotton-like structure. However, poor evaporation rate is experienced for the highest RH leading to beaded fibers as well as a better fiber-fiber contact leading to efficient charge release and finally avoiding the formation of the cotton-like structure.

In conclusion, the control of humidity is important in order to help the formation of such cotton-like structure which has poor mechanical properties but large pore size which can be beneficial for biological applications necessitating cell invasion [22–24].

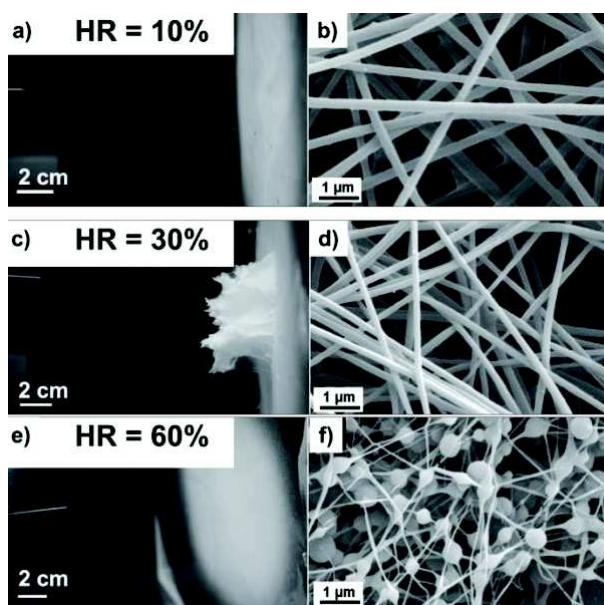


**Figure 1.14.** Effect of humidity on the formation of cotton-like structure after 40 minutes of electrospinning of alginate solubilized in water. Reprinted with permission from [78].

#### FIBER ORIENTATION AND STRUCTURATION

Electrospinning leads to the elaboration of a nonwoven mat. However, when patterned collectors are used it is possible to induce a regular structuration of the deposited fibers [79]. As for the formation of cotton-like structures, the charges remaining on the deposited fibers play an important role. Indeed, the use of patterned collectors allows keeping some portions of the deposited fibers without a direct contact with the ground allowing to form an electrostatic template at the vicinity of the top surface of the mat [80]. This electrostatic template is responsible of the force inducing the controlled deposition of the electrospun jet which can be maintained for long time of deposition allowing the fabrication of thick structured membranes [81]. However, if the charges are released during electrospinning, the structuration of the fibers is lost. As previously discussed, humidity plays an important role on the amount of charges carried by the jet as well as on the capacity to keep the charges on the surface of the deposited fiber. Thus, humidity affects the quality of such fiber structuration. As an example, Zucchelli et al. [82] succeeded in tailoring the degree of orientation and fiber patterning by modifying the humidity during the electrospinning of PLLA in DCM and DMF at room

temperature. During the electrospinning process, fibers retain some charges when deposited on the collector and can influence the deposition of new fibers by electrostatic repulsion [64]. At high humidity, the partial discharge of the electrospinning jet, associated with a less vigorous solidification rate of the fibers, reduces electrostatic repulsion between portions of fibers. Consequently fibers become less orientated with an increase in humidity. Similarly to Zucchelli et al., Li et al. [83] could control the alignment and assembly of PVP fibers electrospun in a mixture of water and ethanol by varying the humidity.

#### NANO-NETS

Relative humidity could also promote the apparition of nano-nets (also called nano-webs) (Figure 1.15). This hierarchical fibrous structure corresponds in nets of very thin nanofibers with diameter in the range of few tens of nm suspended between larger fibers with diameter in the range of several hundreds of nm to few microns [84]. Different theories could explain the formation of this structure and no consensus has been yet reached. Wang et al. [85] emphasized the role of the formation of hydrogen bonds during the electrospinning/-netting. Hydrogen bonds are supposed to connect nano-nets together and could explain their formation (Figure 1.16). Ding et al. [13] hypothesized that nano-nets are formed from charged microsized droplets generated during the process of electrospinning which are subjected to fast phase separation. Phase separation happens very fast in the case of PAA dissolved in water and ethanol at low RH, and nano-nets can be seen in the structure of the PAA nonwovens when RH is decreased. Zhang et al. (2015) [86] suggested two critical charge to mass formulas enabling to predict the generation of jets and microsized droplets. If the charge to mass ratio exceeds the first and lowest critical value, only jets are formed. If the charge to mass ratio exceeds the second critical value, microsized droplets and jets are fabricated.

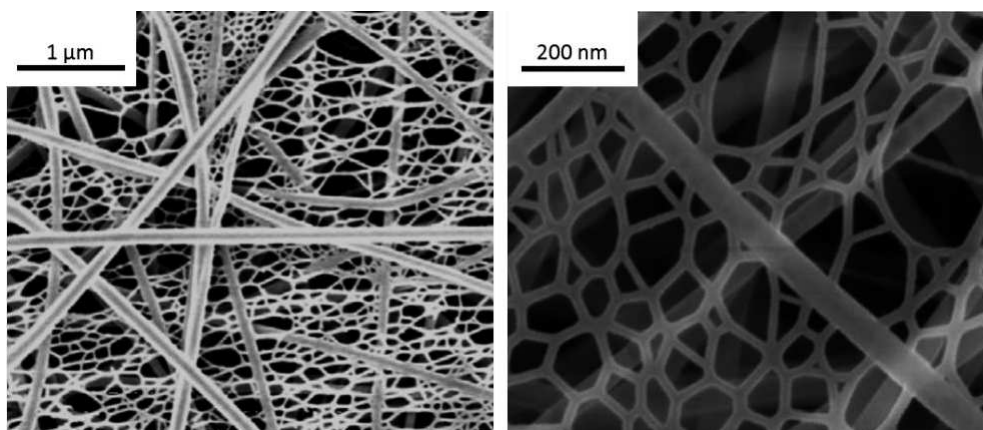


**Figure 1.15.** (a) Nylon 6 fibers and nano-nets electrospun in formic acid at 25°C and 20% RH. Reprinted with permission from [69]. (b) Gelatin-NaCl fibers and nano-nets electrospun in formic acid at 24°C and 25% RH. Reprinted with permission from [85].



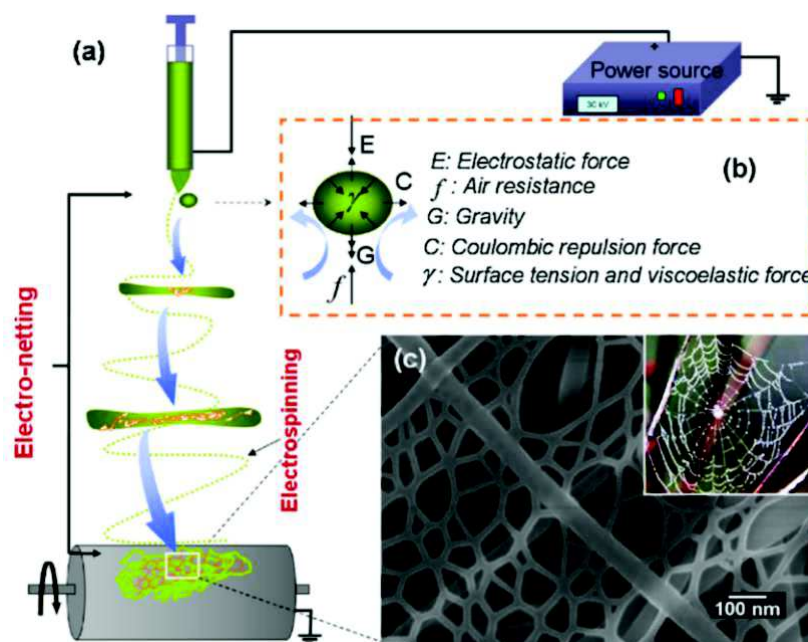


**Figure 1.16.** Mechanism of nano-net formation. Reprinted with permission from [85].

Ref	Polymer	Solvent	Temperature (°C)	RH (%)	Effects
[12]	PS	DMF	20	5-10	Bead-on-string fibers
[40]	PEO	Water	22	$\geq 53$	Bead-on-string fibers
[84]	Gelatin-	Formic acid	24	60	Bead-on-string fibers
[39]	PVA	Water	24	70	Beads
[39]	PEO	Acetic acid	24	50	Beads
[48]	PAN	DMF	22	$\geq 20$	Rough surface
[70]	PS	THF/DMF 1/4	24	20	Rough surface
[11]	PS	THF	20	$\geq 30$	Pores on the surface
[56]	PLA	DCM	RT	75	Pores on surface
[50]	PCL	Chloroform/DMF 80/20	21	$\geq 50$	Pores on the surface
[73]	PCL	CHCl <sub>3</sub>	RT	$\geq 35$	Pore on surface
[51]	PS	THF	24	$\geq 30$	Pores on the surface
[87]	PMMA	DMF	n.g.	$\geq 35$	Pores on surface
[87]	PMMA	toluene	n.g.	$\geq 40$	Pores on surface
[87]	PVC	DMF	n.g.	$\geq 60$	Pores on surface

Ref	Polymer	Solvent	Temperature (°C)	RH (%)	Effects
[74]	PS	DCM/Ethanol 90/10	19	≥40	Pores on the surface
[48]	PSU	DMF	21-22	≥ 40	Pores on the surface (inside?)
[12]	PS	THF	40	≥60	Pores on the surface
[12]	PS	DMF	20	≥ 30	Internal porosity
[57]	PS	THF	20	22	Internal porosity
[88]	PS	THF/DMF	n.g.	60	Internal porosity
[70]	PS	THF/DMF 1/4	24	45	Internal porosity
[89]	PS	THF	25	≥ 30	Internal porosity
[66]	SAN	Ethanol/DMF 2/3	23	60	Internal porosity
[13]	PAA	Ethanol	25	75	Fiber-sticking
[42]	PVP	Ethanol	20	60	Film
[68]	HA	DMF/Water v/v	25	38	Film
[39]	PEO	Acetic acid	24	70	Film
[75]	PEO	Water/Ethanol 5/1	30	70	Film
[76]	PEO	Water	25	83-93	Film
[48]	PAN	DMF	22	≥ 40	Cotton-like structure
[48]	PSU	DMF	22	≥ 30	Cotton-like structure
[13]	PAA	Ethanol	25	20	Nanonets
[13]	PA6	Formic acid	25	20 and 75	Nanonets
[85]	Gelatin-	Formic acid	24	45	Nanonets

**Table 1.2.** Effects of RH on the morphology of the fibers regarding various polymer/solvent electrospinning systems. n.g.: not given. RT: room temperature.

In conclusion, due to the fact that a variation of RH shortens or delays the solidification time, the structure of electrospun mats is therefore affected. Table 1.2 gives typical examples for which humidity influences the structure of electrospun nonwoven mats. Fast solidification is linked with the appearance of cotton-like structure and nano-nets. Slow solidification with the fabrication of fiber-sticking and films. Last but not least, the choice of solvent and polymer promotes either fast or slow solidification. So, most of the time, mats electrospun from solutions containing water, a hydrophilic solvent or a polymer able to plasticize with water yield at low RH nano-nets and at high RH fiber sticking and films. Mats, electrospun from solutions containing a hydrophobic solvent and a polymer not able to plasticize with water, lead at high RH to cotton-like structures and potentially also nano-nets. No tendency has been noticed at low RH.

Relative humidity plays a major role in controlling the fiber morphology and the structure of electrospun nonwovens as it influences the evaporation rate of solvents and the solidification rate of fibers. Whether the solidification of the electrospun fibers occur rapidly or slowly, the morphology of the fibers and the structure of the mats may change depending on electrospinning solutions. Indeed, humidity influences the solidification rate differently according to both the solvent (aqueous, hydrophilic or hydrophobic) and the polymer (hydrophilic, hygroscopic or hydrophobic) (Figure 1.17). For hydrophilic and hygroscopic polymers solubilized in aqueous or hydrophilic solvents, the increase of humidity delays the solidification of the fibers due to water absorption and polymer plasticizing. Consequently, fibers are coarser at low humidity than at high humidity. Besides, high humidity favors the apparition of bead-on-string fibers and films. In the case of hydrophobic polymers, the increase of humidity usually shortens the solidification time of the fibers. Consequently, low humidity leads to thin fibers while in contrast high humidity yields coarser fibers, and possibly porous fibers, cotton-like structure and nano-nets. Furthermore, fiber orientation can disappear at high humidity due to jet discharge. Choosing the humidity (for a fixed temperature) can be a way to tailor a desired structure and/or morphology, knowing the composition of the electrospinning solution, for a targeted application. Thus, humidity also plays on various properties of nonwoven mats such as the mechanical strength [48,90], the electrical conductivity of conductive fibers [91] and various biological properties (controlled release rates, cytocompatibility, cell penetration rate). As final conclusion, humidity is an unneglectable parameter during electrospinning experiments, whatever the solvent is. This is why the control of humidity has to be implemented in all electrospinning devices.

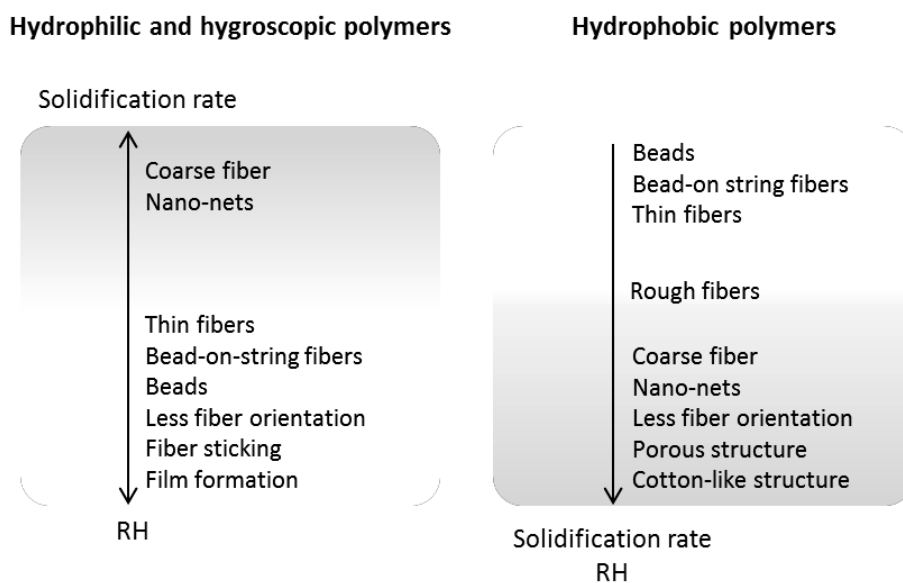


**Figure 1.17.** Fiber and mat structures as a function of RH, the solidification rate and the polymer type mostly obtained.

## 1.2 Liquid microfiltration

### 1.2.1 Principles

Liquid microfiltration is a process allowing the separation of specific elements from a mix of liquid and solid phases, through a filter media. It is a pressure-driven process used for a wide range of fields including oil, fuel, water, wine [92] and food industries. The main goal of this process is either to collect solid particles or to clarify a liquid of interest from solid particles contamination. Microfiltration filter media are composed of pores with a size between 0.1  $\mu\text{m}$  and 10  $\mu\text{m}$  [93].

During liquid microfiltration, three main retention mechanisms can occur (Figure 1.18): sieving, depth and adsorption mechanisms [92,93]. These various filtration mechanisms occur alone or jointly, depending on the filter media, on the to-be filtered liquid and on the solid particles contained in the liquid [94]. In sieving mechanism, particles are stopped on the up-stream side of the filter media and piled-up, thereby giving birth to a filtration cake. This phenomenon occurs when particles are significantly larger than the pore size of the filtering membrane. The cake build-up increases the pressure drop during filtration and creates smaller passages. Smaller passages enable the removal of smaller particles than the ones initially targeted, thus inducing an impoverishment of the liquid of interest. In many applications, this type of filtration mechanism is avoided in order to ensure good filtration duration and efficiency. The second mechanism that can occur during liquid microfiltration is depth filtration. In this case, particles are trapped inside the filter media. This mechanism is affected by both the pore characteristics (the pore size, the pore shape and the material constituting the filter) and the particles' characteristics (size and physical/chemical properties). This trapping process is sought as it helps extending duration and efficiency of the filtration. The last mechanism is adsorption which occurs either on the surface of the filter or in the pores. This holding mechanism is based on electrostatic interactions and on Van der Waals forces. Particles having an affinity with the filter media are adsorbed and retained on or within the filter media. This phenomenon allows the trapping of particles having smaller diameters than the pore size.

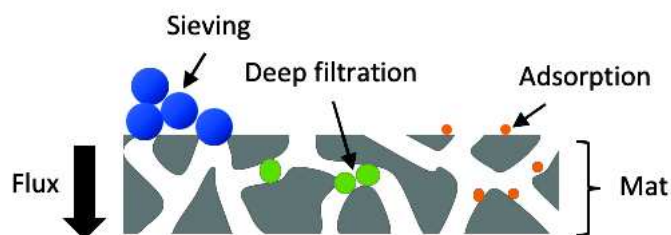


**Figure 1.18.** Retention mechanisms during liquid filtration.

Two geometries are conceivable to perform liquid microfiltration trials: a dead-end or a cross-flow geometry (Figure 1.19). For the dead-end geometry, the flux is directed perpendicularly to the filter in such a way that the liquid flows entirely through the filter. Two phases can be distinguished: the retentate and the permeate. The retentate is the liquid withheld by the filter on the up-stream side of the filter whereas the permeate is the liquid in the down-stream side of the filter. Dead-end geometries have the drawback of being rapidly fouled, above all when a solution, highly concentrated in particles, is used. In cross-flow geometries, the flux is directed alongside the filter, creating three phases: the filtrate, the retentate and the permeate [92]. The filtrate is the liquid on the up-stream side of the filter. The retentate is the liquid on the down-stream side of the filter

that did not flow through the filter. The liquid on the down-stream side of the filter that went through the filter is called permeate. Cross-flow geometries are slower fouled than dead-end ones and are, thereby, more efficient. However, cross-flow geometries are more expansive.

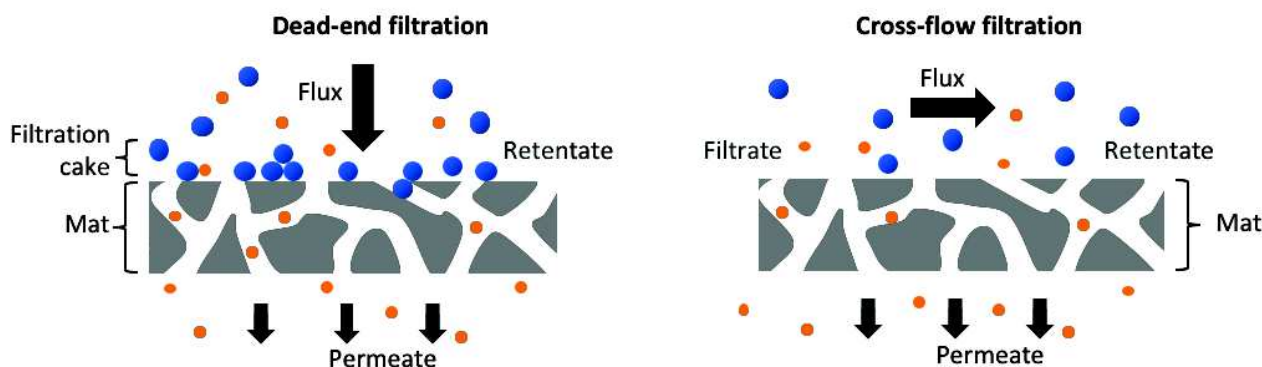


**Figure 1.19.** Dead-end and cross-flow filtration setups.

Generally, microfiltration membranes are non-fibrous membranes prepared either by sintering, stretching, track-etching, phase inversion or sol-gel process. The resulting porosity of these non-fibrous microfiltration membranes is low, around 40%, which induces either long filtration cycles or large filtration surfaces to overcome the lack of flow rate. As a consequence, nonwoven fibrous filters, traditionally developed for air filtration, are becoming a serious alternative to the previously described filter media. Nonwoven fibrous filters can be principally fabricated by dry-laid, wet-laid, spunbond [95], meltblown [96], electrospinning and force-spinning processes [93,97]. As a matter of fact, nonwoven fibrous filters combine low basic weight, high permeability, high porosity, interconnected open pore structure, small pore size and large specific area. Electrospun mats for liquid filtration are highly interesting due to the small pore size (pore size in the same range than the fiber diameter) and due to the high porosity of the mats, generally above 80%.

### 1.2.2 Parameters

Filtration properties (good efficiency, low pressure drop, high permeability, clean filtrate, low fouling, easy discharged filter cake, economic filtration time, high mechanical and chemical resistance and good lifetime) of a filter are determined by its structure parameters (material choice, fiber morphology, specific surface area, porosity, pore size distribution, thickness). Therefore, filtration properties and structure parameters determine whether a filter is appropriate to a specific application. Definitions as well as relations between structure parameters and filtration properties are detailed below.

#### STRUCTURAL PARAMETERS

##### *Material(s) choice*

Fibrous microfiltration mats can be either organic or mineral. The material has an impact on the mechanical, thermal, chemical and biological resistance, and can induce modifications in the filtration efficiency. Mats can be symmetric (same composition on the entire thickness) or asymmetric (stack of various layers).

### ***Fiber morphology and pore size***

Filters can be composed of fibers with different cross-sections and diameters giving birth to pores with different shapes and sizes. Modifying the cross-sections of fibers can enlarge the surface area of a filter and thus the filtration surface. Furthermore, reducing the fiber diameter leads to a reduction of the pore size and to an increasing of the filtration efficiency [93].

### ***Specific surface area***

The specific surface area is the ratio between the interface area and the total volume of the filter media. Therefore, it is expressed in  $\text{m}^2/\text{m}^3$  ( $\text{m}^{-1}$ ). The morphology of fibers, pores and the thickness of the mat have a large influence on this parameter. Specific surface area is a major parameter considering adsorption filtration mechanisms [98].

### ***Porosity***

The porosity is the ratio between the void and the total volume of the media. Considering the pores are interconnected, which is the case in electrospinning, and that their interconnectivity allows the liquid to go through the media, the porosity refers to the amount of space in the media that is available to trap particles.

### ***Thickness***

Thickness is a prominent parameter in filtration. A thick mat has more space to stop and collect particles. It has consequently a longer lifetime. In addition, increasing the thickness is generally linked with a decrease of the pore size [99] and thus to better efficiencies [100], up to a certain thickness where the pore size cannot be reduced anymore. However, a large thickness is also correlated to high pressure drops and low permeabilities [101]. Optimized filters are thus usually thin but resistant and efficient. To this aim, filtering membranes are consequently generally composed of several layers to combine the advantages of the different layers as high filtration efficiencies and high mechanical properties. In that regard, it is worth noting that electrospinning mats used as liquid filtering membranes quite always require an additional layer to ensure mechanical support. For example, Li et al. prepared filtering membranes by combining solution electrospinning and melt electrospinning methods. The layer produced by melt electrospinning is the support layer while the layer fabricated by solution electrospinning ensures high efficiencies [101]. Spunbond-Meltblown-Spunbond (SMS) structures are also quite popular industrially. Mats produced by spunbond are composed of thicker fibers (usual range of fiber diameters: 10 to 50  $\mu\text{m}$  [95]) inducing bigger pores than the ones fabricated by meltblown (usual range of fiber diameters: 1 to 5  $\mu\text{m}$  [96]). So, the first spunbond-meltblown layers are placed in order to create a gradient density of fibers, so that the coarsest particles are removed by the first spunbond filtering layer while the finest particles are filtrated by the meltblown layer. This kind of structure assures a depth filtration of particles and postpones the formation of a cake layer. The last spunbond layer guarantees mechanical strength.

## **FILTRATION PROPERTIES**

### ***Filtration efficiency and retention threshold***

The filtration efficiency is the capacity of a filter to stop the concerned particles. It is often calculated with the separation factor (SF):



$$SF (\%) = \frac{C_{feed} - C_{permeate}}{C_{feed}} * 100 \quad \text{Equation 1.2}$$

With:  $C_{feed}$  : Concentration of particles in the feed solution (%)

$C_{permeate}$  : Concentration of particles in the permeate (%)

The retention threshold is generally defined by the size of the smallest particles retained up to 90% by the filter media.

### ***Permeability***

The permeability of a filter media is its ability to allow a pure liquid to go through it more or less easily, regarding the effective surface of the media and the differential pressure. The permeability can also be defined as the resistance of the filter media to a liquid. A high permeability means that the liquid is able to go through the media easily. With the same retention threshold, the highest the permeability is, the better the filter is. The permeability of a filter media is calculated based on Darcy's law:

$$Lp = \frac{J}{\Delta P} \quad \text{Equation 1.3}$$

With:  $Lp$  : permeability ( $L \cdot h^{-1} \cdot m^2 \cdot bar^{-1}$ )

$J$ : volumetric flow rate ( $m \cdot s^{-1}$ )

$\Delta P$ : pressure drop (Pa)

The volumetric flow rate can be expressed as the ratio of the pure solvent flow rate by the filtration surface.

$$J = \frac{Q}{S} \quad \text{Equation 1.4}$$

With:  $Q$ : pure solvent flow ( $m^3 \cdot s^{-1}$ )

$S$ : effective surface of the filter ( $m^2$ )

### ***Fouling and lifetime***

Each filter, regarding its structure, has its own fouling behavior toward the filtration of particles regarding its shape, composition and size [102]. Fabricating long lasting filters is quite challenging as one wants to use filters with high efficiencies and low pressure drop which are slowly fouled. It is a compromise between high efficiency, low pressure drop and cost-effective filtration process and, consequently, an interplay between small fibers, high porosity and high thickness.

### ***Mechanical resistance***

Filters should resist the imposed flux (even when the filter is deep-fouled or has formed a cake layer). The fabrication of filters with high mechanical resistance is very attractive as high flux can be used during the filtration process leading to high productivity.

### *Chemical resistance*

Filters should be chemically resistant to the liquid to be filtered. The choice of the material regarded filtration trials must, in consequence, be adapted.

## **1.3 Electrospun membranes for liquid filtration**

Electrospun filters have gained more and more interests due to increasing demands for high efficiency filters with low cut-off thresholds and low pressure drop, which can be reached thanks to the low fiber diameter, the excellent pore connectivity and the high porosity. For instance, NANOWEB® filter media, produced by Hollingsworth and Vose for liquid filtration, reach a micron rating as low as 0.5 – 0.8 for a thickness of 0.38 mm, a mean pore size of 0.55  $\mu\text{m}$  and a maximal pore size of 2.5  $\mu\text{m}$  (grade CTR8015S1). The electrospinning process is, thus, the most promising process nowadays to answer such demands. Today's research focuses, above all, on developing high efficient and long-lasting filters which have overall good mechanical properties and high hydrophilicity in order to withstand high flux. Different strategies aiming at improving the properties of electrospun membranes used for liquid microfiltration are summed up in this part.

### *Enhancement of the filtration efficiency*

Improving the filtration efficiency can be achieved by various strategies. First reduction of the pore size is obtained by decreasing the average fiber diameter, by orienting fibers, by adding particles into the fibrous web or by applying a post-treatment such as a thermal treatment to the electrospun mesh. The relation between the pore size and the fiber diameter was put forward by Wang et al. [99]. Measures by capillary flow porometry were made on electrospun membranes with the same thickness ( $100 \pm 10 \mu\text{m}$ ) but with different average fiber diameters. Decreasing the average fiber diameter, from 450 nm to 100 nm, leads to a reduction of the maximal pore size from  $4.0 \pm 0.5 \mu\text{m}$  to  $0.62 \pm 0.05 \mu\text{m}$  and of the mean flow pore size from  $1.8 \pm 0.2 \mu\text{m}$  to  $0.22 \pm 0.01 \mu\text{m}$ . The reduction of the average fiber diameter not only decreases the mean flow pore size, but also the maximal pore size and narrows the pore size distribution. Moreover, they showed that an increase of the thickness of the electrospun layer also shifts the pore size distribution to lower values. However, a thicker membrane also increases the fluid driving pressure, which is not favorable for many applications. The thinnest membrane with lower fiber diameters as possible will thus be preferred. This explains why electrospun filters have higher efficiency than meltblown and spunbond filters. The main advantage of reducing the mean fiber diameter in order to decrease the pore size is that the porosity remains unchanged. Another strategy to reduce the pore size would be to orient the electrospun fibers. Indeed, it was shown by Li et al. [103] for PP fibers of a few microns, electrospun from the melt, that the mean pore size of oriented fibers was 18.96  $\mu\text{m}$  whereas the mean pore size of random fibers was 27.29  $\mu\text{m}$ . In their article, they stacked several layers of oriented fibers with different angles to increase the rejection ratio of 0.5 $\mu\text{m}$  particles from 70% for random fibers to 98.5% for four layers of oriented fibers. However, this strategy also reduces the pure water flux probably because the overall porosity is reduced. A thermal treatment also decreases the pore size. It can be performed either by hot pressing [104,105] or by thermal annealing [106,107]. During a thermal treatment, fibers fuse together and thicken. This leads to the shrinkage of the membrane, to the reduction of its thickness and to the reduction of its pores. The pore size is reduced even more during a hot pressing as the membrane is, in addition, pressed. Reducing the pore size thanks to a thermal treatment presents the advantage that it also reinforces the mechanical properties of electrospun mats. Yet its major drawback is that it decreases also the porosity and the



permeability. For instance, after a hot pressing, Zhou et al. measured a decrease of the porosity from 90% to 65% of cellulose acetate fibers [104]. The addition of particles inside electrospun mats is another way to decrease the pore size and to thereby increase the filtration efficiency. Burger et al. particularly underlined the link between addition of nanoparticles, pore size and filtration [107]. They discovered that by loading fibers with cellulose nanowhiskers which are then heated to cross-link the nanowhiskers to the fibers, they could adjust the mean pore size and the pore distribution. Unloaded membranes had a mean pore size of 0.38  $\mu\text{m}$  and the retention towards 0.2  $\mu\text{m}$  particles was of 13.8%. On the contrary particle loaded membranes gained a mean pore size of 0.22  $\mu\text{m}$  and exhibited retention towards 0.2  $\mu\text{m}$  particles of 97.7%. In this case, the addition of nanowhiskers also had the advantage of increasing the mechanical properties of the mat and providing for negatively charged surfaces that increase the adsorption capacity toward positively charged species. Finally, many approaches are conceivable to decrease the pore size of electrospun filters in order to improve the filtration efficiency. All those strategies have advantages and drawbacks which impact on other filtration properties as the mechanical strength or the permeability. One must bear in mind that all filtration properties are interdependent before tailoring the filtration efficiency.

### *Enhancement of mechanical properties*

Improving the mechanical resistance of a mat is another crucial issue for liquid filtration as it allows to perform experiments with high flux and to get high yields. The mechanical resistance of a mat can be improved on two levels. On the one hand, the intrinsic mechanical strength of electrospun mats can be first enhanced. On the other hand, support layers can be used when the intrinsic strength of electrospun mats is not high enough. When support layers are used, it becomes noteworthy to pay attention to the adhesion of both of the layers together. Improving the intrinsic mechanical strength of the electrospun membrane can be done by performing a post-treatment such as thermal treatment [108], exposure to solvent vapor [109], or polymerization at the surface of the fibers and cross-linking [110]. These three post-treatments result in the formation of junction points between the fibers, by fusing them at intersections. For example, Homaieghar et al. prepared polyethersulfone (PES) membranes which were heated and then slowly cooled down [108]. The heat-treated mats were more rigid, with a higher tensile modulus and lower elongation at break due to fusion points, while the fibers of the untreated mat were able to slide freely over one another, resulting in lower tensile modulus but longer elongation at break. [108]. When the strength of electrospun mats required to withstand the flux is not high enough despite the above strategies, support layers are solutions of choice provided a good adhesion between the layers. Tang et al. particularly work on the adhesion between fibers and between layers in electrospinning [111]. They directly electrospun polyethersulfone (PES) onto a poly(ethylene terephthalate) (PET) nonwoven and were concerned about the poor adhesion between the electrospun PES layer and the PET nonwoven layer and between the electrospun nanofibers themselves, which could result in low mechanical resistance of the filter and delamination. They were able to produce wet fibers that bond the fibers together and to the support, by adding NMP, a solvent with low vapor pressure to DMF, thus decreasing the evaporation rate and by playing with the solution flow rate. A “primer layer”, made of wet electrospun fibers was thus electrospun on the PET microfibrillar support layer before electrospinning a dry layer of more uniform selective nanofibers to enhance the adhesion between the layers.

It should be pointed out that certain strategies performed to improve the mechanical strength, such as hot pressing or coating, have side effects: on the one hand, it improves the mechanical resistance, enabling the use of a high flux, but on the other hand it reduces the pore size. Therefore, the flux must be adapted (or lowered) to maintain mechanical integrity. This is the case of the polyacrylonitrile (PAN) fibers coated or not with

polydopamine (PDA) fabricated by Huang et al. [112]. During flux performance tests, they noticed that the coated fibers exhibit a slightly lower water flux than the uncoated ones. They incriminated the coating to reduce the pore size and the pore volume and to consequently reduce the permeability of the mat. They also noted an interesting relation between the pure water permeability and the applied pressure as the pure water permeability of PAN mats (coated or not) decrease with higher applied pressures. They pointed out the fact that electrospun mats are prone to compression during flux performance tests and explained that the compression of the mats blocks the pore connectivity, reduces the pore volume and diminishes the pore size. Choong et al. [113] also noticed the compression undergone by electrospun PSU mats related to a loss of porosity during flux performance tests as the permeability drops by 60% between 5 kPa and 140 kPa.

### ***Enhancement of the permeability***

A high permeability enables to get a high flux with a low applied pressure. Therefore, it is crucial for high filtration yields. Applying a low pressure is also interesting for cost saving reasons and to limit the compression of electrospun mats. The permeability of a mat can be first improved by increasing the porosity. In the case of electrospinning, average porosity of the mats is around 80% [114–116]. Hussain et al. measured porosity of  $85 \pm 2$  % independently of the fiber diameter. Similar values were obtained by Yoon et al., there produced an electrospun with a porosity of  $\approx 73$  %. As porosity has an important impact on flow rates, electrospun filters allow greater flow rates, for the same pore size, than non-fibrous filtration membranes (porosity of around 40%). Enhancing the hydrophilicity of a filter allows reducing its resistance to the passing through of an aqueous solution and it enables to increase its permeability. The hydrophilicity can be tailored by a strategy called blending consisting in introducing into the electrospinning solutions, before electrospinning, a small amount of a hydrophilic polymer [117–119]. Kaur et al. highlighted the relation between hydrophilicity and permeability by blending into their electrospinning solution poly(vinylidene fluoride) (PVDF) with surface modifying macromolecules based on hydrophilic polyurethane (PU) containing, between others, poly(ethylene glycol) (PEG) [117]. They measured that the water flux of blend electrospun membranes could be 20% higher than the water flux of pure PVDF membranes for the same applied pressure. Asmatulu et al. also improved the hydrophilicity and the permeability of polyvinyl chloride (PVC) mats by adding polyvinylpyrrolidone (PVP) into their electrospinning solutions [118]. They found out that the filtration rate was much higher with the introduction of PVP into PVC fibers. They furthermore linked permeability with contact angles. As a matter of fact, they measured the water contact angles of PVC fibers blended with different amount of PVP. The contact angle decreases when the amount of PVP into the fibers is increased (from  $135.7^\circ$  for pure PVC fibers to  $16.12^\circ$  for PVC fibers blended with 5 wt% PVP). They concluded that the permeability is at its highest when the contact angle is low.

### ***Enhancement of the lifetime***

Besides, expanding the lifetime of a filter is a major challenge in order to save costs. The lifetime of a filter is determined by its fouling process [120–123] which is itself determined by the structural properties of the filter. Indeed, each membrane, regarding its structure, has its own behavior toward the filtration of a particle regarding its shape, composition and size. For instance, Gopal et al. [122] illustrated the different fouling behavior of a same membrane during the filtration of polystyrene particles with different size (1, 5 and 10  $\mu\text{m}$ ). The membranes had an average fiber diameter of  $380 \pm 106$  nm, a thickness of 300  $\mu\text{m}$  and a pore size ranging from 10.6  $\mu\text{m}$  to 4  $\mu\text{m}$ . A stirring system that does not disturb the flux lifted, during the experiment,

the PS particles from the surface of the membrane. For the 10  $\mu\text{m}$  PS particles the separation factor reached 96%, no permanent fouling was mentioned, and the permeation flux was unchanged. In the case of the 5  $\mu\text{m}$  PS particles, the separation factor was of 91% because of the smaller size of the PS particles, some particles could be seen on the surface of the membrane, and the flux was rather unaffected. The filtration of the 1  $\mu\text{m}$  PS particles took place differently as the flux reduction was immediate, the membrane was fouled and consequently the separation factor was at its highest (98%). Gopal et al. [122] explained that the 1  $\mu\text{m}$  PS particles are closely packed together on the surface of the membrane due to their size because small particles, between 0.1  $\mu\text{m}$  and 1  $\mu\text{m}$ , are more influenced by Brownian diffusion than by the imposed and the stirring flux. The cake layer, composed of the closely packed PS particles, is thought to be accounting for the high separation factor. The structural properties of a filter must in the end be correctly chosen in accordance with the application.

### *Addition of specific filtration properties*

Finally, for some applications, it can be interesting to functionalize fibers, namely enhancing the affinity of the mats with some particles or providing mats with new properties. This can be realized by adding particles in the electrospinning solution or after electrospinning [112]. As an example, silver nanoparticles were added to polyamide nanofibers for their antimicrobial activity [124,125]. Functionalization of the electrospun filters has also been performed by addition of chitosan in the electrospinning solution because of its ability to bind heavy metals ions and its antibacterial properties [98,119,126]. Finally, chemical post-treatment has also been used by Mahanta et al. [127] who chemically modified the hydroxyl groups of PVA nanofibers with amine and thiol groups in order to increase gold or silver nanoparticles adsorption during filtration.

In conclusion, electrospun filters have extremely interesting filtration capacities. Many ways are possible to improve the filtration properties which are interdependent. According to the application, the right properties must thus be carefully chosen, and the filter structure tailored in consequence. In addition, despite the superior properties of electrospun filters, the electrospinning process encounters also lots of industrial limits [128], which explains the few electrospun membranes on the market for liquid filtration (Table 1.3). Electrospun membranes have rather low mechanical strength and require a support layer. In addition, the productivity is also extremely low, a high voltage is needed during the process and a special treatment of the solvents' vapors must be set up when toxic solvents are used in the composition of the electrospinning solutions [129]. However, all these drawbacks put aside, electrospun filters could find applications in many fields such as filtration of beverage [100], in biorefinery [130], for metallic ions adsorption [98], as affinity membranes [131], for water filtration [132–136], for antibacterial applications [110,119,137], as prefilter [120,121] and for oil/water filtration [138–140].

Company	Product	Raw material	Thickness (µm)	Mean pore size (µm)	Max pore size (µm)	Applications
Finetex Technology Global Ltd.	Technoweb™ Filtrepro	PU, PVDF, Nylon, PES (and others)	4-12	0.20-0.45	0.27-0.73	Food & Beverage, Wastewater treatment, Micro-electronics, Biopharmaceutica
Hollingsworth and Vose Company	NANOWEB®	PP	66- 267	0.55-10.2	2.5-30.1	Water filtration

**Table 1.3.** Commercial electrospun membranes designed for liquid microfiltration.

## Abbreviations

CA: cellulose acetate, DCM: dichloromethane, DMAc: N,N-dimethylacetamide, DMF: N,N-dimethylformamide, HA: hyaluronic acid, Mc: methylene chloride, NaCl: sodium chloride, NMP: 1-methyl-2-pyrrolidinone, PA: polyamide, PAA: poly(acrylic acid), PAN: poly(acrylonitrile), PCL : polycaprolactone, PCU: poly(carbonate urethane), PDLLA: poly(L-lactide-co-DL-Lactide), PEG : poly(ethylene glycol), PEI: polyetherimide, PEO: poly(ethylene oxide), PLLA: poly(L-lactide), PS: polystyrene, PSU: polysulfone, PVA: polyvinyl alcohol, PVP: polyvinylpyrrolidone, SAN: styrene/acrylonitrile copolymer, THF: tetrahydrofuran.

## References

- [1] A. Greiner, J.H. Wendorff, Functional Self-Assembled Nanofibers by Electrospinning, in: T. Shimizu (Ed.), *Self-Assem. Nanomater. I*, Springer Berlin Heidelberg, 2008: pp. 107–171.
- [2] T. Subbiah, G.S. Bhat, R.W. Tock, S. Parameswaran, S.S. Ramkumar, Electrospinning of nanofibers, *J. Appl. Polym. Sci.* 96 (2005) 557–569. doi:10.1002/app.21481.
- [3] N. Bhardwaj, S.C. Kundu, Electrospinning: A fascinating fiber fabrication technique, *Biotechnol. Adv.* 28 (2010) 325–347. doi:10.1016/j.biotechadv.2010.01.004.
- [4] D. Li, Y. Xia, Electrospinning of Nanofibers: Reinventing the Wheel?, *Adv. Mater.* 16 (2004) 1151–1170. doi:10.1002/adma.200400719.
- [5] R. Sahay, V. Thavasi, S. Ramakrishna, Design Modifications in Electrospinning Setup for Advanced Applications, *J. Nanomater.* (2011).
- [6] M. Yu, R.-H. Dong, X. Yan, G.-F. Yu, M.-H. You, X. Ning, Y.-Z. Long, Recent Advances in Needleless Electrospinning of Ultrathin Fibers: From Academia to Industrial Production, *Macromol. Mater. Eng.* (2017). doi:10.1002/mame.201700002.
- [7] A. Varesano, R.A. Carletto, G. Mazzuchetti, Experimental investigations on the multi-jet electrospinning process, *J. Mater. Process. Technol.* 209 (2009) 5178–5185. doi:10.1016/j.jmatprotec.2009.03.003.
- [8] G. Kim, Y.-S. Cho, W.D. Kim, Stability analysis for multi-jets electrospinning process modified with a cylindrical electrode, *Eur. Polym. J.* 42 (2006) 2031–2038. doi:10.1016/j.eurpolymj.2006.01.026.
- [9] Z.M. Huang, Y.Z. Zhang, M. Kotaki, S. Ramakrishna, A review on polymer nanofibers by electrospinning and their applications in nanocomposites, *Compos. Sci. Technol.* 63 (2003) 2223–2253. doi:10.1016/S0266-3538(03)00178-7.
- [10] C.-L. Pai, M.C. Boyce, G.C. Rutledge, Morphology of Porous and Wrinkled Fibers of Polystyrene Electrospun from Dimethylformamide, *Macromolecules.* 42 (2009) 2102–2114. doi:10.1021/ma802529h.
- [11] G.-T. Kim, J.-S. Lee, J.-H. Shin, Y.-C. Ahn, Y.-J. Hwang, H.-S. Shin, J.-K. Lee, C.-M. Sung, Investigation of pore formation for polystyrene electrospun fiber: Effect of relative humidity, *Korean J. Chem. Eng.* 22 (2005) 783–788. doi:10.1007/BF02705799.
- [12] H. Fashandi, M. Karimi, Pore formation in polystyrene fiber by superimposing temperature and relative humidity of electrospinning atmosphere, *Polymer.* 53 (2012) 5832–5849. doi:10.1016/j.polymer.2012.10.003.
- [13] B. Ding, C. Li, Y. Miyauchi, O. Kuwaki, S. Shiratori, Formation of novel 2D polymer nanowebs via electrospinning, *Nanotechnology.* 17 (2006) 3685. doi:10.1088/0957-4484/17/15/011.
- [14] S.L. Shenoy, W.D. Bates, H.L. Frisch, G.E. Wnek, Role of chain entanglements on fiber formation during electrospinning of polymer solutions: Good solvent, non-specific polymer-polymer interaction limit, *Polymer.* 46 (2005) 3372–3384. doi:10.1016/j.polymer.2005.03.011.

- [15] M.G. McKee, G.L. Wilkes, R.H. Colby, T.E. Long, Correlations of Solution Rheology with Electrospun Fiber Formation of Linear and Branched Polyesters, *Macromolecules*. 37 (2004) 1760–1767. doi:10.1021/ma035689h.
- [16] K. Riazi, J. Kübel, M. Abbasi, K. Bachtin, S. Indris, H. Ehrenberg, R. Kádár, M. Wilhelm, Polystyrene comb architectures as model systems for the optimized solution electrospinning of branched polymers, *Polymer*. 104 (2016) 240–250. doi:10.1016/j.polymer.2016.05.032.
- [17] M.G. McKee, M.T. Hunley, J.M. Layman, T.E. Long, Solution Rheological Behavior and Electrospinning of Cationic Polyelectrolytes, *Macromolecules*. 39 (2006) 575–583. doi:10.1021/ma051786u.
- [18] N. Lavielle, A.-M. Popa, M. de Geus, A. Hébraud, G. Schlatter, L. Thöny-Meyer, R.M. Rossi, Controlled formation of poly( $\epsilon$ -caprolactone) ultrathin electrospun nanofibers in a hydrolytic degradation-assisted process, *Eur. Polym. J.* 49 (2013) 1331–1336. doi:10.1016/j.eurpolymj.2013.02.038.
- [19] Z.M. Huang, Y.Z. Zhang, M. Kotaki, S. Ramakrishna, A review on polymer nanofibers by electrospinning and their applications in nanocomposites, *Compos. Sci. Technol.* 63 (2003) 2223–2253. doi:10.1016/S0266-3538(03)00178-7.
- [20] J. Doshi, D.H. Reneker, Electrospinning process and applications of electrospun fibers, *J. Electrostat.* 35 (1995) 151–160. doi:10.1016/0304-3886(95)00041-8.
- [21] S. Agarwal, J.H. Wendorff, A. Greiner, Use of electrospinning technique for biomedical applications, *Polymer*. 49 (2008) 5603–5621. doi:10.1016/j.polymer.2008.09.014.
- [22] M. Cheng, Z. Qin, S. Hu, H. Yu, M. Zhu, Use of electrospinning to directly fabricate three-dimensional nanofiber stacks of cellulose acetate under high relative humidity condition, *Cellulose*. 24 (2017) 219–229. doi:10.1007/s10570-016-1099-3.
- [23] W. Yang, F. Yang, Y. Wang, S.K. Both, J.A. Jansen, In vivo bone generation via the endochondral pathway on three-dimensional electrospun fibers, *Acta Biomater.* 9 (2013) 4505–4512. doi:10.1016/j.actbio.2012.10.003.
- [24] S. Lee, S. Cho, M. Kim, G. Jin, U. Jeong, J.-H. Jang, Highly Moldable Electrospun Clay-Like Fluffy Nanofibers for Three-Dimensional Scaffolds, *ACS Appl. Mater. Interfaces*. 6 (2014) 1082–1091. doi:10.1021/am404627r.
- [25] X. Li, Y. Zhang, H. Li, H. Chen, Y. Ding, W. Yang, Effect of oriented fiber membrane fabricated via needleless melt electrospinning on water filtration efficiency, *Desalination*. 344 (2014) 266–273. doi:10.1016/j.desal.2014.04.003.
- [26] B.B. Rothrauff, B.B. Lauro, G. Yang, R.E. Debski, V. Musahl, R.S. Tuan, Braided and Stacked Electrospun Nanofibrous Scaffolds for Tendon and Ligament Tissue Engineering, *Tissue Eng. Part A*. 23 (2017) 378–389. doi:10.1089/ten.tea.2016.0319.
- [27] V. Milleret, T. Hefti, H. Hall, V. Vogel, D. Eberli, Influence of the fiber diameter and surface roughness of electrospun vascular grafts on blood activation, *Acta Biomater.* 8 (2012) 4349–4356. doi:10.1016/j.actbio.2012.07.032.
- [28] R. Wang, Y. Liu, B. Li, B.S. Hsiao, B. Chu, Electrospun nanofibrous membranes for high flux microfiltration, *J. Membr. Sci.* 392 (2012) 167–174. doi:10.1016/j.memsci.2011.12.019.
- [29] N. Tomczak, N.F. van Hulst, G.J. Vancso, Beaded Electrospun Fibers for Photonic Applications, *Macromolecules*. 38 (2005) 7863–7866. doi:10.1021/ma051049y.
- [30] S. Somvipart, S. Kanokpanont, R. Rangkupan, J. Ratanavarnaporn, S. Damrongsakkul, Development of electrospun beaded fibers from Thai silk fibroin and gelatin for controlled release application, *Int. J. Biol. Macromol.* 55 (2013) 176–184. doi:10.1016/j.ijbiomac.2013.01.006.
- [31] T. Li, X. Ding, L. Tian, J. Hu, X. Yang, S. Ramakrishna, The control of beads diameter of bead-on-string electrospun nanofibers and the corresponding release behaviors of embedded drugs, *Mater. Sci. Eng. C*. 74 (2017) 471–477. doi:10.1016/j.msec.2016.12.050.



- [32] N. Thakur, A.S. Ranganath, K. Agarwal, A. Baji, Electrospun Bead-On-String Hierarchical Fibers for Fog Harvesting Application, *Macromol. Mater. Eng.* 302 (2017) 1700124. doi:10.1002/mame.201700124.
- [33] N.H.A. Ngadiman, N.M. Yusof, A. Idris, E. Misran, D. Kurniawan, Development of highly porous biodegradable  $\gamma$ -Fe<sub>2</sub>O<sub>3</sub>/polyvinyl alcohol nanofiber mats using electrospinning process for biomedical application, *Mater. Sci. Eng. C.* 70 (2017) 520–534. doi:10.1016/j.msec.2016.09.002.
- [34] J. Lin, B. Ding, J. Yang, J. Yu, G. Sun, Subtle regulation of the micro- and nanostructures of electrospun polystyrene fibers and their application in oil absorption, *Nanoscale.* 4 (2012) 176–182. doi:10.1039/C1NR10895F.
- [35] H.-S. Bae, A. Haider, K.M.K. Selim, D.-Y. Kang, E.-J. Kim, I.-K. Kang, Fabrication of highly porous PMMA electrospun fibers and their application in the removal of phenol and iodine, *J. Polym. Res.* 20 (2013) 158. doi:10.1007/s10965-013-0158-9.
- [36] W.G. Jang, K.S. Jeon, H.S. Byun, The preparation of porous polyamide-imide nanofiber membrane by using electrospinning for MF application, *Desalination Water Treat.* 51 (2013) 5283–5288. doi:10.1080/19443994.2013.768755.
- [37] B. Ding, X. Wang, J. Yu, M. Wang, Polyamide 6 composite nano-fiber/net functionalized by polyethyleneimine on quartz crystal microbalance for highly sensitive formaldehyde sensors, *J. Mater. Chem.* 21 (2011) 12784–12792. doi:10.1039/C1JM11847A.
- [38] A.L. Yarin, S. Koombhongse, D.H. Reneker, Bending instability in electrospinning of nanofibers, *J. Appl. Phys.* 89 (2001) 3018–3026. doi:10.1063/1.1333035.
- [39] J. Pelipenko, J. Kristl, B. Janković, S. Baumgartner, P. Kocbek, The impact of relative humidity during electrospinning on the morphology and mechanical properties of nanofibers, *Int. J. Pharm.* 456 (2013) 125–134. doi:10.1016/j.ijpharm.2013.07.078.
- [40] S. Tripatanasuwan, Z. Zhong, D.H. Reneker, Effect of evaporation and solidification of the charged jet in electrospinning of poly(ethylene oxide) aqueous solution, *Polymer.* 48 (2007) 5742–5746. doi:10.1016/j.polymer.2007.07.045.
- [41] Y. Cai, M. Gevelber, The effect of relative humidity and evaporation rate on electrospinning: fiber diameter and measurement for control implications, *J. Mater. Sci.* 48 (2013) 7812–7826. doi:10.1007/s10853-013-7544-x.
- [42] S. De Vrieze, T. Van Camp, A. Nelvig, B. Hagström, P. Westbroek, K. De Clerck, The effect of temperature and humidity on electrospinning, *J. Mater. Sci.* 44 (2008) 1357–1362. doi:10.1007/s10853-008-3010-6.
- [43] G. Collins, J. Federici, Y. Imura, L.H. Catalani, Charge generation, charge transport, and residual charge in the electrospinning of polymers: A review of issues and complications, *J. Appl. Phys.* 111 (2012) 44701. doi:10.1063/1.3682464.
- [44] V.A. Mohnen, Formation, Nature, and Mobility of Ions of Atmospheric Importance, in: *Electr. Process. Atmospheres*, Steinkopff, 1976: pp. 1–17.
- [45] C.C. Wu, G.W.M. Lee, S. Yang, K.-P. Yu, C.L. Lou, Influence of air humidity and the distance from the source on negative air ion concentration in indoor air, *Sci. Total Environ.* 370 (2006) 245–253. doi:10.1016/j.scitotenv.2006.07.020.
- [46] B. Zhang, J. He, Y. Ji, Dependence of the average mobility of ions in air with pressure and humidity, *IEEE Trans. Dielectr. Electr. Insul.* 24 (2017) 923–929. doi:10.1109/TDEI.2017.006542.
- [47] I. Dogu, Fundamentals of Electrostatic Spinning Part IV:-: Ionization of Atmospheric Air under Action of an Electric Field, *Text. Res. J.* 54 (1984) 111–119. doi:10.1177/004051758405400207.
- [48] L. Huang, N.-N. Bui, S.S. Manickam, J.R. McCutcheon, Controlling electrospun nanofiber morphology and mechanical properties using humidity, *J. Polym. Sci. Part B Polym. Phys.* 49 (2011) 1734–1744. doi:10.1002/polb.22371.

- [49] O. Hardick, B. Stevens, D.G. Bracewell, Nanofibre fabrication in a temperature and humidity controlled environment for improved fibre consistency, *J. Mater. Sci.* 46 (2011) 3890–3898. doi:10.1007/s10853-011-5310-5.
- [50] R.M. Nezarati, M.B. Eifert, E. Cosgriff-Hernandez, Effects of Humidity and Solution Viscosity on Electrospun Fiber Morphology, *Tissue Eng. Part C Methods.* 19 (2013) 810–819. doi:10.1089/ten.tec.2012.0671.
- [51] C.L. Casper, J.S. Stephens, N.G. Tassi, D.B. Chase, J.F. Rabolt, Controlling Surface Morphology of Electrospun Polystyrene Fibers: Effect of Humidity and Molecular Weight in the Electrospinning Process, *Macromolecules.* 37 (2004) 573–578. doi:10.1021/ma0351975.
- [52] S. Megelski, J.S. Stephens, D.B. Chase, J.F. Rabolt, Micro- and Nanostructured Surface Morphology on Electrospun Polymer Fibers, *Macromolecules.* 35 (2002) 8456–8466. doi:10.1021/ma020444a.
- [53] G. Yazgan, A.M. Popa, R.M. Rossi, K. Maniura-Weber, J. Puigmartí-Luis, D. Crespy, G. Fortunato, Tunable release of hydrophilic compounds from hydrophobic nanostructured fibers prepared by emulsion electrospinning, *Polymer.* 66 (2015) 268–276. doi:10.1016/j.polymer.2015.04.045.
- [54] H. Fashandi, M. Karimi, Characterization of porosity of polystyrene fibers electrospun at humid atmosphere, *Thermochim. Acta.* 547 (2012) 38–46. doi:10.1016/j.tca.2012.08.003.
- [55] H. Fashandi, M. Karimi, Comparative Studies on the Solvent Quality and Atmosphere Humidity for Electrospinning of Nanoporous Polyetherimide Fibers, *Ind. Eng. Chem. Res.* 53 (2014) 235–245. doi:10.1021/ie4028846.
- [56] L. Natarajan, J. New, A. Dasari, S. Yu, M.A. Manan, Surface morphology of electrospun PLA fibers: mechanisms of pore formation, *RSC Adv.* 4 (2014) 44082–44088. doi:10.1039/C4RA06215A.
- [57] P. Lu, Y. Xia, Maneuvering the Internal Porosity and Surface Morphology of Electrospun Polystyrene Yarns by Controlling the Solvent and Relative Humidity, *Langmuir.* 29 (2013) 7070–7078. doi:10.1021/la400747y.
- [58] R.A. Basheer, A.R. Hopkins, P.G. Rasmussen, Dependence of Transition Temperatures and Enthalpies of Fusion and Crystallization on Composition in Polyaniline/Nylon Blends, *Macromolecules.* 32 (1999) 4706–4712. doi:10.1021/ma981935r.
- [59] G.J. Kettle, Variation of the glass transition temperature of nylon-6 with changing water content, *Polymer.* 18 (1977) 742–743. doi:10.1016/0032-3861(77)90244-0.
- [60] S. De Vrieze, B. De Schoenmaker, Ö. Ceylan, J. Depuydt, L. Van Landuyt, H. Rahier, G. Van Assche, K. De Clerck, Morphologic study of steady state electrospun polyamide 6 nanofibres, *J. Appl. Polym. Sci.* 119 (2011) 2984–2990. doi:10.1002/app.33036.
- [61] E. Marsano, L. Francis, F. Giunco, Polyamide 6 nanofibrous nonwovens via electrospinning, *J. Appl. Polym. Sci.* (2010) 1754–1765. doi:10.1002/app.32118.
- [62] B.D. Schoenmaker, L.V. der Schueren, R. Zuggle, A. Goethals, P. Westbroek, P. Kiekens, T. Nyokong, K.D. Clerck, Effect of the relative humidity on the fibre morphology of polyamide 4.6 and polyamide 6.9 nanofibres, *J. Mater. Sci.* 48 (2012) 1746–1754. doi:10.1007/s10853-012-6934-9.
- [63] H.I. İçoğlu, R.T. Ogulata, Effect of Ambient Parameters on Morphology of Electrospun Polyetherimide (PEI) Fibers, *Tekst. Ve Konfeksiyon.* 23 (2013) 313–318.
- [64] V.E. Kalayci, P.K. Patra, Y.K. Kim, S.C. Ugbohue, S.B. Warner, Charge consequences in electrospun polyacrylonitrile (PAN) nanofibers, *Polymer.* 46 (2005) 7191–7200. doi:10.1016/j.polymer.2005.06.041.
- [65] C. Thammawong, S. Buchatip, A. Petchsuk, P. Tangboriboonrat, N. Chanunpanich, M. Opaprakasit, P. Sreearunothai, P. Opaprakasit, Electrospinning of poly(l-lactide-co-dl-lactide) copolymers: Effect of chemical structures and spinning conditions, *Polym. Eng. Sci.* 54 (2014) 472–480. doi:10.1002/pen.23576.



- [66] A. Bandegi, M.R. Moghbeli, Effect of solvent quality and humidity on the porous formation and oil absorbency of SAN electrospun nanofibers, *J. Appl. Polym. Sci.* 135 (2018) 45586. doi:10.1002/app.45586.
- [67] C.-L. Pai, M.C. Boyce, G.C. Rutledge, Morphology of Porous and Wrinkled Fibers of Polystyrene Electrospun from Dimethylformamide, *Macromolecules.* 42 (2009) 2102–2114. doi:10.1021/ma802529h.
- [68] S. Yao, X. Wang, X. Liu, R. Wang, C. Deng, F. Cui, Effects of Ambient Relative Humidity and Solvent Properties on the Electrospinning of Pure Hyaluronic Acid Nanofibers, *J. Nanosci. Nanotechnol.* 13 (2013) 4752–8. doi:10.1166/jnn.2013.7197.
- [69] M. Putti, M. Simonet, R. Solberg, G.W.M. Peters, Electrospinning poly( $\epsilon$ -caprolactone) under controlled environmental conditions: Influence on fiber morphology and orientation, *Polymer.* 63 (2015) 189–195. doi:10.1016/j.polymer.2015.03.006.
- [70] J. Lin, F. Tian, Y. Shang, F. Wang, B. Ding, J. Yu, Facile control of intra-fiber porosity and inter-fiber voids in electrospun fibers for selective adsorption, *Nanoscale.* 4 (2012) 5316–5320. doi:10.1039/C2NR31515G.
- [71] L. Pauchard, C. Allain, Buckling instability induced by polymer solution drying, *EPL Europhys. Lett.* 62 (2003) 897. doi:10.1209/epl/i2003-00457-7.
- [72] M. Srinivasarao, D. Collings, A. Philips, S. Patel, Three-Dimensionally Ordered Array of Air Bubbles in a Polymer Film, *Science.* 292 (2001) 79–83. doi:10.1126/science.1057887.
- [73] G. Yazgan, R.I. Dmitriev, V. Tyagi, J. Jenkins, G.-M. Rotaru, M. Rottmar, R.M. Rossi, C. Toncelli, D.B. Papkovsky, K. Maniura-Weber, G. Fortunato, Steering surface topographies of electrospun fibers: understanding the mechanisms, *Sci. Rep.* 7 (2017) 158. doi:10.1038/s41598-017-00181-0.
- [74] J.-Y. Park, I.-H. Lee, Relative Humidity Effect on the Preparation of Porous Electrospun Polystyrene Fibers, *J. Nanosci. Nanotechnol.* 10 (2010) 3473–3477. doi:10.1166/jnn.2010.2349.
- [75] Y. Yang, Z. Jia, Q. Li, Z. Guan, Experimental investigation of the governing parameters in the electrospinning of polyethylene oxide solution, *IEEE Trans. Dielectr. Electr. Insul.* 13 (2006) 580–585. doi:10.1109/TDEI.2006.1657971.
- [76] T. Liang, M. Parhizkar, M. Edirisinghe, S. Mahalingam, Effect of humidity on the generation and control of the morphology of honeycomb-like polymeric structures by electrospinning, *Eur. Polym. J.* 61 (2014) 72–82. doi:10.1016/j.eurpolymj.2014.09.020.
- [77] M.M. Li, Y.Z. Long, Fabrication of Self-Assembled Three-Dimensional Fibrous Stackings by Electrospinning, *Mater. Sci. Forum.* 688 (2011) 95–101. doi:10.4028/www.scientific.net/MSF.688.95.
- [78] C.A. Bonino, K. Efimenko, S.I. Jeong, M.D. Krebs, E. Alsberg, S.A. Khan, Three-Dimensional Electrospun Alginate Nanofiber Mats via Tailored Charge Repulsions, *Small.* 8 (2012) 1928–1936. doi:10.1002/sml.201101791.
- [79] N. Lavielle, A. Hébraud, C. Mendoza-Palomares, A. Ferrand, N. Benkirane-Jessel, G. Schlatter, Structuring and Molding of Electrospun Nanofibers: Effect of Electrical and Topographical Local Properties of Micro-Patterned Collectors, *Macromol. Mater. Eng.* 297 (2012) 958–968. doi:10.1002/mame.201100327.
- [80] S. Nedjari, A. Hébraud, S. Eap, S. Siegwald, C. Mélar, N. Benkirane-Jessel, G. Schlatter, Electrostatic template-assisted deposition of microparticles on electrospun nanofibers: towards microstructured functional biochips for screening applications, *RSC Adv.* 5 (2015) 83600–83607. doi:10.1039/C5RA15931H.
- [81] S. Nedjari, G. Schlatter, A. Hébraud, Thick electrospun honeycomb scaffolds with controlled pore size, *Mater. Lett.* 142 (2015) 180–183. doi:10.1016/j.matlet.2014.11.118.
- [82] A. Zucchelli, D. Fabiani, C. Gualandi, M.L. Focarete, An innovative and versatile approach to design highly porous, patterned, nanofibrous polymeric materials, *J. Mater. Sci.* 44 (2009) 4969–4975.

- [83] D. Li, G. Ouyang, J.T. McCann, Y. Xia, Collecting Electrospun Nanofibers with Patterned Electrodes, *Nano Lett.* 5 (2005) 913–916. doi:10.1021/nl0504235.
- [84] X. Wang, B. Ding, G. Sun, M. Wang, J. Yu, Electro-spinning/netting: A strategy for the fabrication of three-dimensional polymer nano-fiber/nets, *Prog. Mater. Sci.* 58 (2013) 1173–1243. doi:10.1016/j.pmatsci.2013.05.001.
- [85] X. Wang, B. Ding, J. Yu, J. Yang, Large-scale fabrication of two-dimensional spider-web-like gelatin nano-nets via electro-netting, *Colloids Surf. B Biointerfaces.* 86 (2011) 345–352. doi:10.1016/j.colsurfb.2011.04.018.
- [86] S. Zhang, K. Chen, J. Yu, B. Ding, Model derivation and validation for 2D polymeric nanonets: Origin, evolution, and regulation, *Polymer.* 74 (2015) 182–192. doi:10.1016/j.polymer.2015.08.002.
- [87] E.S. Medeiros, L.H.C. Mattoso, R.D. Offeman, D.F. Wood, W.J. Orts, Effect of relative humidity on the morphology of electrospun polymer fibers, *Can. J. Chem.* 86 (2008) 590–599. doi:10.1139/v08-029.
- [88] W. Liu, C. Huang, X. Jin, Tailoring the grooved texture of electrospun polystyrene nanofibers by controlling the solvent system and relative humidity, *Nanoscale Res. Lett.* 9 (2014) 1–10. doi:10.1186/1556-276X-9-350.
- [89] J. Zheng, H. Zhang, Z. Zhao, C.C. Han, Construction of hierarchical structures by electrospinning or electro spraying, *Polymer.* 53 (2012) 546–554. doi:10.1016/j.polymer.2011.12.018.
- [90] E. Zampetti, A. Muzyczuk, A. Macagnano, S. Pantalei, S. Scalese, C. Spinella, A. Bearzotti, Effects of temperature and humidity on electrospun conductive nanofibers based on polyaniline blends, *J. Nanoparticle Res.* 13 (2011) 6193–6200. doi:10.1007/s11051-011-0310-6.
- [91] M.S. Peresin, Y. Habibi, A.-H. Vesterinen, O.J. Rojas, J.J. Pawlak, J.V. Seppälä, Effect of Moisture on Electrospun Nanofiber Composites of Poly(vinyl alcohol) and Cellulose Nanocrystals, *Biomacromolecules.* 11 (2010) 2471–2477. doi:10.1021/bm1006689.
- [92] Y. El Rayess, C. Albasi, P. Bacchin, P. Taillandier, J. Raynal, M. Mietton-Peuchot, A. Devatine, Cross-flow microfiltration applied to oenology: A review, *J. Membr. Sci.* 382 (2011) 1–19. doi:10.1016/j.memsci.2011.08.008.
- [93] I.M. Hutten, G. Pelletier, G. Smaldon, J. Simpson, C. Dawes, L. Jones, *Handbook of Nonwoven Filter Media*, Elsevier, 2007.
- [94] P. Czekaj, F. López, C. Güell, Membrane fouling by turbidity constituents of beer and wine: characterization and prevention by means of infrasonic pulsing, *J. Food Eng.* 49 (2001) 25–36. doi:10.1016/S0260-8774(00)00181-3.
- [95] H. Lim, A Review of Spunbond Process, *J. Text. Appar. Technol. Manag.* 6 (2010).
- [96] K.C. Dutton, Overview and Analysis of the Meltblown Process and Parameters, *J. Text. Appar. Technol. Manag.* 6 (2008).
- [97] R. Nayak, R. Padhye, I.L. Kyratzis, Y.B. Truong, L. Arnold, Recent advances in nanofibre fabrication techniques, *Text. Res. J.* 82 (2012) 129–147. doi:10.1177/0040517511424524.
- [98] Z. Li, T. Li, L. An, H. Liu, L. Gu, Z. Zhang, Preparation of chitosan/polycaprolactam nanofibrous filter paper and its greatly enhanced chromium(VI) adsorption, *Colloids Surf. Physicochem. Eng. Asp.* 494 (2016) 65–73. doi:10.1016/j.colsurfa.2016.01.021.
- [99] R. Wang, Y. Liu, B. Li, B.S. Hsiao, B. Chu, Electrospun nanofibrous membranes for high flux microfiltration, *J Membr Sci.* 392 (2012) 167–174. doi:10.1016/j.memsci.2011.12.019.
- [100] C.A. Fuenmayor, S.M. Lemma, S. Mannino, T. Mimmo, M. Scampicchio, Filtration of apple juice by nylon nanofibrous membranes, *J. Food Eng.* 122 (2014) 110–116. doi:10.1016/j.jfoodeng.2013.08.038.
- [101] X. Li, W. Yang, H. Li, Y. Wang, M.M. Bubakir, Y. Ding, Y. Zhang, Water Filtration Properties of Novel Composite Membranes Combining Solution Electrospinning and Needleless Melt Electrospinning Methods, *J. Appl. Polym. Sci.* 132 (2015) 41601. doi:10.1002/app.41601.

- [102] R. Kumar, A.F. Ismail, Fouling control on microfiltration/ultrafiltration membranes: Effects of morphology, hydrophilicity, and charge, *J. Appl. Polym. Sci.* 132 (2015) 42042. doi:10.1002/app.42042.
- [103] X. Li, Y. Zhang, H. Li, H. Chen, Y. Ding, W. Yang, Effect of oriented fiber membrane fabricated via needleless melt electrospinning on water filtration efficiency, *Desalination*. 344 (2014) 266–273. doi:10.1016/j.desal.2014.04.003.
- [104] Z. Zhou, W. Lin, X.-F. Wu, Electrospinning ultrathin continuous cellulose acetate fibers for high-flux water filtration, *Colloids Surf. Physicochem. Eng. Asp.* 494 (2016) 21–29. doi:10.1016/j.colsurfa.2015.11.074.
- [105] X. Zhuang, L. Shi, K. Jia, B. Cheng, W. Kang, Solution blown nanofibrous membrane for microfiltration, *J. Membr. Sci.* 429 (2013) 66–70. doi:10.1016/j.memsci.2012.11.036.
- [106] L. Li, R. Hashaikeh, H.A. Arafat, Development of eco-efficient micro-porous membranes via electrospinning and annealing of poly (lactic acid), *J. Membr. Sci.* 436 (2013) 57–67. doi:10.1016/j.memsci.2013.02.037.
- [107] H. Ma, C. Burger, B.S. Hsiao, B. Chu, Nanofibrous Microfiltration Membrane Based on Cellulose Nanowhiskers, *Biomacromolecules*. 13 (2012) 180–186. doi:10.1021/bm201421g.
- [108] S. Homaeigohar, J. Koll, E.T. Lilleodden, M. Elbahri, The solvent induced interfiber adhesion and its influence on the mechanical and filtration properties of polyethersulfone electrospun nanofibrous microfiltration membranes, *Sep Purif Technol.* 98 (2012) 456–463. doi:10.1016/j.seppur.2012.06.027.
- [109] L. Huang, S.S. Manickam, J.R. McCutcheon, Increasing strength of electrospun nanofiber membranes for water filtration using solvent vapor, *J Membr Sci.* 436 (2013) 213–220. doi:10.1016/j.memsci.2012.12.037.
- [110] H. Ma, B.S. Hsiao, B. Chu, Functionalized electrospun nanofibrous microfiltration membranes for removal of bacteria and viruses, *J. Membr. Sci.* 452 (2014) 446–452. doi:10.1016/j.memsci.2013.10.047.
- [111] Z. Tang, C. Qiu, J.R. McCutcheon, K. Yoon, H. Ma, D. Fang, E. Lee, C. Kopp, B.S. Hsiao, B. Chu, Design and fabrication of electrospun polyethersulfone nanofibrous scaffold for high-flux nanofiltration membranes, *J Polym Sci B Polym Phys.* 47 (2009) 2288–2300. doi:10.1002/polb.21831.
- [112] L. Huang, J.T. Arena, S.S. Manickam, X. Jiang, B.G. Willis, J.R. McCutcheon, Improved mechanical properties and hydrophilicity of electrospun nanofiber membranes for filtration applications by dopamine modification, *J Membr Sci.* 460 (2014) 241–249. doi:10.1016/j.memsci.2014.01.045.
- [113] L.T. (Simon) Choong, Z. Khan, G.C. Rutledge, Permeability of electrospun fiber mats under hydraulic flow, *J. Membr. Sci.* 451 (2014) 111–116. doi:10.1016/j.memsci.2013.09.051.
- [114] Y. Liu, R. Wang, H. Ma, B.S. Hsiao, B. Chu, High-flux microfiltration filters based on electrospun polyvinylalcohol nanofibrous membranes, *Polymer.* 54 (2013) 548–556. doi:10.1016/j.polymer.2012.11.064.
- [115] D. Hussain, F. Loyal, A. Greiner, J.H. Wendorff, Structure property correlations for electrospun nanofiber nonwovens, *Polymer.* 51 (2010) 3989–3997. doi:10.1016/j.polymer.2010.06.036.
- [116] K. Yoon, K. Kim, X.F. Wang, D.F. Fang, B.S. Hsiao, B. Chu, High flux ultrafiltration membranes based on electrospun nanofibrous PAN scaffolds and chitosan coating, *Polymer.* 47 (2006) 2434–2441. doi:10.1016/j.polymer.2006.01.042.
- [117] S. Kaur, D. Rana, T. Matsuura, S. Sundarrajan, S. Ramakrishna, Preparation and characterization of surface modified electrospun membranes for higher filtration flux, *J. Membr. Sci.* 390–391 (2012) 235–242. doi:10.1016/j.memsci.2011.11.045.
- [118] R. Asmatulu, H. Muppalla, Z. Veisi, W.S. Khan, A. Asaduzzaman, N. Nuraje, Study of hydrophilic electrospun nanofiber membranes for filtration of micro and nanosize suspended particules, *Membranes*. 3 (2013) 375–88. doi:10.3390/membranes3040375.

- [119] A. Cooper, R. Oldinski, H. Ma, J.D. Bryers, M. Zhang, Chitosan-based nanofibrous membranes for antibacterial filter applications, *Carbohydr. Polym.* 92 (2013) 254–259. doi:10.1016/j.carbpol.2012.08.114.
- [120] D. Aussawasathien, C. Teerawattananon, A. Vongachariya, Separation of micron to sub-micron particles from water: {Electrospun} nylon-6 nanofibrous membranes as pre-filters, *J. Membr. Sci.* 315 (2008) 11–19. doi:10.1016/j.memsci.2008.01.049.
- [121] R. Gopal, S. Kaur, C.Y. Feng, C. Chan, S. Ramakrishna, S. Tabe, T. Matsuura, Electrospun nanofibrous polysulfone membranes as pre-filters: Particulate removal, *J. Membr. Sci.* 289 (2007) 210–219. doi:10.1016/j.memsci.2006.11.056.
- [122] R. Gopal, S. Kaur, Z. Ma, C. Chan, S. Ramakrishna, T. Matsuura, Electrospun nanofibrous filtration membrane, *J. Membr. Sci.* 281 (2006) 581–586. doi:10.1016/j.memsci.2006.04.026.
- [123] S.S. Homaeigohar, K. Buhr, K. Ebert, Polyethersulfone electrospun nanofibrous composite membrane for liquid filtration, *J. Membr. Sci.* 365 (2010) 68–77. doi:10.1016/j.memsci.2010.08.041.
- [124] D. Bjorge, N. Daels, S. De Vrieze, P. Dejans, T. Van Camp, W. Audenaert, P. Westbroek, K. De Clerck, C. Boeckaert, S.W.H. van Hulle, Initial testing of electrospun nanofibre filters in water filtration applications, *Water SA.* 36 (2010) 151–155.
- [125] D. Bjorge, N. Daels, S. De Vrieze, P. Dejans, T. Van Camp, W. Audenaert, J. Hogie, P. Westbroek, K. De Clerck, S.W.H.H. Van Hulle, Performance assessment of electrospun nanofibers for filter applications, *Desalination.* 249 (2009) 942–948. doi:10.1016/j.desal.2009.06.064.
- [126] K. Desai, K. Kit, J. Li, P. Michael Davidson, S. Zivanovic, H. Meyer, Nanofibrous chitosan non-wovens for filtration applications, *Polymer.* 50 (2009) 3661–3669. doi:10.1016/j.polymer.2009.05.058.
- [127] N. Mahanta, S. Valiyaveetil, Surface modified electrospun poly(vinyl alcohol) membranes for extracting nanoparticles from water, *Nanoscale.* 3 (2011) 4625–4631. doi:10.1039/C1NR10739A.
- [128] F.E. Ahmed, B.S. Lalia, R. Hashaikeh, A review on electrospinning for membrane fabrication: Challenges and applications, *Desalination.* 356 (2015) 15–30. doi:10.1016/j.desal.2014.09.033.
- [129] L. Persano, A. Camposeo, C. Tekmen, D. Pisignano, Industrial Upscaling of Electrospinning and Applications of Polymer Nanofibers: A Review, *Macromol. Mater. Eng.* 298 (2013) 504–520. doi:10.1002/mame.201200290.
- [130] A.K. Gautam, C. Lai, H. Fong, T.J. Menkhaus, Electrospun polyimide nanofiber membranes for high flux and low fouling microfiltration applications, *J. Membr. Sci.* 466 (2014) 142–150. doi:10.1016/j.memsci.2014.04.047.
- [131] Z. Ma, M. Kotaki, S. Ramakrishna, Electrospun cellulose nanofiber as affinity membrane, *J. Membr. Sci.* 265 (2005) 115–123. doi:10.1016/j.memsci.2005.04.044.
- [132] H.-C. Kim, B.G. Choi, J. Noh, K.G. Song, S. Lee, S.K. Maeng, Electrospun nanofibrous PVDF–PMMA MF membrane in laboratory and pilot-scale study treating wastewater from Seoul Zoo, *Desalination.* 346 (2014) 107–114. doi:10.1016/j.desal.2014.05.005.
- [133] H. Ma, C. Burger, B.S. Hsiao, B. Chu, Ultra-fine cellulose nanofibers: new nano-scale materials for water purification, *J Mater Chem.* 21 (2011) 7507–7510. doi:10.1039/C0JM04308G.
- [134] S. Ramakrishna, R. Jose, P.S. Archana, A.S. Nair, R. Balamurugan, J. Venugopal, W.E. Teo, Science and engineering of electrospun nanofibers for advances in clean energy, water filtration, and regenerative medicine, *J Mater Sci.* 45 (2010) 6283–6312. doi:10.1007/s10853-010-4509-1.
- [135] A.W. Zularisam, A.F. Ismail, R. Salim, Behaviours of natural organic matter in membrane filtration for surface water treatment - a review, *Desalination.* 194 (2006) 211–231. doi:10.1016/j.desal.2005.10.030.
- [136] S. Homaeigohar, M. Elbahri, Nanocomposite Electrospun Nanofiber Membranes for Environmental Remediation, *Materials.* 7 (2014) 1017–1045. doi:10.3390/ma7021017.
- [137] N. Daels, S. De Vrieze, I. Sampers, B. Decostere, P. Westbroek, A. Dumoulin, P. Dejans, K. De Clerck, S.W.H.W.H. Van Hulle, Potential of a functionalised nanofibre microfiltration membrane as an antibacterial water filter, *Desalination.* 275 (2011) 285–290. doi:10.1016/j.desal.2011.03.012.

- [138] M. Khamforoush, O. Pirouzram, T. Hatami, The evaluation of thin film composite membrane composed of an electrospun polyacrylonitrile nanofibrous mid-layer for separating oil-water mixture, *Desalination*. 359 (2015) 14–21. doi:10.1016/j.desal.2014.12.016.
- [139] W. Ma, Q. Zhang, D. Hua, R. Xiong, J. Zhao, W. Rao, S. Huang, X. Zhan, F. Chen, C. Huang, Electrospun fibers for oil-water separation, *RSC Adv.* 6 (2016) 12868–12884. doi:10.1039/c5ra27309a.
- [140] X. Wang, J. Yu, G. Sun, B. Ding, Electrospun nanofibrous materials: a versatile medium for effective oil/water separation, *Mater. Today*. (2016). doi:10.1016/j.mattod.2015.11.010.

# 2

## **ELECTROSPINNING OF BIO-BASED POLYAMIDE 11 MATS**

*A bio-based polymer, polyamide 11, was chosen for fabricating nanofibrous mats for liquid microfiltration. The first objective was to develop mats with an average pore size ranging between 0.2 and 0.8  $\mu\text{m}$ , a specification of the CLARIFIL project. To this aim, electrospinning parameters have been adjusted to reach such thin pores by reducing the average fiber diameter by playing on solvent proportions, humidity, polymer concentration and on the distribution of the molar mass. Electrospun mats have been then characterized towards liquid microfiltration applications with their pore size (related to the fiber diameter and the thickness) and with their mechanical and hydrophilic properties.*



## 2.1 Introduction

Polyamide 11 (PA11) is an aliphatic semi-crystalline thermoplastic polymer. It is composed of amide groups regularly spaced thanks to a linear carbon chain composed of 11 carbon atoms. Historically, PA11 was first polymerized from 11-aminoundecanoic in 1938 by a group of researchers directed by Michel Génas at the French company Organico. They worked on the synthesis of 11-aminoundecanoic acid from castor oil as well as on its polymerization in PA11 and patented it. Since 1949, PA11 is commercialized by Arkema under the trade name Rilsan®. It is a high-performance polymer used nowadays mainly for automotive, transport, textile, oil and gas applications due to its excellent properties, namely high chemical resistance, ease of processing, wide range of working temperature, high dimensional stability, etc. The Rilsan® brand has celebrated in 2017 its 70 years of growth [1].

PA11 is a bio-based polymer as it is derived from castor oil. It is recyclable but not biodegradable. Castor beans are grown in arid landscapes that are difficult to cultivate. Consequently, its use does not compete with the human or animal food chain. PA11 is therefore very attractive from an industrial point of view as an environmentally friendly polymer. During the thesis, no additives were added to polyamide 11 solutions in order to facilitate future recycling steps. The synthesis of 11-aminoundecanoic is performed in five steps as described in Figure 2.1. First, castor oil is transformed into methyl ricinoleate via methanolysis. Second, methyl 10-undecenoate is obtained from the elimination of heptanal at 550°C and hydrolyzed, in a third step, into 10-undecenoic acid. The fourth step corresponding to a bromination yields 11-bromoundecanoic acid. Last, 11-aminoundecanoic acid is finally formed after addition of aqueous ammonia [2]. Even if PA11 is bio-based and thus environmentally friendly, its synthesis involves methanol, which is highly toxic for human, hydrobromic acid, a corrosive compound, and ammonia which is corrosive and hazardous when concentrated. The polymerization of 11-aminoundecanoic in polyamide 11 is performed by polycondensation of 11-aminoundecanoic acid in inert atmosphere at high temperature (between 250 and 280°C) (Figure 2.2).

PA11 is chemically very resistant and can only be solubilized in few solvents. A list of the main solvents of PA11 found in the literature is given in Table 2.1. For the present work, a mixture composed of formic acid and dichloromethane was retained as solvent for its relative low health impact, as industrial upscaling is foreseen, because PA11 solubilization happens at room temperature and due to the fact that it had already been used for electrospinning trials [3].

Reference	Solvent
Behler et al. (2007) [3]	Formic acid/Dichloromethane
Dhanalakshmi et al. (2008) [4]	Formic acid (at 70°C)
Carponcin et al. (2012) [5]	Dimethylacetamide (at 160°C)
Mago et al. (2011) [6]	1,4-butanediol (at 160–165°C)

**Table 2.1.** List of some PA11 solvents.

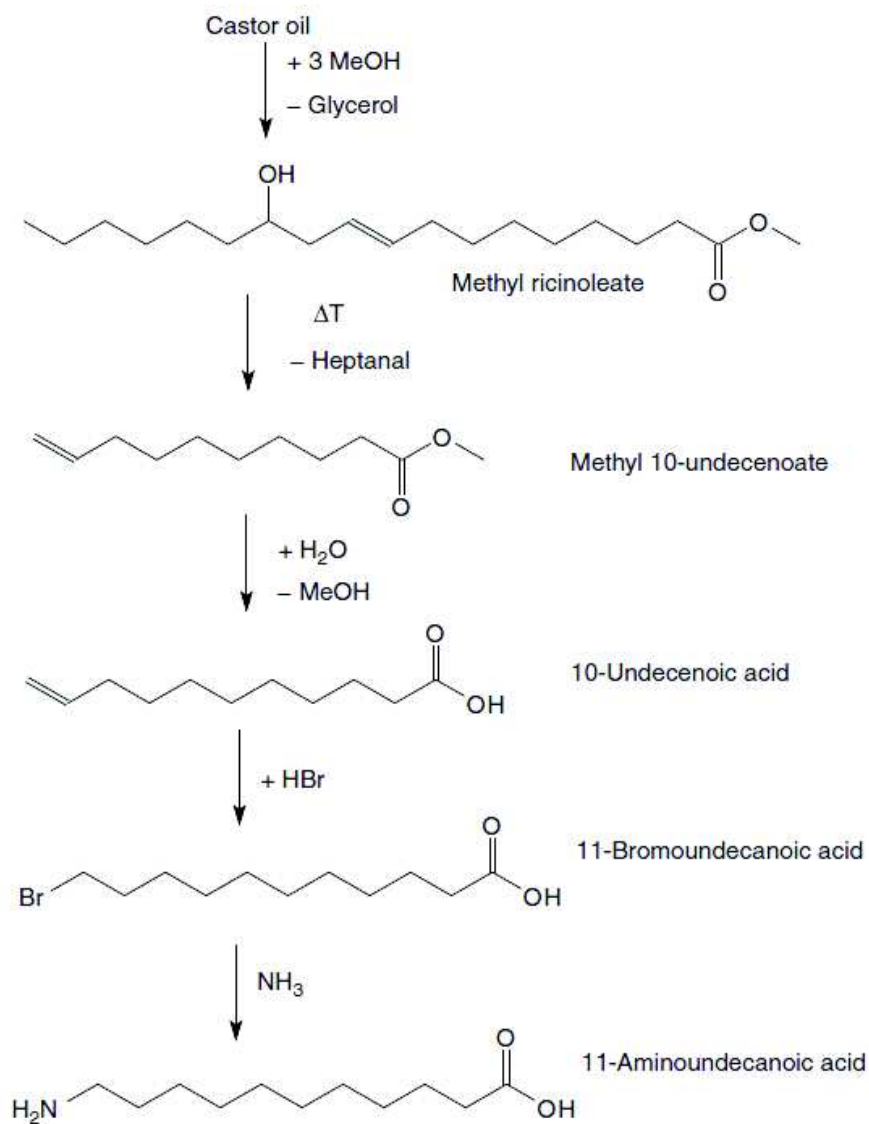


**Figure 2.1.** Reaction scheme of 11-aminoundecanoic acid production from castor oil. Taken from Rulkens and Koning (2012) [2].

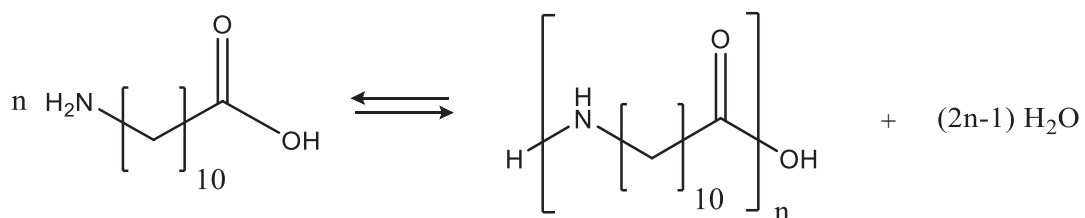


**Figure 2.2.** Polycondensation reaction of PA11.

In liquid filtration, the pore size is the main parameter characterizing a mat and its reduction leads to better efficiencies (Chapter 1). Various strategies can lead to the decrease of the mean pore size: hot pressing [7], annealing [8], coating [9] or decreasing the fiber diameter [10] for instance. However, hot pressing, annealing and coating also participate in decreasing the porosity via a decrease of the thickness or, for the coating strategy, via an increase of the main fiber diameter. The reduction of the porosity leads to two major drawbacks: the decrease of the permeability and the increase of the pressure drop across the filter that must be applied in order to keep the same filtering productivity. These drawbacks are costly, energy-consuming and mats must be mechanically stronger to resist to the flow. On the contrary, for the strategy consisting in decreasing the mean fiber diameter, Wang et al. explained that small fibers lead to higher density of fiber crossings and shorter average length between crossings, thus decreasing the average pore size [10,11]. Decreasing the mean fiber diameter in order to decrease the mean pore size has the advantage to maintain a high porosity [11]. This strategy has consequently been chosen for the fabrication of liquid filtration membranes by electrospinning.

The diameter of fibers is defined by the choice of the electrospinning parameters, and generally electrospun fibers have a mean fiber diameter between 100 nm and 1  $\mu\text{m}$  [12]. To tailor the fiber diameter, different levers can be considered [13]. For instance, Lavielle et al. [14] degraded polycaprolactone solutions in mixtures of formic acid and acid acetic in order to broaden the polydispersity of the molar mass resulting in the decrease of the fiber diameter. Riazi et al. [15] could adjust the diameter of electrospun polystyrene fibers by playing on the polymer architecture of linear and comb polymers. They found out that comb solutions with few but long branches yielded by electrospinning thicker fibers than linear and comb solutions with shorter but more numerous branches when electrospun in the same conditions. In the case of polyamides, Huang et al. [16] could reduce the mean fiber diameter by decreasing the concentration of polymer into the solution. Yet, at low concentrations continuous fibers turn into beaded fibers. Differently, Mi-uppatham et al. [17] carefully chose the solvent system in favor for a system with a slow evaporation rate in order to produce thin fibers. Solvent systems with slow evaporation rates allow fibers to be elongated during longer times and to be thinner. Finally, humidity can be changed to promote the fabrication of fine fibers as seen in Chapter 1 [18].

High productivity is nowadays one of the major drawback of the electrospinning process [19,20], and neither of these strategies lead to an increase of productivity, above all the solution consisting in decreasing the concentration. New multi-jet setups have recently flourished in the literature to solve the issue [21–24]. Differently, we propose here a new strategy allowing reducing the fiber diameter while increasing the concentration of the electrospinning solution and therefore the productivity that does not require changing from electrospinning setup, but which could be used in multi-jet setups. Inspired by the work of Lavielle et al [14], our strategy consists in mixing two PA11 with two different molar masses in order to fabricate mats composed of PA11 only which is advantageous for recycling perspectives. This strategy can be extended to other polymers. Usually, the electrospinning of a polymer blend is performed to provide electrospun fibers with new properties such as antibacterial properties [25,26], high hydrophilicity [27], possibly promoting cell adhesion properties [28] and better mechanical properties [29]. In our case, the aim of the blend is to fabricate thin fibers from concentrated solutions for industrial state-of-the art applications, with the polymer of highest molar mass being the carrier polymer bringing the chain entanglements necessary for the formation of a continuous electrospun fiber [30]. Blend electrospinning has until now never been tailored to such extend. This strategy could open new doors towards high yields electrospinning processes producing thin fibers for industrial applications.

So, throughout the following, we will first play on four major parameters with the aim to reduce the mean fiber diameter of PA11 fibers: the composition of the solvent, the humidity, the polymer concentration and the

distribution of the molar mass (by blending a polymer of low molar mass to a polymer of higher molar mass). We will seek in the same time to understand the role of the carrier polymer on the ability to electrospin the blend. Finally, a PA11 mat composed of fibers with a mean diameter of approximately 100 nm is compared with a PA11 mat composed of fibers with a mean diameter of approximately 500 nm by their pore size (in relation with the thickness), their mechanical properties and their hydrophilic properties.

## 2.2 Materials and methods

### 2.2.1 Materials

Three polyamides 11 Rilsan® (PA11) of different molar masses ( $M_w = 5600$  g/mol, 36000 g/mol and 47400 g/mol) were furnished by Arkéma (see Appendix 1 for rheological characterizations). They are referred as PA11(5.6) ( $M_w = 5600$  g/mol), PA11(36) ( $M_w = 36000$  g/mol) and PA11(47.4) ( $M_w = 47400$  g/mol). The molar masses were obtained by size exclusion chromatography (SEC) in hexafluoroisopropanol and using PMMA calibration. Dichloromethane (Pure-stabilized with amylene) (DCM) was purchased from Carlo Erba. Formic acid (puriss. p.a., ACS reagent, reag. Ph. Eur.,  $\geq 98\%$ ) (FA) was purchased from Sigma-Aldrich.

### 2.2.2 Solution preparation

PA11 pellets were dissolved in the solvent 4 hours prior to the experiments. The solvent is composed of FA and DCM (FA/DCM) in an equivalent volume ratio (v/v).

### 2.2.3 Electrospinning

Electrospinning was performed using a home-made electrospinning setup. A difference of potential was established between a needle and a collector using a high-voltage power supply (Spellmann SL 10). The collector was rotated through a high-speed laboratory stirrer (Ika® Eurostar 20). A syringe pump (Fischer Scientific) pushed the solution through the needle. The distance between the needle and the collector was kept at 15 cm. The rotation speed of the collector was set at 150 rpm. Experiments were performed at 22°C and relative humidity was maintained at  $50 \pm 10\%$ . The mass concentration of PA11(5.6) was changed from 2 wt% to 14 wt% whereas it was changed between 2 wt% and 10 wt% for PA11(36) and PA11(47.4). The flow rate was kept at  $1.0 \pm 0.2$  mL/h for all electrospinning experiments. All electrospinning experiments lasted 3 minutes in part 2.3. For the measurement of the pore size, fibers were deposited on a PA11 nonwoven placed on the collector (Appendix 2).

### 2.2.4 Membrane characterization

Before Scanning Electron Microscopy (SEM) examination, samples were coated with a thin layer of gold with a gold coater (Quorum Q 150 R S, Quorum Technologies). The SEM (Vega-3, Tescan) was used in high vacuum mode using accelerating voltages of 5 kV and working distances in the range of 10 mm. For each sample showing fibers, the diameter of 100 fibers was measured on 5 different SEM images with the image analysis software Image J. Pore size was measured on a gas-liquid porometer at the IFTS institute (Institut de la Filtration et des Techniques Séparatives (Fr) - International Filter Testing Services (En)). Tensile tests were conducted on a Physica MCR301 rheometer (Anton Paar) equipped with homemade grips for tensile tests. Mats were cut into sample with dimensions 20 x 10 mm<sup>2</sup>. The traction velocity was 0.002 mm/s. Thicknesses

were measured by SEM. Contact angles of 4  $\mu\text{L}$  deionized water drops on electrospun mats and on films were measured 5 times for 1 minute and averaged with a tensiometer (DSA25S) from Krüss.

#### 4.2.5 Solution characterization

Conductivity of solutions was measured with an electrical conductivity meter (Consort K610). Surface tension was measured with a tensiometer (Tracker, Teclis Instruments). Before surface tension measurement, density of solutions was measured by weighing a fixed volume of solution in a pycnometer. Viscosity of solutions was measured with a rheometer (Physica MCR 301, Anton Paar). Cone-Plate geometry (CP50-1) with an angle of  $1^\circ$  was used. A gradient of shear was imposed from  $10 \text{ s}^{-1}$  to  $1000 \text{ s}^{-1}$ . Over this range of shear rates, only Newtonian behavior was observed for all tested concentrations. All measurements were performed at  $22^\circ\text{C}$ . An anti-evaporation system was used to avoid evaporation of solvents during the measures. The viscoelastic properties, characterized by the elastic modulus  $G'$  and the loss modulus  $G''$ , were assessed in the pulsation range of  $1 \text{ rad}\cdot\text{s}^{-1}$  to  $100 \text{ rad}\cdot\text{s}^{-1}$  at  $20^\circ\text{C}$  and with a strain amplitude of 3% using a rheometer (TA Instruments Discovery HR3) with a cone plate-plate geometry having a diameter of 50 mm and an angle of  $1^\circ$ .

## 2.3 Fabrication of thin PA11 fibers by electrospinning

Four strategies were investigated in order to play on the fiber diameter. The three first strategies consist in changing three electrospinning parameters that are the solvent proportions, the humidity and the polymer concentration. The fourth strategy involves blending two polyamides of different molar masses.

### 2.3.1 Effect of the solvent composition

FA/DCM ratio has been changed from 80/20 to 30/70 in order to evaluate the impact of the proportion of the solvents on fibers and to fabricate the thinnest continuous and regular fibers without beads. These experiments were conducted with PA11(36) and PA11(47.4) with a concentration of 4 wt% and 6 wt% at fixed relative humidity ( $42 \pm 3 \%$ ) and temperature ( $22 \pm 2^\circ\text{C}$ ). It can be seen from Figure 2.3 and Figure 2.4 that when the proportion of formic acid increases, fibers become thinner. This can be explained by the fact that formic acid has a lower evaporation rate than dichloromethane at  $22^\circ\text{C}$  due to its higher boiling point (Table 2.2). Consequently, fibers can be elongated during a longer time before drying. Nevertheless, when the proportion of formic acid exceeds 60%, the solidification time is long enough to also allow the apparition of instabilities, resulting in defects (bead-on-string fibers mainly). A 50/50 ratio has been found to be the best ratio allowing the fabrication of the thinnest defect-free fibers.



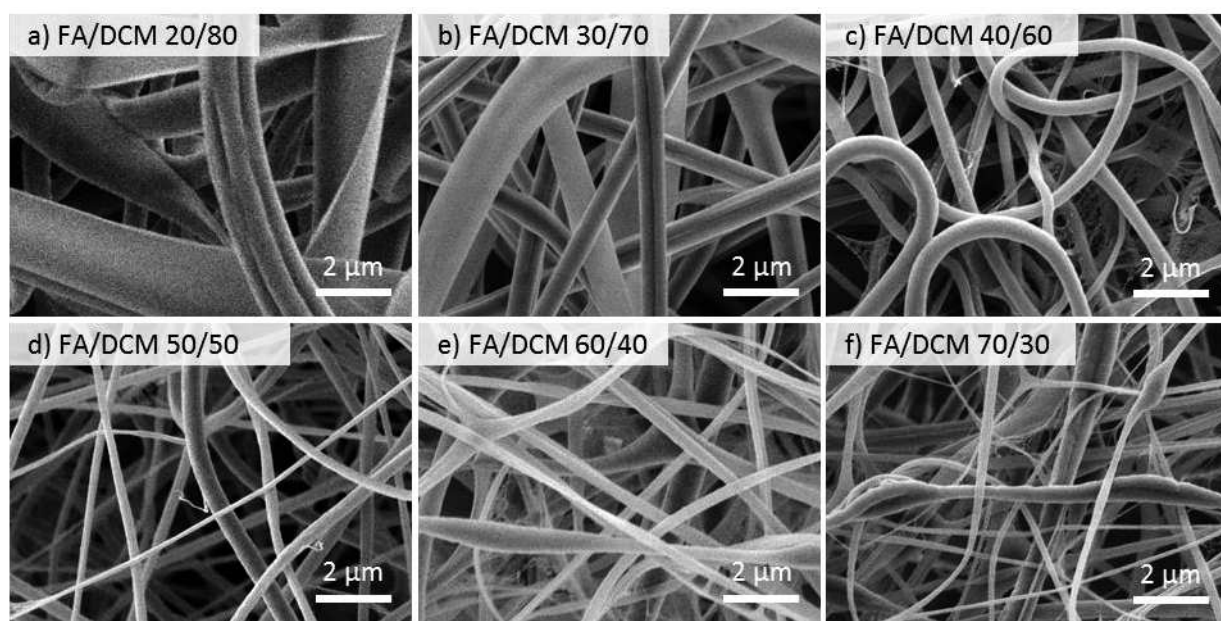


**Figure 2.3.** SEM images of PA11 fibers electrospun from 6 wt% of PA11(47.4) in FA/DCM v/v in different proportions: a) 20/80, b) 30/70, c) 40/60, d) 50/50, e) 60/40 and f) 70/30.

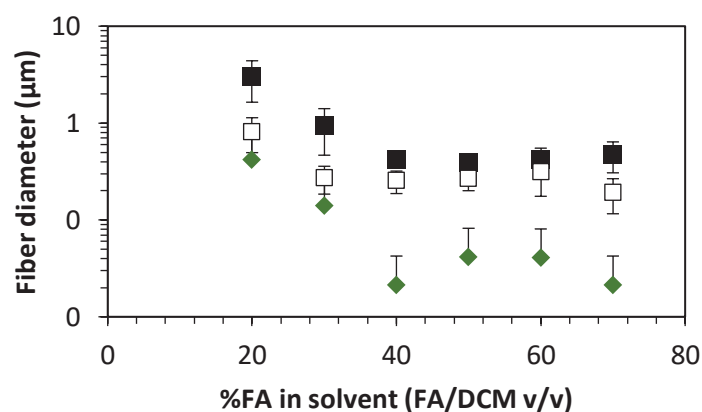


**Figure 2.4.** Fiber diameter of PA11 fibers electrospun from 6 wt% PA11(36) (dark green diamonds), 4 wt% PA11(47.4) (white squares) and 6 wt% PA11(47.4) (black squares) in FA/DCM v/v as a function of the proportion in FA (in v%) in the FA/DCM v/v solvent.

Property	Formic acid	Dichloromethane
Melting point (°C)	8.2 - 8.4 °C	-95.1
Boiling point (°C)	100 - 101 °C	40
Density at 25 °C (g/mL)	1.22	1.33

**Table 2.2.** Melting point, boiling point and density of formic acid and dichloromethane (Source: Sigma-Aldrich and Carlo Erba, accessed March 13, 2018).



### 2.3.2 Role of humidity

Relative humidity has been changed between 20 and 60% during electrospinning experiments at 22°C. Figure 2.5 presents the results with a solution composed of 4 wt% and 6 wt% of PA11(47.4) in FA/DCM 50/50 v/v. Our goal is to find the best conditions allowing the fabrication of continuous fibers with thin diameters. A relative humidity below 30% leads to the fabrication of the thickest fibers whereas the thinnest fibers are formed above 40%. The result can be explained by the fact that polyamides can absorb a certain amount of water during the electrospinning process depending on the temperature and on the relative humidity at which the process is performed (before electrospinning, polyamides 11 contain approximatively 1% of water, see Appendix 3). The absorption of water is sufficient to decrease the glass transition temperature [31,32] and to stretch fibers out more before solidification. The phenomenon, called “plasticizing effect”, has been evidenced in the literature [33–35] and is detailed in Chapter 1.

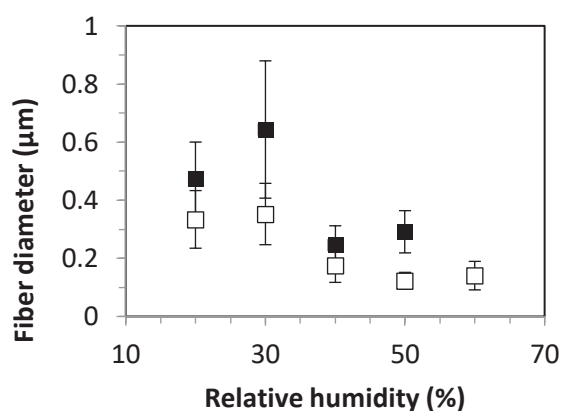


**Figure 2.5.** Fiber diameter resulting from the electrospinning of 4 wt% PA11(47.4) (white squares) and 6 wt% PA11(47.4) (black squares) in FA/DCM 50/50 v/v as a function of the relative humidity at 22°C.

### 2.3.3 Effect of PA11 concentration

The influence of the PA11 concentration on the fiber diameter has been highlighted for PA11(36) and PA11(47.4) in FA/DCM 50/50 v/v. It was possible to successfully electrospin PA11(36) and PA11(47.4) into bead-free fibers for concentrations between 5 wt% and 10 wt% (Figure 2.6). At 10 wt%, the electrospinning process became unstable and fibers were ribbon-shaped. Between 2 wt% and 5 wt% bead-on-string fibers were fabricated. Below 2 wt% only particles were produced. In the end, the fiber diameter increases with the increase of concentration (Figure 2.7). The mean fiber diameter of PA11(47.4) mats is always higher than the one of PA11(36) mats due to the difference in molar mass. Thus, the mat having the thinnest mean fiber diameter without beads,  $178 \pm 41$  nm, was electrospun from the electrospinning of PA11(36) with a concentration of 6 wt% (Figure 2.6d).

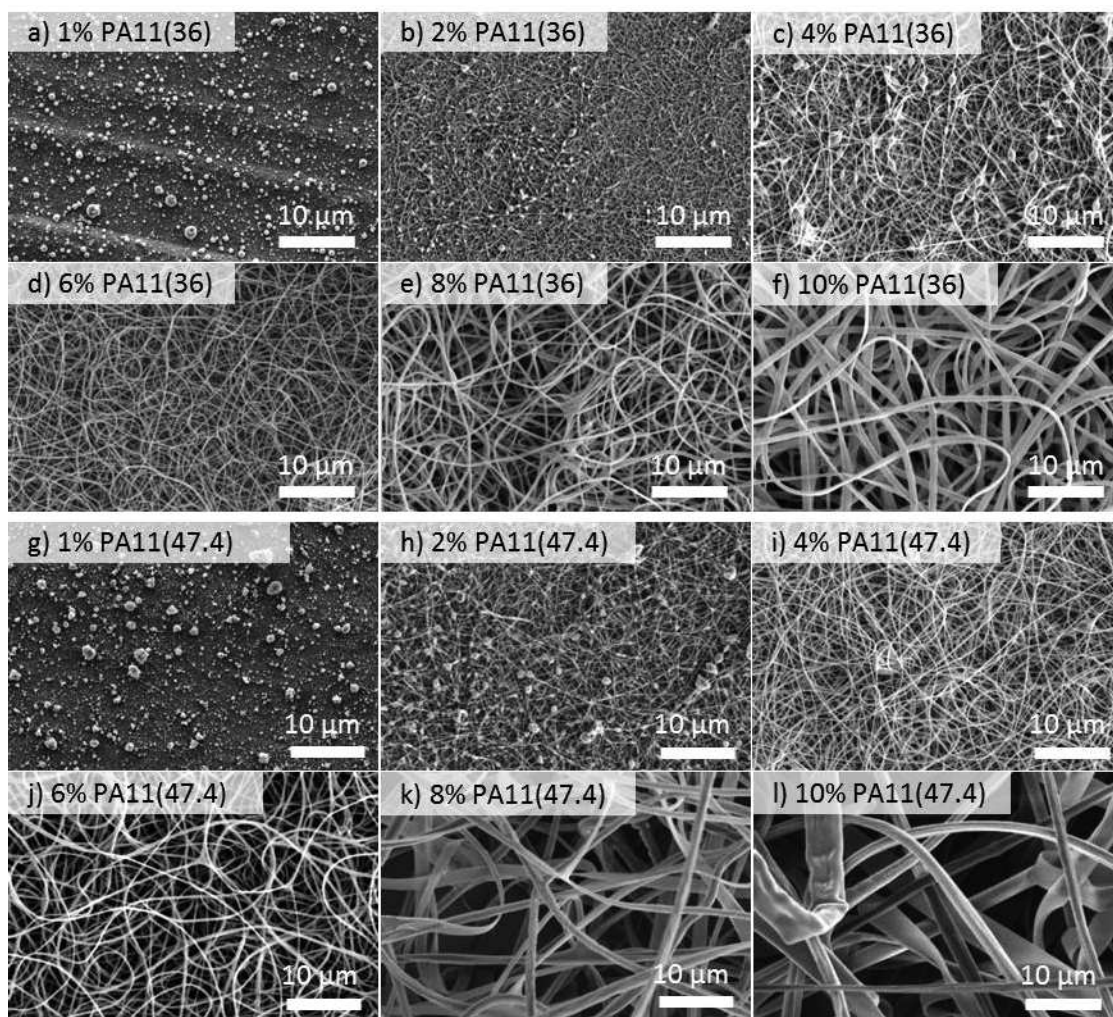


**Figure 2.6.** Electrospinning of a-f) PA11(36) and g-l) PA11(47.4) with concentrations between 1 wt% and 10 wt% in FA/DCM 50/50 v/v.

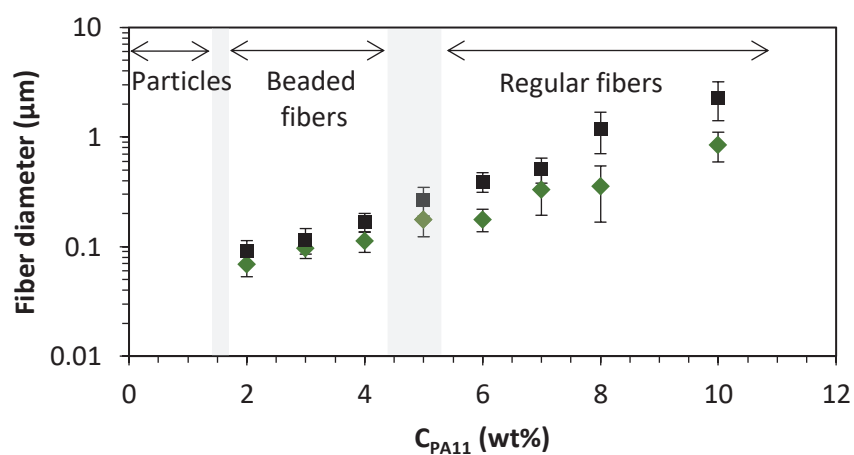


**Figure 2.7.** Fiber diameter of PA11(36) (dark green diamonds) and PA11(47.4) (black squares) as a function of the concentration in FA/DCM 50/50 v/v.

The concentration dependence of the specific viscosity is shown in Figure 2.8 for PA11(36) and PA11(47.4). The viscosity scaling relationships of neutral solutions in good solvents are expressed by  $\eta_{sp} \propto C$  in the dilute regime,  $\eta_{sp} \propto C^{1.3}$  in the semi-dilute unentangled regime, and  $\eta_{sp} \propto C^{3.9}$  in the semi-dilute entangled regime [36]. Our results with PA11(36) as well as with PA11(47.4) are in good agreement with the theoretical predictions.  $C^* \approx 0.7$  wt% for PA11(36) and PA11(47.4).  $C_e$  for PA11(36) is  $\approx 5.4$  wt% whereas it is  $\approx 4.5$  wt% for PA11(47.4).  $C^*$  and  $C_e$  values for PA11(47.4) are higher than that of PA11(36) due to the molar mass difference. The obtained values are coherent with the fact that bead-on-string fibers were obtained for PA11 solutions concentrated at 2 wt% (Figure 2.6b and h) meaning that polymer chains were already interacting together for such low concentrations.

Bead-free fibers of PA11(36) and PA11(47.4) were obtained at 6 wt% and above, or in other words above  $C_e$ . Generally, for neutral solutions, fibers can be obtained above 2-2.5 $C_e$  [37,38].

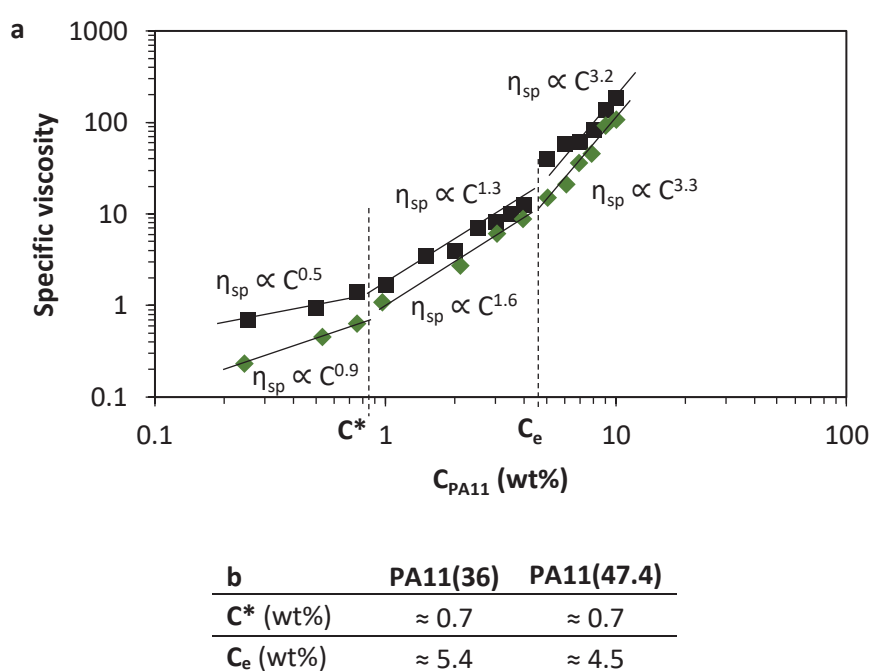


**Figure 2.8.** a) Specific viscosity as a function of PA11(36) (dark green diamonds) and PA11(47.4) (black squares) mass concentration in FA/DCM v/v 50/50. b)  $C^*$  and  $C_e$  values for PA11(36) and PA11(47.4).

### 2.3.4 Effect of the distribution of the molar mass

The main problem linked with decreasing the concentration to form thin fiber is that productivity is also reduced. In this part, with the goal to fabricate mats with thin fibers from concentrated solutions, the effect of the distribution of the molar mass on the fiber diameter was investigated. The distribution of the molar mass was varied by blending PA11(36) or PA11(47.4) with PA11(5.6). More specifically, a small amount of PA11(36) or PA11(47.4) was added to a solution of PA11 having the lowest molar mass (here: PA11(5.6)). Different PA11(5.6/36) and PA11(5.6/47.4) blends were electrospun: 14/0.25 wt%, 14/0.5 wt% and 14/1 wt% on the one hand (PA11 (5.6) concentration being constant) (Figure 2.9) and 8/1 wt%, 10/1 wt%, 12/1 wt% and 14/1 wt% (PA11 (36) and PA11(47.4) concentrations being constant) on the other hand (Figure 2.11).

When PA11(5.6) was electrospun alone, only particles were obtained irrespectively of the concentration. As a matter of fact, the electrospinning of PA11(5.6), up to a concentration of 14 wt% which is the highest concentration that can be dissolved in the solvent, only particles are formed (Figure 2.9a). The inability to electrospin PA11(5.6) into fibers is due to its low molar mass. PA11(5.6) polymer chains are not long enough to provide enough entanglements in the range of concentration where PA11(5.6) is soluble in FA/DCM v/v. On the opposite, regular fibers were obtained for all blends. Excepted in the cases of 14/0.25 wt% and 14/0.5 wt% blends, beads and bead-on-string fibers are fabricated (Figures 2.9b,c,e,f). PA11(36) and PA11(47.4) play here the role of a carrier polymer as it was not possible to electrospin fibers with pure PA11(5.6) solutions.

The mean fiber diameter could be first decreased by using PA11(36) instead of PA11(47.4) due to the fact that PA11(36) has a lower molar mass than PA11(47.4) (Figure 2.10 and Figure 2.12). Second, decreasing the overall PA11 concentration leads to the formation of thinner fibers as developed in the previous part (Figure 2.10 and Figure 2.12). Consequently here, the thinnest fibers that were fabricated were obtained from the 8/1 wt% PA11(5.6/36) blend solution (total PA11 concentration of 9 wt%). The corresponding fibers have a mean diameter of  $82 \pm 14$  nm. Without the blending strategy, the thinnest fibers that could be fabricated,  $178 \pm 41$  nm, were obtained from a solution composed of 6 wt% of PA11(36) for the same flow rate ( $1.0 \pm 0.2$  mL/h). In comparison, the fiber diameter of 8/1 wt% PA11(5.6/36) fibers is decreased by 54% while the solution concentration is increased by 50%. Third, taking into account the productivity issues, the optimal strategy to electrospin thin fibers from concentrated solutions is to maximize PA11(5.6) concentration while minimizing PA11(36) or PA11(47.4) concentrations provided the formation of regular fibers. Here, for instance, for a concentration of 14 wt% in PA11(5.6), which is very close to the solubility threshold, the concentration in PA11(36) must be raised above 0.5 wt% to ensure to formation of regular and continuous fibers (Figure 2.9). Finally, the most concentrated blend solution (15 wt%) which could be electrospun into regular fibers was 14/1 wt% PA11(5.6/36). Fibers with an average diameter of  $143 \pm 43$  nm were then fabricated. In that case, in comparison with the electrospinning of 6 wt% of PA11(36) in FA/DCM v/v 50/50 (fiber diameter of  $178 \pm 41$  nm), the mean fiber diameter could be decreased by 20% and the concentration increased by 150%. In the end, even if PA11(5.6) does not play the major part in the formation of fibers, its presence is essential for the electrospinning of concentrated solutions and for the obtaining of thin fibers.



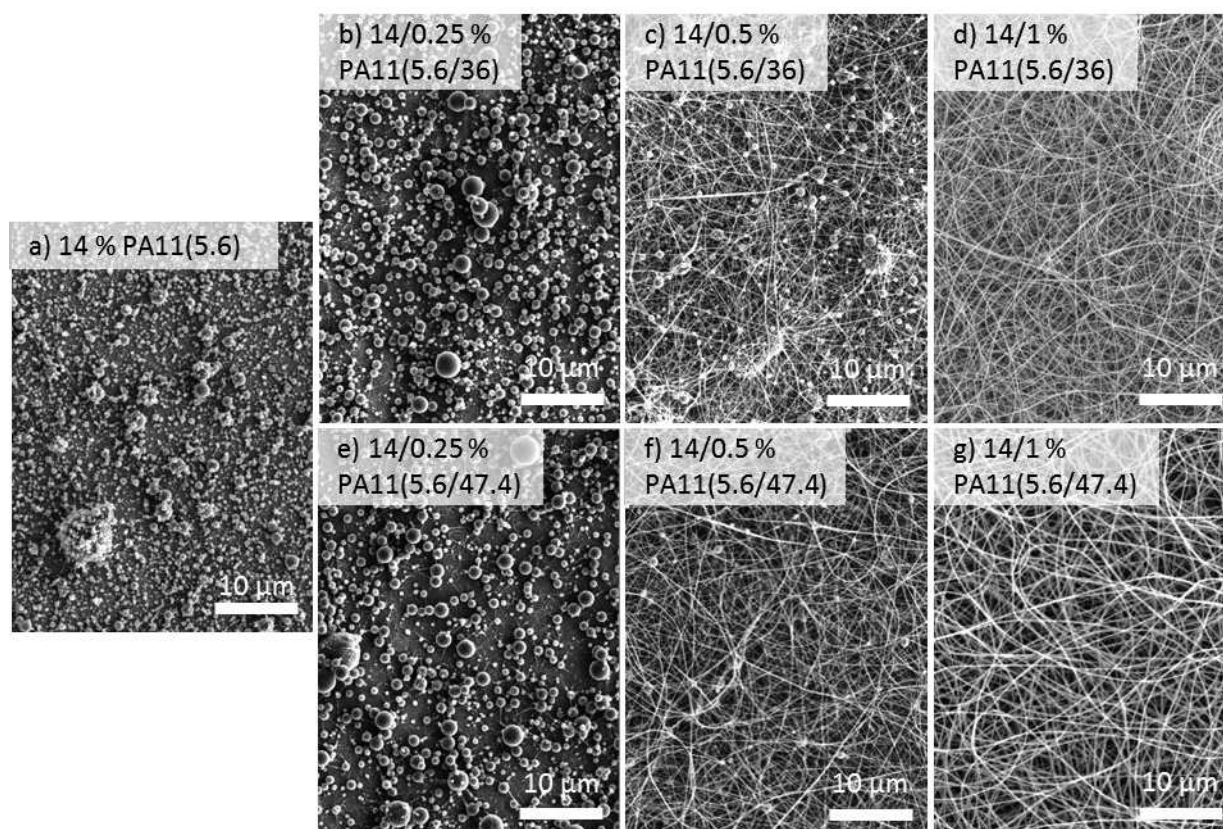


**Figure 2.9.** Electrospinning of a) 14 wt PA11(5.6) in FA/DCM 50/50 v/v; b) 14/0.25 wt%, c) 14/0.5 wt%, d) 14/1 wt% PA11(5.6/36) blends in FA/DCM 50/50 v/v; and e) 14/0.25 wt%, f) 14/0.5 wt%, g) 14/1 wt% PA11(5.6/47.4) blends in FA/DCM 50/50 v/v.

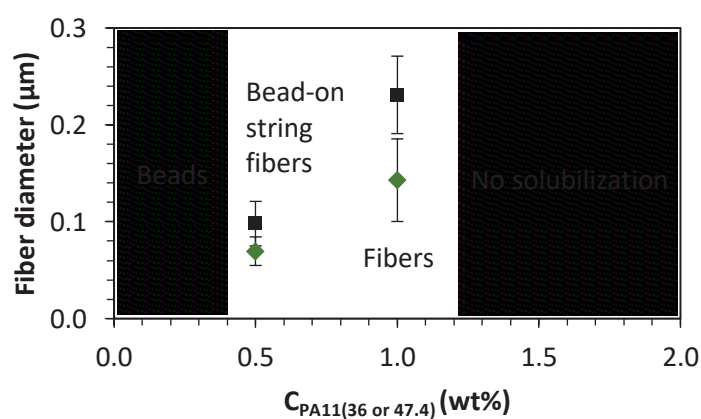


**Figure 2.10.** Mean fiber diameter of different PA11(5.6/36) and PA11(5.6/47.4) blends in FA/DCM v/v 50/50 as a function of PA11(36) (green diamonds) or PA11(47.4) (black squares) concentration keeping PA11(5.6) concentration at 14 wt%.

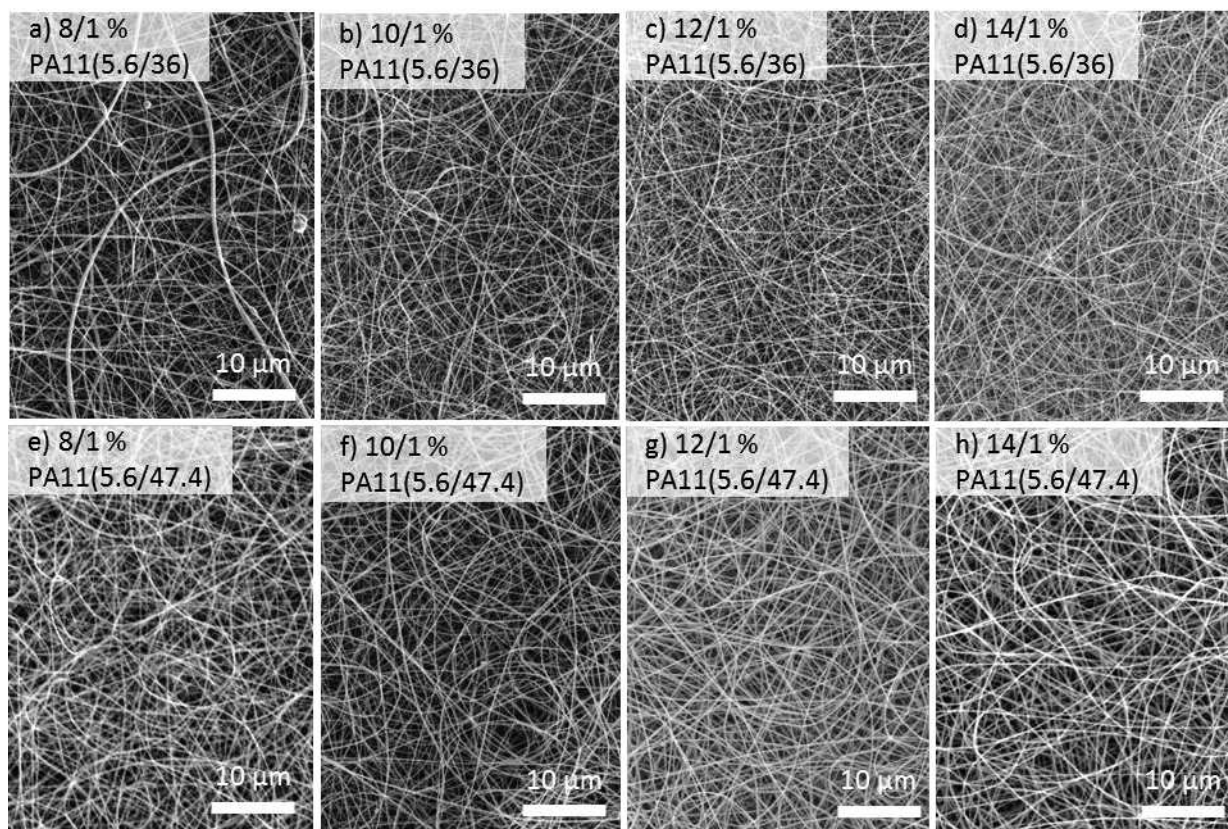


**Figure 2.11.** Electrospinning of a) 8/1, b) 10/1, c) 12/1, d) 14/1 wt% PA11(5.6/36) and e) 8/1, f) 10/1, g) 12/1, h) 14/1 wt% PA11(5.6/47.4) blends in FA/DCM v/v 50/50.

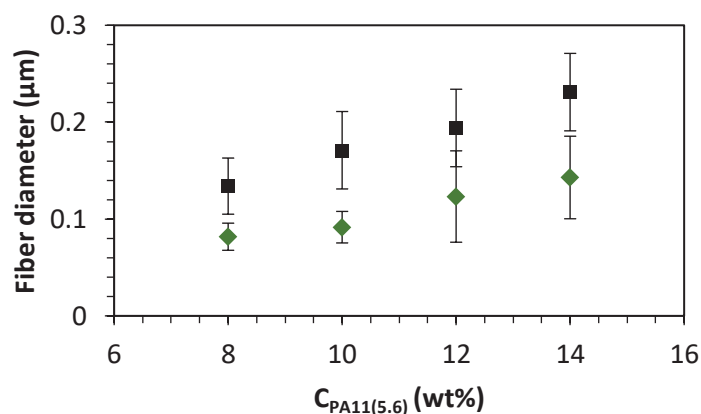


**Figure 2.12.** Mean fiber diameter of PA11(5.6/36) (green diamonds) and PA11(5.6/47.4) (black squares) blends in FA/DCM v/v 50/50 as a function of PA11(5.6) concentration keeping PA11(36) and PA11(47.4) concentrations at 1 wt%.

In order to understand how fibers could be fabricated from PA11(5.6/36) or PA11(5.6/47.4) blend solutions and not from PA11(5.6) solutions, we investigated the role played by the PA11s during the process of fiber formation. The conductivity and the surface tension of the solvent 12 wt% PA11(5.6), 1 wt% PA11(36) and 12/1 wt% PA11(5.6/36) were compared. Surface tension does not affect the electrospin-ability of the solutions (Table 2.3) as surface tension values of 1% PA11(36), 12% PA11(47.4) and 12/1 wt% PA11(5.6/36) are rather similar.



Mean surface tension (mN/m)	
Solvent	$32.9 \pm 0.6$
6%PA11(5.6)	$32.8 \pm 0.6$
6%PA11(36)	$33.6 \pm 0.6$
1%PA11(36)	$31.7 \pm 0.9$
12%PA11(5.6)	$35.4 \pm 0.5$
12/1% PA11(5.6/36)	$34.4 \pm 0.7$
14%PA11(5.6)	$33.6 \pm 1.3$
14/1% PA11(5.6/36)	$34.4 \pm 0.3$

**Table 2.3.** Surface tension of PA11 solutions in FA/DCM 50/50 v/v.

Conductivity measurements are given in Figure 2.13. The comparison between the conductivities of 12 wt% PA11(5.6) and 12/1 wt% PA11(5.6/36) and between the conductivities of 14 wt% PA11(5.6) and 14/1 wt% PA11(5.6/36) do not explain the difference between the morphologies obtained after electrospinning. Thus, a change in conductivity is not at the origin of the formation of fibers.

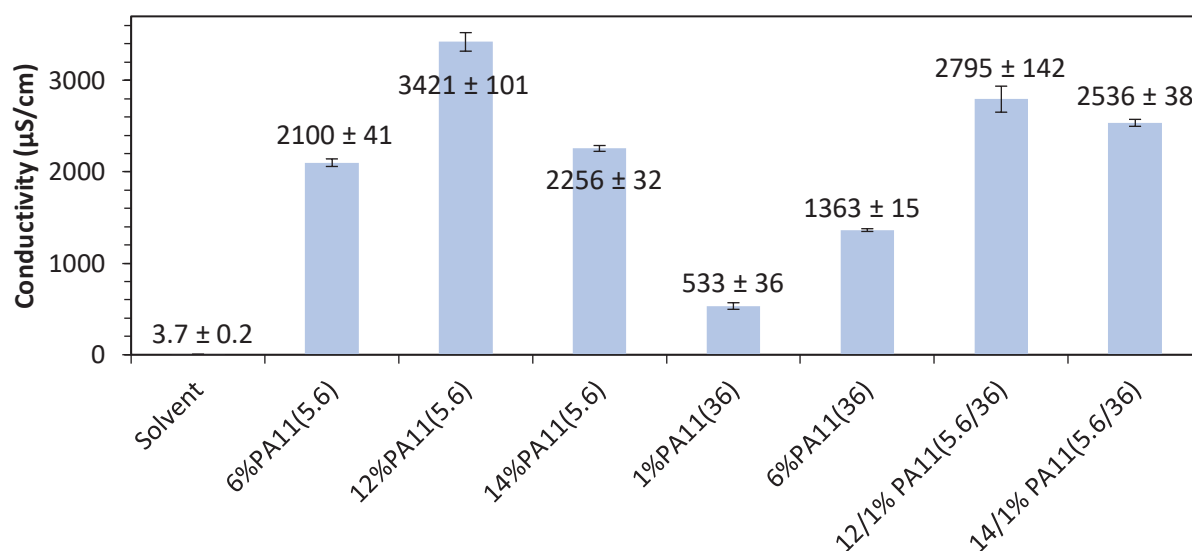


**Figure 2.13.** Conductivity of PA11 solutions in FA/DCM 50/50 v/v.

The concentration dependence of the specific viscosity was also measured in order to compare the specific viscosity evolutions of PA11(5.6), 12/1 PA11(5.6/36) and 14/1 PA11(5.6/36) in FA/DCM v/v as a function of the concentration (Figure 2.14). Saquing et al. [30] evidenced the role played by polyethylene oxide (PEO), the carrier polymer, on the formation of PEO/alginate fibers thanks to the measure of the concentration dependence of the specific viscosity. They could see an increase in  $C_e$  as well as in the viscosity scaling relationships for the alginate/PEO blend compared to neat alginate thanks to the influence of PEO. However here, the evolution of the specific viscosity of 12/1 PA11(5.6/36) and 14/1 PA11(5.6/36) as a function of the concentration is identical to the evolution of pure PA11(5.6). The influence of PA11(36) is not visible. It can be due to the fact that the PA11 ratios (5.6/36) (12/1 and 14/1) are higher than the PEO/alginate (7/3) ratio used by Saquing et al.

Palangetic et al. [39] showed that in the case of highly polydispersed polymer solutions, the formation of fibers is better related to the extensibility average molecular weight as the spinnability of the solution is dependent on the extensibility of the highest molecular weight fractions. Thus, viscoelastic properties of 12/1 PA11(5.6/36) were compared with those of pure PA11(5.6) at 12 wt% (Figure 2.15). The addition of 1 wt% PA11(36) did not significantly affect the loss modulus  $G''$  and the complex viscosity. A slight increase of the elastic modulus  $G'$  is observed with the addition of 1 wt% PA11(36). However, such effect could not explain the huge difference in the behavior during electrospinning where regular fibers were obtained in the case of 12/1 PA11(5.6/36) blend whereas only beads were obtained with 12 wt% of PA11(5.6). However, it is worth noting that the addition of 1 wt% PA11(36) played an important role on the precipitation behavior of the solution. Indeed, the viscoelastic properties of the pure PA11(5.6) solution at 12 wt% was much more stable during the measurements than the 12/1 PA11(5.6/36) solution which experienced rapid and significant increase of all viscoelastic properties. Such behavior is probably due to DCM evaporation which leads to rapid precipitation and gelification of PA11(36). Such an effect could explain the different behaviors during electrospinning of each solution. Thus, it is not the initial rheological properties which could explain the fabrication of regular fibers with the 12/1 PA11(5.6/36) solution but their rapid increase during the solvent evaporation.

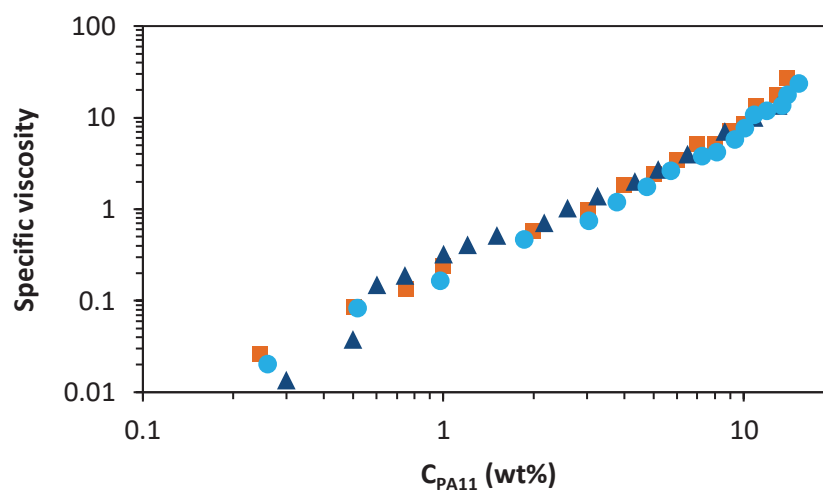


**Figure 2.14.** Specific viscosity as a function of the total PA11 mass concentration (light blue circles: PA11(5.6), orange squares: PA11(5.6/36) with a ratio 14/1 and dark blue triangles: PA11(5.6/36) with a ratio 12/1) in a solvent composed of FA and DCM 50/50 v/v.

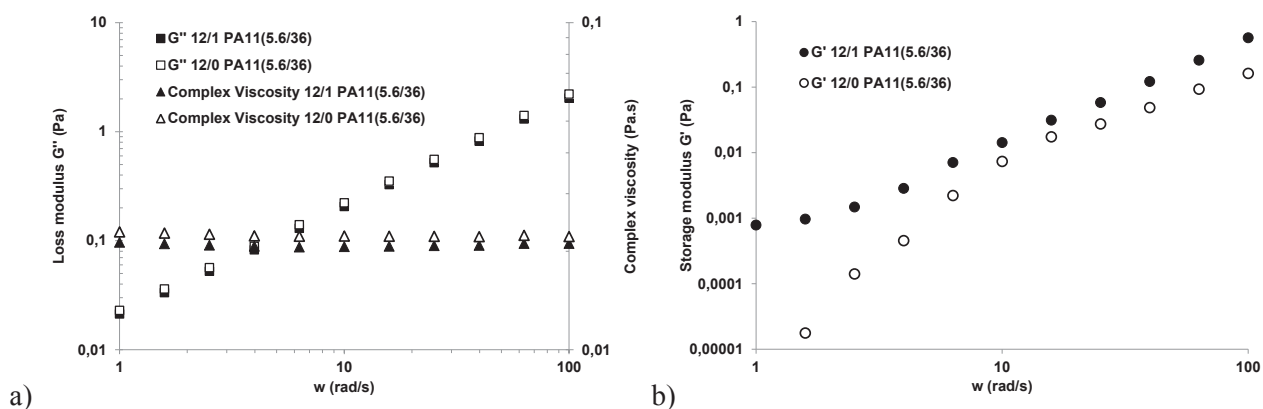


**Figure 2.15.** Viscoelastic properties of 12/1 and 12/0 PA11 (5.6/36) blends.

In conclusion, the use of two polymers of low and higher molar mass allows decreasing the mean fiber diameter. The PA11 of high molar mass ensures the continuity of the nanofiber produced by electrospinning whereas the introduction into the formulation of the PA11 of low molar mass makes it possible to increase the mass concentration in polymer without significantly increasing the nanofiber diameter. The fabrication of fibers, which is linked with a high number of entanglements between polymer chains, could sadly neither be evidenced by a variation in surface tension, nor by a variation in conductivity, nor by a variation in viscosity of the used solution. Further viscoelastic measurements should be conducted in order to evidence the physical impact of the addition of a small amount of high molar mass PA11 in the blend on the gelification during solvent evaporation. Nevertheless, the variation of the distribution of the molar mass enabled the fabrication of mats which are composed of fibers having a mean diameter of 100 nm from a solution concentrated at 13 wt% in PA11. Without this strategy, the thinnest continuous fibers (178 nm) were obtained from a solution concentrated at 6 wt% in PA11. Tailoring the distribution of the molar mass allows thus the fabrication of nanofibrous mats composed of thin fibers from concentrated solutions. Consequently, it guarantees high productivities.

## 2.4 Characterization of electrospun PA11 mats

The advantages linked to the fabrication of mats with thin fibers are highlighted in this part in the light of liquid filtration applications. Two kinds of mats with different average fiber diameters have been fabricated: mats composed of fibers with diameters of approximately 100 nm and mats composed of fibers with diameters of approximately 500 nm. They are compared by their pore size (in relation with the thickness), their mechanical properties and their hydrophilic properties.

Mats with ultrathin diameters of approximately 100 nm ( $100 \pm 25$  nm) were produced with the 12/1 wt% PA11(5.6/36) blend in FA/DCM v/v. They are called D100. Mats were not produced with the 14/1 wt% PA11(5.6/36) blend because of drying problems at the tip of the needle during the electrospinning process. Mats composed of fibers with mean diameters of 500 nm ( $489 \pm 199$  nm) were electrospun from a solution composed of 6 wt% PA11(36) in FA/DCM v/v and are called D500. SEM images of the electrospun mats can be seen in Figure 2.16.

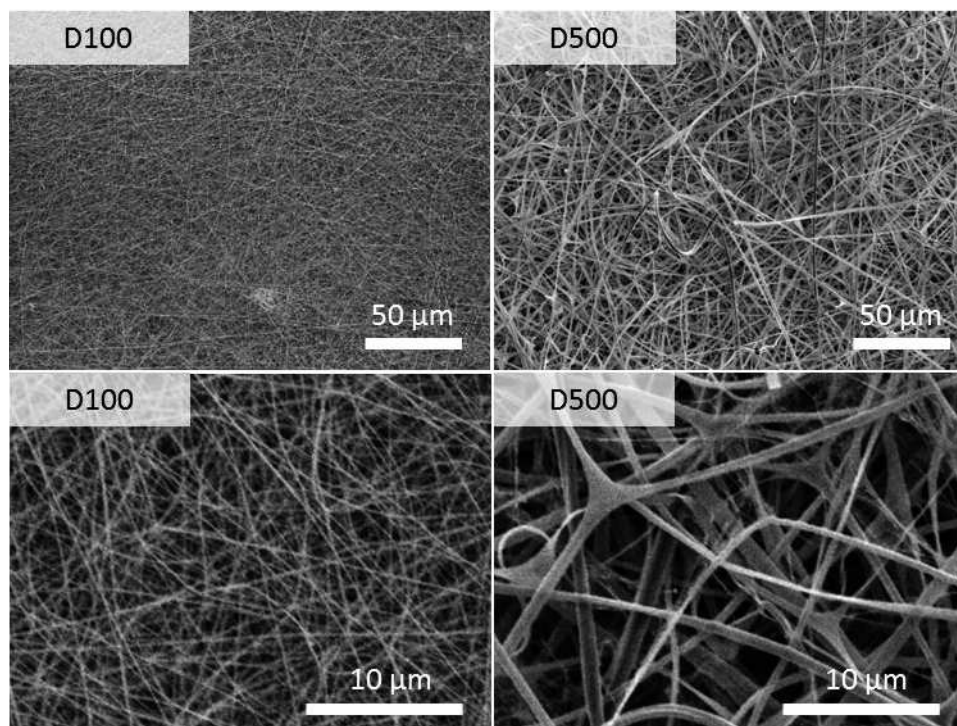


**Figure 2.16.** D100 and D500 liquid filtration mats.

#### 2.4.1 Hydrophilic properties

Contact angles of deionized water on D100 and D500 mats have been measured and compared with the contact angles of deionized water on a PA11(5.6) film, on a PA11(36) film and on a film composed of a PA11(5.6):PA11(36) ratio of 12:1, which is equivalent to the composition of D100 mats (Figure 2.17). The contact angle on films is approximately of  $62^\circ$  whereas it increased to  $128^\circ$  on nanofibrous mats due to the roughness of the surface. The contact angle value is here independent of the fiber diameter contrary to previous findings [40]. It is worth noting that D100 and D500 could be prone to fast fouling during aqueous filtration trials as the contact angle is high and as mats are more easily fouled when the hydrophobicity is enhanced [41]. Diverse strategies could be used in order to decrease the hydrophobicity of D100 and D500 mats such as coating, blending or grafting [40] and to consequently postpone fouling phenomena.

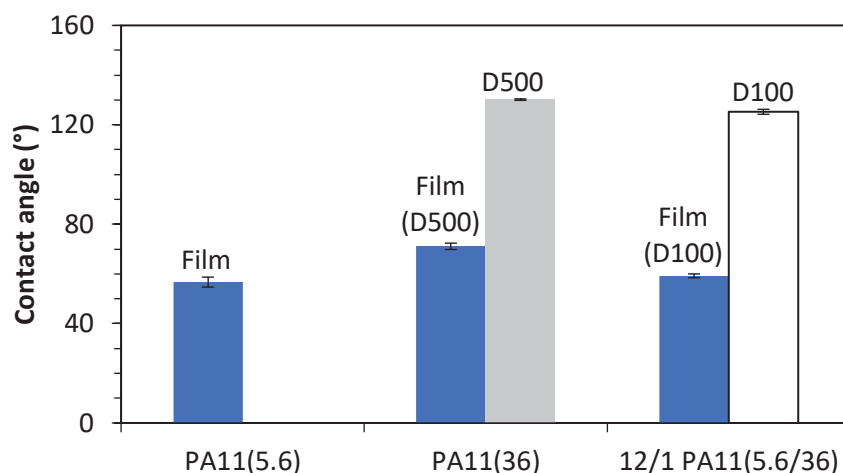


**Figure 2.17.** Contact angles of water droplets on films (in blue of PA11(5.6), PA11(36) and 12/1 PA11(5.6/36)) and on electrospun mats (D100 in white and D500 in grey).

#### 2.4.2 Mechanical properties

Mechanical tests were performed on D100 and D500 mats under uniaxial tension (Figure 2.18). The elastic modulus remains unchanged but the yield strength and the elongation at break increase with the fiber diameter. Generally, in the case of individual electrospun fibers smaller than 1  $\mu\text{m}$ , the young's modulus and the yield strength increase as the fiber diameter decreases contrary to the elongation at break which is reduced [42,43]. Pai et al. [44] correlated this behavior with an increase of the molecular level of orientation of fibers when the fiber diameter decreases due to the fact that smaller fibers have undergone greater extensional deformation during the electrospinning process. However, for non-woven mats, different deformation mechanisms take place during mechanical trials: fiber alignment, fiber bending and network consolidation which are influenced by the structure of mats as fibers are entangled, can be fused together at fiber-fiber junction points and may be composed of some defects such as beaded-fibers. More precisely, first, fibers oriented in the direction of the applied strain align along this direction whereas fibers oriented transverse to the applied strain are prone to bending [45]. Second, Huang et al. [46] highlighted the fact that mats containing beads and beaded fibers show poorer mechanical properties than bead-free fibers. Indeed, beads reduce cohesive forces between fibers. Third, a lack of bonding facilitates fiber orientation and stretching [47] but inter-bonded fibrous structures promote nevertheless an enhancement of the mechanical properties [48,49]. Fourth, concerning the fiber diameter, a difference in crystallinity and in molecular orientation affect the mechanical properties as in the case of individual electrospun fibers [47]. In addition, mechanical properties are influenced by the core and the skin morphology of fibers which vary with the fiber diameter as the core part diminished when the diameter is reduced [47]. Finally, fifth, Pai et al. [50] evidenced the role of the fiber curvature on nonwoven mats' mechanical properties. They observed that the fibers with the smallest diameters are the most curved ones as a consequence of low flexural rigidity of the submicron diameter fibers. In our case the higher mechanical properties of D500 compared to D100 can be explained by the fact that the density of nonwoven mats increases when the fiber diameter decreases [51], and that consequently D100 fibers are more crossed than D500 inducing more friction between fibers. Furthermore, fiber-fiber junction points are far more numerous in D500 mats than in D100 mats (Figure 2.16). Even if it suggests that D500 fibers can less orientate and stretch than D100 fibers, inter-bonded fibers reinforce D500 mechanical

properties. So, on the one end, mats composed of fibers with small diameter induce fine pores which are crucial for high filtration efficiencies. On the other hand, they are mechanically weaker. Optimal fiber diameter can be adjusted according to the application depending on efficiency and mechanical strength specifications.

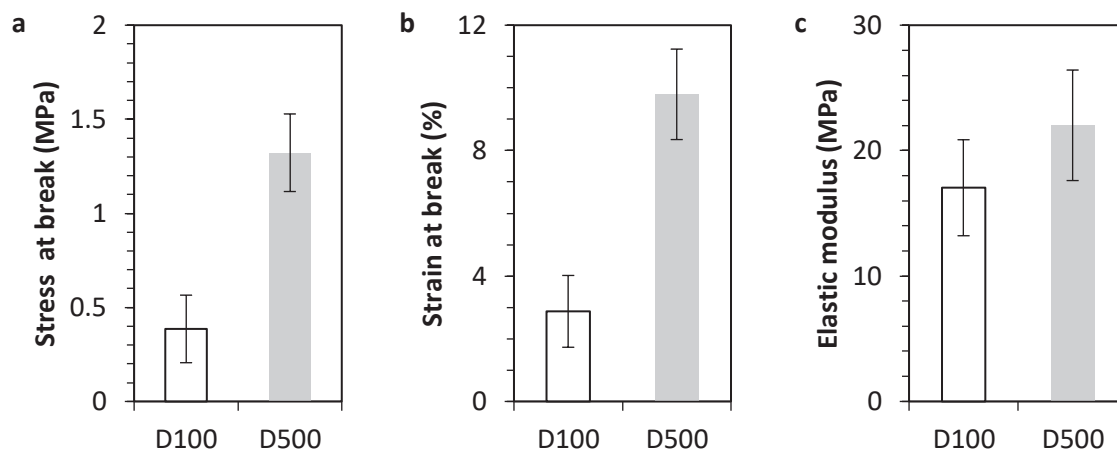


**Figure 2.18.** a) Stress at break, b) Strain at break and c) Elastic modulus of D100 (in white) and D500 (in grey).

#### 2.4.3 Pore size, thickness and fiber diameter

First, as predicted in the literature [10], at equal thicknesses, the pore size decreases with the mean fiber diameter (Figure 2.19). Indeed, the mean pore size of D100 mats is always lower than the mean pore size of D500 for the same thickness. Second, it can be seen that for both D100 and D500, an increase of the thickness is linked with a decrease of the pore size. This result has already been observed by Wang et al. [10]. The explanation lies in the fact that as fibers are deposited on the collector, fibers can intersect and divide pores, forming thus new smaller pores. Nevertheless, they add that this process reaches a plateau above a critical thickness. It seems that for D100 mats, this plateau is reached above a mat thickness of 45  $\mu\text{m}$  whereas it is reached approximately for a thickness of 70  $\mu\text{m}$  for D500 mats. In conclusion, above 40  $\mu\text{m}$ , the pore size of D100 mats remains constant at approximately  $0.37 \pm 0.01 \mu\text{m}$ . This value is in agreement with the specification of the CLARIFIL project (pore size between 0.2 and 0.8  $\mu\text{m}$ ).



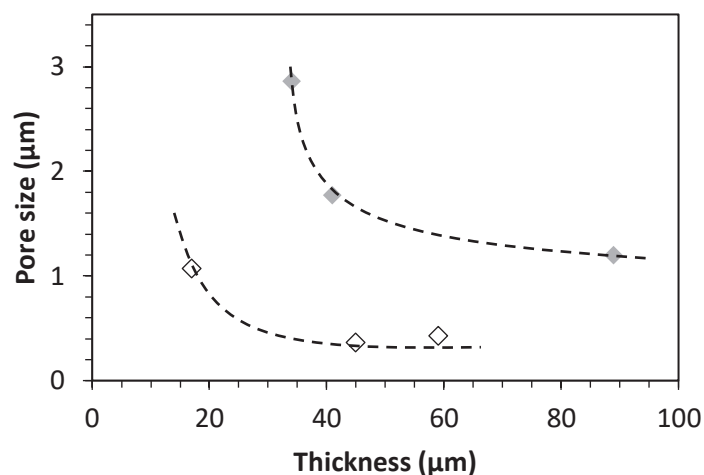


**Figure 2.19.** Pore size as a function of the mat thickness and the fiber diameter for D500 mats (grey diamonds) and D100 mats (white diamonds).

## 2.5 Conclusion

The chapter evidences four strategies allowing the decrease to the mean fiber diameter of PA11 fibers: choosing a solvent which evaporation rate is slow at the working temperature but that nevertheless enables the fabrication of dried nanofibrous mats, increasing the humidity, decreasing the concentration and mixing two polyamides 11 of different molar mass. This last strategy is very advantageous as it allows the fabrication of thin fibers from concentrated solutions which means that productivity is simultaneously enhanced. Furthermore, it can be used with other solutions and can be implemented on any electrospinning setups, even multi-jet setups. Thanks to this method, fibers as thin as 100 nm were electrospun from a polymer concentration of 13 wt%. Mats composed of fibers with average diameters of 100 nm fulfill the specifications of the CLARIFIL project as the pore size ( $0.37 \pm 0.01 \mu\text{m}$ ) is comprised between 0.2 and 0.8  $\mu\text{m}$ . Mats with fibers measuring in diameter 500 nm have pores bigger than the range targeted. These values justify the study of this whole chapter, namely the search for the fabrication of thin fibers. Finally, it should be noted that PA11 mats are hydrophobic and that PA11 mats with thin diameters are mechanically weaker than mats with thicker diameters. The main perspective of this work is to perform filtration trials. This was not achieved here as the toxicity of the solvent compelled us to work with a “greener” solvent for environmentally friendly reasons.

## References

- [1] <https://www.arkema.com/en/products/product-finder/product-viewer/Rilsan-Polyamide-11-Resin/> (accessed March 22, 2018).
- [2] R. Rulken, C. Koning, 5.18 - Chemistry and Technology of Polyamides, in: K. Matyjaszewski, M. Möller (Eds.), *Polym. Sci. Compr. Ref.*, Elsevier, Amsterdam, 2012: pp. 431–467.
- [3] K. Behler, M. Havel, Y. Gogotsi, New solvent for polyamides and its application to the electrospinning of polyamides 11 and 12, *Polymer*. 48 (2007) 6617–6621. doi:10.1016/j.polymer.2007.08.058.
- [4] M. Dhanalakshmi, Preparation and characterization of electrospun fibers of Nylon 11, *EXPRESS Polym. Lett.* 2 (2008) 540–545. doi:10.3144/expresspolymlett.2008.65.
- [5] D. Carponcin, E. Dantras, G. Aridon, F. Levallois, L. Cadiergues, C. Lacabanne, Evolution of dispersion of carbon nanotubes in Polyamide 11 matrix composites as determined by DC conductivity, *Compos. Sci. Technol.* 72 (2012) 515–520. doi:10.1016/j.compscitech.2011.12.012.
- [6] G. Mago, D.M. Kalyon, F.T. Fisher, Nanocomposites of polyamide-11 and carbon nanostructures: Development of microstructure and ultimate properties following solution processing, *J. Polym. Sci. Part B Polym. Phys.* 49 (2011) 1311–1321. doi:10.1002/polb.22311.
- [7] Z. Zhou, W. Lin, X.-F. Wu, Electrospinning ultrathin continuous cellulose acetate fibers for high-flux water filtration, *Colloids Surf. Physicochem. Eng. Asp.* 494 (2016) 21–29. doi:10.1016/j.colsurfa.2015.11.074.
- [8] L. Li, R. Hashaikeh, H.A. Arafat, Development of eco-efficient micro-porous membranes via electrospinning and annealing of poly (lactic acid), *J. Membr. Sci.* 436 (2013) 57–67. doi:10.1016/j.memsci.2013.02.037.
- [9] H. Ma, B.S. Hsiao, B. Chu, Functionalized electrospun nanofibrous microfiltration membranes for removal of bacteria and viruses, *J. Membr. Sci.* 452 (2014) 446–452. doi:10.1016/j.memsci.2013.10.047.
- [10] R. Wang, Y. Liu, B. Li, B.S. Hsiao, B. Chu, Electrospun nanofibrous membranes for high flux microfiltration, *J. Membr. Sci.* 392 (2012) 167–174. doi:10.1016/j.memsci.2011.12.019.
- [11] D. Hussain, F. Loyal, A. Greiner, J.H. Wendorff, Structure property correlations for electrospun nanofiber nonwovens, *Polymer*. 51 (2010) 3989–3997. doi:10.1016/j.polymer.2010.06.036.
- [12] A. Greiner, J.H. Wendorff, Electrospinning: A Fascinating Method for the Preparation of Ultrathin Fibers, *Angew. Chem. Int. Ed.* 46 (2007) 5670–5703. doi:10.1002/anie.200604646.
- [13] N. Bhardwaj, S.C. Kundu, Electrospinning: A fascinating fiber fabrication technique, *Biotechnol. Adv.* 28 (2010) 325–347. doi:10.1016/j.biotechadv.2010.01.004.
- [14] N. Lavielle, A.-M. Popa, M. de Geus, A. Hébraud, G. Schlatter, L. Thöny-Meyer, R.M. Rossi, Controlled formation of poly( $\epsilon$ -caprolactone) ultrathin electrospun nanofibers in a hydrolytic degradation-assisted process, *Eur. Polym. J.* 49 (2013) 1331–1336. doi:10.1016/j.eurpolymj.2013.02.038.
- [15] K. Riazi, J. Kübel, M. Abbasi, K. Bachtin, S. Indris, H. Ehrenberg, R. Kádár, M. Wilhelm, Polystyrene comb architectures as model systems for the optimized solution electrospinning of branched polymers, *Polymer*. 104 (2016) 240–250. doi:10.1016/j.polymer.2016.05.032.
- [16] C. Huang, S. Chen, C. Lai, D.H. Reneker, H. Qiu, Y. Ye, H. Hou, Electrospun polymer nanofibres with small diameters, *Nanotechnology*. 17 (2006) 1558. doi:10.1088/0957-4484/17/6/004.
- [17] C. Mit-uppatham, M. Nithitanakul, P. Supaphol, Ultrafine Electrospun Polyamide-6 Fibers: Effect of Solution Conditions on Morphology and Average Fiber Diameter, *Macromol. Chem. Phys.* 205 (2004) 2327–2338. doi:10.1002/macp.200400225.
- [18] S. De Vrieze, T.V. Camp, A. Nelvig, B. Hagström, P. Westbroek, K. De Clerck, The effect of temperature and humidity on electrospinning, *J. Mater. Sci.* 44 (2008) 1357–1362. doi:10.1007/s10853-008-3010-6.

- [19] L. Persano, A. Camposeo, C. Tekmen, D. Pisignano, Industrial Upscaling of Electrospinning and Applications of Polymer Nanofibers: A Review, *Macromol. Mater. Eng.* 298 (2013) 504–520. doi:10.1002/mame.201200290.
- [20] F.E. Ahmed, B.S. Lalia, R. Hashaikeh, A review on electrospinning for membrane fabrication: Challenges and applications, *Desalination*. 356 (2015) 15–30. doi:10.1016/j.desal.2014.09.033.
- [21] J. Kula, A. Linka, M. Tunak, D. Lukas, Image analysis of jet structure on electrospinning from free liquid surface, *Appl. Phys. Lett.* 104 (2014) 243114. doi:10.1063/1.4884597.
- [22] D. Lukas, A. Sarkar, P. Pokorny, Self-organization of jets in electrospinning from free liquid surface: A generalized approach, *J. Appl. Phys.* 103 (2008) 84309. doi:10.1063/1.2907967.
- [23] M. Yu, R.-H. Dong, X. Yan, G.-F. Yu, M.-H. You, X. Ning, Y.-Z. Long, Recent Advances in Needleless Electrospinning of Ultrathin Fibers: From Academia to Industrial Production, *Macromol. Mater. Eng.* (2017). doi:10.1002/mame.201700002.
- [24] S. Moon, M. Gil, K.J. Lee, Syringeless Electrospinning toward Versatile Fabrication of Nanofiber Web, *Sci. Rep.* 7 (2017) 41424. doi:10.1038/srep41424.
- [25] K. Desai, K. Kit, J. Li, P. Michael Davidson, S. Zivanovic, H. Meyer, Nanofibrous chitosan non-wovens for filtration applications, *Polymer*. 50 (2009) 3661–3669. doi:10.1016/j.polymer.2009.05.058.
- [26] A. Cooper, R. Oldinski, H. Ma, J.D. Bryers, M. Zhang, Chitosan-based nanofibrous membranes for antibacterial filter applications, *Carbohydr. Polym.* 92 (2013) 254–259. doi:10.1016/j.carbpol.2012.08.114.
- [27] S. Kaur, D. Rana, T. Matsuura, S. Sundarajan, S. Ramakrishna, Preparation and characterization of surface modified electrospun membranes for higher filtration flux, *J. Membr. Sci.* 390–391 (2012) 235–242. doi:10.1016/j.memsci.2011.11.045.
- [28] S.E. Kim, D.N. Heo, J.B. Lee, J.R. Kim, S.H. Park, S.H. Jeon, I.K. Kwon, Electrospun gelatin/polyurethane blended nanofibers for wound healing, *Biomed. Mater.* 4 (2009) 44106. doi:10.1088/1748-6041/4/4/044106.
- [29] B. Ding, E. Kimura, T. Sato, S. Fujita, S. Shiratori, Fabrication of blend biodegradable nanofibrous nonwoven mats via multi-jet electrospinning, *Polymer*. 45 (2004) 1895–1902. doi:10.1016/j.polymer.2004.01.026.
- [30] C.D. Saquing, C. Tang, B. Monian, C.A. Bonino, J.L. Manasco, E. Alsberg, S.A. Khan, Alginate–Polyethylene Oxide Blend Nanofibers and the Role of the Carrier Polymer in Electrospinning, *Ind. Eng. Chem. Res.* 52 (2013) 8692–8704. doi:10.1021/ie302385b.
- [31] R.A. Basheer, A.R. Hopkins, P.G. Rasmussen, Dependence of Transition Temperatures and Enthalpies of Fusion and Crystallization on Composition in Polyaniline/Nylon Blends, *Macromolecules*. 32 (1999) 4706–4712. doi:10.1021/ma981935r.
- [32] G.J. Kettle, Variation of the glass transition temperature of nylon-6 with changing water content, *Polymer*. 18 (1977) 742–743. doi:10.1016/0032-3861(77)90244-0.
- [33] B.D. Schoenmaker, L.V. der Schueren, R. Zügler, A. Goethals, P. Westbroek, P. Kiekens, T. Nyokong, K.D. Clerck, Effect of the relative humidity on the fibre morphology of polyamide 4.6 and polyamide 6.9 nanofibres, *J. Mater. Sci.* 48 (2012) 1746–1754. doi:10.1007/s10853-012-6934-9.
- [34] S. De Vrieze, B. De Schoenmaker, Ö. Ceylan, J. Depuydt, L. Van Landuyt, H. Rahier, G. Van Assche, K. De Clerck, Morphologic study of steady state electrospun polyamide 6 nanofibres, *J. Appl. Polym. Sci.* 119 (2011) 2984–2990. doi:10.1002/app.33036.
- [35] E. Marsano, L. Francis, F. Giunco, Polyamide 6 nanofibrous nonwovens via electrospinning, *J. Appl. Polym. Sci.* (2010) 1754–1765. doi:10.1002/app.32118.
- [36] R.H. Colby, Structure and linear viscoelasticity of flexible polymer solutions: comparison of polyelectrolyte and neutral polymer solutions, *Rheol. Acta*. 49 (2010) 425–442. doi:10.1007/s00397-009-0413-5.

- [37] M.G. McKee, G.L. Wilkes, R.H. Colby, T.E. Long, Correlations of Solution Rheology with Electrospun Fiber Formation of Linear and Branched Polyesters, *Macromolecules*. 37 (2004) 1760–1767. doi:10.1021/ma035689h.
- [38] S.L. Shenoy, W.D. Bates, H.L. Frisch, G.E. Wnek, Role of chain entanglements on fiber formation during electrospinning of polymer solutions: Good solvent, non-specific polymer-polymer interaction limit, *Polymer*. 46 (2005) 3372–3384. doi:10.1016/j.polymer.2005.03.011.
- [39] L. Palangetic, N.K. Reddy, S. Srinivasan, R.E. Cohen, G.H. McKinley, C. Clasen, Dispersity and spinnability: Why highly polydisperse polymer solutions are desirable for electrospinning, *Polymer*. 55 (2014) 4920–4931. doi:10.1016/j.polymer.2014.07.047.
- [40] R. Kumar, A.F. Ismail, Fouling control on microfiltration/ultrafiltration membranes: Effects of morphology, hydrophilicity, and charge, *J. Appl. Polym. Sci.* 132 (2015) 42042. doi:10.1002/app.42042.
- [41] D. Rana, T. Matsuura, Surface Modifications for Antifouling Membranes, *Chem. Rev.* 110 (2010) 2448–2471. doi:10.1021/cr800208y.
- [42] E.P.S. Tan, S.Y. Ng, C.T. Lim, Tensile testing of a single ultrafine polymeric fiber, *Biomaterials*. 26 (2005) 1453–1456. doi:10.1016/j.biomaterials.2004.05.021.
- [43] S.-C. Wong, A. Baji, S. Leng, Effect of fiber diameter on tensile properties of electrospun poly( $\epsilon$ -caprolactone), *Polymer*. 49 (2008) 4713–4722. doi:10.1016/j.polymer.2008.08.022.
- [44] C.-L. Pai, M.C. Boyce, G.C. Rutledge, Mechanical properties of individual electrospun PA 6(3)T fibers and their variation with fiber diameter, *Polymer*. 52 (2011) 2295–2301. doi:10.1016/j.polymer.2011.03.041.
- [45] M.N. Silberstein, C.-L. Pai, G.C. Rutledge, M.C. Boyce, Elastic–plastic behavior of non-woven fibrous mats, *J. Mech. Phys. Solids*. 60 (2012) 295–318. doi:10.1016/j.jmps.2011.10.007.
- [46] Z.-M. Huang, Y.Z. Zhang, S. Ramakrishna, C.T. Lim, Electrospinning and mechanical characterization of gelatin nanofibers, *Polymer*. 45 (2004) 5361–5368. doi:10.1016/j.polymer.2004.04.005.
- [47] A. Baji, Y.-W. Mai, S.-C. Wong, M. Abtahi, P. Chen, Electrospinning of polymer nanofibers: Effects on oriented morphology, structures and tensile properties, *Compos. Sci. Technol.* 70 (2010) 703–718. doi:10.1016/j.compscitech.2010.01.010.
- [48] J. Park, E.-S. Lee, T. Amna, Y. Jang, D.H. Park, B.-S. Kim, Effects of heat-treatment on surface morphologies, mechanical properties of nanofibrous poly(propylene carbonate) biocomposites and its cell culture, *Colloids Surf. Physicochem. Eng. Asp.* 492 (2016) 138–143. doi:10.1016/j.colsurfa.2015.11.075.
- [49] S.-S. Choi, S.G. Lee, C.W. Joo, S.S. Im, S.H. Kim, Formation of interfiber bonding in electrospun poly(etherimide) nanofiber web, *J. Mater. Sci.* 39 (2004) 1511–1513. doi:10.1023/B:JMSC.0000013931.84760.b0.
- [50] C.-L. Pai, M.C. Boyce, G.C. Rutledge, On the importance of fiber curvature to the elastic moduli of electrospun nonwoven fiber meshes, *Polymer*. 52 (2011) 6126–6133. doi:10.1016/j.polymer.2011.10.055.
- [51] I.M. Hutten, G. Pelletier, G. Smaldon, J. Simpson, C. Dawes, L. Jones, *Handbook of Nonwoven Filter Media*, Elsevier, 2007.



# 3

## ELECTROSPINNING IN AQUEOUS SOLVENTS

*Contrary to Chapter 2, where the electrospinning process required the use of toxic solvents to solubilize water insoluble polymers (such as formic acid and dichloromethane in the case of polyamide 11) a new strategy has been developed in Chapter 3 to carry out the process in aqueous solvents for environmentally friendly reasons. Two ways have been investigated. The first one is based on the electrospinning of aqueous suspensions of water-insoluble polymer. The second one consists in electrospinning a non-polymeric and water-soluble molecule, tannic acid, by exploiting the supramolecular interactions present in the solution which account for the formation of a nanofiber by electrospinning.*

*Parts of the chapter are published in:*

Domitille Mailley, Allais, Manon, Pascal Hébraud, Dris Ihiawakrim, Vincent Ball, Florent Meyer, Anne Hébraud, and Guy Schlatter. “Polymer-Free Electrospinning of Tannic Acid and Cross-Linking in Water for Hybrid Supramolecular Nanofibres.” *Nanoscale* 10, no. 19 (2018): 9164–73. <https://doi.org/10.1039/C8NR01067F>.



## 3A ELECTROSPINNING OF AQUEOUS SUSPENSIONS OF WATER INSOLUBLE POLYMERS

The electrospinning of aqueous suspensions of water insoluble polymers is detailed in this part. The solvent is composed of water only. Four polymers were electrospun as suspensions: co-polyamide (coPA), polypropylene (PP), a copolymer of vinylidene fluoride and methyl methacrylate (PVDF-PMMA) and polyvinylidene fluoride (PVDF).

### 3A.1 Introduction

The electrospinning of water insoluble polymers such as polyvinylidene fluoride [1], poly(methyl methacrylate) [2], polypropylene [3] and polyamides [4] require most of the time organic solvents. Unfortunately, their evaporation during the electrospinning process is harmful. In addition, removing residual solvent from scaffold after processing is environmentally unfriendly, costly and time consuming. In order to avoid organic solvents, water can be used. Nevertheless, the choice of water-soluble polymer is limited and electrospun mats need to be post-processed after electrospinning to become insoluble in water. For instance, poly(vinyl alcohol) (PVA) mats become insoluble in water after crosslinking with maleic acid [5,6] or glyoxal [7] after a heat treatment. Melt electrospinning is another method which does not require any solvent [8]. Different water insoluble polymers have even been successfully electrospun with this strategy such as polyethylene [9] and polypropylene [10]. However, the melt electrospinning setup is uneconomical and yields fiber diameters larger than solution electrospinning [8]. A last alternative consists in electrospinning aqueous suspensions of water insoluble polymers. Several polymer suspensions such as polystyrene [11], poly(hexanmethylene adipate)-polyethylene glycol block copolymers [12], polyurethane [13] or polycaprolactone [14] dispersions have already been electrospun. The fabrication of mats composed of continuous fibers from aqueous suspensions is achieved in two or three steps: electrospinning, an optional post treatment and washing. First, a suspension blended with a template polymer are electrospun. Throughout this step, the template polymer allows the formation of fibers thanks to entanglements between its polymer chains. Then, a post treatment, crosslinking [15,16] or curing, is required for polymers having a glass transition temperature close to room temperature or above. The post treatment allows the particles contained in the fibers to fuse and/or bond together. After the post treatment, particles bond together and contribute to the inner cohesion of fibers. If the glass transition temperature of polymer particles is sufficiently low, the post treatment step is unnecessary as particles merge together during electrospinning due to the fact that they are prone to deformation and film formation [11,17]. Finally, washing allows the elimination of the template polymer. After washing, fibers are composed of bonded or fused particles, possibly coated with a small amount of template polymer when not properly washed [16]. Regarding the application, hydrophobic fibers (composed of hydrophobic polymer suspensions) covered with a small amount of a hydrophilic polymer might be interesting. This is the case of the filtration of aqueous liquids as hydrophilic filters have a high permeability and thus allow reducing applied filtration pressures. A reduction of the applied filtration pressure is linked to energy saving and costs reduction which goes along with an economically friendly process.

In this part, conditions allowing the fabrication of fibers from aqueous suspensions by this strategy were first established using the co-polyamide suspension (coPA). The influence of the formulation, the curing step and the washing step on the morphology of fibers were studied. Mats composed of polyvinylidene fluoride (PVDF), a copolymer of vinylidene fluoride and methyl methacrylate (PVDF-PMMA) and maleic anhydride

grafted polypropylene (MAPP) suspensions were then electrospun, characterized and compared towards liquid filtration applications. Optimal conditions for the electrospinning of fibers and the fabrication of water-stable mats were thereby established. Further mechanical, hydrophilic and liquid filtration properties of mats were assessed and compared. This part aims finally at proving that this environmentally friendly strategy, yielding liquid filtration mats comparable to those fabricated by solution electrospinning, could be a serious alternative to the traditional solution electrospinning process. It would then solve issues linked to the evaporation of organic solvents and ease the industrialization of the electrospinning process. Finally, the reader might be interested in reading Appendix 4 which deals with the fabrication of fibers from aqueous suspensions by another strategy: co-axial electrospinning.

## 3A.2 Materials and methods

### 3A.2.1 Materials

Co-polyamide (coPA) suspensions (D5030), polyvinylidene fluoride (PVDF) suspensions and a copolymer of vinylidene fluoride and methyl methacrylate (PVDF-PMMA) in suspensions were provided by Arkema. Maleic anhydride grafted polypropylene (MAPP) suspension (FGLASS X35) was provided by Michelman. Solid content and particle size of suspensions, measured by DLS (Appendix 5), are given in Table 3A.1. The template polymer is polyvinyl alcohol Mowiol® 18-88 ( $M_w = 130\,000$  g/mol, 86.7-88.7 mol% hydrolysis) (PVA) purchased from Sigma-Aldrich.

Suspension	Solid content	Diameter of particles
coPA	$29.2 \pm 0.6$ wt%	$104 \pm 34$ nm
MAPP	$33.8 \pm 0.8$ wt%	$61 \pm 10$ nm
PVDF-PMMA	$45.7 \pm 0.8$ wt%	$133 \pm 15$ nm
PVDF	$24.7 \pm 0.8$ wt%	$142 \pm 14$ nm

**Table 3A.1.** Solid content of aqueous suspensions and diameter of particles contained in the suspensions.

### 3A.2.2 Blend preparation and electrospinning

PVA solutions are prepared and first heated at 50°C to help PVA solubilization during 12 hours. CoPA, MAPP and PVDF-PMMA suspensions are then blended 1 hour prior to the experiments with the adequate aqueous PVA solution at room temperature. Aqueous PVDF/PVA blends are prepared by directly adding solid PVA to the PVDF suspension due to the low solid content in the initial suspension. Aqueous PVDF/PVA blends are then heated at 50°C to help PVA solubilization during 12 hours.

A horizontal homemade electrospinning setup is used. It is composed of a uniaxial stainless-steel needle connected to a high-power voltage supply (Spellman SL10), a syringe pump (Intertek) and a rotary cylinder collector (rotation speed of 150 rpm). The distance between the needle and the collector was 15cm; the infusion rate was 0.3mL/h; the applied voltage at the needle was 18 kV and at the collector -2 kV. The

temperature was  $22 \pm 1$  °C and the humidity was approximately 40%. Electrospun mats were collected on a bakery paper to peel it off more easily.

### 3A.2.3 Fiber curing and removal of template polymers

Samples containing coPA, PP, PVDF and PVDF-PMMA were cured at 120°C, 150°C, 200°C and 120°C respectively for 1h. After curing, template polymers were removed by washing in water at room temperature during 24 hours.

### 3A.2.4 Film preparation

Films were prepared by casting from the suspensions. Three films were fabricated in MAPP, PVDF-PMMA and PVDF.

### 3A.2.5 Characterization of the materials

A differential scanning calorimetry apparatus (TA Q200) has been used to determine melting points (Appendix 5).

	<b>Melting point</b>
PVA	190°C
coPA	110 °C
MAPP*	155°C
PVDF-PMMA	94°C**
PVDF	148°C

**Table 3A.2.** Glass transition temperatures and melting points of utilized polymers.

\* A first fusion is observed around 30°C. This fusion could not be explained.

\*\* The melting temperature given for PVDF-PMMA might also just be a relaxation temperature as no crystallization is observed in the cooling ramp (and consequently no fusion on the second heating ramp). The fact that no crystallization was observed might be related to the speed of the cooling ramp which might be too high.

Solid contents in suspensions were measured with a Ohaus MB45 moisture weighing scale.

Dried particles from suspensions and surface morphologies of the samples at each step were imaged by scanning electron microscopy (SEM, VEGA 3, TESCAN) in high vacuum mode using accelerating voltages of 5 kV. The observation of the surface of fibers was achieved by SEM (ZEISS GMINI SEM 500) in high vacuum mode using accelerating voltages of 2 kV. The samples were pre-coated with gold (Q1500R S) before analysis. For each sample showing particles/fibers, the diameter of 100 particles/fibers was measured on 5 different SEM images with the image analysis software Image J.

Conductivity of blends was measured with an electrical conductivity meter (Consort K610). Surface tension was measured from pendant drops with a tensiometer (Tracker, Teclis Instruments). Before surface tension measurement, density of blends was measured by weighing a fixed volume in a pycnometer.

Mats from each step (initial, after curing, after curing and washing) were used for tensile tests. At least 5 samples from each step were mechanically tested. Tensile tests were conducted on TA Discovery HR3 Rheometer equipped with a linear tension geometry, the velocity for the samples was 5  $\mu\text{m/s}$ .

Contact angles of five 4  $\mu\text{L}$  deionized water drops on electrospun mats were measured with a tensiometer (DSA25S) from Krüss.

The infrared analysis of the fibers from each step was performed on a Nicolet 380 Fourier-transform infrared spectrometer (Thermo Electron Corporation) equipped with ATR Smart Omni Sampler. The IR spectra were collected from 4000-400  $\text{cm}^{-1}$ .

Liquid permeability of mats was measured at the IFTS institute (Institut de la Filtration et des Techniques Séparatives (Fr) - International Filter Testing Services (En)). The mean thickness of mats was  $28 \pm 9 \mu\text{m}$ .

### 3A.2.6 Characterization of the filtration efficiency

For filtration trials, silica ( $\text{SiO}_2$ ) micro-particles of 1  $\mu\text{m}$  in size were purchased from Fiber Optic Center. Aqueous suspensions of silica of 0.1 and 0.4  $\mu\text{m}$  in size were purchased from Nissan Chemical Industries. Size distributions of silica particles were assessed by dynamic light scattering (DLS) with an ALV CGS-3 goniometer system equipped with a He-Ne laser (wavelength=633 nm). All experiments were performed at a scattering angle of  $90^\circ$ . Results are displayed in Appendix 10. Suspensions composed of 0.2 wt% of silica particles in water were prepared from each suspension. They are used as feed suspensions for filtration trials. Calibration curves were determined for each micro-filtration feed suspension using a UV-VIS spectrophotometer (UV-2600 from Shimadzu) (Appendix 10). Filtration trials were carried out on a frontal downward Millipore micro syringe filter holder (diameter of the filter holder of 25 mm). A polyamide 11 nonwoven was used as prefilter. The prefilter is characterized in Appendix 2. It does not disturb filtration trials as the silica concentration in the feed suspension and in the filtrate was found to be similar when filtration trials occurred with the prefilter only. For each filtration trials, 10 mL of the feed suspension were filtered, and a flux of 50 mL/h was applied. Separation performance was performed three times per mat for each micro-particles/water mixture. The average thickness of electrospinning filtering membranes is approximately 30  $\mu\text{m}$  ( $29 \pm 8 \mu\text{m}$ ). The presence of any silica particles in the permeate was detected via UV-VIS spectrophotometry (UV-2600, Shimadzu). Calibration curves are given in Appendix 10. The filtration efficiency was determined from the concentration in silica of the feed suspension ( $C_{feed}$ ) and from that of the permeate ( $C_{permeate}$ ) using the separation factor (SF) given by the following formula:

$$SF (\%) = \frac{C_{feed} - C_{permeate}}{C_{feed}} * 100 \quad \text{Equation 3A.1}$$

(Equation 1.1)

### 3A.3 Fabrication of continuous fibers

The fabrication of mats composed of continuous fibers was achieved in three steps: electrospinning, curing and washing. Electrospinning was performed from a blend of a suspension and a template polymer solubilized in water leading to continuous fibers. Throughout this step, the template polymer provides the polymer entanglements necessary to prevent rupture of the jet into droplets, thus ensuring the formation of a

continuous nanofiber (Figure 3A.1a). Curing enables the particles contained in the fibers (and coming from the suspension) to bond and/or fuse together (Figure 3A.1b). Bonded particles form within fibers a new fibrous network and contribute to the inner cohesion of fibers. Finally, washing allows the elimination of the carrier polymer (Figure 3A.1c). After washing, fibers are composed of bonded particles coated with a small amount of template polymer when not properly washed. During the three steps, numerous parameters must be fixed in order to fabricate continuous fibers. The template polymer and its concentration must be chosen as well as the concentration in particles. The choice of the curing temperature is crucial to bond particles together without losing the fibrous structure. Finally, it is important to keep the mat's integrity after washing. This first part details the choices that were made in order to elaborate continuous fibers with a co-polyamide suspension. Co-polyamide (coPA) has been chosen by continuity with the previous chapter. The same study was undergone for all suspensions. Results are presented in Appendix 7.

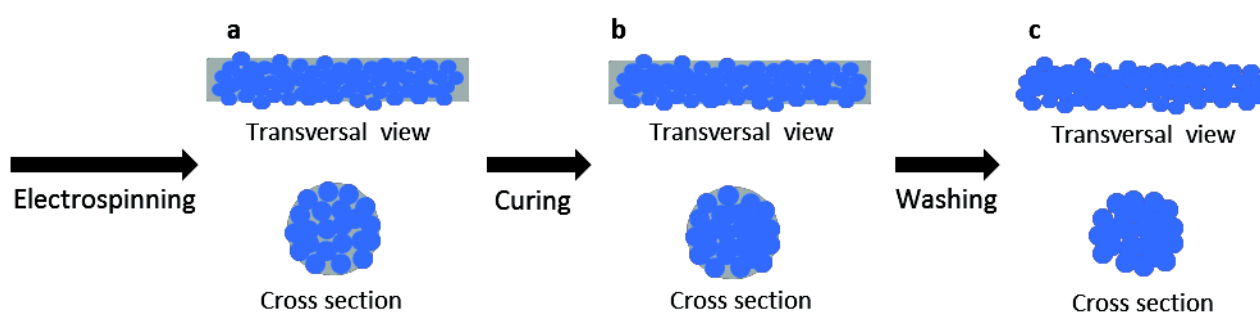


**Figure 3A.1.** Transversal views and cross sections of fibers after a) electrospinning, b) curing and c) washing.

### 3A.3.1 Particles and template polymer concentrations

First and foremost, the template polymer must be water soluble as we decided to electrospin in pure water. In addition, the template polymer is necessary to the formation of fibers during electrospinning. To form fibers either the molar mass or the concentration or both should be high enough to enable the formation of entanglements between polymer chains. However, as particles contained in fibers must be very close to one another in order to be able to bond to the others during the curing step, the concentration of template polymer must be kept as low as possible. A low concentration also eases its removal during the washing step. So, we aim at choosing a template polymer which does not require a high concentration to form continuous fibers. This requirement suggests a template polymer with a high molar mass [16,18,19]. Then, the template polymer should stay solid at the curing temperature in order to keep the fibrous shape. Therefore, its glass transition temperature ( $T_g$ ) for amorphous polymers or its melting temperature for semi-crystalline polymers should be above the curing temperature. The curing temperature depends on the melting temperature of the particles. In the end, at the optimal curing temperature, particles bond or fuse together while the template polymer state remains unchanged. Last but not least, the template polymer should be removed after washing. PVA Mowiol 18-88 (PVA) was chosen as template polymer as it fulfilled the above requirements. It is water-soluble and its melting point (190°C) is above the melting point of the dried co-polyamide particles (110°C) (Table 3A.2 and Appendix 5). Other template polymers were unsuccessfully used (Appendix 6).

The concentration of template polymer plays on the formation of continuous fibers. The effect of PVA concentration is detailed in Figure 3A.2a,b,c. Low concentrations do not allow the formation of continuous fibers as entanglements between polymer chains are not sufficient to form fibers by electrospinning. When the



concentration increases, continuous fibers can be electrospun [20]. The optimal template polymer is obtained for the lowest template polymer concentration allowing the formation of fibers, namely 5 wt% of PVA for 20 wt% of coPA. Fibers are continuous and homogenous in Figure 3A.2c which denotes a good homogeneity of the initial electrospinning suspension. Indeed, Jiang et al. [21] demonstrated that aggregates present in electrospinning suspensions lead to the presence of aggregates in fibers, which is not the case. The surface of fibers is rough which evidences the presence of the particles inside fibers. In colloidal electrospinning, the surface the fibers can be smooth depending on the glass transition temperature of the polymer constituting the particles. The lower the glass transition temperature is, the smoother fibers are due to the fact that particles are prone to deformation and to film formation. When the glass transition temperature is sufficiently low, particles merge together during the electrospinning step. The template polymer can thus be eliminated by washing without curing or crosslinking steps [11,17].

The concentration in coPA also plays an important role on the formation of fibers (Figure 3A.2d,e,f). When the concentration in particles is too low, particles contained in fibers are not close enough to one another. Consequently, they cannot bond together during thermal treatment and the mat is destroyed during the washing step. Above a critical concentration, particles are numerous enough to bond together during the thermal treatment. CoPA concentration was not increased more than 20 wt% due to the fact that the solid content in suspensions was a limiting factor and because 20/5 wt% coPA/PVA blends were viscous.

Finally, for a maximal concentration of 20 wt% of coPA particles, a concentration of 5 wt% of PVA was necessary to fabricate continuous fibers. Similar ratios to our (coPA: PVA 4:1) were also reported in the literature [11,17,22].

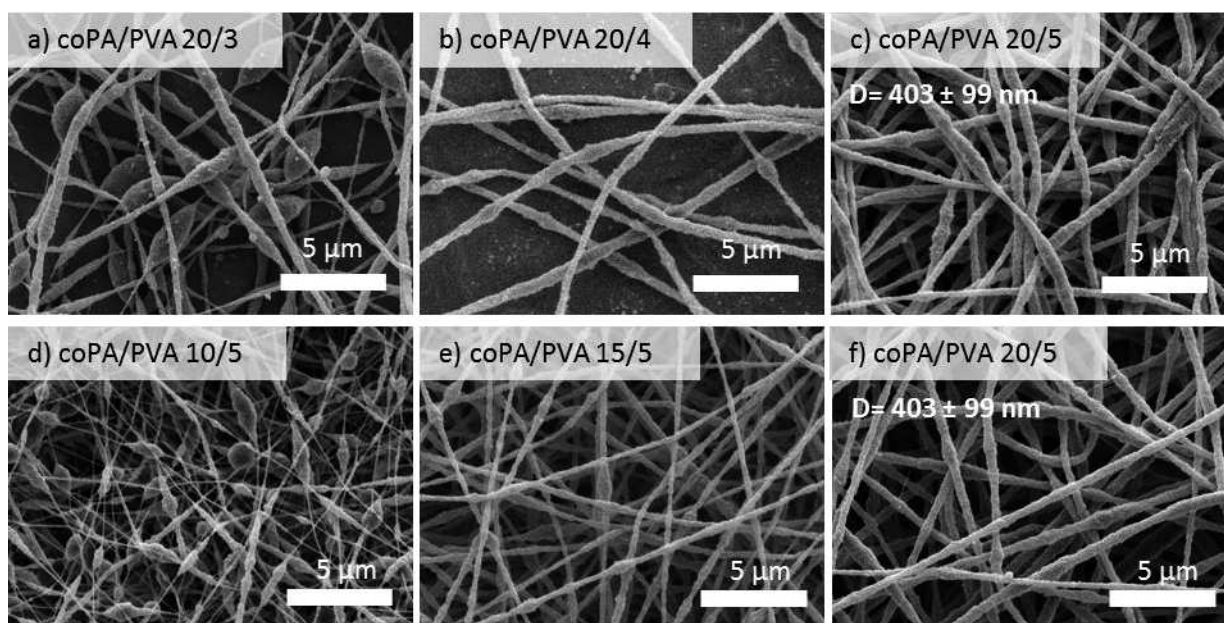


**Figure 3A.2.** SEM images of mats electrospun from a blend of coPA/PVA as a function of PVA concentration: a) 20/3, b) 20/4 and c) 20/5 and as a function of coPA concentration: d) 10/5, e) 15/5 and f) 20/5.



### 3A.3.2 Effect of curing temperature

Curing is here a compulsory step in the process of fiber formation to bond particles together. The choice of the curing temperature is essential as if the temperature is too low, particles cannot bond, and the structure is lost during the washing step. On the contrary, if the curing temperature is too high, the fibrous mat becomes a film. Different curing temperatures were tested in order to determine the optimal curing temperature. It can be seen in Figure 3A.3, that a treatment of 1 hour at a temperature equal or below 120°C preserves the fibrous structure contrary to higher curing temperatures. As a matter of fact, at 140°C, a film is formed. It is recalled that the melting temperature of coPA is 110°C and that of PVA 190°C.

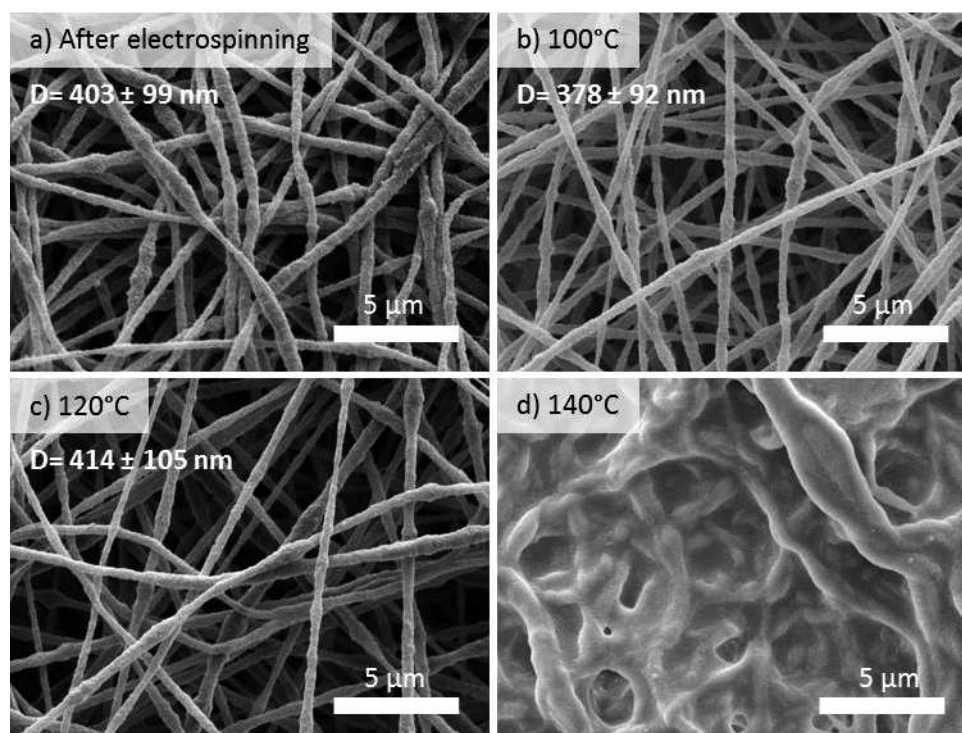


**Figure 3A.3.** SEM images of 20/5 wt% coPA/PVA mats a) after electrospinning and cured at temperatures of b) 100°C, c) 120°C and d) 140°C.

### 3A.3.3 Washing

The polymer template should be removed during the washing step by re-solubilization in water. Contrary to the mat cured at 120°C which was water-stable and washed during 24h (Figure 3A.4c and d), the mat cured at 100°C was immediately destroyed when in contact with water meaning that coPA particles had not been properly bonded during thermal treatment (Figure 3A.4a and b). The result proves the necessity of a thermal treatment. Besides, the shape of coPA particles can still be distinguished in Figure 3A.4d showing that, even if particles have to some extent bonded together during the curing step, they have not yet merged. A better merging of particles is here unthinkable as the curing temperature cannot be increased well above 120°C. Indeed, a thermal treatment of 1h at 140°C turns coPA/PVA fibrous mats into films. So, a curing temperature of 120°C is the optimal temperature allowing the fabrication of coPA fibers. The proportion of PVA remaining in coPA mats was rather difficult to estimate either by DSC or IR spectroscopy even when the washing step was performed at 50°C. As a matter of fact, variations in DSC were too slight. In IR spectrometry, the wave length of coPA and PVA bands were too close to be analyzed (Appendix 8).

Nevertheless, in the literature, PVA as template polymer could easily be removed by washing electrospun mats with the same method [11]. We infer that, at least, some PVA could be removed during the washing step. Regarding the application, hydrophobic fibers (formed from water-insoluble polymer suspensions) covered with a hydrophilic polymer may be interesting in some applications. This is the case of the filtration of aqueous liquids as hydrophilic filters allow a reduction of the applied filtration pressure.

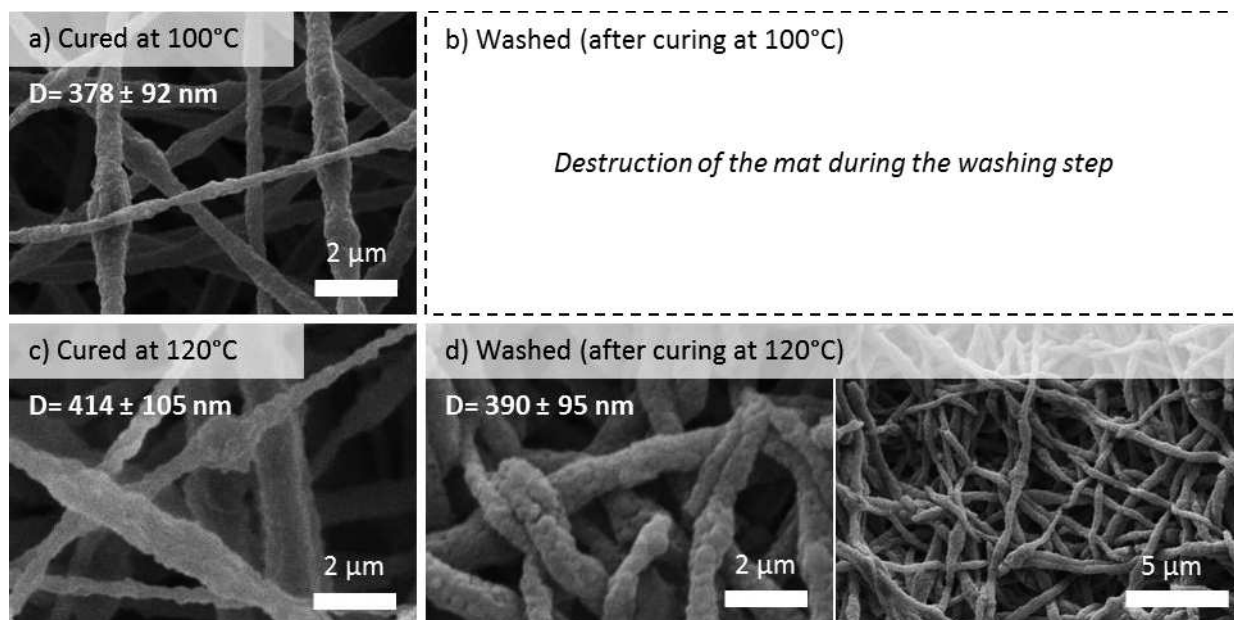


**Figure 3A.4.** SEM images of mats 20/5 wt% coPA/PVA mats a) cured at 100°C and b) washed; c) cured at 120°C and d) washed during 24h.

In conclusion, after choosing the adequate template polymer and determining the optimal parameters for each step, continuous fibers could be fabricated from a 20/5 wt% coPA/PVA blend in water. Mats where cured at 120°C for 1 hour and washed during 24 hours in water. However, these mats had poor mechanical properties. They could hardly be carried by hand after washing. So, in the following, mats based on other suspensions were electrospun with the goal to fabricate fibrous mats for liquid filtering applications.

## 3A.4 Fabrication of liquid filtration mats

### 3A.4.1 Fabrication of mats

PVDF, PVDF-PMMA and MAPP suspensions were blended with PVA and electrospun in water (Figure 3A.5a-b-c). Particles and PVA concentrations were adjusted in order to form continuous fibers as presented in the previous part (Appendix 7). The optimal ratio for MAPP/PVA mats was 20/5 wt% and the curing temperature 150°C. After curing (Figure A3.5d and A3.6a) mats are still fibrous and fibers are poorly interconnected. This might be due to the fact that the temperature of the curing step (150°C) was slightly below the melting point of MAPP (155°C). In addition, the curing temperature chosen for MAPP/PVA mats might also enable PVA to react with the maleic functions of MAPP particles through an esterification reaction [5,23] which may increase the cohesion of MAPP/PVA fibers. Finally, fibers become rougher after washing

proving that some PVA was eliminated. It was calculated that maximum 50 wt% of the initial PVA content could be removed by weighing dried mats before and after washing (Appendix 8).

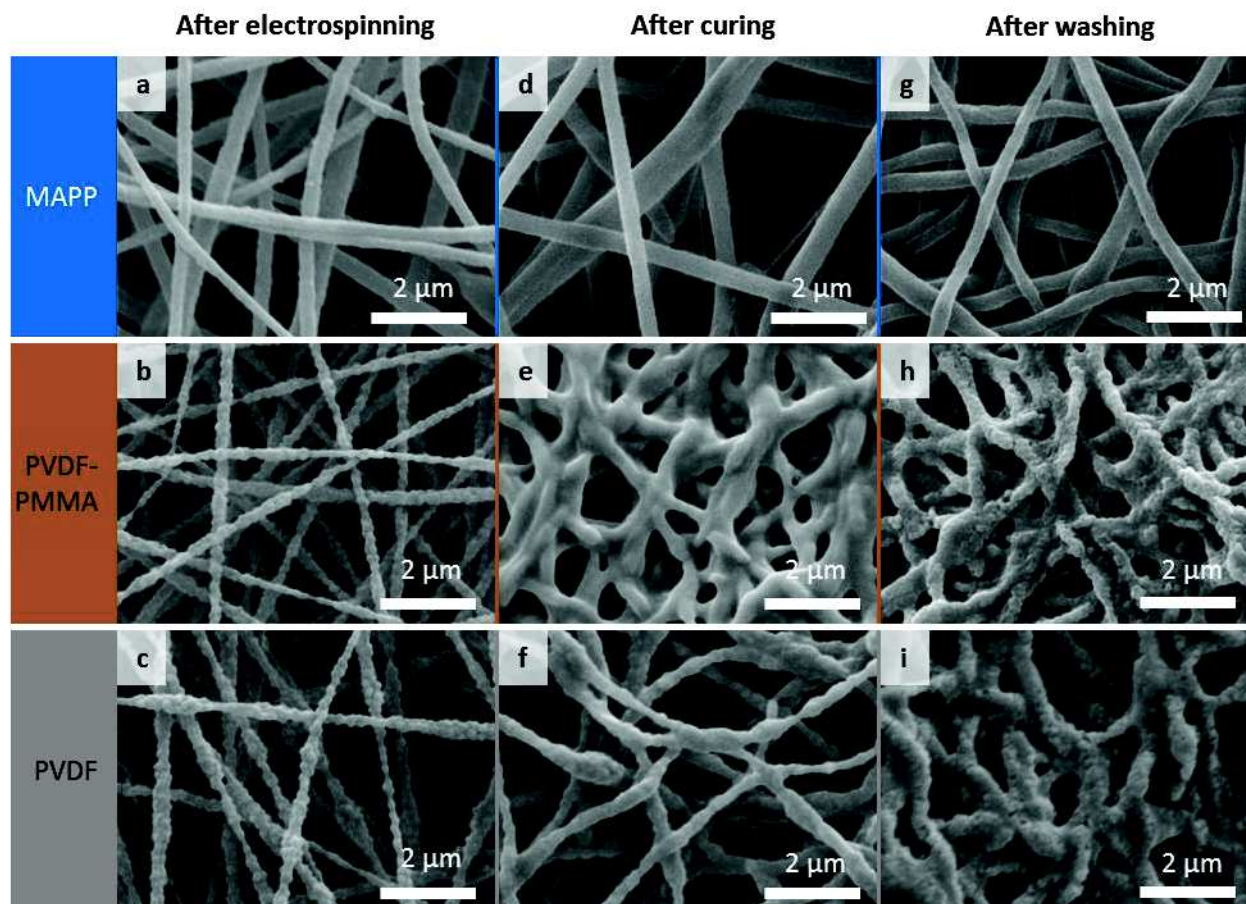


**Figure 3A.5.** SEM images of a,d,g) MAPP/PVA, b,e,h) PVDF-PMMA/PVA and c,f,i) PVDF/PVA fibrous mats after electrospinning, curing and washing.

For PVDF-PMMA/PVA, the optimal ratio was 20/5 wt% and the curing temperature 120°C. PVDF-PMMA/PVA fibers are highly interconnected, certainly due to the fact that the transition temperature of PVDF-PMMA (94°C) is well below the curing temperature. The removal of PVA from the fibers after washing is evidenced in Figure 3A.6d as fibers are rougher than in Figure 3A.6c and that some particles can even be distinguished after washing. The diameter of particles in fibers ( $133 \pm 20$  nm) is equal to the size of dried particles observed by SEM ( $133 \pm 15$  nm). By weighing dried PVDF-PMMA/PVA mats before and after washing, it was estimated that PVA had probably entirely been eliminated (Appendix 8). This is in agreement with the fact that the diameter of particles in fibers and dried are similar.

The optimal ratio for PVDF/PVA mats was 20/8 wt% and the curing temperature 200°C. Here, the curing temperature is slightly above the melting point of PVA (190°C) and well above that of PVDF (148°C). However, mats are still porous after curing even though fibers are highly interconnected. PVDF particles have the lowest glass transition temperature of all considered polymer particles. Consequently, they would be the most prone to deformation. However, particles can be seen in Figure 3A.6f. Their size is  $136 \pm 17$  nm which is close to the size of dried PVDF particles ( $142 \pm 14$  nm). This proves that a certain amount of PVA was washed, uncovering particles. It was inferred from the measure of the mass difference between before and



after washing of dried PVDF/PVA mats that maximum 33 wt% of PVA could be removed during the washing step (Appendix 8). The fact that less PVA is removed in PVDF/PVA mats (up to 33 wt%) compared to PVDF-PMMA/PVA mats (up to 100 wt%) and MAPP/PVA mats (up to 50 wt%) could come from the fact that the initial PVA amount in PVDF/PVA fibers (particles:PVA ratio of 20:8) is higher than in PVDF-PMMA/PVA and in MAPP/PVA fibers (particles:PVA ratio of 20:5).

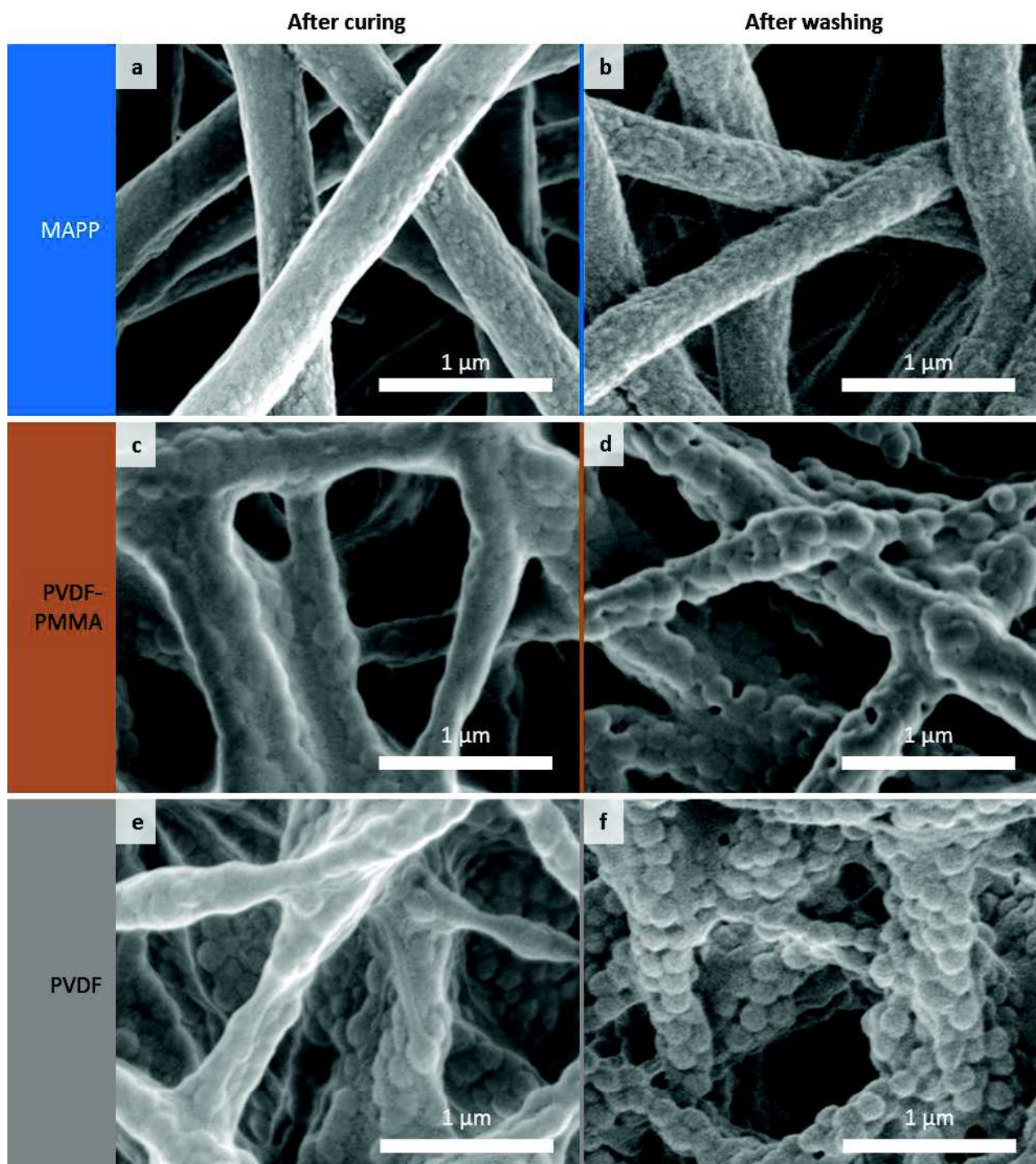


**Figure 3A.6.** SEM close-ups of a,b) MAPP/PVA, c,d) PVDF-PMMA/PVA and e,f) PVDF/PVA fibrous mats after curing and washing.

The mean fiber diameter slightly increases after curing due to fiber sticking at contact points and softening, and after washing probably due to fiber flattening (Figure 3A.7). However, the mean fiber diameter is equivalent for each mat ( $471 \pm 47$  nm) after washing which is important for further characterizations as for instance mechanical properties, which is influenced by the fiber diameter [24].

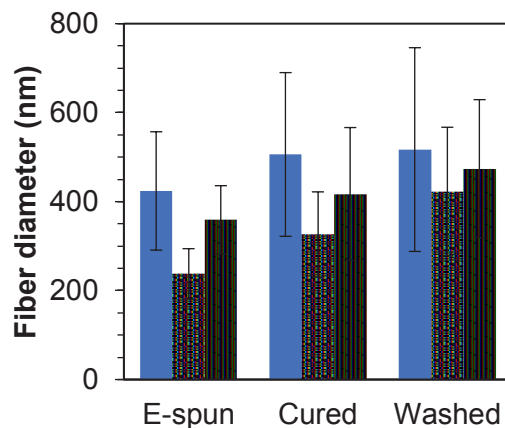


**Figure 3A.7.** Mean fiber diameter after electrospinning (E-spun), curing and washing of PVDF/PVA (in blue), PVDF-PMMA/PVA (orange square patterned) and MAPP/PVA mats (grey with white points).

### 3A.4.2 Mechanical properties

Mats have been mechanically characterized by tensile tests at  $5 \mu\text{m/s}$  for each sample. Mats had a thickness of  $43 \pm 17 \mu\text{m}$ . Results are displayed in Figure 3A.8 and stress-strain curves in Appendix 9. On the overall, the mechanical properties (elastic modulus, stress at break and strain at break) are higher after washing than after electrospinning for all mats. Moreover, it can be seen that the increase of the mechanical properties is principally due to the curing step.

First, curing increases the mechanical properties of mats for all suspensions as the elastic modulus, the stress at break and the strain at break are enhanced. Before curing, the mechanical strength of mats is mainly due to the template polymer (PVA) as particles are disjointed. After curing, particles are bonded together and contribute to reinforce the mechanical properties of mats. Similar results were observed by Giebel et al [15] for PVA fibers containing acrylate particles. Mats having the best particle merging have the best mechanical properties. During curing, fiber merging also occurs between fibers to produce a highly inter-bonded fibrous structure and a denser mat as it can be seen in Figure 3A.5e-f. Inter-bonded fibrous structure also contribute to the enhancement of the mechanical properties [25,26]. The observation of the surface of rupture highlights the fact that the rupture becomes brittle after the curing step for all mats. Indeed, while the rupture is unclear for mats after electrospinning as fibers are elongated and torn apart during traction trials, the rupture is clear for mats after curing (Figure 3A.9). This highlights the fact that during thermal treatment, particles contained in fibers and fibers tend to merge together. Consequently, mats become more rigid.

After washing, the stress at break and the elastic modulus of MAPP/PVA mats remain unchanged. This result can be linked to the fact that PVA is mainly removed from the surface of the fibers. As a matter of fact, fibers become rougher after washing (Figure 3A.6a and b). Furthermore, it was calculated that a maximum 50 wt% of PVA (Appendix 8) could be removed from mats during the washing step. This was attributed to the fact



that PVA can react with the maleic functions of MAPP particles during the heat treatment through an esterification reaction [5, 23]. In the end, the removal of PVA only creates surface roughness in fibers (it does not “break” fibers) and therefore does not lower mechanical properties.

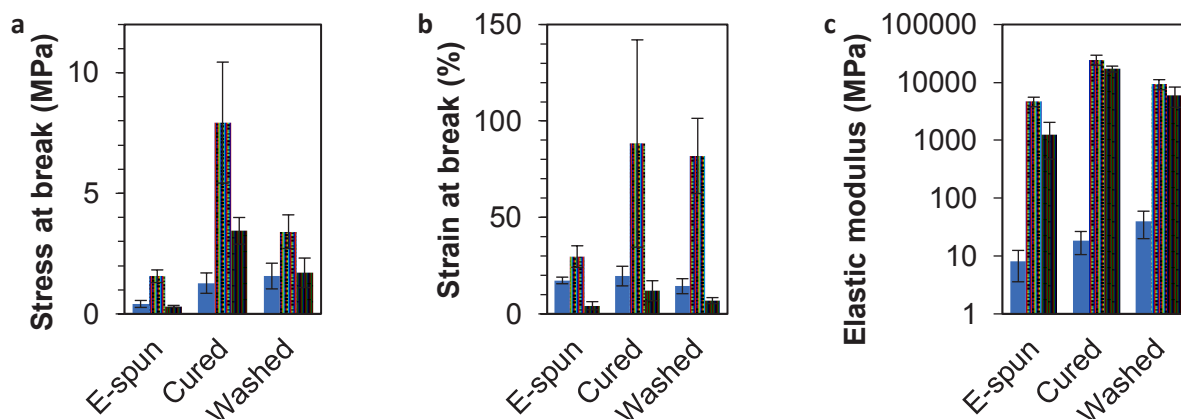


**Figure 3A.8.** a) Stress at break, b) strain at break and c) elastic modulus of mats at each step for MAPP/PVA mats (in blue), PVDF-PMMA/PVA mats (orange square patterned) and PVDF/PVA mats (grey with white points).

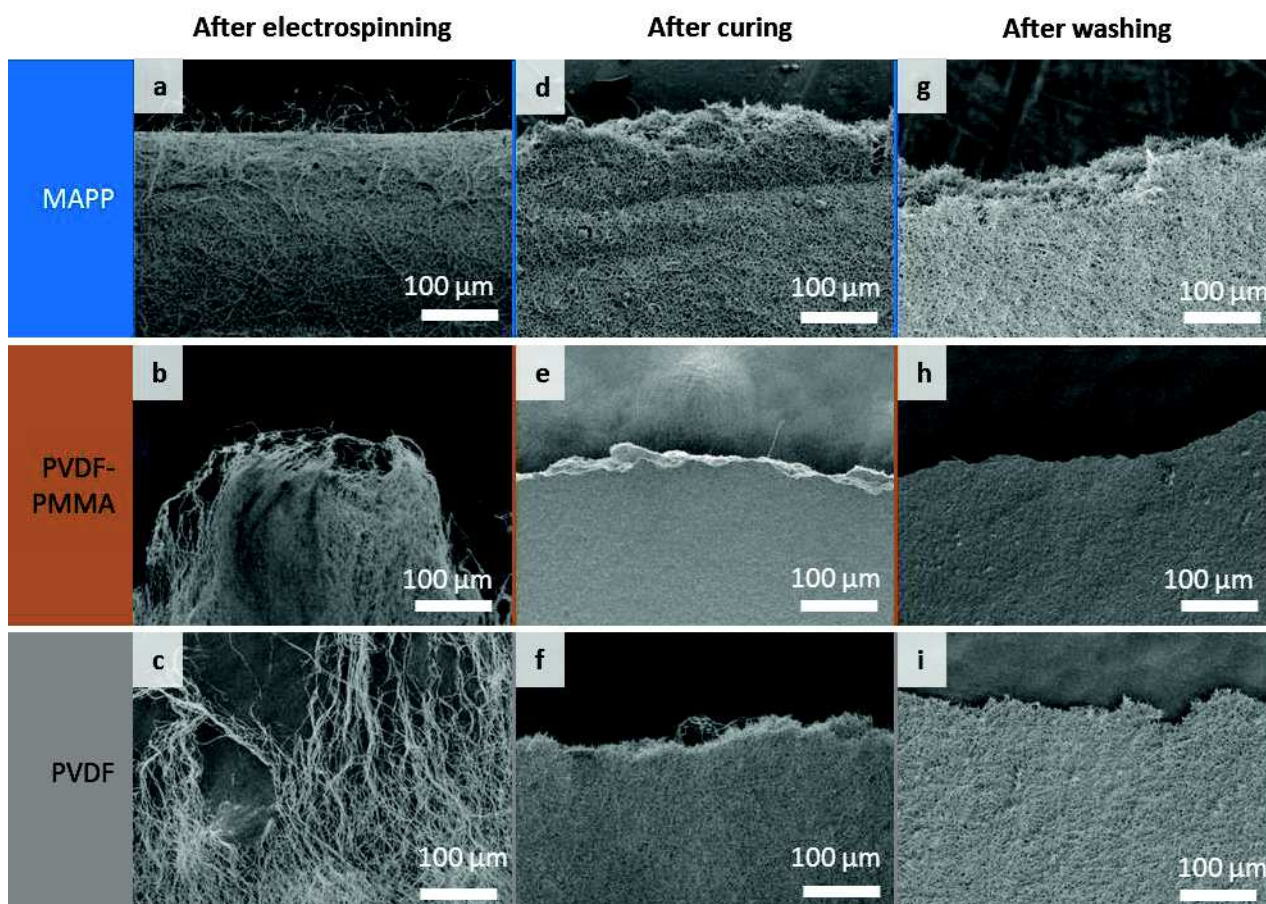


**Figure 3A.9.** SEM images of the surface of rupture after mechanical tests of mats.

On the contrary, the stress at break and the elastic modulus of PVDF-PMMA/PVA mats and PVDF/PVA mats decrease after washing. This result was related to PVA removal. Indeed, the removal of PVA uncovers uncoated bonded PVDF-PMMA and PVDF particles after washing as proved in Figure 3A.6d and f. The lower mechanical properties after washing can be explained by the fact that a part of PVA before washing was situated between particles. During the heat treatment, particles were thus unable to merge. Consequently, after washing, some particles are disjointed, which lower the mechanical properties of mats.

In the end, after washing, PVDF-PMMA/PVA mats show the best mechanical properties (highest strain at break, stress at break and elastic modulus) and a strain at break as high as  $82 \pm 19$  %. (Figure 3A.8) Mats electrospun from suspensions of water-insoluble polymers can be compared to some extent to mats composed of the same polymers but which were electrospun by classical solution electrospinning in organic solvents, keeping in mind that mechanical properties depend on the diameter of fibers, sample size and test velocity.

Polymer	Test velocity (mm/min)	Sample length (mm)	Fiber diameter (nm)	Stress at break (MPa)	Strain at break (%)
MAPP/PVA (washed)	0.3	20	$471 \pm 47$	1.6	14
PVDF-PMMA/PVA (washed)	0.3	20	$471 \pm 47$	3.4	82
PVDF/PVA (washed)	0.3	20	$471 \pm 47$	1.7	7

Polymer	Test velocity (mm/min)	Sample length (mm)	Fiber diameter (nm)	Stress at break (MPa)	Strain at break (%)	Ref
PP	10	n.g.	$760 \pm 370$	2.1	77.6	[27]
PP	10	n.g.	$530 \pm 130$	4.1	128	[27]
PVDF	1	25	$954 \pm 90$	$\approx 80$	$\approx 250$	[28]
PVDF	5	n.g.	100-500	3.3	16.9	[29]
PVDF	5	60	$355 \pm 99$	17.6	171	[30]
PVDF	5	70	50-300	4.4	10	[31]
PVDF	10	50	700	14.5	28.8	[32]
PVDF	10	n.g.	180	2.84	45	[1]

**Table 3A.3.** Up: Stress and strain at break of MAPP/PVA, PVDF-PMMA/PVA and PVDF/PVA mats fabricated here after washing. Down: Stress and strain at break of PP, PVDF-PMMA and PVDF mats found in the literature. n.g.: not given.

### 3A.4.3 Hydrophilic properties

Contact angles (Figure 3A.10) with water were assessed to estimate the hydrophilicity of mats after the washing step, which is relevant for filtration trials regarding the to-be filtrated liquid.

MAPP/PVA mats and films are the most hydrophilic mats due to the fact that MAPP particles are hydrophilic thanks to its maleic functions which can react with PVA during curing through an esterification reaction [5,23]. The contact angle decreases rapidly over time from an initial value of  $40^\circ$ - $50^\circ$ . It is close to zero after 20s. Thus, the presence of maleic functions and PVA in MAPP/PVA mats after washing imposed the hydrophilic properties.

PVDF-PMMA/PVA mats are, on the opposite, more hydrophobic. The mean contact angle calculated during 30s is  $115 \pm 6^\circ$ . This is due to the mat composition as PVDF-PMMA is itself hydrophobic (the contact angle of films composed of pure PVDF-PMMA is around  $81 \pm 1^\circ$  during 30s as it can be read on Figure 3A.10b). It is also linked with the roughness of the surfaces of electrospun mats leading to a higher value than the one of the pure PVDF-PMMA film. The fact that PVDF-PMMA/PVA mats are hydrophobic also proves that PVA has certainly been totally eliminated during the washing step.

PVDF/PVA mats are also hydrophobic due to their composition (the contact angle of pure PVDF films is  $115 \pm 1^\circ$  during 30s). The initial contact angle of PVDF/PVA mats is  $113 \pm 8^\circ$ . However, it decreases overtime to reach  $38 \pm 18^\circ$  after 30s. This behavior can be attributed to the incomplete removal of PVA from PVDF/PVA fibers (Appendix 8). The presence of PVA in PVDF/PVA mats after washing conveys hydrophilic properties to PVDF/PVA mats. The fabrication of PVDF/PVA mats having hydrophilic properties is interesting, as for example in the case of liquid filtration to increase the permeability. Other strategies have also been investigated in the literature to increase the hydrophilic behavior of electrospun PVDF mats [33,34].

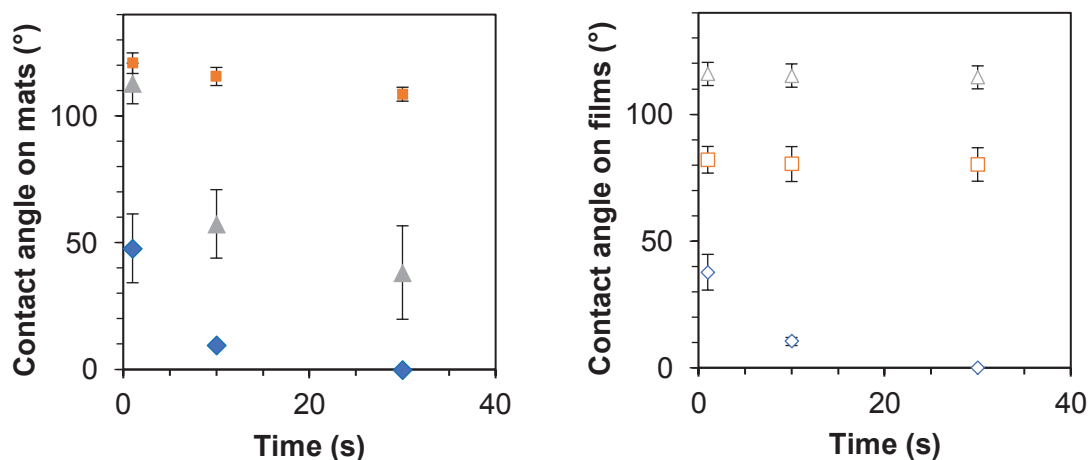


**Figure 3A.10. Left.** Contact angle on mats over time: MAPP/PVA (blue diamonds), PVDF-PMMA/PVA (orange squares) and PVDF/PVA (grey triangles). **Right.** Contact angle on films (containing no PVA) over time: MAPP (unfilled blue diamonds), PVDF-PMMA (unfilled orange squares) and PVDF (unfilled grey triangles).

#### 3A.4.4 Filtration properties

Permeability to pure water of MAPP/PVA mats and PVDF-PMMA/PVA mats were measured in Appendix 10. The average thickness of both mats were  $28 \pm 9 \mu\text{m}$ . The permeability of MAPP/PVA mats is  $(18 \pm 2) \cdot 10^4 \text{ L/h/m}^2/\text{bar}$  whereas the permeability of PVDF-PMMA/PVA mats is  $(2.4 \pm 0.1) \cdot 10^4 \text{ L/h/m}^2/\text{bar}$ . The permeability of MAPP/PVA mats is higher than the permeability of PVDF-PMMA/PVA mats. This is first

due to the inner morphology of both mats: PVDF-PMMA/PVA mats are denser than MAPP/PVA mats due to the thermal treatment, thus reducing the permeability. In addition, MAPP/PVA mats are more hydrophilic than PVDF-PMMA/PVA mats which leads to an increase of the permeability of MAPP/PVA mats.

Filtration trials were carried out at 50 mL/h to understand the performance and the selectivity of mats towards silica particles in aqueous suspensions having diameters of 0.1  $\mu\text{m}$ , 0.4  $\mu\text{m}$  and 1  $\mu\text{m}$ . Two mats have been selected: MAPP/PVA mats and PVDF-PMMA/PVA mats. The mean thickness is  $29 \pm 8 \mu\text{m}$ . MAPP/PVA mats have been selected for their high hydrophilicity whereas PVDF-PMMA/PVA mats were chosen for their high mechanical properties and their hydrophobicity. Both mats were electrospun from aqueous suspensions, cured and washed as seen before. Filtration efficiencies were measured by UV-VIS spectrometry and are depicted in Figure 3A.11. The separation factors of MAPP/PVA mats decrease sharply when the size of particles decreases. It is superior to 99% for 1  $\mu\text{m}$  silica particles, of  $63 \pm 42\%$  for 0.4  $\mu\text{m}$  silica particles and  $12 \pm 9\%$  for 0.1  $\mu\text{m}$  silica particles. On the contrary, the separation factors of PVDF-PMMA/PVA mats remain high even with the 0.1  $\mu\text{m}$  silica particles. The separation factor is superior to 99% for 1 and 0.4  $\mu\text{m}$  silica particles and of  $95 \pm 4\%$  for 0.1  $\mu\text{m}$  silica particles. Pictures of solutions before and after filtration are displayed in Appendix 10.

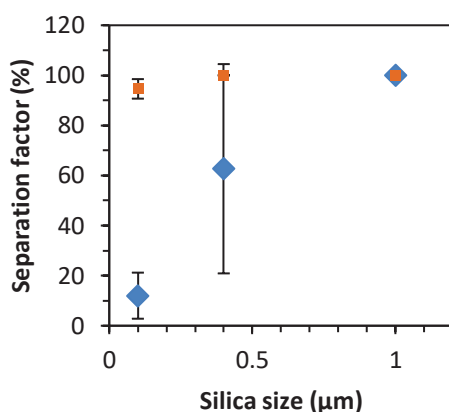


**Figure 3A.11.** Separation factors as a function of the size of the silica particles for MAPP/PVA mats (blue diamonds) and PVDF-PMMA/PVA mats (orange squares).

MAPP/PVA and PVDF-PMMA/PVA mats are fouled by 1  $\mu\text{m}$  silica particles (Figure 3A.12 and Figure 3A.13). Cake layers can be observed on the top surfaces of the electrospinning layers contrary to the bottom surfaces, where seldom particles can be observed. Quasi no particles can be found within the layer. The high separation factors (above 99%) can be attributed to the formation of the cake layers.

Silica particles of size 0.4  $\mu\text{m}$  also fouled MAPP/PVA and PVDF-PMMA/PVA mats. However, they penetrate inside the filtering layers as well. Silica particles are also visible on the bottom surface of MAPP/PVA mats. This result is coherent with the separation factor of 63% of MAPP/PVA mats. The large error bar ( $\pm 42\%$ ) is attributed to the fact that small variations in morphology between MAPP/PVA mats (such as defects) can postpone the formation of the cake layer. The cake layer reduces the effective pore size and leads to higher retention thresholds [35]. Thus, the sooner it is formed, the higher the separation factor is. For PVDF-PMMA/PVA mats, particles can also be observed on the bottom surface. PVDF-PMMA mats act therefore as a depth filter for 0.4  $\mu\text{m}$  silica particles since the separation factor is above 99%.



Silica particles measuring  $0.1\ \mu\text{m}$  in size could be found on the top surface, in the cross-section and on the bottom surface of MAPP/PVA and PVDF-PMMA/PVA mats. Nevertheless, the separation factor of PVDF-PMMA/PVA mats remains high ( $95 \pm 4\%$ ) contrary to MAPP/PVA mats ( $12 \pm 9\%$ ). PVDF-PMMA/PVA mats act thus also as a depth filter for  $0.1\ \mu\text{m}$  silica particles. On the opposite, MAPP/PVA mats are unsuitable for the filtration of  $0.1\ \mu\text{m}$  silica particles.

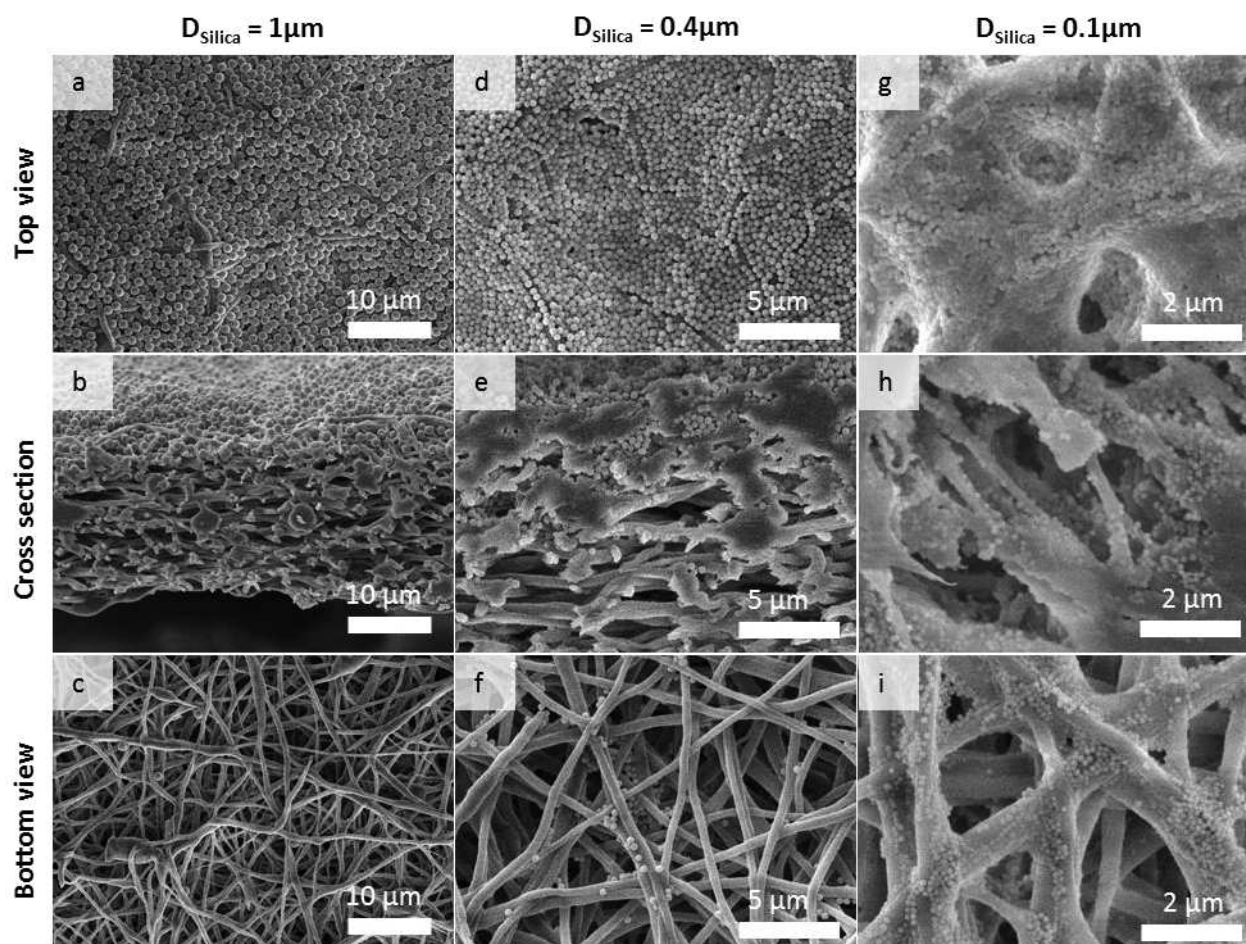


**Figure 3A.12.** MAPP/PVA mats after  $1\ \mu\text{m}$  particle separation a) top surface, b) cross-section, c) bottom surface, after  $0.4\ \mu\text{m}$  particle separation d) top surface, e) cross-section, f) bottom surface, and after  $0.1\ \mu\text{m}$  particle separation g) top surface, h) cross-section, i) bottom surface.

The differences between filtering behaviors of MAPP/PVA and PVDF-PMMA/PVA mats are linked with their morphologies, their mean pore sizes, their hydrophilic properties and their permeability. As a matter of fact, MAPP/PVA mats have a fibrous structure creating pores whereas PVDF-PMMA/PVA mats are better referred as “porous” than “fibrous” (Figure 3A.5g and h). The pore size was not measured here but should be in a future work. It can be inferred that the structure of mats greatly affects filtration efficiencies. However, the mat with the highest efficiencies (PVDF-PMMA/PVA mat) was not the mat for which the highest permeability was measured (MAPP/PVA mat), mainly due to the fact that MAPP/PVA mats were more hydrophilic than PVDF-PMMA/PVA mats. Filtration efficiency and permeability are both crucial parameters in liquid filtration. According to the application, they should be both optimized.

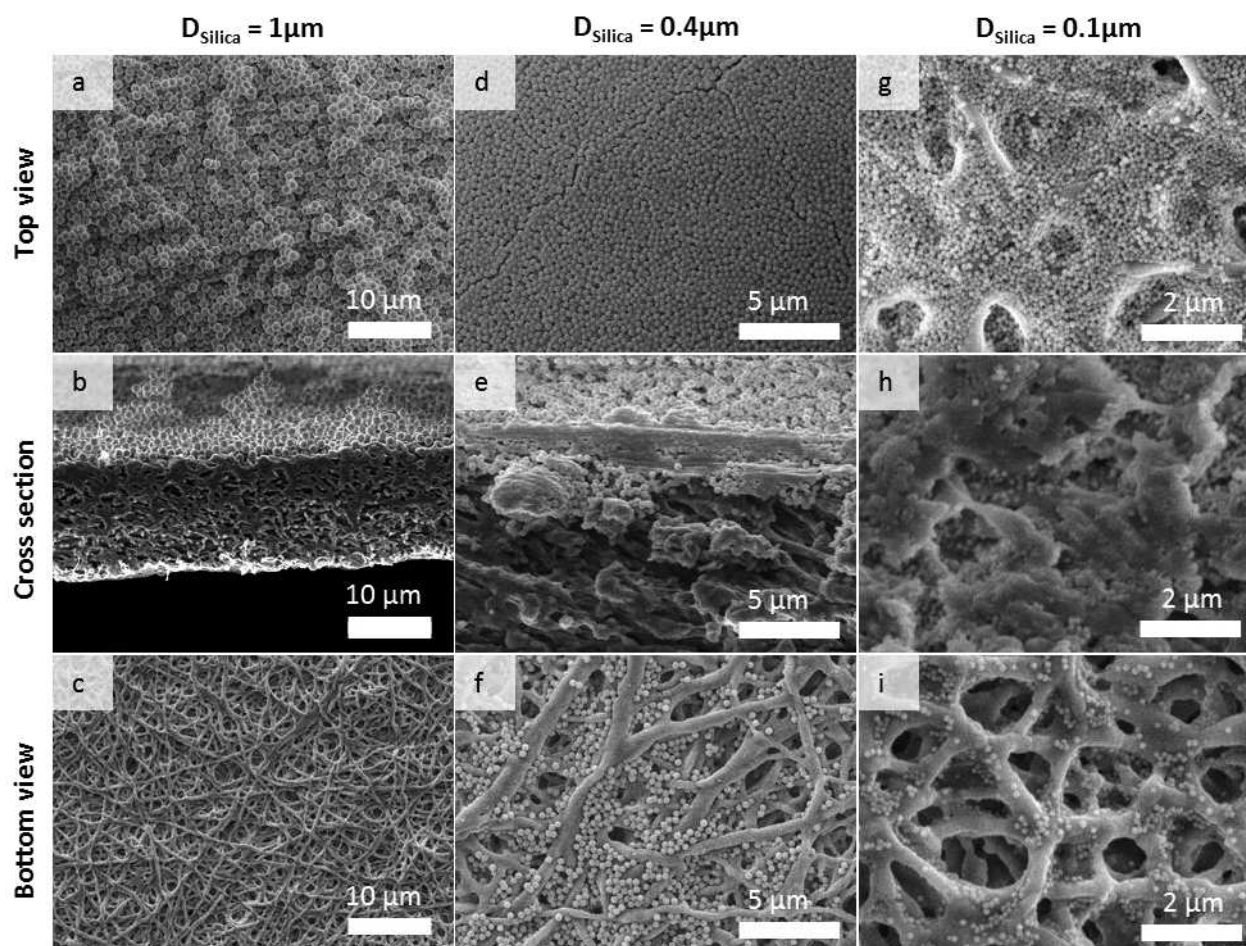


**Figure 3A.13.** PVDF-PMMA/PVA mats after 1  $\mu\text{m}$  particle separation a) top surface, b) cross-section, c) bottom surface, after 0.4  $\mu\text{m}$  particle separation d) top surface, e) cross-section, f) bottom surface, and after 0.1  $\mu\text{m}$  particle separation g) top surface, h) cross-section, i) bottom surface.

### 3A.5 Conclusion

Mats electrospun from suspensions of water-insoluble polymers present a serious alternative to mats electrospun from solutions of these polymers solubilized in organic solvents. As a matter of fact, the process is carried out in water, the polymers constituting the suspension would only dissolve in toxic solvents otherwise and fine and regular fibers were obtained. The strategy is environmentally friendly and may in conclusion ease the industrialization of the electrospinning process. In addition, mats showed overall good mechanical properties. PMMA-PVDF/PVA mats even showed a strain at break as high as approximately 80% after curing and washing. Contact angle measurements showed that depending on the PVA content remaining after washing, mats could either be hydrophilic or hydrophobic. Finally, micro filtration trials could be successfully performed with mats fabricated by the strategy developed in this part, and above all with PMMA-PVDF/PVA mats. The electrospinning of aqueous suspensions composed of water insoluble polymers is thus a strategy that could be further used to develop new “green” membranes for liquid micro filtration but could also be considered for other areas of applications.



## 3B. ELECTROSPINNING OF PURE POLYMER-FREE TANNIC ACID SOLUTIONS

In this part, polymer-free mats of pure tannic acid are electrospun and studied with a focus on the process stability using an eco-friendly solvent composed of a mixture of water and ethanol. A study was conducted to understand why it is possible to obtain tannic acid fibers since tannic acid is a non-polymeric molecule. Before considering liquid filtration trials, attempts were made to crosslink tannic acid mats.

### 3B.1 Introduction

Electrospinning is a process allowing the preparation of nanofibrous materials from a solution usually based on a high molar mass polymer. To obtain continuous fibers, polymers with a high molar mass are generally used. Their concentration has to be high enough to ensure chain entanglements in solution and to avoid breakage of the jet into droplets [36–38]. Recently, a few publications have also demonstrated the possibility to electrospin non-polymeric systems, producing continuous fibers from low molar mass molecules, such as phospholipids or Gemini surfactants [39,40]. These amphiphilic molecules exhibit a behavior similar to polymers in solution. When increasing their concentration, they form micelles, first spherical, then cylindrical, until these cylindrical micelles overlap and entangle at high concentration. As for polymer solutions, when sufficient entanglements are obtained, continuous fibers can be electrospun. Electrospinning was also possible with diphenylalanine [41], a small peptide which self-aggregates in nanotubes in solution through  $\pi$ - $\pi$  interactions [42]. Other molecules such as cyclodextrins (CDs), cyclic oligosaccharides having 6, 7 or 8 glucose units, were also processed by electrospinning to obtain nanofibers [43,44]. CDs are well known to self-assemble in solution [45] forming hydrogen bonds which are crucial to obtain homogeneous fibers [46]. From these examples, it appears that molecules exhibiting sufficient intermolecular forces in solution to self-assemble could be used to produce continuous fibers by electrospinning.

With the idea to enlarge the repertoire of small molecules able to undergo electrospinning, we investigated tannic acid (TA) as a possible target due to its high potential of applications. TA is a water soluble molecule and can be found in plants such as oak bark [47]. TA is a hydrolysable polyphenol consisting of a mixture of polygalloyl glucose molecules having different degrees of esterification [48] but with a preponderant amount of decagalloyl glucose as shown in Figure 3B.1. Contrary to CD which has a cone-shape structure, TA is planar but, as CD, it can be expected to form aggregates through hydrogen bonding thanks to its phenol groups. Aggregation of polyphenols found in wine is a phenomenon which is studied in oenology. Indeed, tannins may form colloidal suspensions in water-ethanol solutions that interfere with wine treatment [49]. The presence of galloyl moieties seems to favor the formation of polyphenol aggregates in a mixture of ethanol-water [50]. In this case, increasing ethanol concentration in solvent led to smaller aggregates or even to wine polyphenols solubilization. As TA is a hydrolysable polyphenol compound, which owns several galloyl moieties, it can be expected to form also aggregates in ethanol-water-mixture. However, contrary to the polyphenols used in the previous study, TA is less soluble in ethanol than in water, another behavior in solution is thus expected.

TA exhibits many interesting properties for biology. Indeed it is antibacterial, anticarcinogenic and inhibits the formation of superoxide radicals [51]. For these reasons, TA-loaded materials were investigated for different applications in many kinds of materials. It was studied in layer-by-layer films, in hydrogels or in nanoparticles

[52–54]. TA, as other polyphenols, is also studied in electrospinning to functionalize polymer electrospun fibers [55–57]. TA was used to render electrospun poly(N-vinylcaprolactam) (PVCL) non hydrosoluble [58]. From a simple blend of TA and PVCL, which are both hydrosoluble, it was possible to make non-hydrosoluble fibers through hydrogen bonding between PVCL and TA. Recently, TA-Fe<sup>III</sup> complexes were found to reinforce polyvinyl alcohol (PVA) fibers [59]. At optimal pH, fibers from a blend of PVA and TA-Fe<sup>III</sup> complexes were electrospun. The membranes showed higher mechanical properties (ie higher tensile strength and percentage of elongation at break) than PVA fibers due to the addition of Fe<sup>III</sup> and had an antioxidant activity due to TA activity. Similar results were observed with electrospun ultra-fine cellulose acetate fibrous mats where TA-Fe<sup>III</sup> complexes aim to improve the packaging conditions of perishable foods [60]. In all these articles, TA was always electrospun with a carrier polymer and to our knowledge nobody explored the possibility to produce pure TA nanofibrous materials.

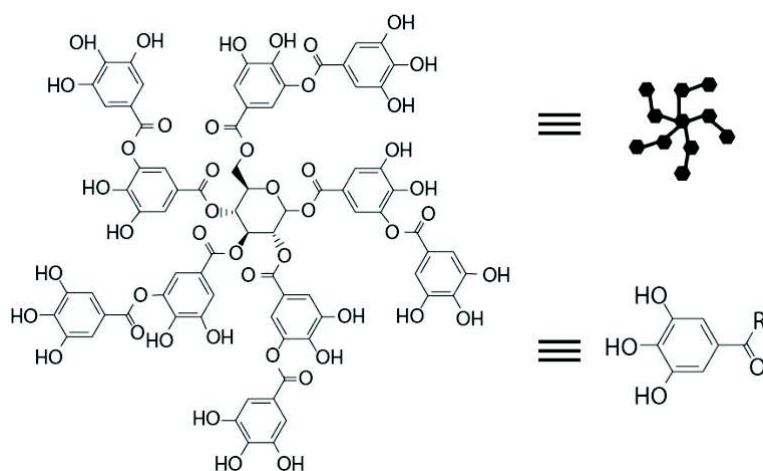


**Figure 3B.1.** Tannic acid molecule and its schematic representations used in this chapter.

In this chapter, we managed to obtain membranes of electrospun fibers from a solution made of ethanol and water highly concentrated in TA without addition of any polymer. TA is a natural molecule and is soluble in non-toxic solvents (water, ethanol) unlike many polymers. It could thus be interesting for green electrospinning perspectives. In this work, the optimal conditions to obtain pure TA fibers were investigated by changing the solvent and TA proportions to study the morphology of the deposit after electrospinning. Furthermore, in view of their potential applications, it appears necessary to cross-link the fibers in order to avoid solubilization when the nonwoven mat enters in contact with water. For this purpose, two different cross-linking routes were studied: the oxidation of TA by sodium periodate as well as a combination of oxidation and complexation of TA by Fe<sup>III</sup>. Finally, Fe-TA mats were successfully electrospun.

## 3B.2 Materials and methods

### 3B.2.1 Materials

Tannic acid (ref. 403040, Mw = 1701.2 g mol<sup>-1</sup>), ethanol (ref. 24103, purity ≥99.8%), sodium periodate (ref. 311448n, purity > 99.8%) were purchased from Sigma-Aldrich. The limit of solubilization of TA given by the

supplier is 100 mg/mL in ethanol and 2.8 g/mL in water. Iron (III) nitrate nonahydrate (99+%, for analysis) was purchased from Acros Organics. All the solutions were prepared with deionized water.

### 3B.2.2 Solution preparation and electrospinning

Solutions were prepared by weighting the solvents 4 to 5 hours prior to electrospinning. TA was dissolved in a mixture of water and ethanol. For the solvent mixture, mass percentage of water varied from 12.5 to 100 wt% relatively to the total mass of solvent. The mass percentage of TA relatively to the total mass of the solution was studied from 30 wt% to 55 wt%.

Electrospinning was performed using a home-made horizontal electrospinning setup with a cylindrical rotating collector. A needle was connected to a positive high-voltage power supply (Spellmann SL 10) while the collector was connected to a negative high-voltage power supply (Spellmann SL 10). The collector was connected to a laboratory stirrer (Ika® Eurostar 20). A syringe pump (Fischer Scientific) pushed the solution through the needle via a feedline connected to a 6 mL syringe. The electrospinning conditions were fixed with a pump flow rate of  $1.2 \pm 0.2$  mL/h, a distance between the needle and the collector surface of 10 cm, and a difference of potential between the needle and the collector of 15 kV with  $V_{\text{needle}} = 10\text{kV}$  and  $V_{\text{collector}} = -5\text{kV}$ . The rotation speed of the collector was set at 150 rpm. The experiments were performed at 22°C and the relative humidity was maintained under 30%.

### 3B.2.3 Solution characterization

Conductivity of solutions was measured with an electrical conductivity meter (Consort K610). Surface tensions were measured with a pendant drop tensiometer (Tracker, Teclis Instruments). Before surface tension measurements, densities of solutions were measured by weighing fixed volume of solutions.

Viscosity of the solution was measured with a rheometer (Physica MCR 301, Anton Paar). Cone-plate geometry (CP50-1) with an angle of  $1.009^\circ$ , and a Pelletier plate was used. All measurements were performed at 22°C with an anti-evaporation system to avoid evaporation of solvents during measurement. The viscosity was measured under steady shear flow for shear rates ranging from  $10\text{ s}^{-1}$  to  $500\text{ s}^{-1}$ . Over this range of shear rates, only Newtonian behavior was observed for all tested TA concentrations. For the highest TA concentrations (i.e. when the measured torque was higher than the minimal torque which can be detected), we verified that the viscosity does not change for shear rates ranging between  $0.1\text{ s}^{-1}$  to  $10\text{ s}^{-1}$ . Thus, it can be concluded that all measurements correspond to the zero-shear viscosities.

Dynamic light scattering (DLS) of TA solutions of various concentrations was studied at 22°C in pure water as well as in water/ethanol 37.5-62.5 wt% with an ALV CGS-3 goniometer system equipped with a He-Ne laser (wavelength=633 nm). All experiments were performed at a scattering angle of  $90^\circ$ . Acquisition time was 5 min and the number of collected photons per unit time was at least ten times the intensity diffused by the solvent. Before measurement, solutions were filtered with  $0.20\text{ }\mu\text{m}$  filters (Filtropur S 0.2).

### 3B.2.4 Cross-linking of the fibers

For this study, a  $300\text{ }\mu\text{m}$  thick nanoweb of TA was electrospun for 3 hours with a solution made of 45 wt% of TA in a solvent composed of 37.5 wt% of water and 62.5 wt% of ethanol (Figure 3B.2).

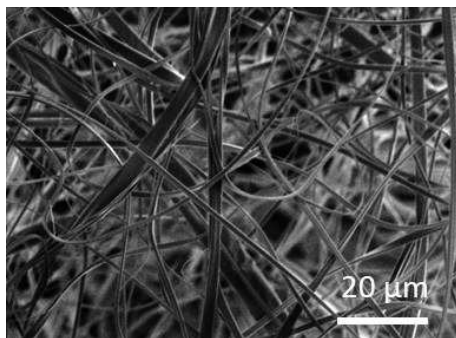


**Figure 3B.2.** SEM picture of the fibers obtained in the water-ethanol mixture 37.5-62.5 wt% at concentration  $C_{TA} = 45$  wt% which were used before cross-linking.

The possibility to cross-link TA fibers was examined through two different mechanisms:

i) Oxidation by  $\text{NaIO}_4$  of galloyl groups of TA into quinones. Solutions of  $\text{NaIO}_4$  were prepared with concentrations of 1 wt% to 9 wt% in water. Small pieces of the nanoweb were then immersed in these solutions for 10 s followed by washing in deionized water for 6 hours.

ii) The oxidation by  $\text{Fe}^{\text{III}}$  of galloyl groups at acidic pH followed by the formation of  $\text{Fe}^{\text{III}}$  - TA coordination complexes at basic pH. Solutions of iron (III) nitrate were made with concentrations in water of 30 wt% and 40 wt%. These solutions have a pH lower than 1. Small pieces of the nanoweb were immersed in these solutions for 10 s followed by washing in PBS buffers (Phosphate Buffered Saline) at pH 8 for 6 h.

### 3B.2.5 Scanning electron microscopy (SEM)

Before SEM examination, samples were coated with a thin layer of gold with a gold coater (Quorum Q 150 RS, Quorum Technologies). A SEM (Vega-3, Tescan) was used in high vacuum mode using an accelerating voltage of 5 kV and working distances in the range of 6-8 mm. For each sample showing fibers, the average diameter was calculated from the measure of 100 diameters obtained on 5 different SEM images with the image analysis software Image J.

### 3B.2.6 Cryogenic transmission electron microscopy (cryo-TEM)

TA at concentration of 2 wt% in water-ethanol 37.5-62.5 wt% was observed by cryo-TEM. A drop of the sample was deposited on a TEM grid covered by a hydrophobic carbon membrane. The drop size was progressively reduced in order to obtain a thin film covering the whole membrane. The grid was subsequently plunged into liquid ethane at liquid nitrogen temperature. By maintaining the specimen at this temperature, the grid was transferred on the cryo-holder and inserted in the high-vacuum column of the TEM. The specimens have been analyzed on a JEOL 2100F TEM microscope working at 200 kV and equipped by a probe aberration corrector, an EELS (Gatan Tridiem) spectrometer and an EDX (Si-Li) detector. This set-up allows a resolution of 2 Å under TEM mode. For limiting irradiation damage, the images were acquired by using a low density of the electron beam irradiation.

### 3B.2.7 Fabrication of Fe-TA solutions

Fe-TA solutions with Fe:TA molar ratios of 1:3, 1:1 and 3:1 have been prepared and electrospun during 1 hour. Solutions are composed of 45 wt% of TA in a mixture of 37.5 wt% of water and 62.5 wt% of ethanol to which  $\text{Fe}(\text{NO}_3)_3$  is added.



### 3B.3 Polymer-free electrospinning of tannic acid

Solutions of TA solubilized in pure water, in pure ethanol and in mixtures of these two solvents were electrospun. Electrospinning of TA in pure water (Figure 3B.3a-c) led to the fabrication of regular fibers when the TA concentration ( $C_{TA}$ ) was raised above 50 wt%. This result is of great importance for green electrospinning perspectives when the use of absolutely non-toxic solvent is needed. However, it was difficult to conduct stable electrospinning in pure water for production time greater than  $\sim 10$  minutes.

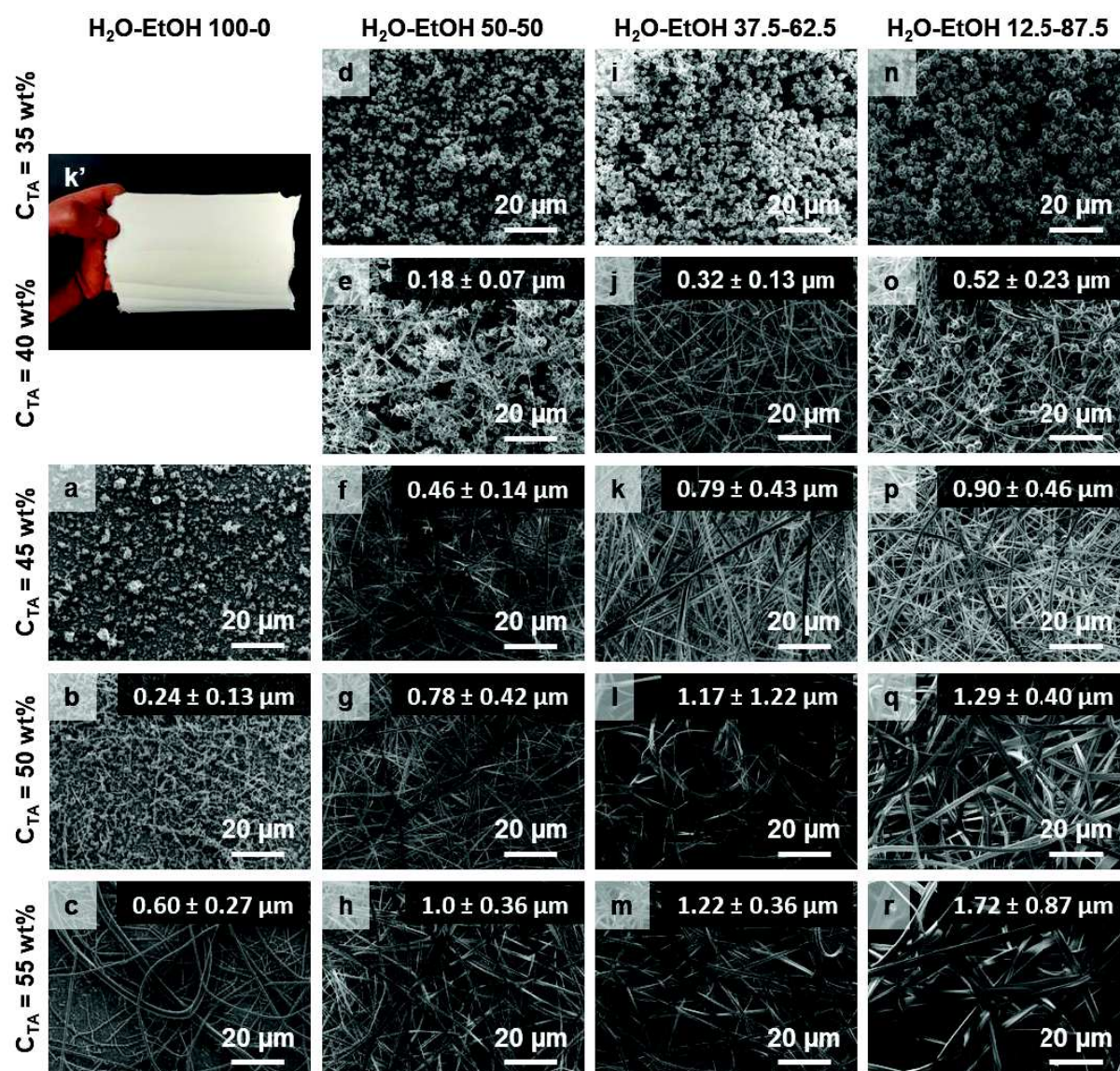


**Figure 3B.3.** SEM images of TA fibers obtained in water-ethanol mixtures (100-0 wt%, 50-50 wt%, 37.5-62.5 wt% and 12.5-87.5 wt%) at concentrations of 35 wt%, 40 wt%, 45 wt%, 50 wt% and 55 wt% of TA in the solvent mixture and their average fiber diameters. k' shows a nanoweb which can be easily handled (obtained from the conditions of picture k).

Besides, it was not possible to electrospin fibers in pure ethanol. At the solubility threshold, only beads could be obtained (Figure 3B.4). Therefore, it was chosen to focus on the electrospinning of TA in water-ethanol mixtures to simultaneously reach high solubility of TA and optimal stability of the electrospinning process.

Indeed, production of continuous fibers from mixtures of water and ethanol (Figure 3B.3d-r) was very stable and much more efficient than in water. The processing window was found for  $C_{TA}$  ranging from 30 to 55 wt% (relatively to the total mass of the solution) and for water-ethanol mixtures containing 12.5 to 87.5 wt% of water (relatively to the total mass of the solvent).

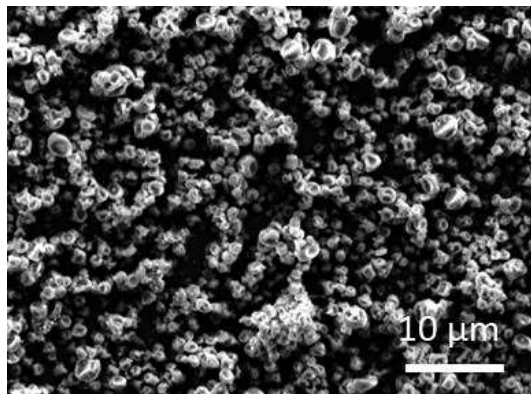


**Figure 3B.4.** Electrospinning of 100 mg/mL of TA in ethanol.

The fiber morphology was studied as a function of the TA concentration and as a function of the water-ethanol ratio. As expected, the fiber morphology evolves with the TA concentration. This observation is detailed for water content of 37.5 wt% in solvent mixture. Indeed, it can be observed from Figure 3B.3i-m that the morphology of the fibers and their related fiber diameter vary as a function of  $C_{TA}$ . Three kinds of morphologies can be noticed: beads (Figure 3B.3i), beads-on-string fibers (Figure 3B.3j) and regular fibers (Figure 3B.3k-m). Beads have been obtained at low concentration, namely for  $C_{TA} \leq 35$  wt%. Bead-on-string structures were observable when the concentration of TA was increased to 40 wt%. Regular fibers were then electrospun for  $C_{TA} \geq 45$  wt%. The diameter of the regular fibers increases with the TA concentration from  $0.79 \pm 0.43$  μm at  $C_{TA} = 45$  wt% to  $1.22 \pm 0.36$  μm at  $C_{TA} = 55$  wt%.

It was also shown that the morphology of the fibers and their average diameter depend on the solvent composition (Figure 3B.3 and Figure 3B.5). The transitions from beads to beads-on-string fibers and from beads-on-string to regular fibers occur at higher TA concentrations for higher water content in the solvent. For instance, solutions with 45 wt% of TA yield fibers for a water content of 12.5 wt% (Figure 3B.3p) whereas only beads are obtained when the solvent is pure water (Figure 3B.3a). In addition, for regular fibers and a given  $C_{TA}$ , the average diameter decreases when the amount of water in the solvent mixture is increased as summarized for  $C_{TA} = 55$  wt% in Figure 3B.5a. This result cannot be linked with the evolution of the solution viscosity as a function of the water content. Indeed, at  $C_{TA} = 55$  wt%, the viscosity is almost constant with the water concentration except for the highest concentrations for which an increase is even observed (Figure 3B.5b). Such a result is not in agreement with a decrease of the fiber diameter with the water content. Thus, the difference in volatility between water and ethanol appears as the dominant parameter. Indeed, solvent mixtures containing the lowest amounts of water (i.e. highest ethanol amount) lead to rapid solvent evaporation during electrospinning due to the high evaporation rate of ethanol. As a consequence, fast jet evaporation induces its rapid solidification limiting thus the effect of the whipping movements which are known to elongate efficiently the jet. In contrast, TA solutions having the highest amount of water (i.e. the lowest amount of ethanol) are subjected to efficient whipping movements during almost all the time of the jet flight leading thus to the thinnest fiber diameters.



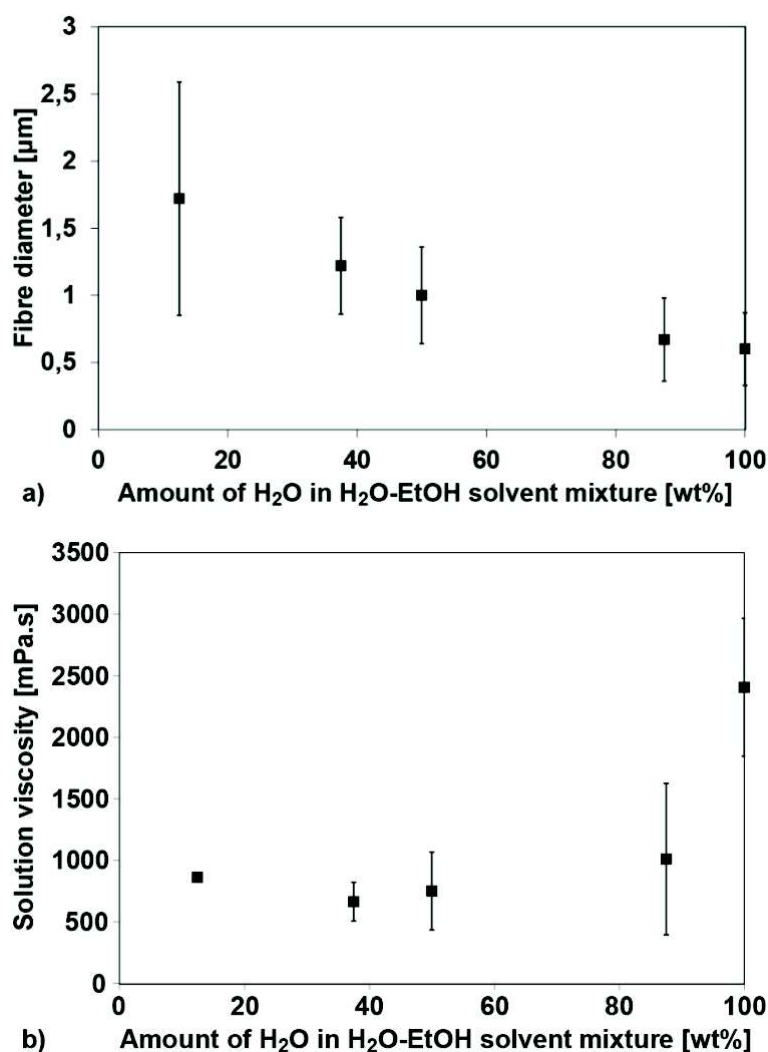


**Figure 3B.5.** a) Evolution of the fiber diameter as a function of the concentration of water in the water-ethanol solvent mixture for  $C_{\text{TA}} = 55$  wt%. b) Viscosity of TA solutions as a function of the mass concentration of water in water-ethanol solvent mixtures for  $C_{\text{TA}}=55\%$ .

Finally, continuous and regular pure tannic acid fibers were successfully and efficiently fabricated in water-ethanol solutions without any addition of polymer. Moreover, electrospinning is stable during several hours without any intervention during the processing. Electrospinning in pure water was also possible but with less efficiency. Last but not least, the resulting nanowebbs are mechanically stable and can be easily handled and wrapped which is of prime importance for their subsequent applications (Figure 3B.3k').

### 3B.4 Aggregation and self-assembling properties of tannic acid in water-ethanol: fiber formation mechanisms

The three main physical parameters of the solution which generally impact the process of electrospinning are the conductivity, the surface tension and the viscosity. In order to get more insight into the process and especially into the mechanisms leading to the fiber formation, we investigated the effect of these parameters for solvent mixtures having a water mass concentration of 37.5 wt%. When TA concentration increases from

30 to 55 wt%, an increase of  $\sim 10\%$  of the surface tension and a decrease of the conductivity from 55 to 20  $\mu\text{S}/\text{cm}$  were observed (Figure 3B.6a). Thus, the conductivity and the surface tension seem not to be the prevailing parameters resulting to the fabrication of the fiber. Contrasting with conductivity and surface tension, the viscosity of the solutions soars by two orders of magnitude when TA concentration increased from 30 to 55 wt% (Figure 3B.6b), suggesting that viscosity plays a key role in the formation of fibers. In order to understand the mechanism behind the fabrication of TA fibers, the specific viscosity  $\eta_{\text{sp}}$  of the solutions was thus analyzed over a broad range of TA concentrations for the two following solvent systems: a water-ethanol mixture with 37.5 wt% of water and pure water.

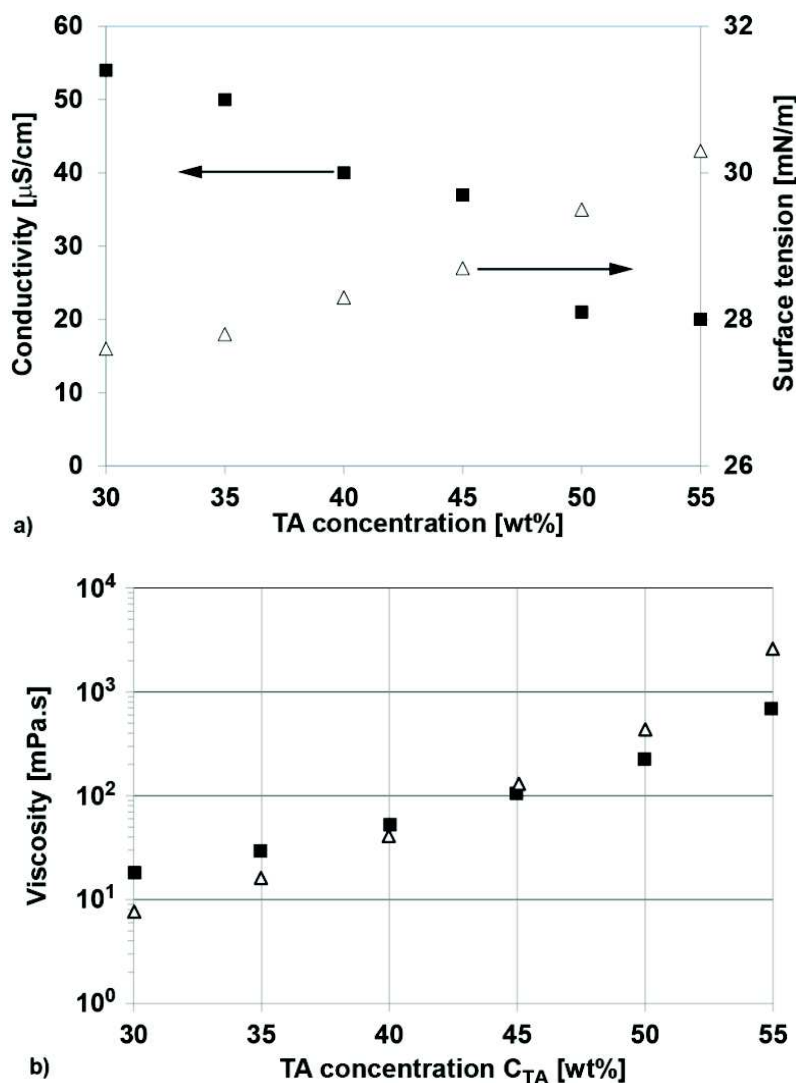


**Figure 3B.6.** a) Conductivity (black squares) and surface tension (white triangle) and b) viscosity as a function of the TA concentration in pure water (white triangles) and water-ethanol at 37.5-62.5 wt% (black squares).

As shown in Figure 3B.7a, four different regimes may be distinguished for which, the specific viscosity follows a power law  $\eta_{\text{sp}} \sim C_{\text{TA}}^\alpha$  with an  $\alpha$  exponent characteristic to each regime of concentration. A dilute regime, at the lowest TA concentration ( $C_{\text{TA}} < C^*$ ) is obtained, where the specific viscosity follows the Einstein's law as it increases linearly with  $C_{\text{TA}}$  (i.e. slope of  $\alpha = 1$  in the log-log plot). Such behavior reveals

the presence of isolated non-interacting TA aggregates [61–64]. The presence of TA aggregates was confirmed in this diluted regime by cryo-TEM performed at  $C_{TA} = 2\text{wt}\%$  for which small isolated TA aggregates having an average size of  $4.1 \pm 0.5$  nm were observed (Figure 3B.7b and Figure 3B.8). The origin of these aggregates could be probably due to hydrogen bonding between TA molecules as shown in Figure 3B.7c. Indeed, although TA is known to be soluble in water and in ethanol, it does not behave like an ideal solute when it is added in a water-ethanol mixture but like a suspension of self-assembled aggregates as also mentioned for cyclodextrins [43]. Indeed, it has been shown that hydrophobic non hydrolysable wine polyphenols form spherical particles or bushy aggregates upon addition of water in an initial ethanolic solution [49]. By analogy, this phenomenon may occur for TA for which hydrogen bonding may thus be envisaged. Then, two intermediate regimes, defined by  $\alpha = 1.5$  for  $C^* < C_{TA} < C_0$  and  $\alpha = 2.5$  for  $C_0 < C_{TA} < C^{**}$  are observed. Finally, a concentrated regime for which  $\alpha = 9$  at  $C_{TA} > C^{**}$  is measured. The overall increase of  $\alpha$  with  $C_{TA}$  suggests the growing of TA aggregates which finally interact to form a network of connected TA structures at the highest concentrations. It is reminiscent of the evolution of the specific viscosity of polymer solutions and of micellar structures. In the former, four regimes are also observed, whose assignation depends on the molar mass  $M_w$  of the polymer [65,66]. At high enough  $M_w$ , the two intermediate regimes correspond to a semi-dilute unentangled and a semi-dilute entangled regime, whereas at lower  $M_w$ , the third regime corresponds to a concentrated unentangled regime. For this reason, electrospinning of polymer is generally performed with high enough molar mass, in order to promote the formation of entanglements. In practice, for linear polymer chains, regular fibers are obtained above a concentration threshold of  $2.5C_e$  corresponding to an average of 2.5 entanglements per chain. For such concentration, the resulting chain entanglements density is high enough to avoid the breaking of the electrospun jet as well as the Rayleigh instabilities responsible of the beads-on-string fiber morphology [36]. Similarly, the specific viscosity of surfactants exhibits a series of regimes with increasing power  $\alpha$  exponent as a function of the concentration ( $\eta_{sp} \sim C_{TA}^\alpha$ ), assigned to the formation of branched and highly branched surfactant structures. The formation of bead free fibers was observed when the surfactant concentration is larger than 2-3 times the branched concentration  $C_0$  [40]. In our case, the increase of the  $\alpha$  exponent indicates the growing of TA aggregates in the first semi-dilute regime which finally interact to form a network of more or less entangled and or connected TA aggregates for the highest concentrations. The behavior of TA in pure water is similar to the one observed in the water-ethanol mixture with the same transitions  $C^*$ ,  $C_0$ ,  $C^{**}$  (Figure 3B.7a). Slight differences are observed for the scaling exponent  $\alpha$  which is equal to 1.35 then 3 for the first two semi-dilute regimes rising to 13 for the concentrated regime. The fact that  $\alpha$  is lower in pure water than in the water-ethanol mixture for  $C^* < C_{TA} < C_0$  suggests a lower rate of aggregation growth in water probably due to the better solubility of TA in water than in water-ethanol. However, for the highest  $C_{TA}$  values ( $C_{TA} > C^{**}$ ), the scaling exponent is larger in water ( $\alpha \sim 13$ ) than in water-ethanol ( $\alpha \sim 9$ ) leading to the crossing of the curves due to higher viscosities and specific viscosities in water than in water-ethanol. This behavior indicates that interactions between the TA aggregates are favored and denser in water than in the water-ethanol mixture.

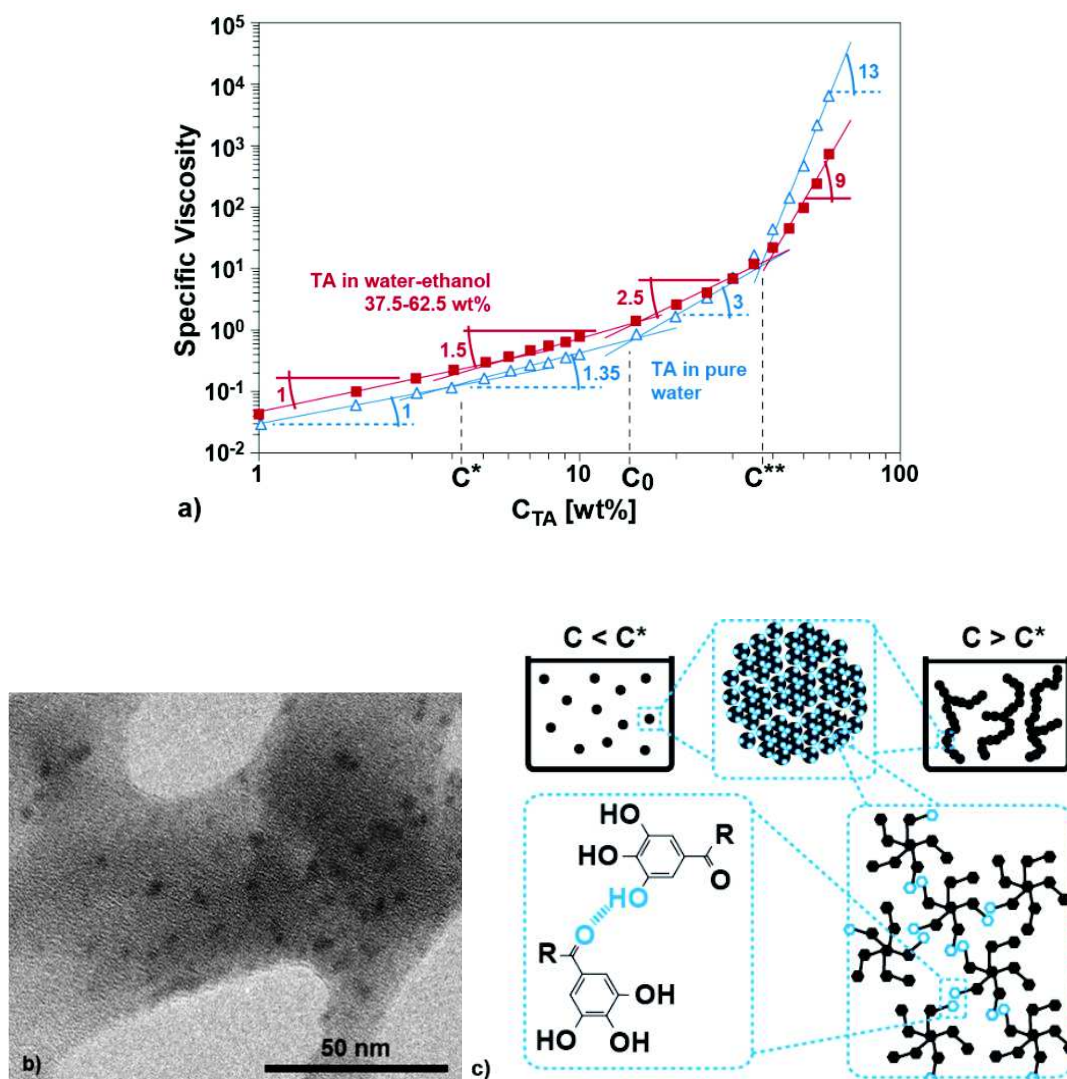


**Figure 3B.7.** a) Specific viscosity of TA solutions as a function of TA concentration at 22°C in pure water (blue triangles) and water-ethanol at 37.5-62.5 wt% (red squares). b) Cryo-TEM picture obtained from a TA solution in water-ethanol at 37.5-62.5 wt% and for  $C_{TA} = 2$  wt% showing dark domains of TA aggregates (cryo-TEM at various scales can be shown Figure 3B.8). c) Schematic representation of a TA solution under and over the critical concentration  $C^*$  and expected TA aggregates resulting from hydrogen interactions.



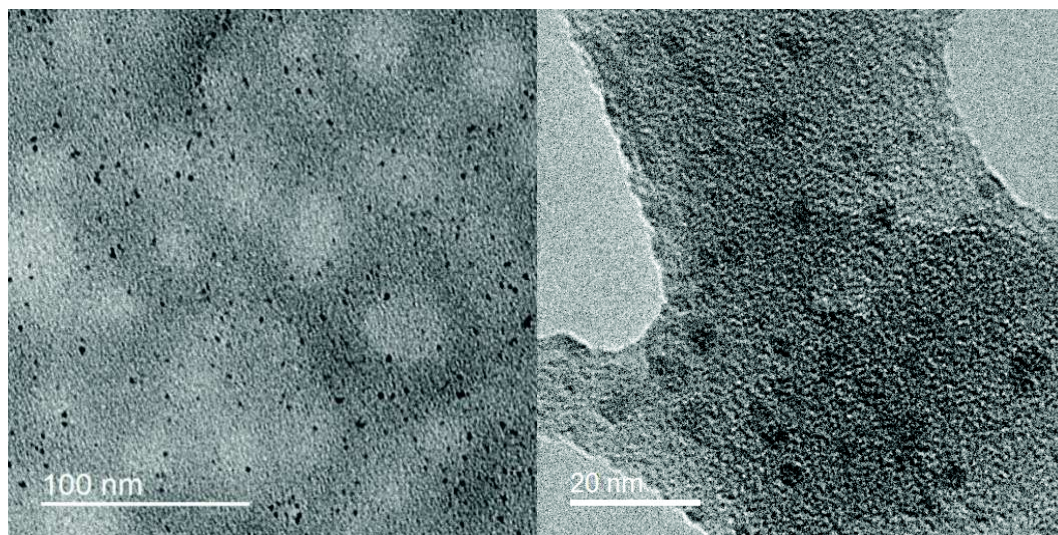


**Figure 3B.8.** Cryo-TEM picture obtained from a TA solution in water-ethanol at 37.5-62.5 wt% and for  $C_{TA} = 2$  wt% showing dark domains of TA aggregates.

In order to get more insight into the structure of TA, DLS measurements were carried out. The intensity autocorrelation functions  $g^{(2)}$  are shown in Figure 3B.9 in the case of TA solutions in water/ethanol 37.5/62.5 wt% as well as in pure water for  $C_{TA} = 2$  wt%, 10 wt% and 35 wt%. Whatever the solvent type and the TA concentration, two modes of decorrelation are observed. The fast mode corresponds to the scattering of small TA aggregates for which the diameter  $D_{TA}$  was calculated (Table 3B.1 and Appendix 11 for the equations allowing their calculation). They slightly increase with the TA concentration and are almost the same in water and in water/ethanol mixture. For the lowest studied concentration  $C_{TA} = 2$  wt%, an average diameter of TA aggregates of 5 nm was measured in water/ethanol which is in the same order than what we observed by cryo-TEM. The slowest relaxation mode may either be attributed to the diffusion of much larger aggregates or to the inner relaxation of less dense structures. Further measurements, in particular varying the scattering angle, would be necessary to unambiguously distinguish between the two hypotheses. Nevertheless, it clearly appears that very large structures of aggregated TA develop. Moreover, the relative amplitude of the slowest mode increases when the concentration of TA increases, proving that the concentration of the largest structures, relative to that of small diffusive aggregates, increases strongly when the TA concentration increases which is in agreement with the growing of a network of aggregated TA as already discussed from rheological measurements.

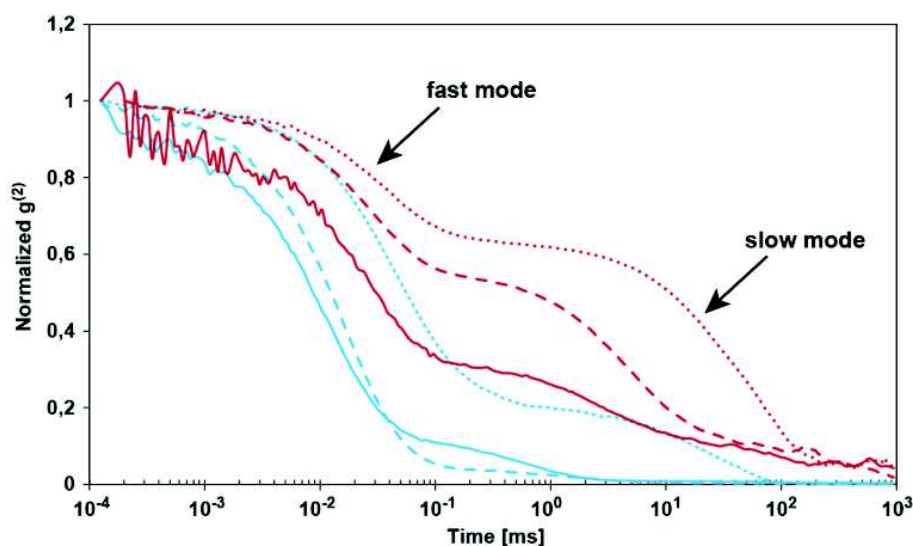


**Figure 3B.9.** Autocorrelation function  $g^{(2)}$  measured by DLS at 22°C in pure water (blue) and water-ethanol at 37.5-62.5 wt% (red) for  $C_{TA} = 2$  wt% (solide lines),  $C_{TA} = 10$  wt% (dashed lines),  $C_{TA} = 35$  wt% (dotted lines).

$C_{TA}$ [wt%]	2	10	35
$D_{TA}$ in pure water [nm]	6	17	34
$D_{TA}$ in water/ethanol [nm]	5	19	29

**Table 3B.1:** Average diameter  $D_{TA}$  of TA aggregates calculated from the fast mode of  $g^{(2)}$ .

Continuous as well as regular fibers were obtained for TA concentration  $C_{TA} > 40$ -45wt% which is indeed higher than  $2.5C_0 \sim 37$  wt% in the studied water-ethanol mixture ( $C_0 \sim 15$  wt%). In water, continuous regular fibers were only obtained from solutions having a much higher TA concentrations  $C_{TA} > 50$ -55wt%. Although, the structure of the associated TA is unknown, the fact that continuous electrospun fibers can be obtained with TA demonstrates that the supramolecular network formed through the self-assembly of TA molecules is strong enough to avoid the breaking of the electrospun jet.

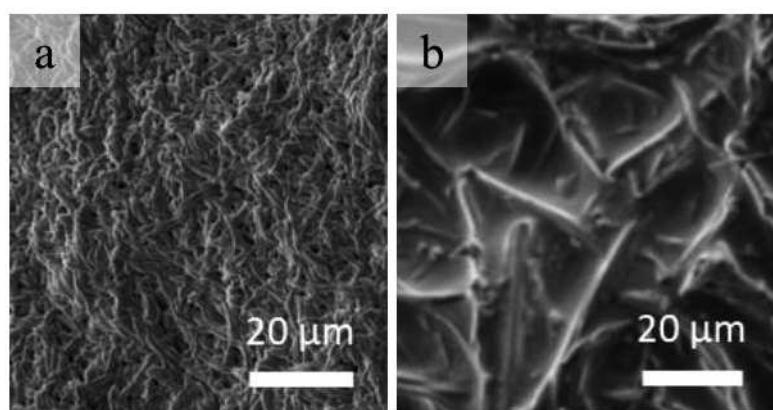
The difference in behavior between the systems in pure water and in water-ethanol mixture may be linked with the topology of the TA supramolecular network formed in the two solvent systems and their energy of association. In the case of the electrospinning of polymer, it was demonstrated that for polymers of given molar mass, the concentration threshold to obtain regular fibers depends on the polymer topology (i.e. linear and combs with controlled length and number of side chains) [67]. In our case, the topology of the TA supramolecular network may be different in water than in the water-ethanol mixture. Indeed, at high  $C_{TA}$  in water-ethanol mixtures, the TA aggregates should be non-homogeneously distributed with TA-rich-water domains (i.e. with a local concentration  $> C_{TA}$ ) and TA-poor-ethanol domains (i.e. with a local concentration  $< C_{TA}$ ). Such heterogeneity could lead to partial phase separation with strong interconnected TA domains plunging in ethanol rich domains. In the case of TA in pure water, the aggregates may be more homogeneously distributed in the volume forming thus a hydrogel with a high degree of interconnectivity between TA aggregates. Such a difference in the network topology may explain the different concentration



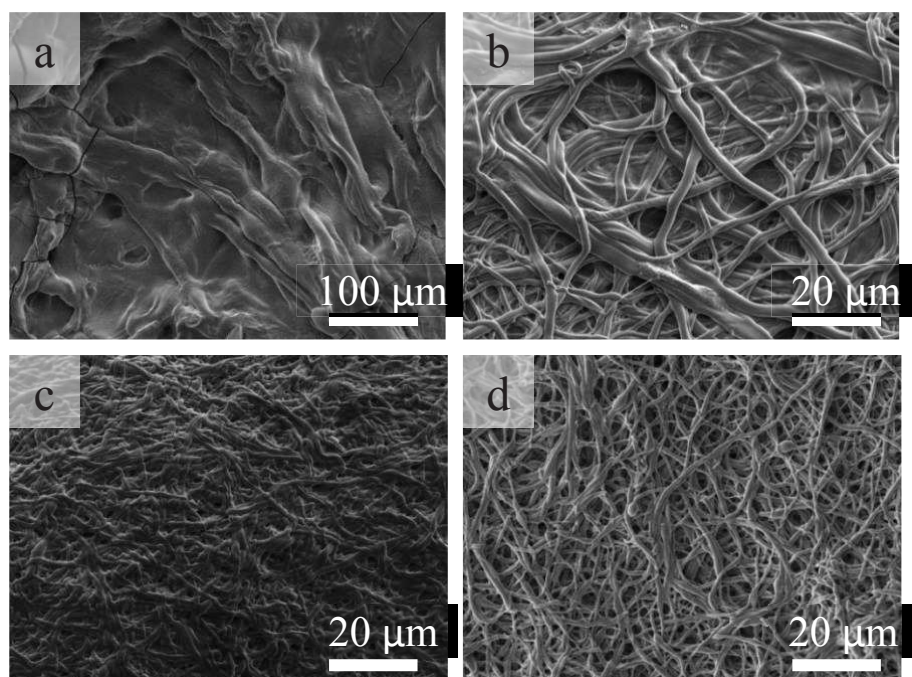
thresholds allowing the production of continuous and regular fibers and more importantly the fact that electrospinning of TA in water-ethanol mixtures is much more efficient and stable than in pure water.

### 3B.5 Cross-linking of tannic acid fibers

TA can be easily cross-linked, contrary to other small molecules for which electrospinning was also possible. Cross-linked TA scaffolds could be interesting for biomedical and filtering applications as TA is an excellent antioxidant, has anti-bacterial properties and interacts strongly with proteins [68]. Moreover, these nanowebs have huge specific surfaces due to the fineness of the fibers, small pore size, in the same order of the diameter of the fibers and high porosity which is essential for high filtering efficiencies and flux [69]. Thus, two strategies have been tested in order to cross-link TA scaffolds. First the galloyl groups of TA were oxidized by sodium periodate ( $\text{NaIO}_4$ ) into quinones, leading to the irreversible creation of covalent bonds between TA molecules [70,71]. The TA scaffolds were immersed in solutions composed of 1, 3, 5 and 9 wt% of  $\text{NaIO}_4$  in water during 10 seconds, followed by washing in distilled water for 6 hours. The washing step was necessary to remove the unreacted molecules forming a film between the fibers (Figure 3B.10a). As the cross-linking step is performed in water, in which TA is very soluble, a competition between dissolution of the scaffold and cross-linking occurs. Therefore, at a  $\text{NaIO}_4$  concentration of 1 wt%, the scaffold was instantly solubilized. At 3 wt% the scaffold turned black showing the presence of quinones and looked macroscopically intact but SEM observation shows that the fibrous structure was lost (Figure 3B.11). Finally, at concentrations of 5 to 9 w%, the fibrous structure of the scaffolds was maintained (Figure 3B.11 and 3B.12a) even after 6 hours of dipping in water. Mechanically, the scaffolds are more brittle than before the  $\text{NaIO}_4$  crosslinking step. It is also worth noting that when the scaffolds are immersed in water for more the one day a progressive degradation is observed. Indeed, after 3 days, a visible degradation can be observed with the eyes and a complete disintegration occurred after one week (Figure 3B.13).

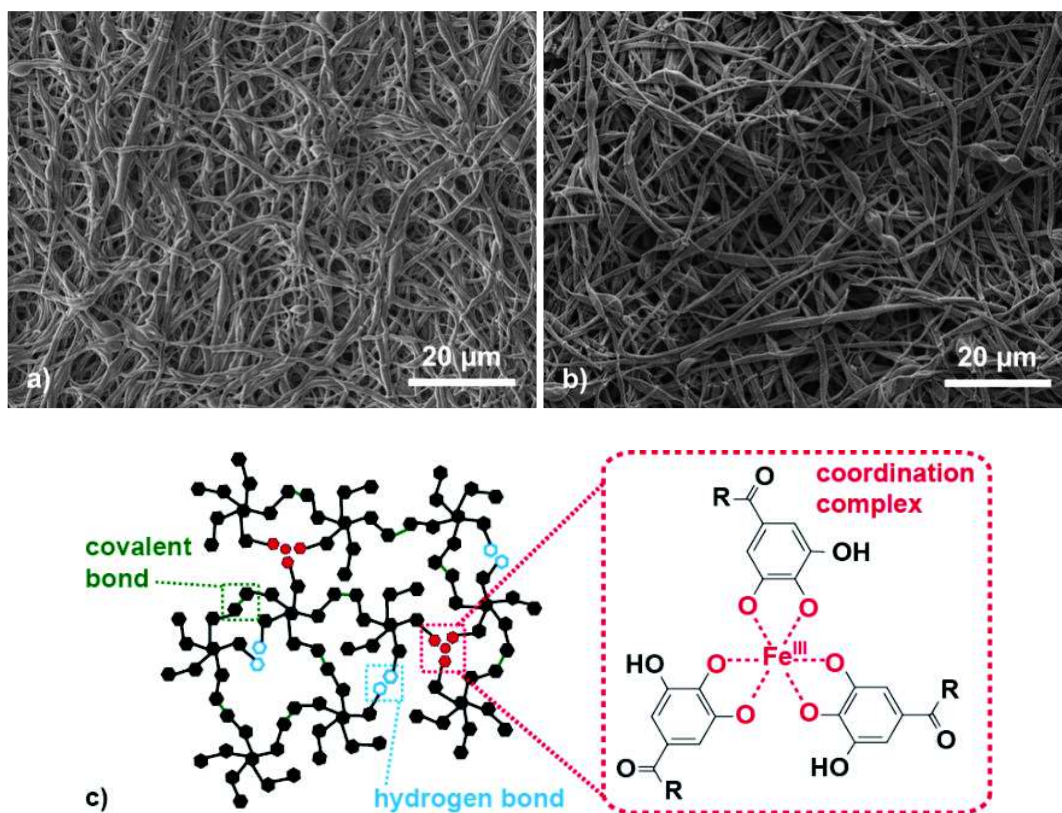


**Figure 3B.10.** SEM picture of the fibers obtained just after crosslinking in aqueous  $\text{NaIO}_4$  solution a) and  $\text{Fe(III)}$  solution b).

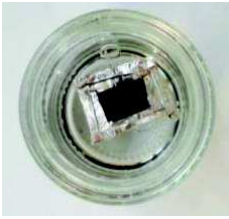
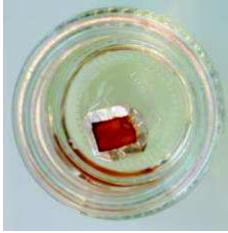
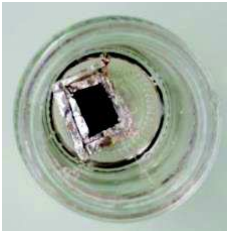
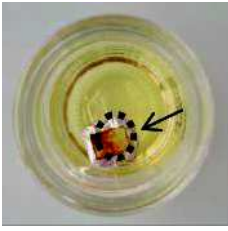
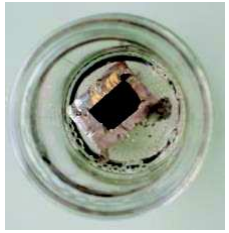


**Figure 3B.11.** SEM picture of the fibers obtained after crosslinking in aqueous  $\text{NaIO}_4$  solution of various concentrations for 10 s followed by washing for 6 hours in distilled water. a) 3 wt%, b) 5 wt%, c) 7 wt%, d) 9 wt%.

The second route proposed to cross-link the tannic acid nanowebs is inspired by the  $\text{Fe}^{\text{III}}$ -catechol interactions occurring in the adhesive threads of the blue mussel, in which a combination of covalent bonds obtained by oxidation reactions and reversible coordination bonds is thought to ensure their strong adhesion to surfaces [72]. The scaffolds were thus first immersed for 10 s in 30 and 40 wt% iron (III) nitrate aqueous solutions. The pH of these solution was lower than 1. A large excess of  $\text{Fe}^{\text{III}}$  as compared to galloyl groups is necessary to ensure a fast oxidation. Indeed, at 30 wt%, the scaffold solubilization was faster than cross-linking and the scaffold disintegrated while at 40 wt% it remained intact and turned black due to oxidation of the galloyl groups by  $\text{Fe}^{\text{III}}$  into quinones and formation of covalent bounds [72]. During this step, part of  $\text{Fe}^{\text{III}}$  ions was reduced to  $\text{Fe}^{\text{II}}$ . However, thanks to the large excess of  $\text{Fe}^{\text{III}}$ , an important proportion of  $\text{Fe}^{\text{III}}$  was still available for the subsequent step. The scaffold was then plunged in a phosphate buffer solution (PBS) at pH 8 for 6 hours in order to allow the complexation between non-oxidized galloyl and remaining  $\text{Fe}^{\text{III}}$  ions. As for the previous crosslinking route, a washing step was necessary to remove unreacted molecules forming a film between the fibers (Figure 3B.10b). SEM observation of the scaffolds carried out after the washing step showed that the fibrous structure was maintained but with some broken fibers (Figure 3B.12b-c). However, although the scaffolds are more brittle than before the crosslinking step, they kept their fibrous structure and their integrity even after one week in water (Figure 3B.13 and Figure 3B.14).



**Figure 3B.12.** SEM pictures of nanofibers after cross-linking. a) TA scaffold after cross-linking with  $\text{NaIO}_4$  at 9 wt% in aqueous solutions for 10s and dipping in distilled water for 6 hours. b) TA scaffold after cross-linking with  $\text{Fe}^{\text{III}}$  at 40 wt% in aqueous solution for 10s, followed by complexation at  $\text{pH} = 8$  in PBS buffer for 6 hours. c) Network of TA molecules after cross-linking with  $\text{Fe}^{\text{III}}$  showing the different types of cross-link points due to oxidative reaction and the formation of coordination complexes.

Time in water	Crosslinking with Fe <sup>3+</sup>		Crosslinking with NaIO <sub>4</sub>	
1 day		The scaffold is still intact. The scaffold is black due to oxidation of the galloyl groups by Fe <sup>III</sup> into quinones and formation of covalent bounds.		The scaffold is still intact.
3 days		The scaffold is still intact.		The scaffold is degraded: a hole appeared (arrow).
7 days		The scaffold is still intact.	No picture	The scaffold is completely degraded.

**Figure 3B.13.** Pictures showing the evolution of crosslinked scaffolds after several days in water.

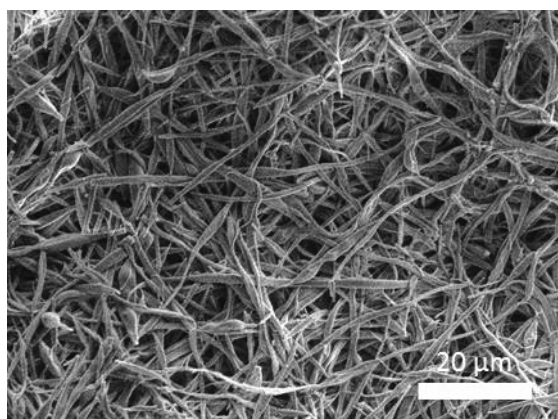


**Figure 3B.14.** SEM picture of the crosslinked fibers with Fe(III) after 7 days in water.

It was recently shown that TA can coordinate with a variety of metals allowing the elaboration of a wide library of metal-TA nanocapsules [73]. Depending on the choice of the metal, various applications can be envisaged such as biomedical [74], selective permeability [75], pH-responsive materials [54] as well as catalysis [73]. Similar strategy could thus be transposed with the cross-linked TA nanowebs having the potential ability for embedding various hybrid metal-TA coordination complexes.



### 3B.6 Electrospinning of a blend composed of TA and $\text{Fe}(\text{NO}_3)_3$

Contrary to the previous part, where Fe-TA complexes were formed after electrospinning during the crosslinking step, the idea in this part is to fabricate TA-Fe mats where  $\text{Fe}(\text{NO}_3)_3$  is added in the TA solution before electrospinning. Three solutions with Fe:TA molar ratio of 3:1, 1:1 and 1:3 have been successfully electrospun (Figure 3B.15). The presence of Fe in electrospun mats is evidenced by the fact that mats are grey after electrospinning. All mats are still fibrous after electrospinning, but upon addition of Fe, mats acquire cotton-like structures. At Fe:TA 3:1, the mat has an interesting structure as the deposit grows along lines perpendicular to the surface of the collector. Yet, the deposit can hardly be seized by hands. This new fluffy structure may arouse interests for biomedical and catalysis applications.

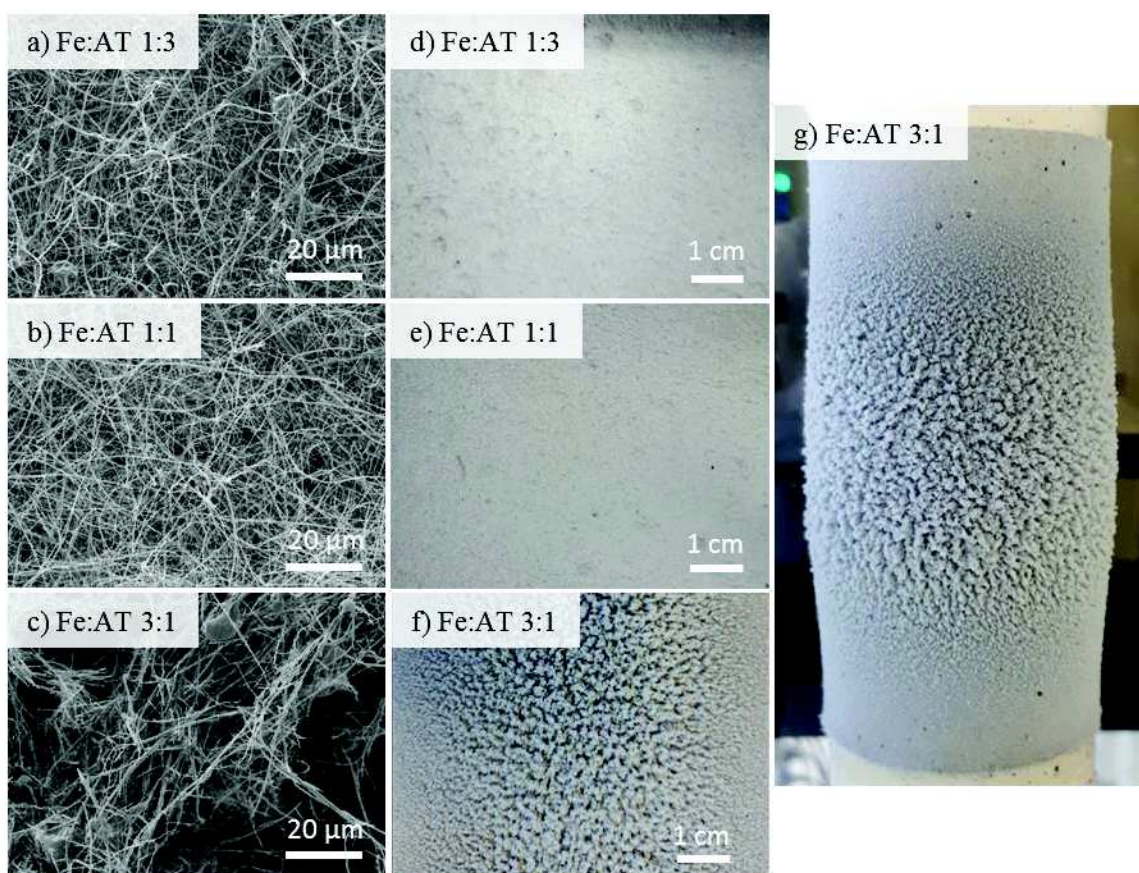


**Figure 3B.15.** a.b.c) SEM pictures of nanofibers after electrospinning with Fe:TA ratios of 1:3, 1:1 and 3:1 respectively. d,e,f) Pictures of Fe:TA mats after electrospinning with Fe:TA ratios of 1:3, 1:1 and 3:1 respectively. g) Picture of Fe:TA 3:1 mat on the collector after electrospinning (collector diameter of 6 cm).

### 3B.7 Conclusion

Homogeneous tannic acid nanofibers were obtained by electrospinning from solutions in water-ethanol mixtures as well as in pure water without any addition of polymer. TA fibers were obtained thanks to favorable hydrogen bonding between the galloyl groups of tannic acid molecules in the solvent. A supramolecular network of TA aggregates is consequently formed in the solvent. The network is strong enough to avoid jet breakage during electrospinning allowing the production of regular fibers above a TA



concentration threshold  $> 3C_0$ , where  $C_0 \sim 15$  wt% is the concentration between the semi-dilute non-entangled and the semi-dilute entangled regimes. Electrospinning was more efficient and stable in water-ethanol mixtures than in pure water. This behavior may be explained by a favorable phase separation in water-ethanol mixtures for which TA-poor-ethanol domains and TA-rich-water domains leads to the formation of a strong interconnected TA network having the optimal topology and rheological properties for efficient electrospinning of continuous and regular nanofibers.

As opposed to the other small molecules for which electrospinning was also demonstrated (e.g. Gemini surfactants and cyclodextrins) we showed that pure tannic acid nanofibrous membranes can be cross-linked. Firstly, cross-linking was possible thanks to oxidation of galloyl groups into quinone with  $\text{NaIO}_4$ . Secondly, cross-linking was also possible by a combination of permanent covalent bonds thanks to the oxidation of galloyl by  $\text{Fe}^{\text{III}}$  at acidic pH and reversible  $\text{Fe}^{\text{III}}$ -TA coordination bounds formed at basic pH mimicking the mussels' adhesive threads. Covalent bonds will provide for good mechanical properties while the reversible bonds should bring self-healing properties to the scaffold [76].

The proposed electrospinning and cross-linking strategy is thus very easy, low cost, scalable and uses non-toxic solvents as well as biocompatible and biofunctional molecules. Furthermore, the strategy could be envisaged and tested by analogy to the whole family of tanins and polyphenols. Last but not least, thanks to the chelation capacity of tannic acid having the ability to coordinate with a wide variety of metals, the proposed smart nanowebs can be envisaged for diverse applications in biomedical, catalysis as well as environment.

## References

- [1] Z. Li, Y. Xu, L. Fan, W. Kang, B. Cheng, Fabrication of polyvinylidene fluoride tree-like nanofiber via one-step electrospinning, *Mater. Des.* 92 (2016) 95–101. doi:10.1016/j.matdes.2015.12.037.
- [2] H. Wang, Q. Liu, Q. Yang, Y. Li, W. Wang, L. Sun, C. Zhang, Y. Li, Electrospun poly(methyl methacrylate) nanofibers and microparticles, *J. Mater. Sci.* 45 (2010) 1032. doi:10.1007/s10853-009-4035-1.
- [3] K.-H. Lee, O. Ohsawa, K. Watanabe, I.-S. Kim, S.R. Givens, B. Chase, J.F. Rabolt, Electrospinning of Syndiotactic Polypropylene from a Polymer Solution at Ambient Temperatures, *Macromolecules.* 42 (2009) 5215–5218. doi:10.1021/ma9006472.
- [4] C. Mit-uppatham, M. Nithitanakul, P. Supaphol, Ultrafine Electrospun Polyamide-6 Fibers: Effect of Solution Conditions on Morphology and Average Fiber Diameter, *Macromol. Chem. Phys.* 205 (2004) 2327–2338. doi:10.1002/macp.200400225.
- [5] J.M. Gohil, A. Bhattacharya, P. Ray, Studies On The Crosslinking Of Poly (Vinyl Alcohol), *J. Polym. Res.* 13 (2006) 161–169. doi:10.1007/s10965-005-9023-9.
- [6] X.-H. Qin, S.-Y. Wang, Electrospun nanofibers from crosslinked poly(vinyl alcohol) and its filtration efficiency, *J. Appl. Polym. Sci.* 109 (2008) 951–956. doi:10.1002/app.28003.
- [7] B. Ding, H.-Y. Kim, S.-C. Lee, C.-L. Shao, D.-R. Lee, S.-J. Park, G.-B. Kwag, K.-J. Choi, Preparation and characterization of a nanoscale poly(vinyl alcohol) fiber aggregate produced by an electrospinning method, *J. Polym. Sci. Part B Polym. Phys.* 40 (2002) 1261–1268. doi:10.1002/polb.10191.
- [8] L.-H. Zhang, X.-P. Duan, X. Yan, M. Yu, X. Ning, Y. Zhao, Y.-Z. Long, Recent advances in melt electrospinning, *RSC Adv.* 6 (2016) 53400–53414. doi:10.1039/C6RA09558E.
- [9] L. Larrondo, R.S.J. Manley, Electrostatic fiber spinning from polymer melts. I. Experimental observations on fiber formation and properties, *J. Polym. Sci. Polym. Phys. Ed.* 19 (1981) 909–920. doi:10.1002/pol.1981.180190601.
- [10] J. Lyons, C. Li, F. Ko, Melt-electrospinning part I: processing parameters and geometric properties, *Polymer.* 45 (2004) 7597–7603. doi:10.1016/j.polymer.2004.08.071.
- [11] A. Stoiljkovic, M. Ishaque, U. Justus, L. Hamel, E. Klimov, W. Heckmann, B. Eckhardt, J.H. Wendorff, A. Greiner, Preparation of water-stable submicron fibers from aqueous latex dispersion of water-insoluble polymers by electrospinning, *Polymer.* 48 (2007) 3974–3981. doi:10.1016/j.polymer.2007.04.050.
- [12] J. Sun, K. Bubel, F. Chen, T. Kissel, S. Agarwal, A. Greiner, Nanofibers by Green Electrospinning of Aqueous Suspensions of Biodegradable Block Copolyesters for Applications in Medicine, Pharmacy and Agriculture, *Macromol. Rapid Commun.* 31 (2010) 2077–2083. doi:10.1002/marc.201000379.
- [13] L. Buruaga, H. Sardon, L. Irusta, A. González, M.J. Fernández-Berridi, J.J. Iruin, Electrospinning of waterborne polyurethanes, *J. Appl. Polym. Sci.* (2010).
- [14] J. Pal, S. Sharma, S. Sanwaria, R. Kulshreshtha, B. Nandan, R.K. Srivastava, Conductive 3D porous mesh of poly( $\epsilon$ -caprolactone) made via emulsion electrospinning, *Polymer.* 55 (2014) 3970–3979. doi:10.1016/j.polymer.2014.06.067.
- [15] E. Giebel, J. Getze, T. Röcker, A. Greiner, The Importance of Crosslinking and Glass Transition Temperature for the Mechanical Strength of Nanofibers Obtained by Green Electrospinning, *Macromol. Mater. Eng.* 298 (2013) 439–446. doi:10.1002/mame.201200080.
- [16] E. Klimov, V. Raman, R. Venkatesh, W. Heckmann, R. Stark, Designing Nanofibers via Electrospinning from Aqueous Colloidal Dispersions: Effect of Cross-Linking and Template Polymer, *Macromolecules.* 43 (2010) 6152–6155. doi:10.1021/ma100750e.
- [17] A. Stoiljkovic, R. Venkatesh, E. Klimov, V. Raman, J.H. Wendorff, A. Greiner, Poly(styrene-co-n-butyl acrylate) Nanofibers with Excellent Stability against Water by Electrospinning from Aqueous Colloidal Dispersions, *Macromolecules.* 42 (2009) 6147–6151. doi:10.1021/ma900354u.

- [18] K. Bubel, Y. Zhang, Y. Assem, S. Agarwal, A. Greiner, Tenside-Free Biodegradable Polymer Nanofiber Nonwovens by “Green Electrospinning,” *Macromolecules*. 46 (2013) 7034–7042. doi:10.1021/ma401044s.
- [19] K. Bubel, D. Grunenber, G. Vasilyev, E. Zussman, S. Agarwal, A. Greiner, Solvent-Free Aqueous Dispersions of Block Copolyesters for Electrospinning of Biodegradable Nonwoven Mats for Biomedical Applications, *Macromol. Mater. Eng.* 299 (2014) 1445–1454. doi:10.1002/mame.201400116.
- [20] W. Yuan, K.-Q. Zhang, Structural Evolution of Electrospun Composite Fibers from the Blend of Polyvinyl Alcohol and Polymer Nanoparticles, *Langmuir*. 28 (2012) 15418–15424. doi:10.1021/la303312q.
- [21] S. Jiang, W. He, K. Landfester, D. Crespy, S.E. Mylon, The structure of fibers produced by colloid-electrospinning depends on the aggregation state of particles in the electrospinning feed, *Polymer*. 127 (2017) 101–105. doi:10.1016/j.polymer.2017.08.061.
- [22] E. Giebel, A. Greiner, Water-Stable Nonwovens Composed of Electrospun Fibers from Aqueous Dispersions by Photo-Cross-Linking, *Macromol. Mater. Eng.* 297 (2012) 532–539. doi:10.1002/mame.201100401.
- [23] W.-Y. Chiang, C.-M. Hu, Studies of reactions with polymers. I. The reaction of maleic anhydride with PVA and the properties of the resultant, *J. Appl. Polym. Sci.* 30 (1985) 3895–3910. doi:10.1002/app.1985.070300928.
- [24] C.-L. Pai, M.C. Boyce, G.C. Rutledge, On the importance of fiber curvature to the elastic moduli of electrospun nonwoven fiber meshes, *Polymer*. 52 (2011) 6126–6133. doi:10.1016/j.polymer.2011.10.055.
- [25] J. Park, E.-S. Lee, T. Amna, Y. Jang, D.H. Park, B.-S. Kim, Effects of heat-treatment on surface morphologies, mechanical properties of nanofibrous poly(propylene carbonate) biocomposites and its cell culture, *Colloids Surf. Physicochem. Eng. Asp.* 492 (2016) 138–143. doi:10.1016/j.colsurfa.2015.11.075.
- [26] S.-S. Choi, S.G. Lee, C.W. Joo, S.S. Im, S.H. Kim, Formation of interfiber bonding in electrospun poly(etherimide) nanofiber web, *J. Mater. Sci.* 39 (2004) 1511–1513. doi:10.1023/B:JMSC.0000013931.84760.b0.
- [27] K. Watanabe, T. Nakamura, B.-S. Kim, I.-S. Kim, Effect of organic solvent on morphology and mechanical properties of electrospun syndiotactic polypropylene nanofibers, *Polym. Bull.* 67 (2011) 2025–2033. doi:10.1007/s00289-011-0618-5.
- [28] M.M. Maciel, S. Ribeiro, C. Ribeiro, A. Francesko, A. Maceiras, J.L. Vilas, S. Lanceros-Méndez, Relation between fiber orientation and mechanical properties of nano-engineered poly(vinylidene fluoride) electrospun composite fiber mats, *Compos. Part B Eng.* 139 (2018) 146–154. doi:10.1016/j.compositesb.2017.11.065.
- [29] S.C. Cheng, Y.Z. Liang, Y.P. Qiu, Effect of Thermal Treatment on the Physical Properties of Electrospun PVDF Membrane, *Adv. Mater. Res.* (2012).
- [30] H.-C. Chen, C.-H. Tsai, M.-C. Yang, Mechanical properties and biocompatibility of electrospun polylactide/poly(vinylidene fluoride) mats, *J. Polym. Res.* 18 (2011) 319–327. doi:10.1007/s10965-010-9421-5.
- [31] Z. Zhao, J. Li, X. Yuan, X. Li, Y. Zhang, J. Sheng, Preparation and properties of electrospun poly(vinylidene fluoride) membranes, *J. Appl. Polym. Sci.* 97 (2004) 466–474. doi:10.1002/app.21762.
- [32] W. Li, Y. Xing, Y. Wu, J. Wang, L. Chen, G. Yang, B. Tang, Study the effect of ion-complex on the properties of composite gel polymer electrolyte based on Electrospun PVdF nanofibrous membrane, *Electrochimica Acta*. 151 (2015) 289–296. doi:10.1016/j.electacta.2014.11.083.
- [33] S. Kaur, D. Rana, T. Matsuura, S. Sundarajan, S. Ramakrishna, Preparation and characterization of surface modified electrospun membranes for higher filtration flux, *J. Membr. Sci.* 390–391 (2012) 235–242. doi:10.1016/j.memsci.2011.11.045.

- [34] F.A. Sheikh, M.A. Zargar, A.H. Tamboli, H. Kim, A super hydrophilic modification of poly(vinylidene fluoride) (PVDF) nanofibers: By in situ hydrothermal approach, *Appl. Surf. Sci.* 385 (2016) 417–425. doi:10.1016/j.apsusc.2016.05.111.
- [35] R. Gopal, S. Kaur, Z. Ma, C. Chan, S. Ramakrishna, T. Matsuura, Electrospun nanofibrous filtration membrane, *J. Membr. Sci.* 281 (2006) 581–586. doi:10.1016/j.memsci.2006.04.026.
- [36] S.L. Shenoy, W.D. Bates, H.L. Frisch, G.E. Wnek, Role of chain entanglements on fiber formation during electrospinning of polymer solutions: Good solvent, non-specific polymer-polymer interaction limit, *Polymer*. 46 (2005) 3372–3384. doi:10.1016/j.polymer.2005.03.011.
- [37] S.L. Shenoy, W.D. Bates, G. Wnek, Correlations between electrospinnability and physical gelation, *Polymer*. 46 (2005) 8990–9004. doi:10.1016/j.polymer.2005.06.053.
- [38] R. Casasola, N.L. Thomas, S. Georgiadou, Electrospinning of poly(lactic acid): Theoretical approach for the solvent selection to produce defect-free nanofibers, *J. Polym. Sci. Part B Polym. Phys.* 54 (2016) 1483–1498. doi:10.1002/polb.24042.
- [39] M.G. McKee, J.M. Layman, M.P. Cashion, T.E. Long, Phospholipid Nonwoven Electrospun Membranes, *Science*. 311 (2006) 353–355. doi:10.1126/science.1119790.
- [40] M.P. Cashion, X. Li, Y. Geng, M.T. Hunley, T.E. Long, Gemini Surfactant Electrospun Membranes, *Langmuir*. 26 (2010) 678–683. doi:10.1021/la902287b.
- [41] G. Singh, A.M. Bittner, S. Loscher, N. Malinowski, K. Kern, Electrospinning of Diphenylalanine Nanotubes, *Adv. Mater.* 20 (2008) 2332–2336. doi:10.1002/adma.200702802.
- [42] M. Reches, E. Gazit, Controlled patterning of aligned self-assembled peptide nanotubes, *Nat. Nanotechnol.* 1 (2006) 195–200. doi:10.1038/nnano.2006.139.
- [43] A. Celebioglu, T. Uyar, Electrospinning of nanofibers from non-polymeric systems: polymer-free nanofibers from cyclodextrin derivatives, *Nanoscale*. 4 (2012) 621–631. doi:10.1039/C1NR11364J.
- [44] A. Celebioglu, T. Uyar, Cyclodextrin nanofibers by electrospinning, *Chem. Commun.* 46 (2010) 6903–6905. doi:10.1039/C0CC01484B.
- [45] A. Ryzhakov, T. Do Thi, J. Stappaerts, L. Bertoletti, K. Kimpe, A.R. Sá Couto, P. Saokham, G. Van den Mooter, P. Augustijns, G.W. Somsen, S. Kurkov, S. Inghelbrecht, A. Arien, M.I. Jimidar, K. Schrijnemakers, T. Loftsson, Self-Assembly of Cyclodextrins and Their Complexes in Aqueous Solutions, *J. Pharm. Sci.* 105 (2016) 2556–2569. doi:10.1016/j.xphs.2016.01.019.
- [46] A. Celebioglu, T. Uyar, Electrospinning of nanofibers from non-polymeric systems: Electrospun nanofibers from native cyclodextrins, *J. Colloid Interface Sci.* 404 (2013) 1–7. doi:10.1016/j.jcis.2013.04.034.
- [47] S. Quideau, D. Deffieux, C. Douat-Casassus, L. Pouységu, Plant Polyphenols: Chemical Properties, Biological Activities, and Synthesis, *Angew. Chem. Int. Ed.* 50 (2011) 586–621. doi:10.1002/anie.201000044.
- [48] T. Mori, K. Rezai-Zadeh, N. Koyama, G.W. Arendash, H. Yamaguchi, N. Kakuda, Y. Horikoshi-Sakuraba, J. Tan, T. Town, Tannic Acid Is a Natural  $\beta$ -Secretase Inhibitor That Prevents Cognitive Impairment and Mitigates Alzheimer-like Pathology in Transgenic Mice, *J. Biol. Chem.* 287 (2012) 6912–6927. doi:10.1074/jbc.M111.294025.
- [49] D. Zanchi, A. Vernhet, C. Poncet-Legrand, D. Cartalade, C. Tribet, R. Schweins, B. Cabane, Colloidal Dispersions of Tannins in Water–Ethanol Solutions, *Langmuir*. 23 (2007) 9949–9959. doi:10.1021/la700694b.
- [50] C. Poncet-Legrand, D. Cartalade, J.-L. Putaux, V. Cheynier, A. Vernhet, Flavan-3-ol Aggregation in Model Ethanolic Solutions: Incidence of Polyphenol Structure, Concentration, Ethanol Content, and Ionic Strength, *Langmuir*. 19 (2003) 10563–10572. doi:10.1021/la034927z.
- [51] K.-T. Chung, T.Y. Wong, C.-I. Wei, Y.-W. Huang, Y. Lin, Tannins and Human Health: A Review, *Crit. Rev. Food Sci. Nutr.* 38 (1998) 421–464. doi:10.1080/10408699891274273.

- [52] N. Sahiner, S. Sagbas, N. Aktas, C. Silan, Inherently antioxidant and antimicrobial tannic acid release from poly(tannic acid) nanoparticles with controllable degradability, *Colloids Surf. B Biointerfaces*. 142 (2016) 334–343. doi:10.1016/j.colsurfb.2016.03.006.
- [53] C. Ringwald, V. Ball, Layer-by-layer deposition of tannic acid and Fe<sup>3+</sup> cations is of electrostatic nature but almost ionic strength independent at pH 5, *J. Colloid Interface Sci.* 450 (2015) 119–126. doi:10.1016/j.jcis.2015.03.009.
- [54] H. Ejima, J.J. Richardson, K. Liang, J.P. Best, M.P. van Koeverden, G.K. Such, J. Cui, F. Caruso, One-Step Assembly of Coordination Complexes for Versatile Film and Particle Engineering, *Science*. 341 (2013) 154–157. doi:10.1126/science.1237265.
- [55] Y. Fei, Y. Chen, H. Wang, W. Gao, R. Yang, Y. Wan, Preparation, characterization of antibacterial PLA/TP nanofibers, *Fibers Polym.* 12 (2011) 340–344. doi:10.1007/s12221-011-0340-9.
- [56] Y.-J. Kim, M.R. Park, M.S. Kim, O.H. Kwon, Polyphenol-loaded polycaprolactone nanofibers for effective growth inhibition of human cancer cells, *Mater. Chem. Phys.* 133 (2012) 674–680. doi:10.1016/j.matchemphys.2012.01.050.
- [57] E. Llorens, L.J. del Valle, A. Díaz, M.T. Casas, J. Puiggali, Polylactide nanofibers loaded with vitamin B6 and polyphenols as bioactive platform for tissue engineering, *Macromol. Res.* 21 (2013) 775–787. doi:10.1007/s13233-013-1090-x.
- [58] J.L. Whittaker, S. Subianto, N.K. Dutta, N.R. Choudhury, Induced insolubility of electrospun poly(N-vinylcaprolactam) fibres through hydrogen bonding with Tannic acid, *Polymer*. 87 (2016) 194–201. doi:10.1016/j.polymer.2016.01.072.
- [59] W. Yang, A.M.M. Sousa, A. Thomas-Gahrng, X. Fan, T. Jin, X. Li, P.M. Tomasula, L. Liu, Electrospun Polymer Nanofibers Reinforced by Tannic Acid/Fe<sup>+++</sup> Complexes, *Materials*. 9 (2016) 757. doi:10.3390/ma9090757.
- [60] W. Yang, A.M.M. Sousa, X. Fan, T. Jin, X. Li, P.M. Tomasula, L. Liu, Electrospun ultra-fine cellulose acetate fibrous mats containing tannic acid-Fe<sup>3+</sup> complexes, *Carbohydr. Polym.* 157 (2017) 1173–1179. doi:10.1016/j.carbpol.2016.10.078.
- [61] A. Einstein, Eine neue Bestimmung der Moleküldimensionen, *Ann. Phys.* 324 (1906) 289–306. doi:10.1002/andp.19063240204.
- [62] A. Einstein, Berichtigung zu meiner Arbeit: „Eine neue Bestimmung der Moleküldimensionen“, *Ann. Phys.* 339 (1911) 591–592. doi:10.1002/andp.19113390313.
- [63] T. Jiang, C.F. Zukoski, Role of Particle Size and Polymer Length in Rheology of Colloid–Polymer Composites, *Macromolecules*. 45 (2012) 9791–9803. doi:10.1021/ma301184t.
- [64] Y. Gnanou, M. Fontanille, Chapter 13: Rheology, Formulation and Polymer Processing Techniques., in: *Org. Phys. Chem. Polym.*, Wiley, 2008.
- [65] Y. Heo, R.G. Larson, The scaling of zero-shear viscosities of semidilute polymer solutions with concentration, *J. Rheol.* 49 (2005) 1117–1128. doi:10.1122/1.1993595.
- [66] W.W. Graessley, Polymer chain dimensions and the dependence of viscoelastic properties on concentration, molecular weight and solvent power, *Polymer*. 21 (1980) 258–262. doi:10.1016/0032-3861(80)90266-9.
- [67] K. Riazi, J. Kübel, M. Abbasi, K. Bachtin, S. Indris, H. Ehrenberg, R. Kádár, M. Wilhelm, Polystyrene comb architectures as model systems for the optimized solution electrospinning of branched polymers, *Polymer*. 104 (2016) 240–250. doi:10.1016/j.polymer.2016.05.032.
- [68] K.J. Siebert, N.V. Troukhanova, P.Y. Lynn, Nature of Polyphenol–Protein Interactions, *J. Agric. Food Chem.* 44 (1996) 80–85. doi:10.1021/jf9502459.
- [69] R.S. Barhate, S. Ramakrishna, Nanofibrous filtering media: Filtration problems and solutions from tiny materials, *J. Membr. Sci.* 296 (2007) 1–8. doi:10.1016/j.memsci.2007.03.038.
- [70] B.P. Lee, J.L. Dalsin, P.B. Messersmith, Synthesis and Gelation of DOPA-Modified Poly(ethylene glycol) Hydrogels, *Biomacromolecules*. 3 (2002) 1038–1047. doi:10.1021/bm025546n.



- [71] M. Allais, F. Meyer, V. Ball, Multilayered films made from tannic acid and alkaline phosphatase with enzymatic activity and electrochemical behavior, *J. Colloid Interface Sci.* 512 (2018) 722–729. doi:10.1016/j.jcis.2017.10.101.
- [72] D.E. Fullenkamp, D.G. Barrett, D.R. Miller, J.W. Kurutz, P.B. Messersmith, pH-dependent cross-linking of catechols through oxidation via Fe<sup>3+</sup> and potential implications for mussel adhesion, *RSC Adv.* 4 (2014) 25127–25134. doi:10.1039/C4RA03178D.
- [73] J. Guo, Y. Ping, H. Ejima, K. Alt, M. Meissner, J.J. Richardson, Y. Yan, K. Peter, D. von Elverfeldt, C.E. Hagemeyer, F. Caruso, Engineering Multifunctional Capsules through the Assembly of Metal–Phenolic Networks, *Angew. Chem. Int. Ed.* 53 (2014) 5546–5551. doi:10.1002/anie.201311136.
- [74] J. Lee, H. Cho, J. Choi, D. Kim, D. Hong, J.H. Park, S.H. Yang, I.S. Choi, Chemical sporulation and germination: cytoprotective nanocoating of individual mammalian cells with a degradable tannic acid–FeIII complex, *Nanoscale.* 7 (2015) 18918–18922. doi:10.1039/C5NR05573C.
- [75] R. Ameloot, F. Vermoortele, W. Vanhove, M.B.J. Roeffaers, B.F. Sels, D.E. De Vos, Interfacial synthesis of hollow metal–organic framework capsules demonstrating selective permeability, *Nat. Chem.* 3 (2011) 382–387. doi:10.1038/nchem.1026.
- [76] A. Andersen, M. Krogsgaard, H. Birkedal, Mussel-Inspired Self-Healing Double-Cross-Linked Hydrogels by Controlled Combination of Metal Coordination and Covalent Cross-Linking, *Biomacromolecules.* (2017). doi:10.1021/acs.biomac.7b01249.



# 4

## DEVELOPMENT OF A MULTI-JET SPINNERET

*Mats fabricated by “green” electrospinning are destined to become liquid filtration membranes. In that optic, as electrospun mats must be wide and large enough as well as homogeneous in thickness to be characterized in standard liquid filtration apparatus, a multi-jet spinneret has been developed in order to increase productivity. After evidencing the major drawbacks linked with the traditional needle electrospinning process, the development of the multi-jet spinneret is presented in this chapter. The main focus was to produce mats with constant thicknesses. Different rotary spinnerets using needles, disks and CDs have also been compared.*

## 4.1 Introduction

Single needle electrospinning setups are quite widespread as they are rather easy to implement. Nevertheless, mainly for productivity reasons, other setups may be used: multi-nozzles setups and free surface electrospinning setups [1,2]. Multi-nozzle electrospinning systems can be composed of needles [3–5] or arrayed holes either located at the side of the nozzle as grooves [6] or channeled in a matrix [7]. This system is convenient for the high-yield electrospinning as the spinneret can account for many electrospinning jets according to the number of nozzles. A spinneret composed of 19 holes has been developed for instance by Zheng et al [8]. The spinneret must nevertheless be properly optimized so that each hole can give birth to one jet. Furthermore, it is inconvenient for stability reasons as nozzles can easily be clogged and washing the spinneret after electrospinning may be arduous. Instead, the number of jets formed from free surface electrospinning systems is independent from the number of nozzles, which cannot be clogged. Different systems have been imagined [2] such as a bubble electrospinning system [9], a porous tube [10,11], a two-layer electrospinning spinneret [12], a grid [13], a cleft spinneret [14], a flat plate [15], or a wire [16]. In this chapter, we developed rotary multi-jet spinnerets composed of needle-disks, disks and CDs (Figure 4.1). They were chosen for their simplicity and their cheapness. Several articles have already developed similar spinnerets. For instance, Moon et al. worked on a helically probed rotating cylinder [17]. They studied the electrical field between the spinneret and the collector and electrospun various kind of polymers. Ali et al. [18] developed a flat wheel spinneret. They studied the influence of the electrical field, the solution concentration and the collecting distance on electrospun fibers. The production rate was found to increase with the applied field. The fiber diameter increases with the concentration as in traditional needle electrospinning. On the contrary, the fiber diameter decreases when the collecting distance is increased as it allows a longer elongation of fibers. Finally, they compared the flat wheel with a cylinder, a disk and a ring in terms of productivity as a function of the applied voltage. The ring and the disk depict the highest production rates. Shuakat et al. [19] used a disk spinneret coupled with a needle to produce yarns. They noted that the thicker the disk was, the thinner fibers were due to higher electrical field intensities on the rim of thin disks. In addition, the disk material played a role on the electrospinning process as higher voltages could be applied on a high density polyethylene disc than on metal discs before corona discharge. Wang et al. [20] developed a multi-ring spinneret, studied the effect of applied voltage, fiber diameter and solution concentration on productivity and analyzed the electrical field. Interestingly, when the viscosity of solutions becomes too high, productivity is dramatically decreased. In needle electrospinning, needles are clogged when the viscosity of solutions is too high. Niu et al. [21] compared a disk spinneret and a cylinder. Under the same conditions, fibers generated from the disk spinneret were thinner than those produced with the cylinder. Moreover, for the cylinder, as the voltage is increased, fibers are first generated from its ends. Then, above a certain voltage, fibers are generated from the whole surface of the cylinder. Ali et al. [22] compared a disk spinneret and a sprocket wheel spinneret with the applied voltage, the solution concentration and the spinning distance. Thicker fibers were produced with the disk spinneret than with the sprocket wheel spinneret as the electrical field is higher at sharps which promote the electrospinning jet. For this reason, lower voltages can also be used to generate fibers from the sprocket wheel spinneret than from the disk spinneret. Niu et al. [23] compared three spinnerets: a cylinder, a disc and a coil. The electrical fields on the edges of the disk and on the coil were higher than the one on the surface of the cylinder, leading to the production of thinner fibers with the disk and the coil. The highest production rate was obtained with the coil. One last very interesting article for the present study was written by Liu et al. [24]. They compared a needle-disk and a disk. The control of jet formation was easier in the case of the needle-disk spinnerets as the number of needles, inducing ultra-high electrical field intensity at needle tips, controls the number of jets.

In this chapter, our first goal is to highlight the difficulties that we faced when we tried to electrospin large PA11 mats and the reasons that led us to choose to develop rotary multi-jet spinnerets. Second, we developed three rotary multi-jet spinnerets. We electrospun different solutions on the one hand to compare the spinnerets. On the other hand, we tried to produce mats of constant thicknesses. Last but not least, a study on the productivity of the developed spinnerets was started.

## 4.2 Materials and methods

### 4.2.1 Materials

Polyamide 11 Rilsan® ( $M_w = 47400$  g/mol) (PA11) was furnished by Arkéma. Dichloromethane (Pure-stabilized with amylene) (DCM) was purchased from Carlo Erba. Formic acid (puriss. p.a., ACS reagent, reagent grade,  $\geq 98\%$ ) (FA) was purchased from Sigma-Aldrich. Polyvinyl alcohol Mowiol® 18-88 ( $M_w = 130\,000$  g/mol) (PVA) was purchased from Sigma-Aldrich. Platamid aqueous suspension (D5030, solid content:  $29.2 \pm 0.6\%$ , particle size:  $104 \pm 38$  nm) (coPA) was provided by Arkema. Pluronic 127 was purchased from Sigma-Aldrich. Deionized water was used as solvent.

### 4.2.2 Solutions preparation

A concentration of 6 wt% of PA11 was dissolved in FA/DCM v/v 4 hours prior to the experiments. Concentrations of 5 wt% and 16.1 wt% of PVA were dissolved in water and heated at 60°C during 12 hours prior to the experiments. The solution concentrated at 16.1 wt% was mixed with coPA suspensions so that the final solution contains 20 wt% of solid coPA particles and 5 wt% of PVA in water. A concentration of 0.5 wt% of pluronic 127 could be added to solutions composed of 5 wt% of PVA in water.

### 4.2.3 Electrospinning setups

Needle electrospinning setup: Electrospinning was performed using a home-made electrospinning set-up. A difference of potential was established between a needle and a collector using a high-voltage power supply (Spellmann SL 10). The collector was rotated through a high-speed laboratory stirrer (Ika® Eurostar 20). A syringe pump (Fischer Scientific) pushed the solution through the needle. The distance between the needle and the collector was kept at 15 cm. The rotation speed of the collector was set at 150 rpm. Experiments were performed at 22°C and relative humidity was maintained at  $40 \pm 2\%$ .

Multi-jet electrospinning setups (Figure 4.1): Three different spinnerets have been developed. They are composed of either needle-disks, disks or CDs. The spinneret composed of needle-disks is a rotary cylinder (diameter of 6 cm) on which several needle-disks are fixed. Needles are 3 cm long and have a diameter of 1 mm. A needle-disk is composed of needles regularly distributed on the rim of the cylinder and their edges describe a circle of 12 cm of diameter. The spinneret composed of disks and CDs is a mandrel on which disks and CDs are fixed. The diameter of disks and CDs is 12 cm. The thickness of disks is 1 mm. A CD is composed of a thin layer of aluminum placed between a thin polymer film protecting the aluminum layer and a 1.2 mm thick polycarbonate support layer. The thickness of the aluminum layer is of few hundreds of nm. Electrospinning solutions are contained into a rectangular tray (10 cm x 10 cm) in which multi-jet spinnerets plunge. By rotating, solution is taken off on the edge of the spinnerets. Half a complete rotation later, the electrospinning process takes place when the part of the spinnerets covered with the electrospinning solution



face the collector. The collector is a flat rectangular surface (30 cm x 21 cm). The collector is located 10 cm away from the edge of the spinnerets. The collector is able to translate along an axis parallel to the spinnerets rotation axis. Multi-jet spinnerets are at potential 0 kV. Temperature was kept at 22°C and relative humidity at  $30 \pm 2$  %.

In part 4.4.2 and 4.4.3, the tension applied to the collector is 40 kV when the spinneret is a multi-needle-disk. It is 55 kV for the multi-disk.

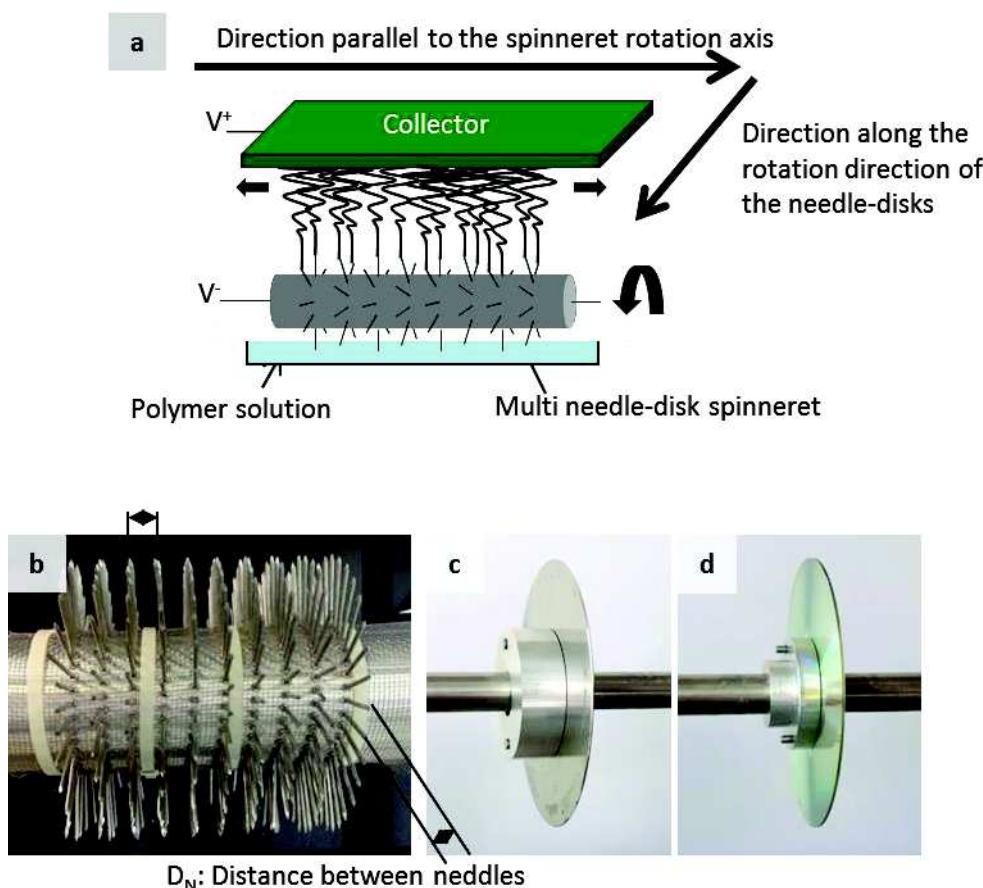


**Figure 4.1.** a) Schematic representation and b) photo of a multi-needle-disk spinneret. The number of needle-disks can be adapted and needle-disks can be replaced by c) disks or d) CDs.

#### 4.2.4 Mat characterization

Before SEM examination, samples were coated with a thin layer of gold with a gold coater (Quorum Q 150 R S, Quorum Technologies). A SEM (Vega-3, Tescan) was used in high vacuum mode using accelerating voltages of 5 kV and working distances in the range of 10 mm. For each sample showing fibers, the diameter of 100 fibers was measured on 5 different SEM images with the image analysis software Image J. Mass of mats was weighted (Sartorius M-power, precision: 0.1 mg). Profiles of mats were measured with a 3D Dektak mechanical profilometer (Veeco). Along the length of the deposit and each centimeter, a profile of the deposit was measured allowing an estimation of the area, as it is shown in Figure 4.2. The volume of fibers deposited on the collector was then calculated with the following formula:

$$V_{Deposit} = (A_1 + \dots + A_n) * L/N \quad \text{Equation 4.1}$$

With  $V_{Deposit}$  the volume of fibers deposited on the collector (in  $\text{cm}^3$ ),  $A_n$  the area of the  $n^{\text{th}}$  transversal section (in  $\text{cm}^2$ ),  $L$  the length of the deposit (in cm) and  $N$  the number of transversal sections.

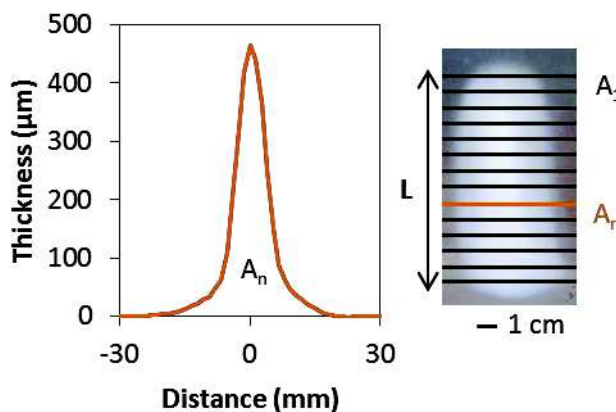


**Figure 4.2.** Profile of a transversal section.

Porosity was calculated from the measurement of the volume of the deposit ( $V_{Deposit}$ ) and from its mass ( $m_{Deposit}$ ) knowing that the density of PA11 is  $1.03 \text{ g/cm}^3$ :

$$Porosity = \frac{V_{Deposit} - (m_{Deposit}/1.03)}{V_{Deposit}} \quad \text{Equation 4.2}$$

The thickness was measured by confocal microscopy (Olympus X 41). To this aim, a flat deposit was electrospun on the collector. To form a flat deposit, the collector was transversally translated during the experiment on 8 cm (Figure 4.12). Then in the middle of the mat, the thickness was measured by subtraction between the height with and without the flat mat.

### 4.3 Drawbacks linked to the electrospinning with a needle

The first mats that were fabricated during this thesis were electrospun with a solution containing PA11 solubilized in formic acid and dichloromethane. Sadly, in addition to the inherent low productivity linked to the use of an electrospinning needle, the solution was found to evolve over time. As a matter of fact, the solvent evaporates so fast that the needle rapidly cloaked. Depending on the polyamide concentration, the electrospinning time could be reduced to 5 minutes. Once the electrospinning needle was cloaked, the whole feeding system had to be cleaned.

In order to evidence this behavior, the evolution of the electrospinning solutions was followed during 40 minutes with a solution composed of 4 wt% of PA11 in formic acid and dichloromethane. It can be seen from Figure 4.3a and c that the fiber diameter increases over time. After 40 minutes of electrospinning, the fiber diameter ( $481 \pm 121 \text{ nm}$ ) is 2.8 times higher than the fiber diameter measured after 3 minutes ( $174 \pm 39 \text{ nm}$ ) and is closed to the fiber diameter of mats electrospun during 3 minutes with a solution composed of 7 wt% of PA11 ( $511 \pm 131 \text{ nm}$ ). It was inferred that the increase of the fiber diameter is linked with an increase in

concentration at the tip of the needle due to solvent evaporation, so that the concentration of the initial 4 wt% of PA11 has, after 10 minutes of electrospinning, a concentration of 6 wt% of PA11 and after 40 minutes of electrospinning a concentration of 7 wt% of PA11 (Figure 3.4b). These results prove that the concentration of PA11 electrospinning solution increases over time. It also means that if a solution with an initial higher concentration is used, then the solubility threshold is reached faster. This explains why, for highly concentrated solutions, the electrospinning needle is rapidly cloaked as only little solvent evaporation is required for the solution to cross the solubility threshold and to precipitate.

From the previous results, it became obvious that thick, large and wide mats could not be electrospun with a needle in a decent time interval. It was chosen to develop a free-surface setup to overcome cloaking and low productivity issues.

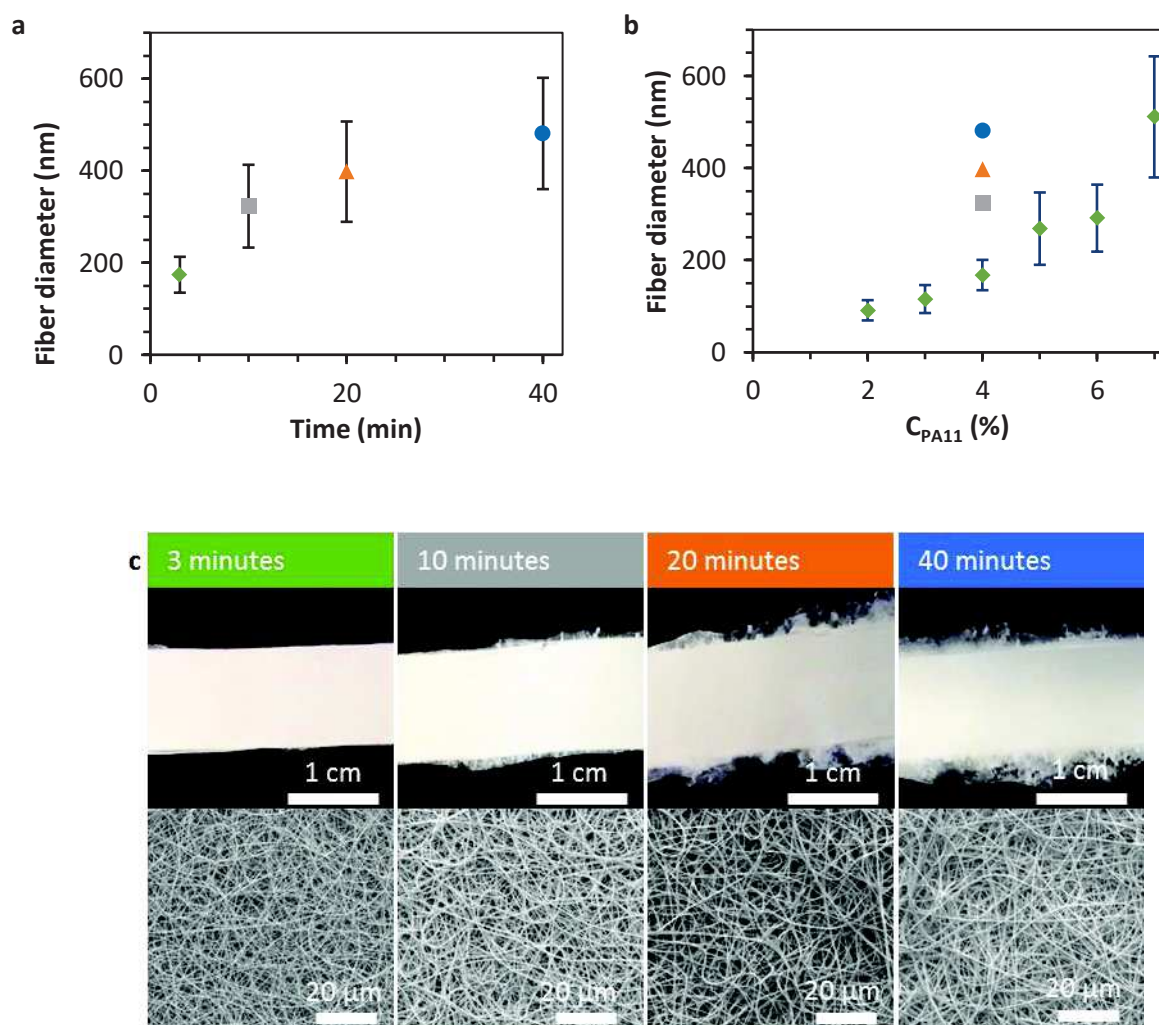


**Figure 4.3.** a) Fiber diameter of PA11 fibers over time. b) Fiber diameter of PA11 fibers over time (after 3 minutes in green, 10 minutes in grey, 20 minutes in orange and 40 minutes in blue) and with the concentration. c) Photo of PA11 mats and fibers over time.

## 4.4 Development of a multi-jet spinneret

Contrary to the traditional needle electrospinning setup, whose productivity is limited, surface free electrospinning setups are very promising. In that regard, three multi needle-jet spinnerets were developed (a multi needle-disk spinneret, a multi disk spinneret and a multi CD spinneret) and various solutions could be electrospun. For filtration application, the development of a new multi-jet setup must ensure the fabrication of flat mats with a constant thickness. A first study was thus conducted in that sense. Second, the productivity of the spinnerets was assessed, and a study was started to understand how the geometry of spinnerets (distance between needle-disks, distance between needles and spinneret's rotation speed) can be optimized.

### 4.4.1 Electrospinning with multi-jet spinnerets

Three solutions have been electrospun. They have been chosen in accordance with chapter 2 (6 wt% PA11 in FA/DCM v/v) and with chapter 3 (5 wt% PVA in water and 20/5 wt% coPA/PVA in water). It was possible to electrospin these solutions with all setups: one needle, a needle-disk, a disk and a CD (Figure 4.4). The electrospinning with one needle allowed using the smallest difference of potential to fabricate fibers for a fixed distance between the spinneret and the collector. The setup using a disk as a spinneret required the highest difference of potential. These results evidence the fact that the geometry of the emitter has a significant influence on the electric field. Sharp needles (present in the needle and in the needle-disk spinnerets) as well as sharp edges (the thin thickness of the aluminum layer constituting CDs) lead to an increase of the electric field at their vicinity. The increase of the electric field thanks to the presence of sharp parts allows a reduction of the applied electric field necessary to electrospin fibers.



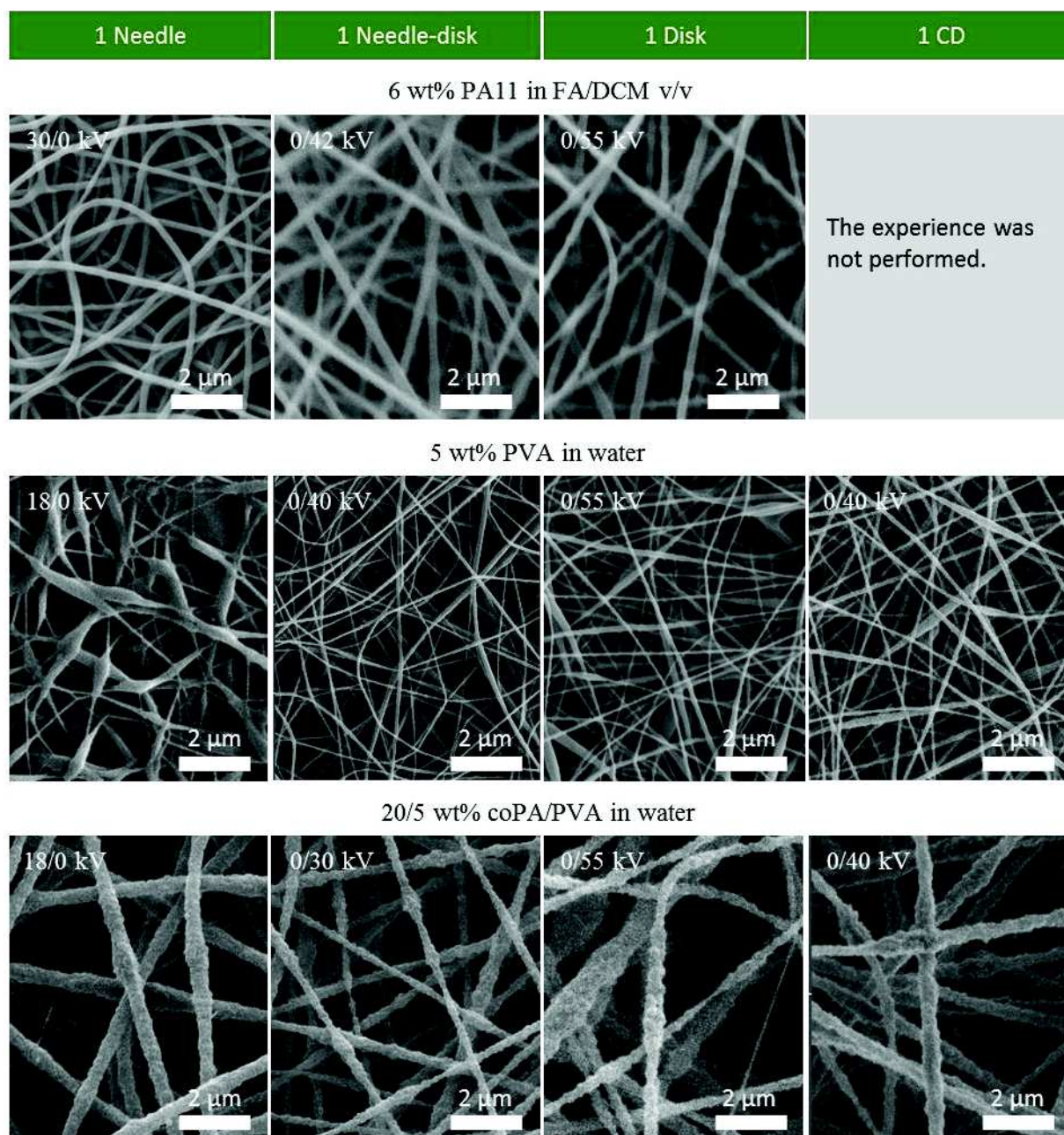


**Figure 4.4.** Electrospinning of 6 wt% PA11 in FA/DCM v/v, 5 wt% PVA in water and 20/5 wt% coPA/PVA in water with 1 needle, 1 needle-disk, 1 disk and 1 CD. Potentials ( $U_{\text{spinneret}}/U_{\text{collector}}$ ) were chosen in order to favor the electrospinning of fibers.

#### 4.4.2 Fabrication of mats with a constant thickness

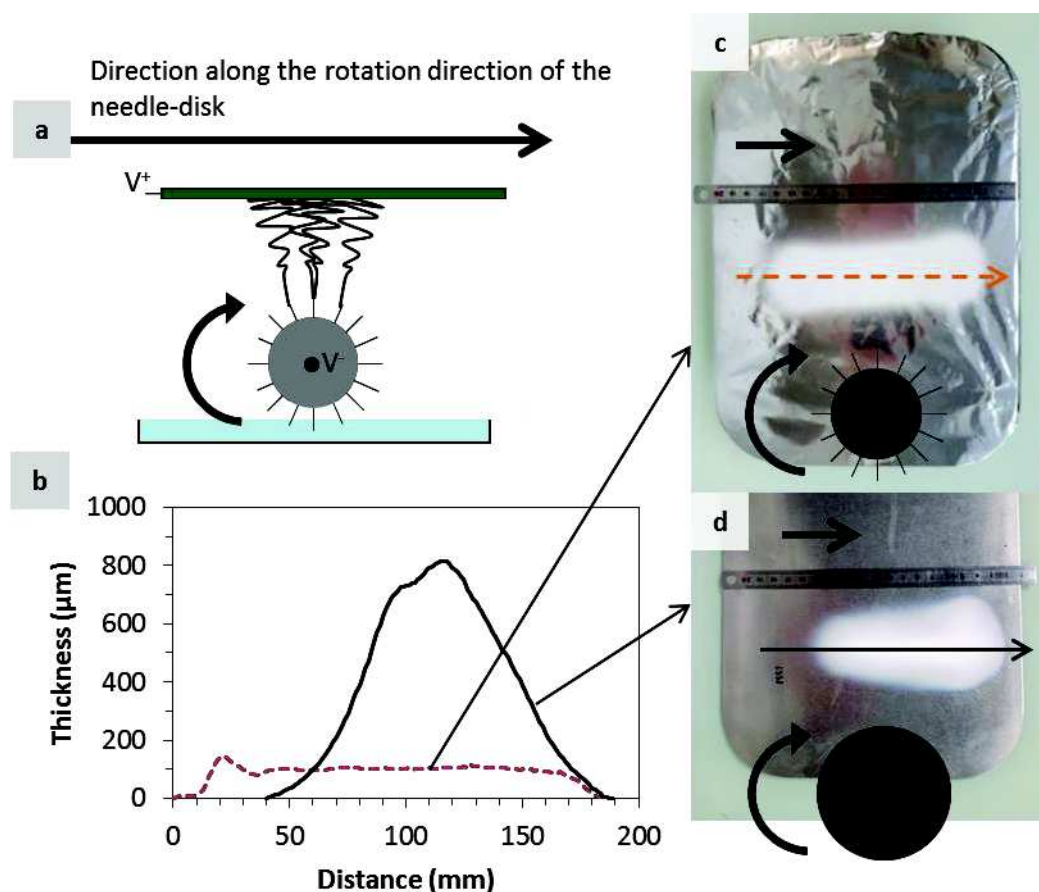
The distribution of the thickness of mats electrospun with one needle-disk, one disk and multi needle-disks was investigated. The study was not conducted for CDs due to the fact that CDs were damaged over time which might have altered results. Thicknesses were evaluated along the direction of rotation of needle-disks and disks and parallel to the spinnerets rotation axis (Figure 4.1a). The electrospinning solution is 6 wt% PA11 in FA/DCM 50/50 v/v and the electrospinning time 20 minutes when not specified.



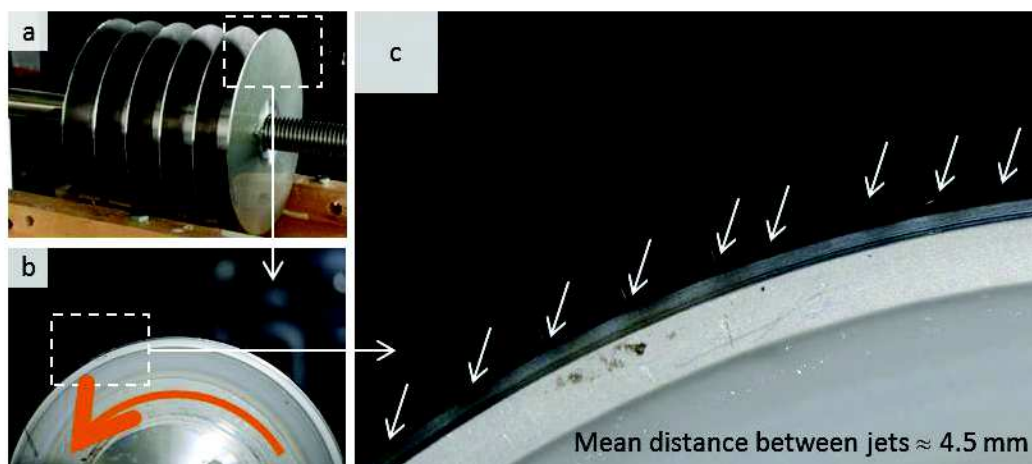
### Thickness along the direction of rotation of needle-disks and disks

The thickness along the direction of rotation was first measured with one needle-disk and with one disk. The collector was static, and the electrospinning time was fixed to 20 minutes. The distance between the needles of the needle-disk is  $D_N = 1$  cm. The rotation speed of both spinnerets is 60 rpm. Profiles of mats are displayed in Figure 4.5. For the nonwoven electrospun with the needle-disk, the deposition of fibers is well distributed on the collector. The deposit is 17 cm long and the thickness ( $103 \pm 4 \mu\text{m}$ ) remains on the overall constant over 10 cm. It can nevertheless be noted that the thickness of the deposit is slightly higher on the 2 first cm where fibers are deposited, meaning that fibers are more attracted to this area. On the contrary, for the nonwoven electrospun with the disk spinneret, the deposition of fibers is more concentrated, hence the shorter length (13 cm) and the higher maximal thickness ( $812 \mu\text{m}$ ). Fibers are deposited differently depending on the geometry of spinnerets which induce different electrical field repartitions. Indeed, for the disk, the number of jet is not restricted by the number of needles. Jets can be emitted from the whole rim (Figure 4.6).

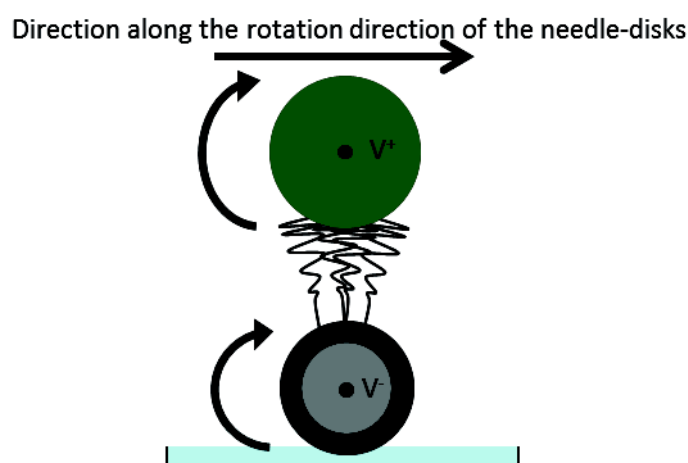
In conclusion, needle-disk spinnerets can be used to fabricate mats that are flat along their rotation direction contrary to disk spinnerets. For disk spinnerets, it is crucial to use rotary collectors so that mats can be of equal thickness along the direction of rotation (An example of such setup is given in Figure 4.7).



**Figure 4.5.** a) Schematic representation of the setup. b) Profiles along the direction of the rotation of the needle-disk (dotted orange line) and of the disk (black line). c) Image of the mat electrospun with the needle-disk spinneret. The orange dotted arrow represents the line along which the thickness was measured. d) Image of the mat electrospun with the disk spinneret. The black arrow represents the line along which the thickness was measured. The black and thick arrow indicates the rotation direction of the needle-disk.

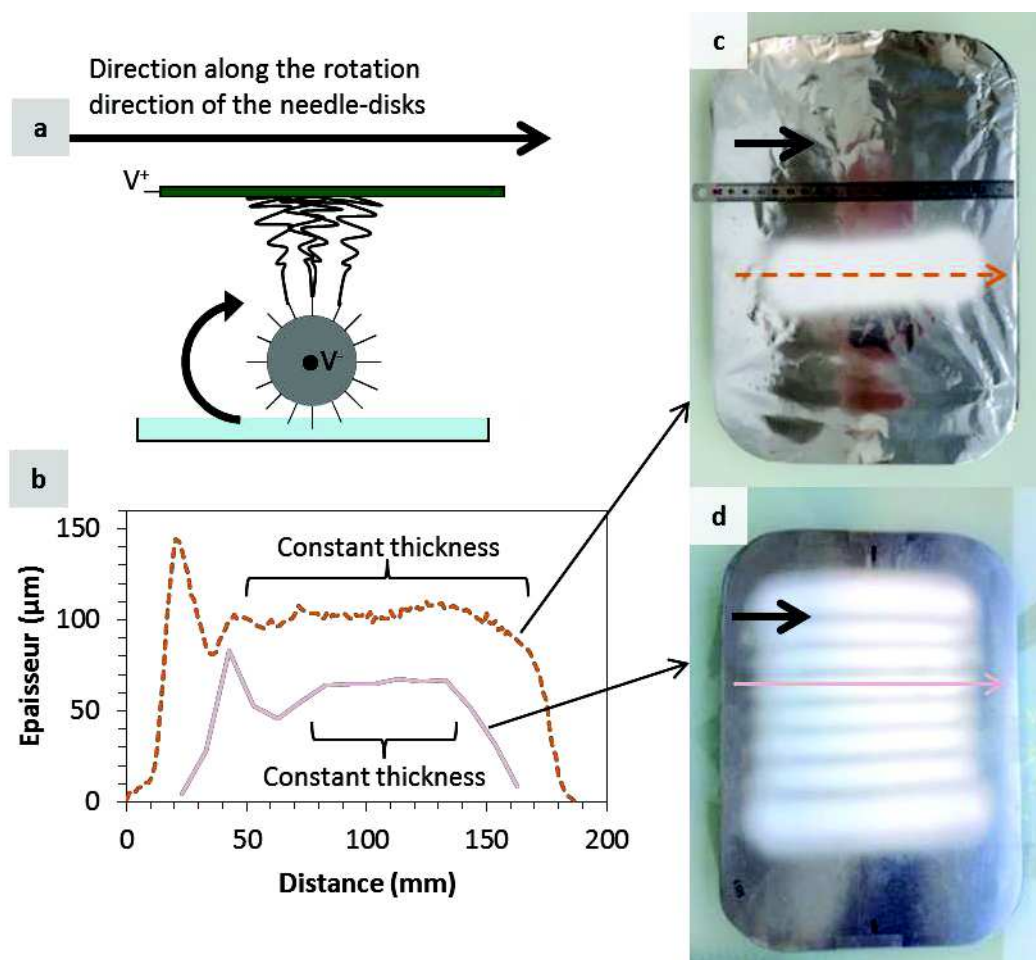


**Figure 4.6.** Photos of a) a multi disk spinneret, b) of a disk and c) of the initiation of jets on the rim of the disk.



**Figure 4.7.** Schematic representation of a setup where both the disk spinneret and the collector are rotary.

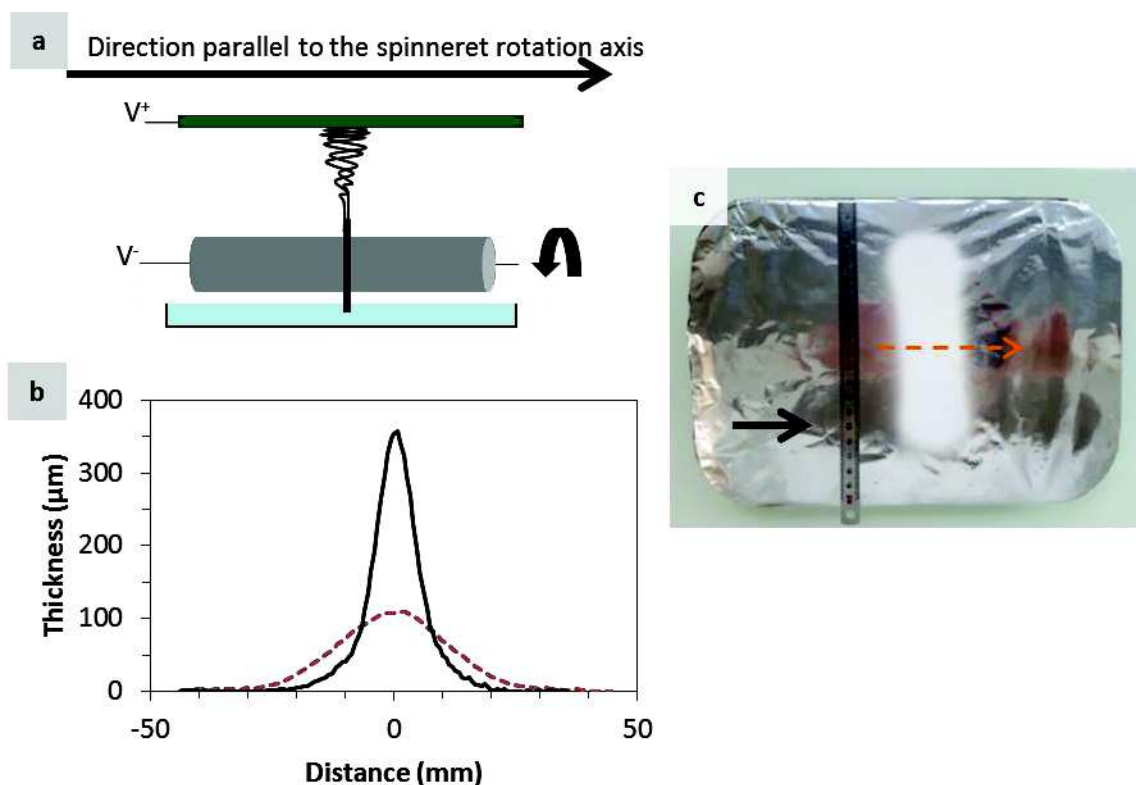
The thickness along the direction of rotation was also measured with a multi needle-disk composed of 8 needle-disks (such as the one see in Figure 4.1.b). Figure 4.8 compares the profiles of mats electrospun with an inner row of an 8 needle-disks spinneret and with one needle-disk. Electrospinning conditions are the same than previously. For the 8 needle-disk spinneret, the distance between needle-disks is 2 cm. The mean thickness of mats (calculated where the distribution of the thickness is a plateau as shown in Figure 4.8b) fabricated with the inner row is smaller ( $63 \pm 6 \mu\text{m}$ ) than that fabricated with a unique needle-disk ( $103 \pm 4 \mu\text{m}$ ). This is due to the fact that the electrical field at the edge of needles of inner needle-disks is disturbed and partially masked by the electrical field of neighboring needle-disks. The thickness of the outer row ( $107 \pm 4 \mu\text{m}$ ) was found to be close to the thickness of the mat electrospun with one row ( $103 \pm 4 \mu\text{m}$ ) Figure 4.11.



**Figure 4.8.** a) Schematic representation of the setup. b) Profiles along the direction of the rotation of the unique needle-disk (dotted orange line) and of the inner needle-disk (pink line). c) Image of the mat electrospun with the unique needle-disk spinneret. d) Image of the mat electrospun with the 8 needle-disk spinneret. The orange dotted and pink arrows represent the lines along which the thicknesses were measured. The black and thick arrows indicate the direction along the rotation of the needle-disks.

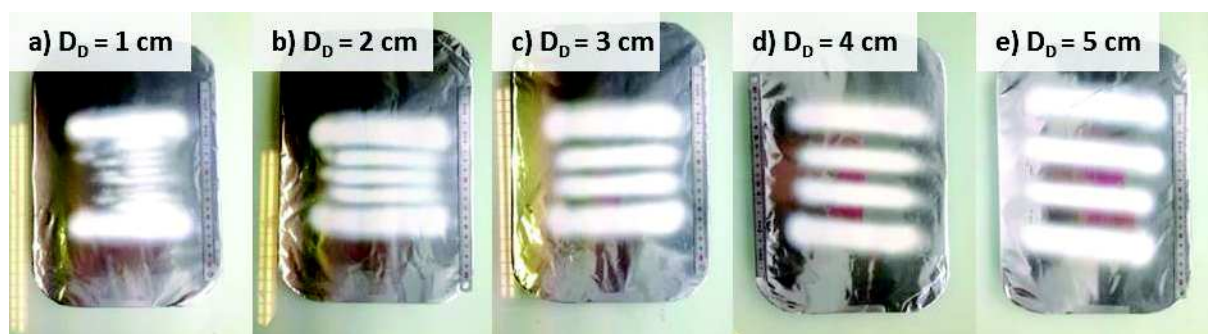
#### *Thickness parallel to the spinnerets rotation axis*

Figure 4.9 shows the profiles of mats parallel to the spinnerets' rotation axis for one needle-disk and for one disk. The collector was fixed. The electrospinning time was 20 minutes. The distance between the needles of the needle-disk is 1 cm and the rotation speed of both spinnerets 60 rpm. The mat fabricated with the needle-disk is 4 cm wide while it is 3 cm wide for the disk. The maximum thickness of mats was  $103 \pm 4 \mu\text{m}$  of the mats fabricated with the needle-disk and  $354 \pm 4 \mu\text{m}$  cm for the mat fabricated with the disk. The thickness might increase or decrease depending on where along the direction of rotation of needle-disks and disks the measure is taken. Profiles can be fitted with a Gaussian function for both spinnerets. Results underline the fact that the collector must be translated along on axis parallel to the spinnerets rotation axis in order to produce mats that are wide and of constant thickness on the whole width.



**Figure 4.9.** a) Schematic representation of the setup. b) Profiles parallel to the spinneret rotation axis for the needle-disk (dotted orange line) and for the disk (black line). c) Image of the mat electrospun with the needle-disk spinneret. The orange dotted arrow represents the line along which the thickness was measured. The black and thick arrow indicates the direction parallel to the spinneret rotation axis.

Multi-needle disk spinnerets were then investigated. The distance between multi needle-disk spinnerets was increased in order to understand how profiles parallel to the spinneret rotation axis are influenced. The distance between needle-disks ( $D_D$ ) was varied from 1 to 5 cm. Figure 4.10 shows mats after 3 minutes. For  $D_D = 1$  cm, the low deposition of fibers suggests a high disruption of the electric field (Figure 4.10a). Liu et al. [25] worked with a distance between rings higher than 1 cm for productivity reasons. When the distance between needle-disks increases from 2 to 5 cm, the electric field becomes less disturbed.



**Figure 4.10.** Deposit as a function of the distance between needle-disks ( $D_D$ ) for a distance between needles equal to 1 cm.



The profiles of an outer row and of 3 inner rows have been measured in the case where the number of needle-disk is 8 and the distance between needle-disks 2 cm. This aim is to evidence the fact that the deposition of fibers is affected differently whether the needle-disks have one or two neighboring needle-disks. It can indeed be seen in Figure 4.11 that the thickness of the outer row is higher than the thickness of the inner rows.

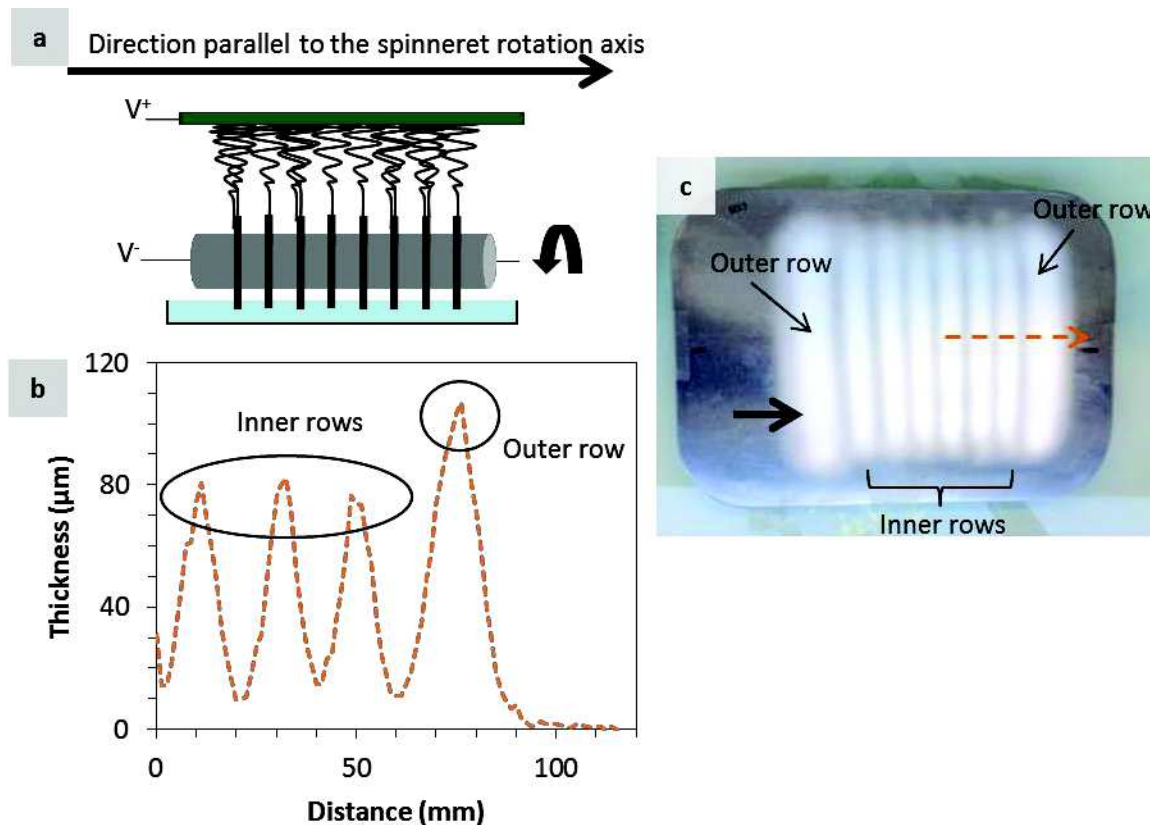


**Figure 4.11.** a) Schematic representation of the setup. b) Profiles parallel to the spinneret rotation axis of the 8 needle-disk spinneret (dotted orange line). c) Image of the mat electrospun with the 8 needle-disk spinneret. The orange dotted arrow represents the line along which the thickness was measured. The black and thick arrow indicates the direction parallel to the spinneret rotation axis.

#### *Thickness as a function of the collector translation distance*

A spinneret composed of 8 needle-disks was used to determine the translation distance that the collector must have in order to electrospin a flat mat (Figure 4.12). The distance between needle-disks is 2 cm and the distance between needles 1 cm. The collector was either fixed, or translated on 4 cm, or translated on 8 cm. Its rotation speed was 60 rpm and the collection time 20 minutes. It can be seen that even if needle-disks are distant from 2 cm, a translation on 4 cm is not enough to obtain a flat mat as the influence of outer rows is still too important, thus leading to higher thicknesses on the edges of mats. A translation distance of 8 cm (+/- 4 cm) is enough to fabricate a flat mat, provided that mats are cut on 2 cm on their edges.



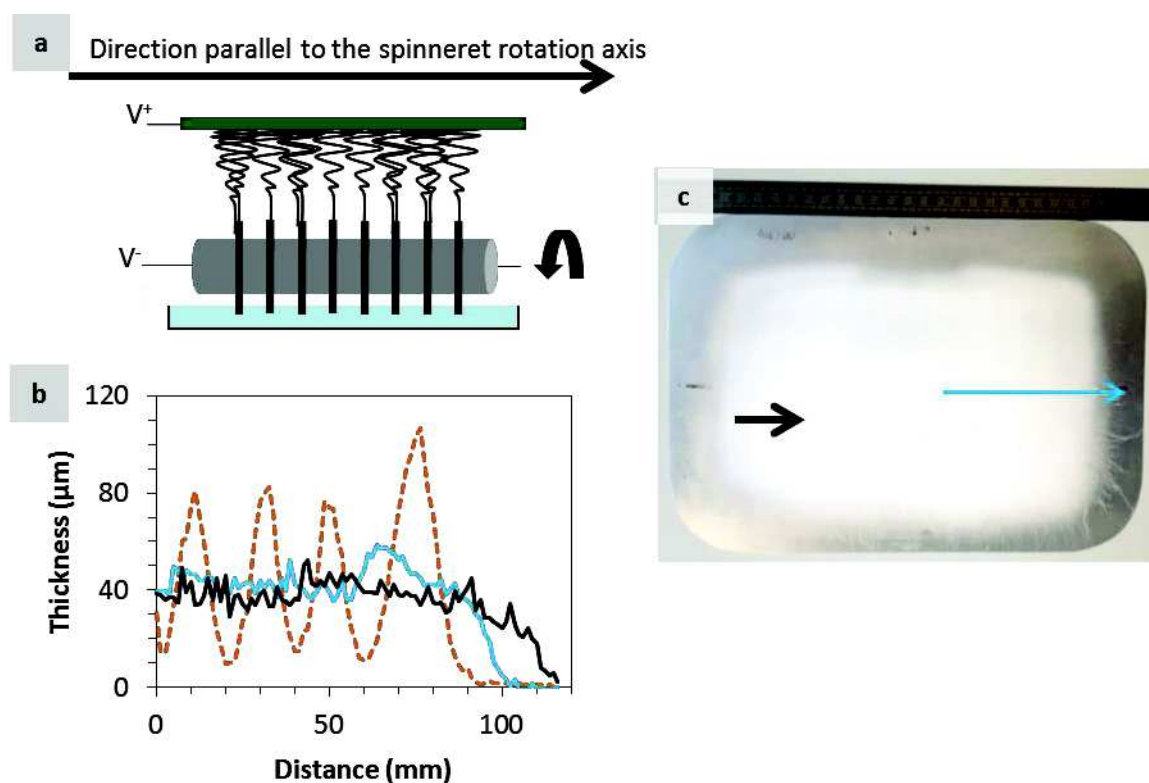


**Figure 4.12.** a) Schematic representation of the setup. b) Profiles parallel to the spinneret rotation axis of the 8 needle-disk spinneret with a fixed collector (orange dotted line), with the collector translated on 4 cm (blue line) and with the collector translated on 8 cm (black line). c) Image of the mat electrospun with the 8 needle-disk spinneret and the collector translated on 8 cm. The blue arrow represents the line along which the thickness was measured. The black and thick arrow indicates the direction parallel to the spinneret rotation axis.

#### 4.4.3 Productivity of multi-jet spinnerets

No proper study was conducted on the increase of productivity as a function of the spinneret or as a function of solutions due to lack of time. Nevertheless, productivity of mats electrospun from a solution composed of 6 wt% of PA11 in FA/DCM with one needle-disk (distance between needles of 1 cm) and with one disk was assessed. Productivity of mats was also measured for the solution 5 wt% of PVA in water to which a small amount of Pluronic 127 was added.

##### 4.4.3.1 Productivity in the case of a solution of 6 wt% of PA11 in FA/DCM 50/50 v/v

###### PRODUCTIVITY WITH THE SOLUTION 6 wt% OF PA11 IN FA/DCM 50/50 V/V

From the measurement of profiles, the volume of mats could be inferred with the solution composed of 6 wt% of PA11 in FA/DCM.

The apparent volume of the nanofibrous mat electrospun by the disk in 20 minutes at 60 rpm in part 4.4.2 was  $\sim 0.55 \text{ cm}^3$  (throughput of  $\sim 1.7 \text{ cm}^3/\text{h}$  taking into account the porosity of mats). The apparent volume of the

nanofibrous mat electrospun by the needle-disk spinneret (distance between needles of 1 cm) in 20 minutes at 60 rpm in part 4.4.2 was  $\sim 0.36 \text{ cm}^3$  (throughput of  $\sim 1.1 \text{ cm}^3/\text{h}$  taking into account the porosity of mats). Comparing the number of jets between emitters is tough as for both emitters either the flow rate per jet and the number of jets may vary. Nevertheless, the fact that the number of jets is not restricted by the number of needles for the disk can explain its higher productivity.

The apparent volume of the nanofibrous mat electrospun by the 8 needle-disk spinneret in 20 minutes in part 4.4.2 was estimated at  $\sim 0.81 \text{ cm}^3$  (throughput of  $\sim 2.4 \text{ cm}^3/\text{h}$  taking into account the porosity of the mat). This value was deduced from the volume of an outer row (throughput of  $\sim 0.46 \text{ cm}^3/\text{h}$  taking into account the porosity of the mat) and of an inner row (throughput of  $\sim 0.25 \text{ cm}^3/\text{h}$  taking into account the porosity of the mat). This value is more than twice higher than the apparent volume electrospun with a single needle-disk. The production rate does not increase linearly with the number of needle-disks. Contrary to what could be expected at first sight, the production rate of the 8 needle-disk spinneret is not equal to 8 times the production rate of the 1 needle-disk. This result has already been observed for rings [20], a cylinder [21] and a coil [23]. Rings and coils on the ends of the spinneret and cylinder's ends produced denser mat's areas due to a higher intensity of the electrical field.

Different mats electrospun with different electrospinning parameters revealed that the porosity of PA11 mats was constant and equivalent to  $91 \pm 1 \%$  (Figure 4.16). By comparison with one needle (the applied flux was  $1.2 \text{ mL/h}$ ) and assuming that the porosity remains the same, the volume of PA11 deposited is of approximately  $0.07 \text{ cm}^3/\text{h}$ . With a porosity of 91%, the apparent volume of the PA11 mat electrospun with a single needle should be theoretically of  $0.8 \text{ cm}^3/\text{h}$ . The productivity of the disks and multi-needle-disks setup was found to be comparable with the theoretical productivity of a single needle. The use of a multi-jet spinneret is here useless if the point is to increase the productivity.

In order to understand more deeply the impact of the geometry of the spinnerets on the electrical field and consequently productivity, the distance between needle-disks ( $D_D$ ), the distance between needles ( $D_N$ ), and the spinneret's rotation speed were changed. The aim is to get an insight of how optimizing rotary multi-jet spinnerets for high productivity.

#### VARIATION OF THE DISTANCE BETWEEN NEEDLES ( $D_N$ )

The distance between the needles composing the needle-disk spinneret was changed from 1 to 3 cm. The spinneret was rotated at 60 rpm and was composed of 8 needle-disks, each distant from one another from 2 cm. The collection time is 20 minutes. The thickness of PA11 mats increases when the distance between needles decreases (Figure 4.13a). Moon et al. [17] noticed a similar trend between the needles constituting their spinneret (referred as helically probed cylindrical rotating cylinder). Electrostatic interactions were found to increase with the increase of the density of needles, thereby disturbing and masking the electric field of neighboring needles. The increase of the thickness can also be explained by the fact that the number of jets is dependent on the number of needles [20]. The higher the number of needle is, the higher the number of jets. The decrease of the fiber diameter with the increase of the distance between needles after 20 minutes of electrospinning (Figure 4.13b) can be explained by the fact that the electric field is less disrupted by the low density of needles, thus promoting jet elongation [22].

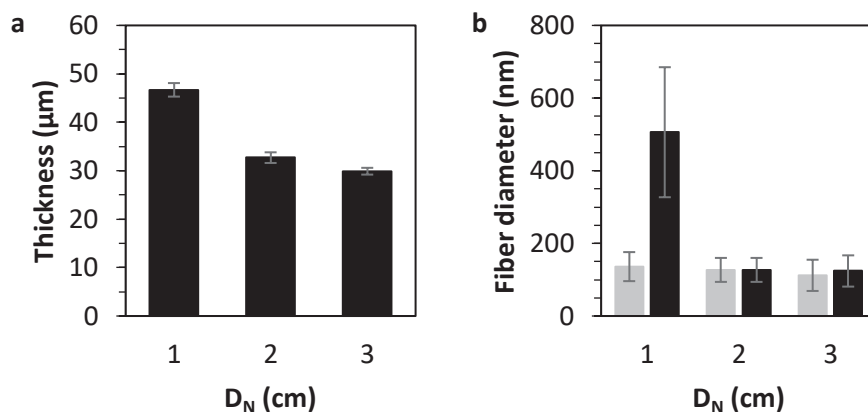


**Figure 4.13.** a) Thickness and b) fiber diameter at  $t=0\text{s}$  (in grey) and after 20 minutes of electrospinning of 6 wt% of PA11 in FA/DCM 50/50 v/v (in black) as a function of the distance between needles ( $D_N$ ).

#### VARIATION OF THE DISTANCE BETWEEN NEEDLE-DISKS ( $D_D$ )

The distance between the needle-disks constituting an 8 needle-disk spinneret was varied from 1 to 4 cm. The distance between the needles of the needle-disks is 2 cm. The rotation speed is 60 rpm and the collection time 20 minutes. As the distance increases, needle-disks are further away from one another forming a wider but thinner deposit (Figure 4.14a).

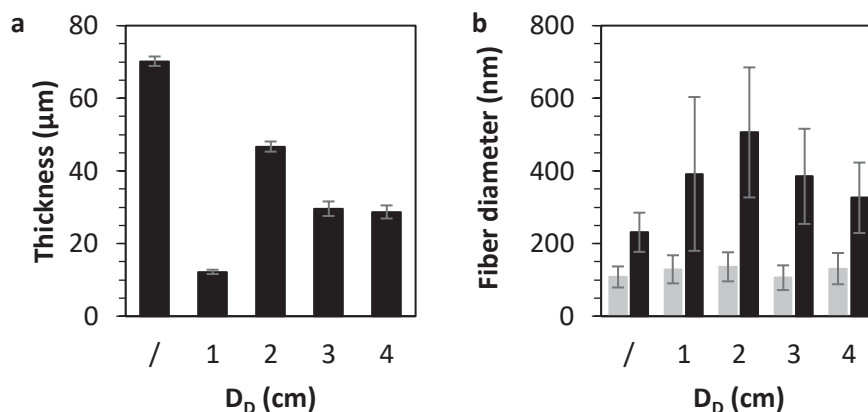


**Figure 4.14.** a) Thickness and b) fiber diameter at  $t=0\text{s}$  in grey and after 20 minutes of electrospinning in black as a function of the distance between needle-disks ( $D_D$ ) for a distance between needles ( $D_N$ ) equal to 1 cm.

For high productivity, the optimal distance between needle-disks was 2 cm. The fiber diameter increases after 20 minutes of electrospinning due to solvent evaporation in the tray and on needles (Figure 4.14b). Fibers with thin diameters were fabricated for a unique needle-disk and when the distance between needle-disk increased. Indeed, the electric field at the rim of each needle-disk is less disturbed by other neighboring needle-disks when the distance between needle-disks increases, leading to high electrical field intensities and strong fiber elongation [20]. The large-scale bar obtain for multi needle-disk spinnerets compared to the unique needle-

disk comes from the fact that smaller fibers are electrospun in the case of the unique needle-disk and from the fact that multi needle-disk spinnerets electrospin fibers with different throughput depending on whether the needle-disk is an inner or an outer one. Different throughputs lead to different solvent evaporation rates and fiber solidification times, and consequently to fibers this various diameters, hence the large bar scales [23].

#### VARIATION OF THE SPEED OF THE SPINNERET

The rotation speed of the spinneret might also affect the productivity of mats as it influences the repartition of the solution on the rim of the disk (Figure 4.15) [21]. However, a relation between the speed of the spinneret and the mass of the deposit was hard to established (Figure 4.16). Further experiments should be performed to confirm the results.

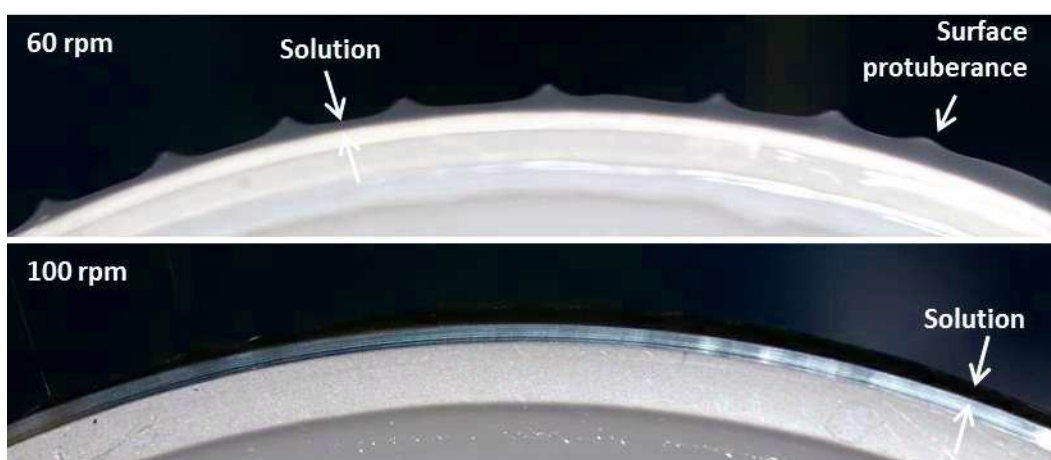


**Figure 4.15.** a) Rim of the disk facing the collector at speeds a) 60 rpm and b) 100 rpm.

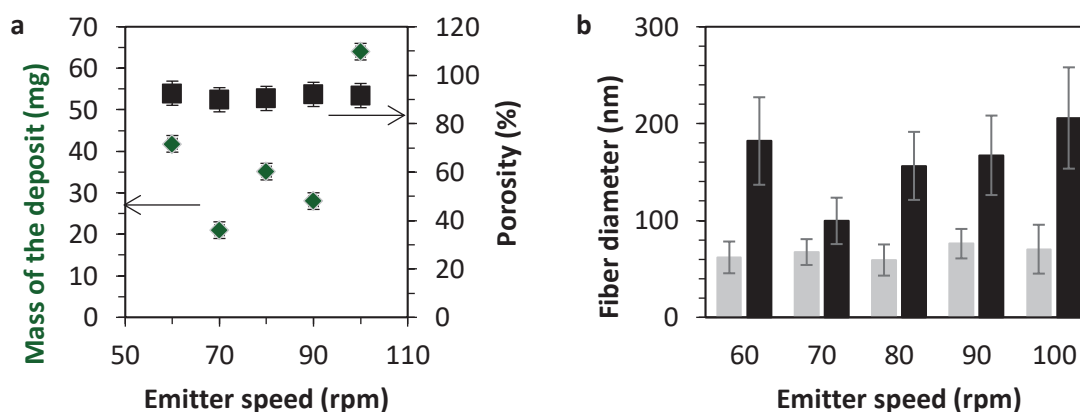


**Figure 4.16.** a) Mass of the deposit (mg), porosity and c) fiber diameter of PA11 fibers ( $t=0s$  in grey and after 20 minutes of electrospinning in black) with a single disk spinneret as a function of the speed on the spinneret (rpm).

#### 4.4.3.2 Productivity in the case of a solution of 5 wt% of PVA - 0.5 wt% of Pluronic 127 in water

For the solution composed of 5 wt% of PVA in water to which a small percentage of pluronic 127 was added (0.5 wt% of the total weight), the same experiment was reproduced 15 times on 4 days (Figure 4.17). The spinneret was a unique disk, the rotation speed was 60 rpm and the collection time 10 minutes. The experiments were not reproducible even if the humidity was controlled during the experiments ( $RH = 40 \pm 5\%$  at  $22^\circ\text{C}$ ) and that we took care about all parameters related to the process as well as the solution and its composition. Nevertheless, for experiment n°1, 101 mg of PVA was deposited on the collector in 10 minutes ( $\sim 0.6$  g/h). By comparison with one needle, where the flow rate had to be fixed at 0.3 mL/h, a mass of 0.017 g/h is approximatively theoretically deposited. The yield is here increased by 35 thanks to the use of the disk spinneret.

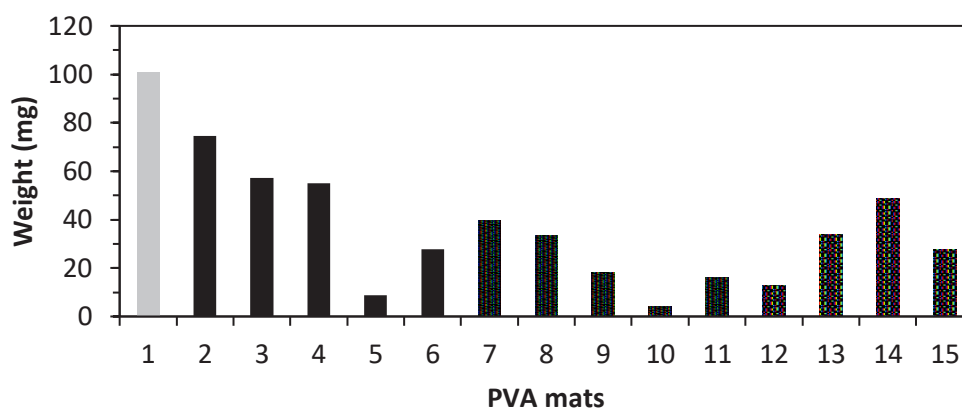


**Figure 4.17.** Weight of mats electrospun from a PVA solution of 5 wt% in water to which a small percentage of pluronic 127 was added (0.5 wt% of the total weight) with a single disk for 10 minutes (in grey day 1, in black day 2, in blue with white strips day 3 and in orange with white points day 4).

Productivities of the multi-jet setups compared to that of the single needle electrospinning setup were very different depending on the electrospinning solution and thus also depending on electrospinning parameters. A study should be continued in order to understand why.

## 4.5 Conclusion

In conclusion, we worked on rotary multi-jet spinnerets in order to produce mats that are wide enough to be characterized for liquid applications and that have a constant thickness. Three rotary multi-jet spinnerets were developed: a multi needle-disk spinneret, a multi disk spinneret and a multi CD spinneret. First, various kind of media (solutions as well as suspensions) could be electrospun. Mats with constant thickness could be fabricated with a multi needle-disk spinneret provided the collector was translated on at least 8 cm along the axis of rotation of the spinneret. For the multi-disk spinneret, mats were not flat along the direction of rotation of the disks. Then, productivity was found to vary a lot depending on the electrospinning solution. Finally, in order to tailor the productivity of spinnerets the distance between multi-disks, the distance between needles in needle-disks and the speed of spinnerets should be optimized. Productivity increases with the number of multi-disks. However, in order to estimate a correct value, one must differentiate inner and outer needle-disks



which productivities differs. The optimal distance between needle-disks is reached for the smallest distance between needle-disks and the lowest disruption of the electrical field. In addition, as the number of jets is linked to the number of needles, the density of needles should be as high as possible per needle-disks, keeping in mind that when the distance between needles is reduced, the electrical field of neighboring needles might disturb one another, thereby reducing productivity. Further experiments and optimizations of the design of the spinneret need to be conducted in order get more insight on productivity. Furthermore, the design of the feeding zone of the solution has also to be optimized in order to limit the evaporation at this stage of the process and thus to keep the viscosity of the solution constant during the whole production time.

## References

- [1] R. Sahay, V. Thavasi, S. Ramakrishna, Design Modifications in Electrospinning Setup for Advanced Applications, *J. Nanomater.* (2011).
- [2] M. Yu, R.-H. Dong, X. Yan, G.-F. Yu, M.-H. You, X. Ning, Y.-Z. Long, Recent Advances in Needleless Electrospinning of Ultrathin Fibers: From Academia to Industrial Production, *Macromol. Mater. Eng.* (2017) 1700002. doi:10.1002/mame.201700002.
- [3] A. Varesano, R.A. Carletto, G. Mazzuchetti, Experimental investigations on the multi-jet electrospinning process, *J. Mater. Process. Technol.* 209 (2009) 5178–5185. doi:10.1016/j.jmatprotec.2009.03.003.
- [4] G. Kim, Y.-S. Cho, W.D. Kim, Stability analysis for multi-jets electrospinning process modified with a cylindrical electrode, *Eur. Polym. J.* 42 (2006) 2031–2038. doi:10.1016/j.eurpolymj.2006.01.026.
- [5] I.G. Kim, J.-H. Lee, A.R. Unnithan, C.-H. Park, C.S. Kim, A comprehensive electric field analysis of cylinder-type multi-nozzle electrospinning system for mass production of nanofibers, *J. Ind. Eng. Chem.* 31 (2015) 251–256. doi:10.1016/j.jiec.2015.06.033.
- [6] M.-H. Duby, W. Deng, K. Kim, T. Gomez, A. Gomez, Stabilization of monodisperse electrosprays in the multi-jet mode via electric field enhancement, *J. Aerosol Sci.* 37 (2006) 306–322. doi:10.1016/j.jaerosci.2005.05.013.
- [7] S.A. Theron, A.L. Yarin, E. Zussman, E. Kroll, Multiple jets in electrospinning: experiment and modeling, *Polymer.* 46 (2005) 2889–2899. doi:10.1016/j.polymer.2005.01.054.
- [8] Y. Zheng, Y. Zeng, Electric field analysis of spinneret design for multihole electrospinning system, *J. Mater. Sci.* 49 (2014) 1964–1972. doi:10.1007/s10853-013-7882-8.
- [9] J.-H. He, Y. Liu, L. Xu, J.-Y. Yu, G. Sun, BioMimic fabrication of electrospun nanofibers with high-throughput, *Chaos Solitons Fractals.* 37 (2008) 643–651. doi:10.1016/j.chaos.2007.11.028.
- [10] J.S. Varabhas, G.G. Chase, D.H. Reneker, Electrospun nanofibers from a porous hollow tube, *Polymer.* 49 (2008) 4226–4229. doi:10.1016/j.polymer.2008.07.043.
- [11] O.O. Dosunmu, G.G. Chase, W. Kataphinan, D.H. Reneker, Electrospinning of polymer nanofibres from multiple jets on a porous tubular surface, *Nanotechnology.* 17 (2006) 1123–1127. doi:10.1088/0957-4484/17/4/046.
- [12] A.L. Yarin, E. Zussman, Upward needleless electrospinning of multiple nanofibers, *Polymer.* 45 (2004) 2977–2980. doi:10.1016/j.polymer.2004.02.066.
- [13] W. Li, G. Zheng, X. Wang, Y. Zhang, L. Li, L. Wang, H. Wang, D. Sun, Directly electrospun ultrafine nanofibres with Cu grid spinneret, *J. Phys. Appl. Phys.* 44 (2011) 135502. doi:10.1088/0022-3727/44/13/135502.
- [14] J. Kula, A. Linka, M. Tunak, D. Lukas, Image analysis of jet structure on electrospinning from free liquid surface, *Appl. Phys. Lett.* 104 (2014) 243114. doi:10.1063/1.4884597.
- [15] M.P. Roman, N.M. Thoppey, R.E. Gorga, J.R. Bochinski, L.I. Clarke, Maximizing Spontaneous Jet Density and Nanofiber Quality in Unconfined Electrospinning: The Role of Interjet Interactions, *Macromolecules.* 46 (2013) 7352–7362. doi:10.1021/ma4013253.
- [16] K.M. Forward, G.C. Rutledge, Free surface electrospinning from a wire electrode, *Chem. Eng. J.* 183 (2012) 492–503. doi:10.1016/j.cej.2011.12.045.
- [17] S. Moon, M. Gil, K.J. Lee, Syringeless Electrospinning toward Versatile Fabrication of Nanofiber Web, *Sci. Rep.* 7 (2017) 41424. doi:10.1038/srep41424.
- [18] U. Ali, A. Abbass, F. Khurshid, S. Aslam, A. Waqar, Needleless Electrospinning Using a Flat Wheel Spinneret, *J. Eng. Fibers Fabr.* 12 (2017).
- [19] M.N. Shukat, T. Lin, Highly-twisted, continuous nanofibre yarns prepared by a hybrid needleless electrospinning technique, *RSC Adv.* 5 (2015) 33930–33937. doi:10.1039/C5RA03906A.

- [20] X. Wang, T. Lin, X. Wang, Scaling up the production rate of nanofibers by needleless electrospinning from multiple ring, *Fibers Polym.* 15 (2014) 961–965. doi:10.1007/s12221-014-0961-x.
- [21] Niu Haitao, Lin Tong, Wang Xungai, Needleless electrospinning. I. A comparison of cylinder and disk nozzles, *J. Appl. Polym. Sci.* 114 (2009) 3524–3530. doi:10.1002/app.30891.
- [22] U. Ali, H. Niu, S. Aslam, A. Jabbar, A.W. Rajput, T. Lin, Needleless electrospinning using sprocket wheel disk spinneret, *J. Mater. Sci.* 52 (2017) 7567–7577. doi:10.1007/s10853-017-0989-6.
- [23] H. Niu, X. Wang, T. Lin, Upward Needleless Electrospinning of Nanofibers, *J. Eng. Fibers Fabr. Special Issue* (2012).
- [24] Z. Liu, K.K.J. Ang, J. He, Needle-disk electrospinning inspired by natural point discharge, *J. Mater. Sci.* 52 (2017) 1823–1830. doi:10.1007/s10853-016-0472-9.
- [25] Z. Liu, R. Chen, J. He, Active generation of multiple jets for producing nanofibres with high quality and high throughput, *Mater. Des.* 94 (2016) 496–501. doi:10.1016/j.matdes.2016.01.075.



# CONCLUDING REMARKS AND OUTLOOK

## CONCLUSION

The fabrication of nanofibrous mats by an environmentally friendly electrospinning process could be achieved by either (1) using a bio-based polymer (PA11) or by electrospinning in aqueous solvents (2a) suspensions of water-insoluble polymers or (2b) a bio-based molecule (tannic acid). Mats were developed for filtration applications. A multi-jet setup was consequently developed for the fabrication of wide mats with constant thickness.

### **Electrospinning of bio-based polyamide 11**

PA11 fibers were electrospun in a mixture of formic acid and dichloromethane. The mean fiber diameter of fibers was first decreased in order to fabricate mats with a pore size adapted for microfiltration applications (mean pore size between 0.2 and 0.8  $\mu\text{m}$ ). Four parameters could efficiently be tailored to this aim: the composition of the solvent, the humidity, the polymer concentration and the distribution of the molar mass. First, increasing the proportion of formic acid in the formic acid-dichloromethane solvent led to a solvent with a slower evaporation rate which enabled a longer elongation of the nanofiber before solidification and promoted the fabrication of thin fibers. Second, working in humid conditions favored the fabrication of thin fibers. Indeed, water absorption in polyamides leads to a decrease of their glass transition temperature and, during electrospinning, to a longer elongation of fibers before solidification. This effect, called “plasticizing” effect, allows the fabrication of thin fibers. Third, decreasing the concentration is related to the fabrication of thin fibers provided the concentration is yet high enough to allow entanglements between polymer chains and to yield regular and continuous fibers by electrospinning. Fourth, playing on the distribution of the molar mass allows the production of thin fibers from concentrated solution in the particular case where a small amount of a polymer of high molar mass is added to the same polymer of lower molar mass. The polymer of high molar mass enables the fabrication of fibers while the polymer of lower molar mass makes it possible to use high concentrated solutions. The use of concentrated solutions is highly interesting for high yield production rates.

By playing on the distribution of the molar mass, it was possible to electrospinning mats composed of fibers as thin as 100 nm approximatively from a polymer concentration of 13 wt%. These mats could be good candidates for microfiltration applications as their mean pore size ( $0.37 \pm 0.01 \mu\text{m}$ ) is in the range of the pore size generally required for liquid filtration applications (0.2 to 0.8  $\mu\text{m}$ ). However, no liquid microfiltration trials were performed as it was decided to first carry the electrospinning process in aqueous solvents. Nevertheless, two mats with average fiber diameters of 100 nm and 500 nm were characterized. Mats with fibers measuring in diameter 500 nm had pores bigger than the range targeted, thus justifying the study aiming at reducing the fiber diameter. Then, both mats were hydrophobic, irrespective of the fiber diameter. Finally, mats with a mean fiber diameter of 100 nm were mechanically weaker than mats with a mean fiber diameter of 500 nm due mainly to the fact that fibers of diameter 100 nm were less bonded.



## **Electrospinning of in aqueous solvents**

### ***Electrospinning of aqueous suspensions of water-insoluble polymers***

The goal of this strategy is to avoid the use of toxic and polluting solvents during the electrospinning of water-insoluble polymers for environmentally friendly reasons. Water-non soluble polymers are consequently electrospun as suspensions with a template polymer. The template polymer prevents the jet from breaking and allows the fabrication of fibers during the electrospinning process as it provides the entanglements necessary for the fabrication of fibers. The fabrication of mats is performed in three steps. First, a blend composed of the particles and of the template polymer is electrospun. In a second step, mats are cured. The heat treatment aims at fusing particles together without destroying the nanofibrous structure. Mats are washed in a third step to remove the template polymer. Four suspensions were electrospun blended with PVA, the template polymer: a co-polyamide (coPA) suspension, a maleic-grafted polypropylene (MAPP) suspension, a copolymer of vinylidene fluoride and methyl methacrylate (PVDF-PMMA) suspension and a polyvinylidene fluoride (PVDF) suspension. Formulations as well as curing conditions were studied in order to fabricate nano-fibrous mats which are water-resistant and which could be used for liquid microfiltration applications. In the end, mats could be successfully fabricated with this strategy from the four suspensions.

CoPA/PVA mats showed very low mechanical properties and were not further characterized. On the contrary, MAPP/PVA, PVDF-PMMA/PVA and PVDF/PVA mats were characterized with their hydrophilic and mechanical properties, and MAPP/PVA, PVDF-PMMA/PVA mats were chosen for filtration trials as MAPP/PVA mats were highly hydrophilic and as PVDF-PMMA/PVA mats showed good mechanical properties with an elongation at break as high as 80%. MAPP/PVA mats could remove more than 99% of 1 $\mu$ m silica particles thanks to the formation of a cake layer. Nevertheless, the efficiency sharply decreased to 63 and 12% for, respectively, 0.4 $\mu$ m and 0.1 $\mu$ m silica particles. On the opposite, PVDF-PMMA/PVA mats depicted efficiencies higher than 99% for 1 $\mu$ m and 0.4 $\mu$ m silica particles and 95% for 0.1 $\mu$ m silica particles. The observation of mats revealed a deep filtration of 0.4 $\mu$ m and 0.1 $\mu$ m silica particles in PVDF-PMMA/PVA mats.

### ***Polymer-free electrospinning of tannic acid by supramolecular self-assembling***

Generally, electrospun mats are prepared from solutions based on high molar mass polymers. The solution must bring enough chain entanglements to avoid any breaking or Raleigh instability of the electrospun jet and to yield by electrospinning a continuous and regular solid nanofibre. It has been however shown that some few non-polymeric molecules can be electrospun without using a carrier polymer. Here, the case of tannic acid was demonstrated. It was possible to electrospin this bio-based molecule solubilized in a mixture of water and ethanol as well as in pure water. Rheology, dynamic light scattering and cryo-TEM highlighted the formation of tannic acid aggregates in solution. Above a critical concentration, these aggregates form a supramolecular interconnected network strong enough to allow the electrospinning of a continuous and regular nanofibre. The resulting nanowebs were mechanically stable and could be handled and wrapped. Furthermore, as opposed to the other small molecules for which polymer-free electrospinning was also demonstrated, tannic acid nanowebs could be efficiently cross-linked in water either by oxidative reaction with sodium periodate or with Fe<sup>III</sup> by a combination of oxidative reaction and the formation of coordination complexes.

### **Development and optimization of a multi-jet spinneret**

A multi-jet spinneret has been developed to fabricate mats which are wide and of constant thickness in order to be used for filtration trials. Three rotary multi-jet spinnerets were developed: a multi needle-disk spinneret, a multi disk spinneret and a multi CD spinneret. Various kinds of media (solutions as well as suspensions) could be electrospun. The distribution of the thickness of mats was studied for the multi needle-disk spinneret and the multi disk spinneret. It was possible to fabricate mats with constant thickness with a multi needle-disk spinneret provided the collector was translated on at least 8 cm along the axis of rotation of the spinneret. On the contrary, mats were not flat along the direction of rotation of the spinneret when a multi disk spinneret and a planar collector were used. With multi disk spinnerets, the fabrication of mats of constant thickness would require the use of a cylindrical and rotary collector. Productivity was found to vary a lot depending on the electrospinning solutions and conditions. Even if productivity, for PA11 solutions, was not significantly increased, it was nevertheless multiplied by 35 for PVA solutions. A study on the impact of the geometry of multi-jet spinnerets on deposits, on electrospinning conditions as well as on interactions between jets was started in order to optimize the geometry of spinnerets. Three parameters were investigated: the distance between needle-disks, the distance between needles (for the multi-needle spinneret) and the rotation speed of spinnerets. On the one hand, productivity can be enhanced by multiplying the number of needle-disks. However, it does not increase linearly since the electric field nearing a row is differently disturbed depending on whether the needle-disk is an inner or an outer needle-disk. On the other hand, as the number of jets is linked to the number of needles, the density of needles should be as high as possible per needle-disks, keeping in mind that when the distance between needles is reduced, the electrical field of neighboring needles might also disturb one another, thereby reducing productivity. Further experiments and optimizations of the design of the spinneret need to be conducted in order to get more insight on productivity. Furthermore, the design of the feeding zone of the solution has also to be optimized in order to limit the evaporation at this stage of the process and to keep thus the viscosity of solutions constant during the whole production time.

### **OUTLOOK**

The fabrication of a new “green” filter for liquid microfiltration by electrospinning started from scratch three years ago. For an uninitiated counterpart, the objective of the thesis can be rather easily fathomed. However, its developments rapidly leveled questions and later unraveled few impediments.

First, the signification of the trendy word “green” was ambiguous. Was the issue about the process or the material(s) constituting the to-be fabricated filter? Was it about both? To which extent could we consider a material “green”? Should it be bio-based? Bio-degradable? Recyclable? Which part of the life cycle of the material, respectful of the environment, should prevail? And finally, how far should and could we go toward the fabrication of an eco-friendly filter? Naturally, the combination of all of these criteria would be very best and the apogee of the thesis but is sadly a utopia. It was, thus, decided to work independently on both sides of the matter, namely to use a “green” material, polyamide 11, which is bio-based and recyclable and to use water-based solutions during the electrospinning process. However, the use of a water-based solutions implied finding cunning strategies allowing to preserve the integrity of mats when in contact, during filtration trials, with water-based liquids. Different from widely used chemical crosslinking strategies of water soluble polymers, which also limit the number of available polymers, we opted for a different approach. The idea was to use insoluble polymers and to find a suitable alternative to the use of toxic solvents. In that regard, we chose to work on the electrospinning of aqueous suspensions of insoluble polymers with the aim to fabricate

filters for liquid microfiltration. Throughout the thesis, we were, in addition, lucky to discover that tannic acid, a molecule, could also be electrospun into fibers in a water-based solvent without the addition of a template polymer. A whole study was conducted to understand the mechanism of fiber formation and to crosslink pure tannic acid nanofibrous mats. Crosslinked tannic acid mats were found to be brittle. An application in liquid microfiltration was consequently inadequate unless a new crosslinking way yielding more flexible mats was found. Nonetheless pure tannic acid mats which are insoluble in aqueous solutions might find other applications in biomedical, catalysis and environment areas.

Second, the type of filtration “microfiltration” and more precisely the specification of the CLARIFIL project “size of pores between 0.2 and 0.8  $\mu\text{m}$ ” was a real challenge. Even if the electrospinning process, due to the fineness of the electrospun fibers, leads to the fabrication of mats with small, regular and interconnected pores, strategies aiming at reducing the diameters of fibers in order to decrease the size of pores even more had to be investigated. This study led us to tackle one to-often neglected parameter: humidity. Depending on the content of water vapor in the air surrounding the electrospinning setup, the evaporation rate of the solvent and the solidification rate of the fibers are altered. In turn, they affect the morphology of fibers and the structure of electrospun nonwoven mats. Adjusting the humidity was ergo one effective way to decrease the diameter of fibers and the size of pores. Yet, the strategy consisting in playing on the distribution of the molar mass was found to be the strategy fulfilling the best the specifications of the project. The strategy consists in adding a small percentage of a polymer of high molar mass without which the electrospinning of continuous fibers would not be possible to a polymer of lower molar mass. Thanks to this method, the specifications of the CLARIFIL project were met. Regular polyamide 11 fibers as thin as 100 nm creating pores with an average size of  $0.37 \pm 0.01 \mu\text{m}$  could be fabricated. The main and very attracting advantage of this strategy was the fabrication of thin fibers from high concentrated solutions (13 wt% for fibers of 100 nm in diameter) which led to an increase of the productivity. Such concentrations could not be reached otherwise. Blending polymers of different molar mass in order to fabricate by electrospinning thin fibers at high yields might inspire other fields of application.

Third, the term “fabrication” refers inevitably to high yield production rates. This was the most arduous hurdle that we faced given the fact that productivity is the main drawback holding back the electrospinning process from many industrial applications and knowing that we had to fabricate membranes that were wide and large enough to be characterized. The development and the optimization of a rotary multi-jet spinneret emphasized the impact of the geometry of the spinneret on the repartition of the electrical field and, in turn, on the production rate. Our work should be transferable to any rotary multi-jet spinneret and might contribute to a better industrialization of the electrospinning process.

Fourth, the word “liquid” had to be correlated to the fabrication of “strong nanofibrous mats being able to support several liquid filtration trials”. To this aim support layers fabricated by spunbond were used. The physical integrity of the membranes tested during the thesis was kept during our filtration trials. Nevertheless, before industrial upscaling, a study should focus on the resistance of electrospun mats towards an applied flux of liquid in industrial conditions based on the thickness of mats and on the average fiber diameter. Indeed, our work highlighted a decrease of the mechanical properties of mats with the decrease of the fiber diameter under uniaxial testing. The pressure applied by a flux of liquid on a membrane during filtration trials is different from the pressure applied during a uniaxial test but our result shows that the mechanical strength of mats may vary with the fiber diameter regardless of the mechanical stress.

Finally, the “filters”, that combined the highest number of “green” advantages, were fabricated from polymer suspensions. This strategy is thus the most promising route towards the fabrication of an eco-friendly filter for

liquid microfiltration by electrospinning and towards a possible industrialization. The process was carried out in water, the polymers constituting the suspensions would only dissolve in toxic solvents otherwise, fine and regular fibers can be obtained, and microfiltration trials could be performed successfully at an experimental scale with silica particles. A future work might entail further filtration trials with new kinds of liquids such as wines and filtration trials in industrial conditions. Wine microfiltration ensures clarification and microbiologic stabilization of wines without altering their organoleptic qualities. Different components are to be removed during the process. This is the case of microorganisms such as yeasts and bacteria responsible for wine alteration and of some particles and colloids which give wines turbid aspects. Such microorganisms, particles and colloids have approximatively the same size than the tested silica particles. It could be interesting to see if filtration efficiencies are similar despite possible new interactions which could modify filtration mechanisms between wine to-be filtrated components and electrospinning filtering membranes. In addition, our “green” strategy using polymer suspensions may interest other areas of applications and be even implemented on any electrospinning setup, even multi-jet setups in order to increase the productivity.

Last but not least, our most promising strategy could even be “greener” by choosing a polymer suspension with a life cycle respecting the environment even more. This was not possible for this work due to the lack of polymer suspensions available on the market compatible with the electrospinning process and our strategy.





# Appendix 1:

## RHEOLOGY OF PA11 AT 200°C

The viscosity of PA11 was measured à 200°C. The initial reason was to calculate a relation between the viscosities of the different studied polyamides 11 and to infer a relation between molar masses in order to verify the values given by Arkema. This was sadly not possible because the viscosity of all PA11 increased over time due to a continuation of the polymerization of PA11 when heated (here: at 200°C). The study, nevertheless, can open doors towards a possible reinforcement of the mechanical properties of polyamide 11 mats thanks to heating treatment.

A temperature of 200°C was chosen as it is above the melting points of the three polyamides (see DSC thermograms in Figure A1.1). Before any experiments, polyamides 11 pellets were dried 48 hours at 80°C. Flat films were then obtained by injection molding. It can be estimated that the residence time of polyamides 11 in the injection molding machine is of approximatively 10 minutes during which polymerization of PA11 could already occur.

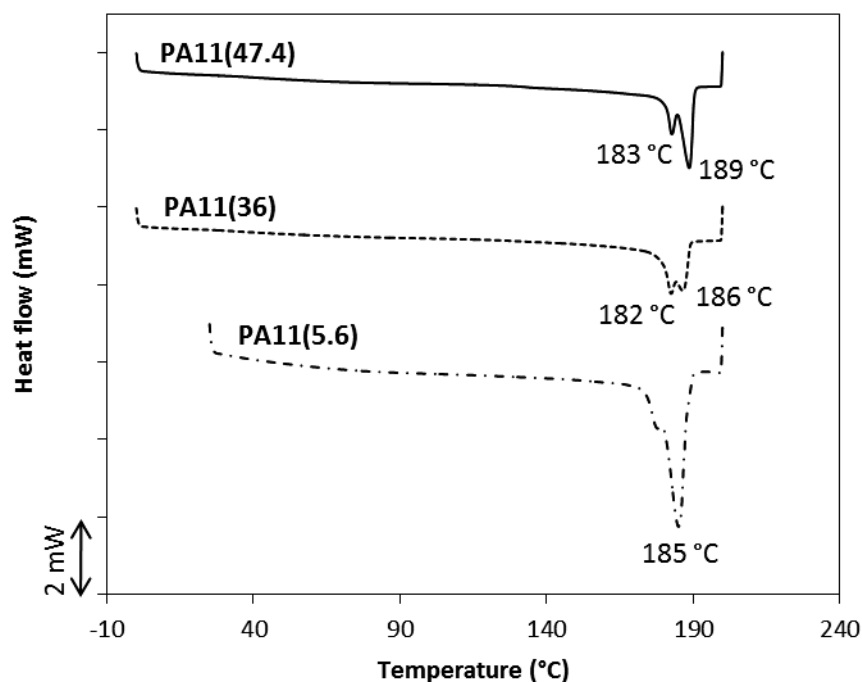


**Figure A1.1.** DSC thermograms of PA11.

PA11 were dried accordingly to Arkema's recommendations in order to prevent their hydrolysis. The viscosity of PA11 was measured under steady shear flow for shear rates ranging from  $0.01 \text{ s}^{-1}$  to  $0.1 \text{ s}^{-1}$  after different waiting times: after 1, 17 and 82 minutes at 200 °C (Figure A1.2). Over this range of shear rates, only Newtonian behaviors were observed on short intervals of time (inferior to 5 minutes). Indeed, on a short

interval of time, the viscosity does not change for shear rates ranging between  $0.01 \text{ s}^{-1}$  to  $0.1 \text{ s}^{-1}$ . For longer interval of time (superior to 5 minutes) the viscosity increased which increase is related to a reaction of polymerization taking place at high temperature.

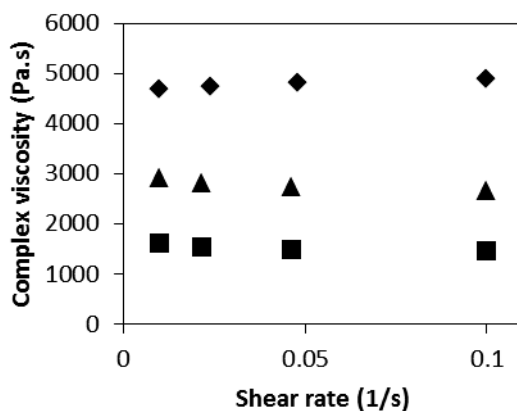


**Figure A1.2.** Modulus of the complex viscosity of PA11 as a function of the shear rate and at different times of measurements (1 minutes (squares), 17 minutes (triangles) and 82 minutes (diamonds) after the beginning of the experiment at  $200^\circ\text{C}$ ).

The complex viscosity was measured over time with a frequency of  $1 \text{ rad/s}$  and a deformation of 5% in order to get an insight about the speeds of polymerization reactions. It can be seen from Figure A1.3 that the viscosity increases over time for all PA11 differently. Table A1.1 shows the variations in viscosity after 30 minutes and after 5 hours for all PA11. The complex viscosity of all PA11 has been multiplied by more than 10 after 5 hours. In addition, PA11(36) presents the highest increase in viscosity as its complex viscosity has been multiplied by 24 after 5 hours, followed by PA11(5.6) and by PA11(47.4). It can be inferred that polymer chains of PA11 are functionalized with different end groups allowing polymerization. As a matter of fact, if all PA11 were functionalized with the same end groups, then the increase in viscosity over time should be the highest for PA11(5.6) followed by PA11(36) and by PA11(47.4) as PA11(5.6) has the shortest polymer chains and therefore the highest number of chains being able to polymerized. PA11(36) end groups allow quicker polymerization reactions.

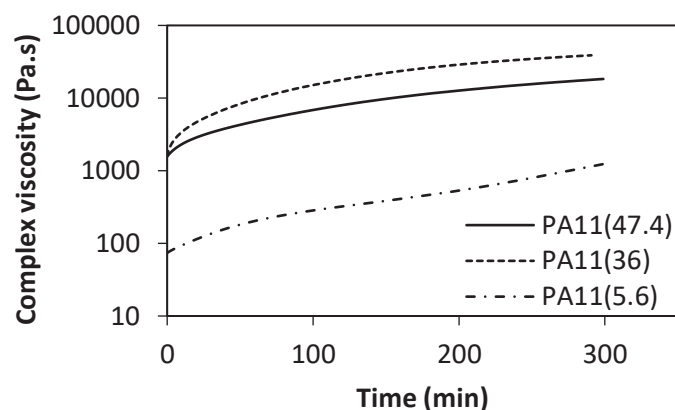


**Figure A1.3.** Complex viscosity of PA11 (frequency of 1 rad/s and deformation of 5%) over time.

	After 30 minutes, the complex viscosity is multiplied by:	After 5 hours, the complex viscosity is multiplied by:
PA11(47.4)	2.1	11
PA11(36)	3.7	24
PA11(5.6)	1.8	14

**Table A1.1.** Increase of the complex viscosity 30 minutes and 5 hours after the beginning of the experiment.

The values of complex viscosity at  $t=0$ min were not compared since PA11 had already been heated during injection molding for 10 minutes and before the beginning of experiments where PA11 are in the rheometer and are heated up to  $200^{\circ}\text{C}$  for 20 minutes approximately. In total, PA11 are heated during about 30 minutes before beginning any experiments. It is consequently highly probable that complex viscosities of PA11 have already begun increasing before starting experiments. Extrapolations are arduous to make as the time during which PA11 are heated previous to the beginning of experiments is an approximation.

In conclusion, PA11 can react together when heated at  $200^{\circ}\text{C}$  and thus increase the overall average molar mass. This effect can be exploited for reinforcing the mechanical properties of polyamide 11 mats thanks to a heating treatment. Indeed, reaction between PA11 chains could occur inside the fibers and maybe between fibers at the fiber-fiber junction points. Tests were performed accordingly and different parameters were varied during the heat treatment: the time, the temperature and the weight applied on mats in the oven. Nevertheless no difference could be noted between the mechanical strength of mats which had been heat-treated and the mats which had not. This result could be attributed to the fact that the mechanical properties of PA11 are mainly due to the crystalline domain which density may not be significantly affected by the heat treatment.

## Materials and methods

### Injection molding

The injection molding apparatus is a Billion Hercules 90. The nozzle temperature was set at 220°C, the holding pressure at 80 bars during 10.5 s. The mold was heated at 60°C.

### Rheology

Viscosity of the solution was measured with a rheometer (Physica MCR 301, Anton Paar). A plate-plate geometry was used with diameter 25 mm. The viscosity of all PA11 was measured under steady shear flow for shear rates ranging from 0.01 s<sup>-1</sup> to 0.1 s<sup>-1</sup>. All tests were performed in this same order: the sample was placed on the rheometer already heated at 200°C. The oven was then closed and a heating period of 5 minutes was observed to give time to samples to adjust to the operating temperature before settling the gap at 1 mm. The test could finally begin if the condition “a temperature of 200 ± 0.25 °C remains unchanged for 3 minutes” is verified.

## Appendix 2:

# CHARACTERIZATION OF THE SPUNBONDED SUPPORT LAYER

Spunbonded nonwovens which were calendered have been used as support layer (SB layer) during the thesis when necessary (for the measurement of the mean pore size in Chapter 2 and for filtration trials in Chapter 3). Calendering is a finishing process aiming at enhancing the mechanical strength of a nonwoven mat. During the process, the nonwoven slides between two heated rollers. Rollers are structured so that when SB layers are pressed between the rollers, it induces punctual fusion points in their structure. SB layers are made of PA11 and were provided by the CETI (Centre Européen des Textiles Innovants) with a basic weight of  $40 \text{ g/m}^2$ , a mean thickness of  $216 \pm 44 \text{ }\mu\text{m}$  and a mean fiber diameter of  $16 \pm 1 \text{ }\mu\text{m}$ . The mean thickness was measured outside fusion points induced by the calendering step (Figure A2.1).

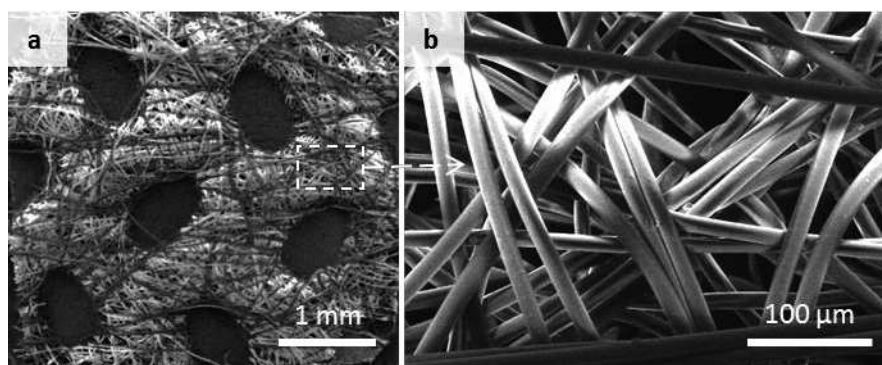


**Figure A2.1.** SEM images of the SB layer.

During the electrospinning process, the deposition of fibers is influenced by the SB layer when they are directly electrospun on it as in Chapter 2. Indeed, fibers are preferentially deposited on fusion points as the thickness of the SB layer is there the thinnest and allows charge release more efficiently than over the porous domains of SB. The thickness of the electrospinning layer is though uneven and is thinner when electrospun fibers are deposited on non-fused spunbonded fibers. So, in Chapter 2, the thickness values of electrospun PA11 mats given in the report are minimums. They are calculated for electrospun fibers deposited on non-fused SB fibers (Figure A2.2).



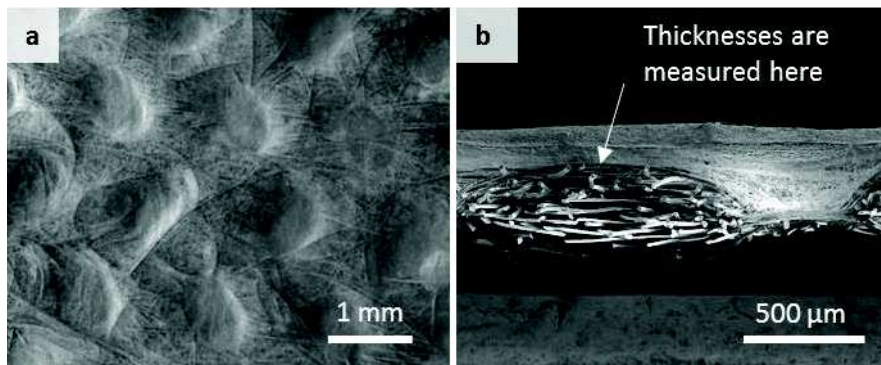


**Figure A2.2.** SEM images of electrospun PA11 fibers on the SB layer: a) top view and b) side view.

In Chapter 3, electrospun fibers are collected on aluminium foils or on backing papers and peeled off. During filtration trials, the SB layer is used as prefilter as in Figure A2.3.

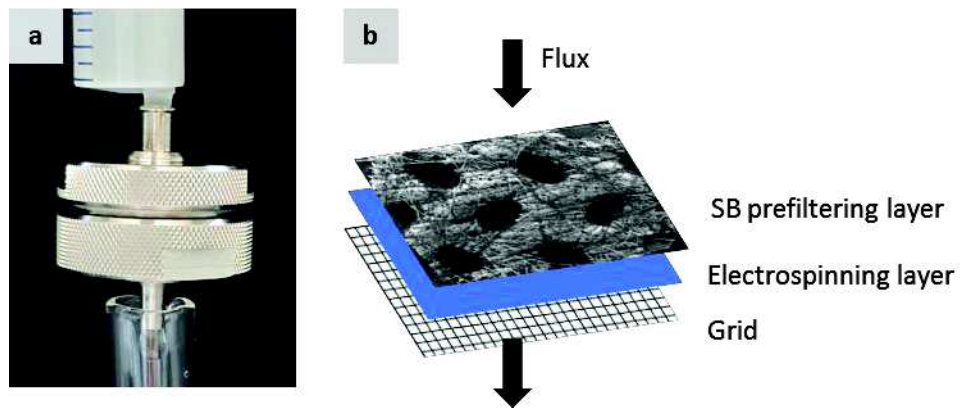


**Figure A2.3.** a) Photo and b) schematic graph of the filtration setup.

# Appendix 3:

## WATER UPTAKE IN PA11

The content of water in PA11, measured as received, was estimated by thermogravimetric analyses (TGA). Thermogravimetric analyses were performed with a TA Instrument Q5000 apparatus. Figure A3.1a-b-c show the TGA spectra of the PA11(47.4), PA11(36) and PA11(5.6). Figure A3.1d depicts a close-up of TGA spectra.

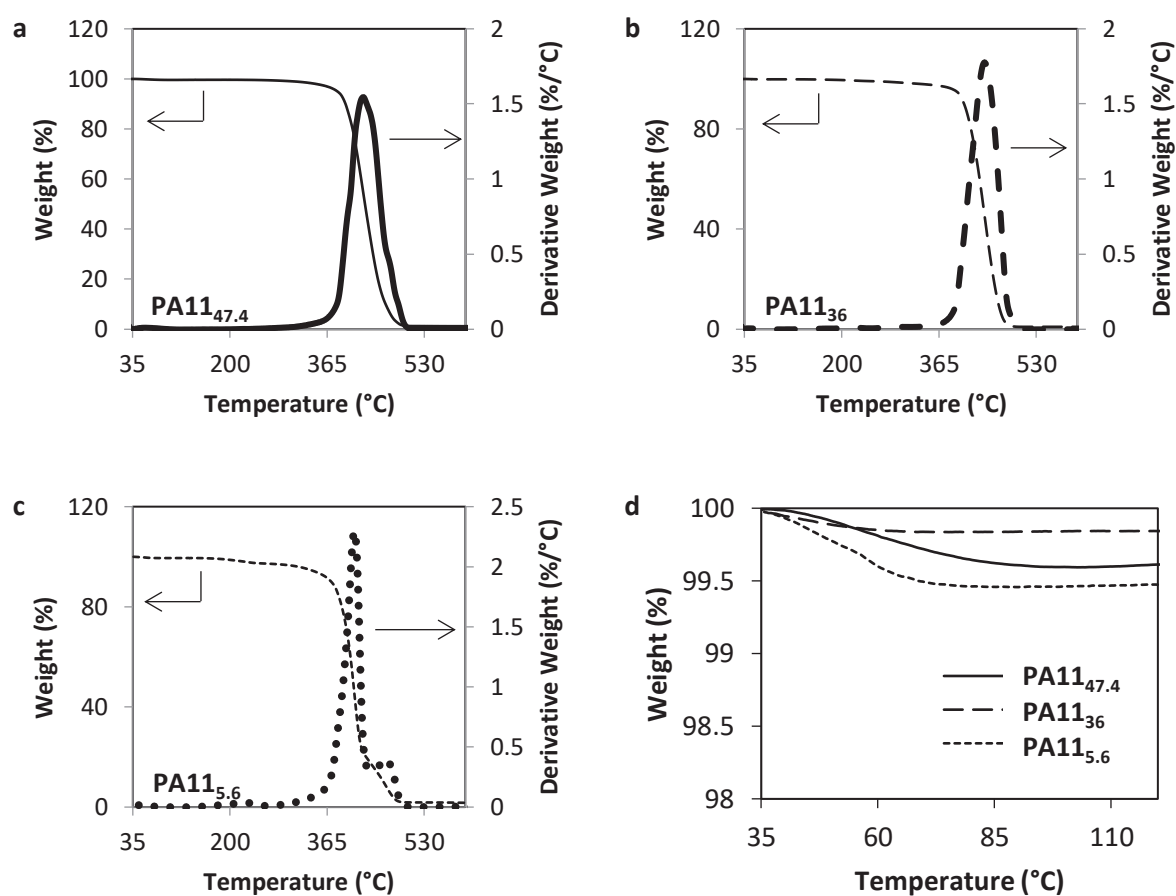


**Figure A3.1.** TGA spectra of a) PA11(47.4), b) PA11(36), c) PA11(5.6) and d) a close-up of PA11(47.4), PA11(36) and PA11(5.6).

The content of water absorbed in PA11 is calculated as the difference between the weight at 35°C and the weight at 100°C divided by the weight at 35°C in percent. The proportion of water absorbed in the received PA11 is below 1% for all PA11.

	PA11(47.4)	PA11(36)	PA11(5.6)
Water uptake (%)	0.4	0.1	0.5

**Table A3.1.** Water uptake in PA11.

# Appendix 4:

## COAXIAL ELECTROSPINNING OF AQUEOUS POLYMER SUSPENSIONS

To avoid organic solvents in electrospinning of hydrophobic polymers, aqueous polymer suspensions can be electrospun by a blend strategy as seen in Chapter 3. Another possible strategy is the coaxial electrospinning of core/shell fibers, where the shell is composed of a template polymer in solution whereas aqueous suspensions (here: Maleic anhydride grafted polypropylene (MAPP)) are present in the core (Figure A4.1). The advantage of the coaxial strategy compared to the blend one is that the polymer template (the shell polymer) should be washed more easily. The template polymer is here PVP, contrary to Chapter 3 where PVA is used, due to the fact that the coaxial electrospinning process was more stable with PVP than PVA. This appendix evidences for the first time the fabrication of fibers from suspensions by coaxial electrospinning. Electrospinning as well as post-treatment conditions allowing the formation of continuous fibers are given. Mats have then been characterized and compared with mats obtained in Chapter 3 from the blend strategy. For the electrospinning of core/shell fibers materials, experimental details on solution preparation and electrospinning setup are given at the end of the appendix. Process parameters of the blend fibers are detailed in Chapter 3. Characterization methods of core/shell fibers are the same as for blend fibers and are given in Chapter 3.

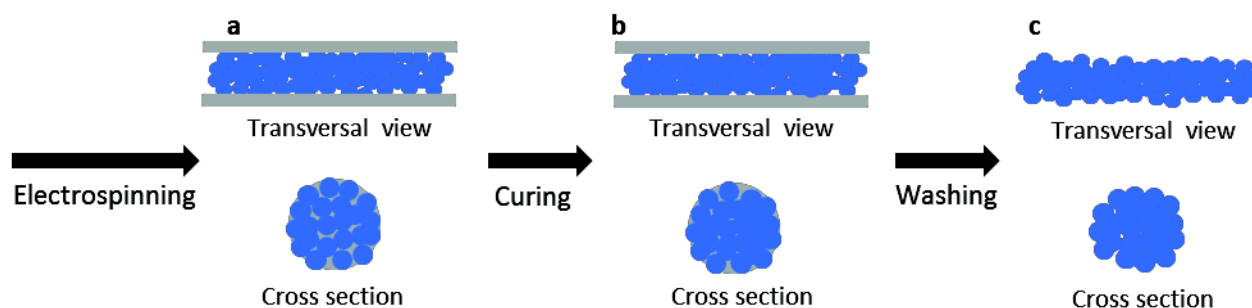


**Figure A4.1.** Transversal views and cross sections of fibers after a) electrospinning, b) curing and c) washing.

Fabrication steps (electrospinning, curing and washing) of mats and schematic graphs of the resulting fibers are displayed on Figure A4.1. First, core/shell fibers are electrospun by coaxial electrospinning. Fibers are composed of a shell of PVP retaining MAPP particles in its inside. The thermal treatment (1 hour at 160°C) allows particles to bond together. After washing (24 hours in water), the water-soluble shell is eliminated by solubilization in water leaving a mat composed of fibers constituted of bonded particles. As for blends, the proportion of PVP eliminated during washing could not be estimated, neither by infrared spectroscopy (IR) nor by DSC. The low absorption of IR spectra led to imprecise values and calibration curves, and variations between DSC thermograms were not significant. At each step of the process, the fiber diameter was calculated (Figure A4.2). It can be seen that the fiber diameter increases a lot after thermal treatment due to gluing of fibers. The slight decrease after washing might be due to the removal of PVP.

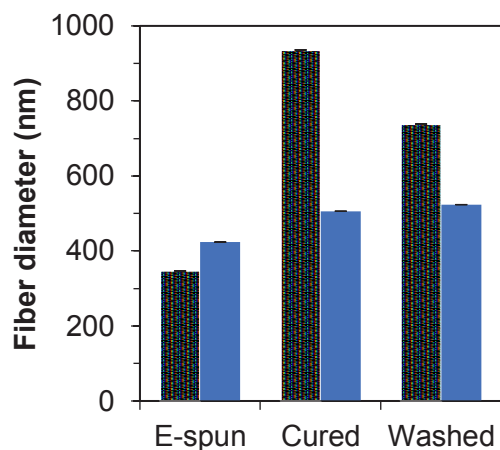


**Figure A4.2.** Fiber diameter of core/shell MAPP/PVP (hatched blue) and blended MAPP/PVA (blue) mats after electrospinning, curing and washing. For each mat, the diameter of 100 fibers were measured.

MAPP/PVP core/shell mats have then been characterized mechanically and compared with MAPP/PVA blend mats. Results are shown in Figure A4.3. Core/shell mats become very brittle after curing and experiments were less reproducible as evidenced by the large bar scales. Surfaces of rupture were observed (Figure A4.4). They highlight the brittleness of mats after curing and washing. Indeed, while the rupture is unclear for electrospun mats as fibers are elongated and torn apart during traction trials, the rupture is clear for mats after curing and washing. During thermal treatment, particles and fibers bond together and mats become more rigid. Thus, during mechanical tests, fibers are not free to move and mats break abruptly. For blend fibers, fibers are less bonded together as proved in Figure A4.5. Mats can therefore stretch more and resist to a higher stress before breaking.

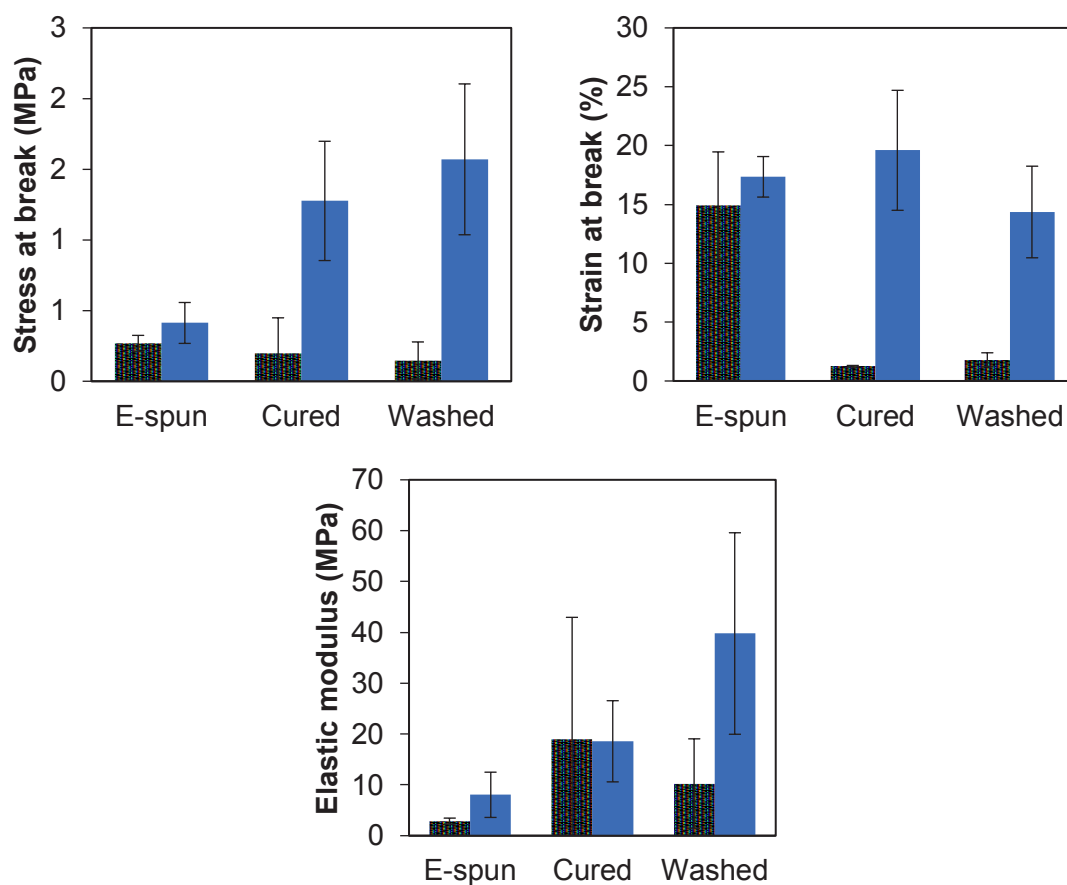


**Figure A4.3.** Stress-strain curves of electrospun core/shell MAPP/PVP (hatched blue) and blended MAPP/PVA (blue) mats at each step: after electrospinning (E-spun), curing and washing. For each mat, 5 tests were performed.

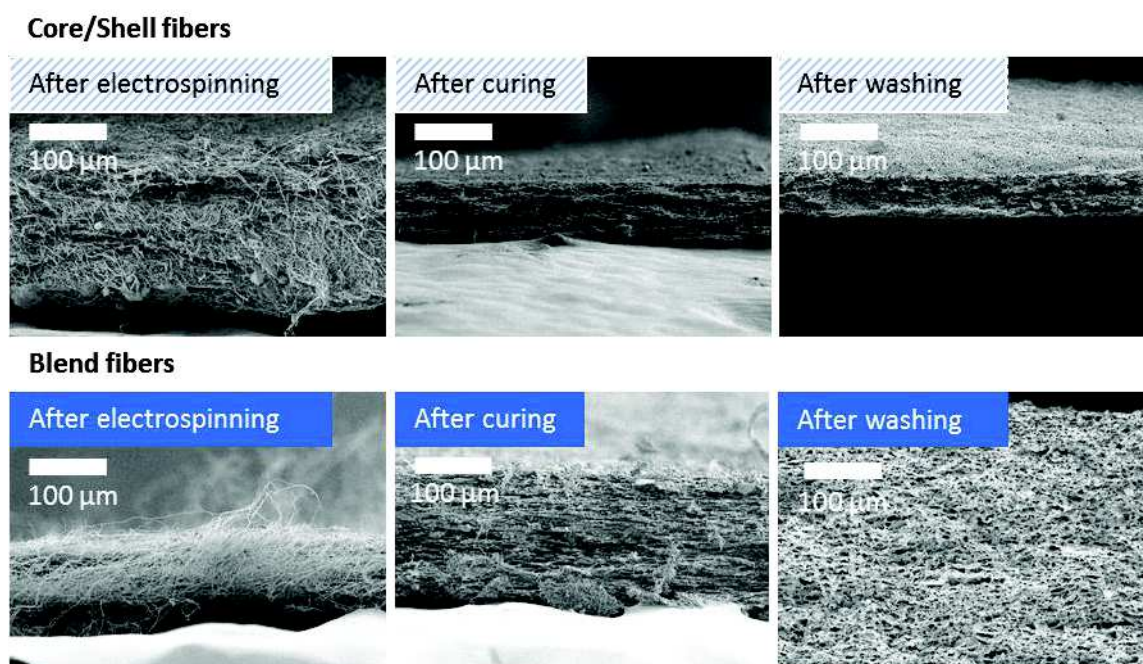


**Figure A4.4.** SEM images of the surface of rupture after mechanical tests of MAPP/PVP core/shell mats and MAPP/PVA blend mats.



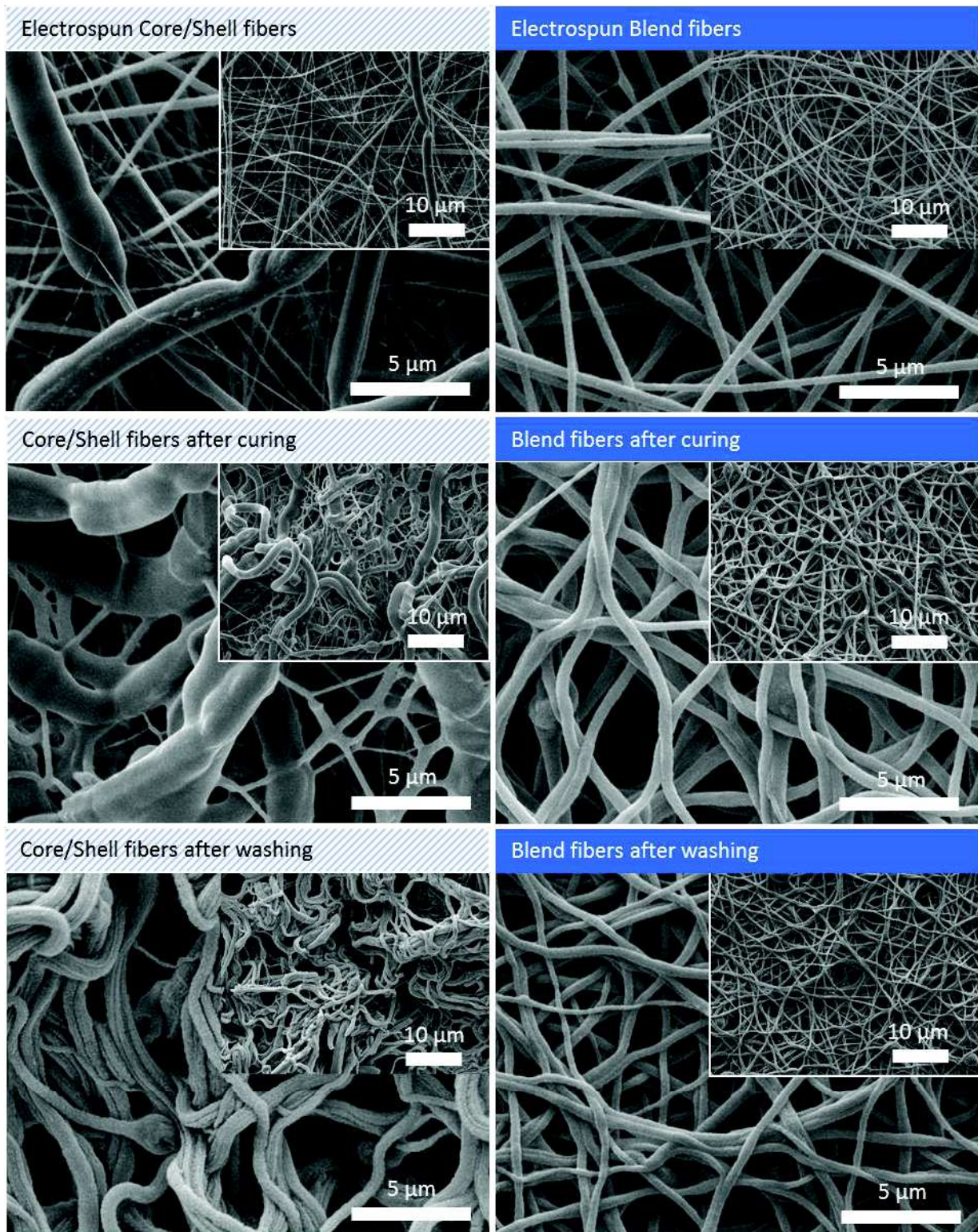


**Figure A4.5.** Core/shell MAPP/PVP fibers and blended MAPP/PVA fibers after curing and washing.

Finally, contact angles have been measured (Figure A4.6). The MAPP film is hydrophilic thanks to its maleic grafted functions and possible residual PVP. Core/shell and blend mats are less hydrophilic than the MAPP film due to the roughness of the nanofibrous surface. Nonetheless, the blend mat is far more hydrophilic than the core/shell mat and exhibits a hydrophilic behavior very close to the one of the MAPP film. It may be linked with the percentage of PVA still present in the structure of blend mats after washing as seen in Chapter 3.

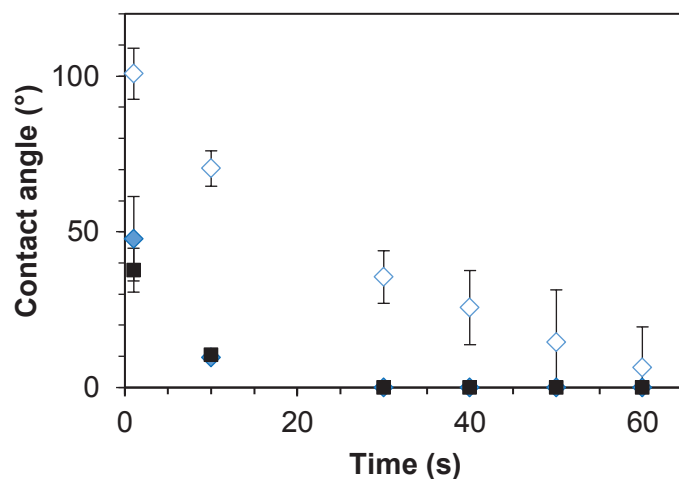


**Figure A4.6.** Contact angles as a function of the time after deposition on the sample of a droplet of water on a film of MAPP (black squares), a mat obtained by blend electrospinning of 20/5 wt% MAPP/PVA cured and washed (blue diamond) and a mat obtain by coaxial electrospinning of MAPP/PVP, cured and washed (white diamond).

In conclusion, MAPP/PVP core/shell mats could be electrospun, cured and washed to obtain MAPP fibers. Nevertheless, because of poor mechanical properties, MAPP/PVP core/shell fibers were not investigated and developed further contrary to MAPP/PVA blended fibers which exhibited higher mechanical properties and higher hydrophilic behavior.

## Materials and methods

### Materials and solution preparation

Maleic anhydride grafted polypropylene (MAPP) suspension (FGLASS X35) was provided by Michelman. Solid content is 33.8 wt% and the average particle size of the suspension is  $96 \pm 30$  nm. Polyvinylpyrrolidone (PVP,  $M_w = 1\,300\,000$  g/mol) and ethanol (ref. 24103, purity  $\geq 99.8\%$ ) were purchased from Sigma-Aldrich. The core is composed of the MAPP suspension. The shell is composed of 8 wt% of PVP in ethanol. The shell solution is prepared 4 hours prior to the experiments.

### Electrospinning, fiber curing and removal of the shell polymer

The homemade coaxial electrospinning setup is composed of a high-power voltage supply, syringe pumps, a stainless steel coaxial needle and a ring-shape ground electrode. The template polymer solution was infused to

the outer needle and the suspension was infused individually into the inner needle. The electric field was provided by a high-power voltage supply (Spellman SL10); two syringe pumps control the core flow rate (0.3 mL/h) and the shell flow rate (0.6 mL/h) (Harvard and Intertek apparatus respectively). The distance between the needle and the collector was kept at 15 cm and the voltage was 18 kV, the temperature was  $22\pm 1$  °C and relative humidity was in a range of 30-40%. After electrospinning, mats were cured in the oven at 160 °C for 1h and washed in distilled water at room temperature for 24 hours.

## References

- [1] J. Brandrup, E.H. Immergut, E.A. Grulke, *Polymer Handbook*, 4th Edition, Wiley, 2004.
- [2] G. Nisato, P. Hébraud, J.-P. Munch, S.J. Candau, Diffusing-wave-spectroscopy investigation of latex particle motion in polymer gels, *Phys. Rev. E.* 61 (2000) 2879–2887. doi:10.1103/PhysRevE.61.2879.



# Appendix 5:

## CHARACTERIZATION OF AQUEOUS POLYMER SUSPENSIONS AND WATER-SOLUBLE POLYMERS

### Size of aqueous suspensions

The diameter of the particles contained in the suspensions was calculated by Dynamic light scattering (DLS, Litesizer™ 500 from Anton Paar or ALV CGS-3 goniometer system. Scattering angles of 90°.) and by Scanning electron microscopy (SEM, VEGA 3, TESCAN). DLS measurements gave a hydrodynamic diameter of particles whereas the diameter of dried particles was calculated by SEM. Measures performed by both methods are presented here for all particles: coPA in Figure A5.1, MAPP in Figure A5.2, PVDF-PMMA in Figure A5.3 and PVDF in Figure A5.4. Table A5.1 gathers the results.

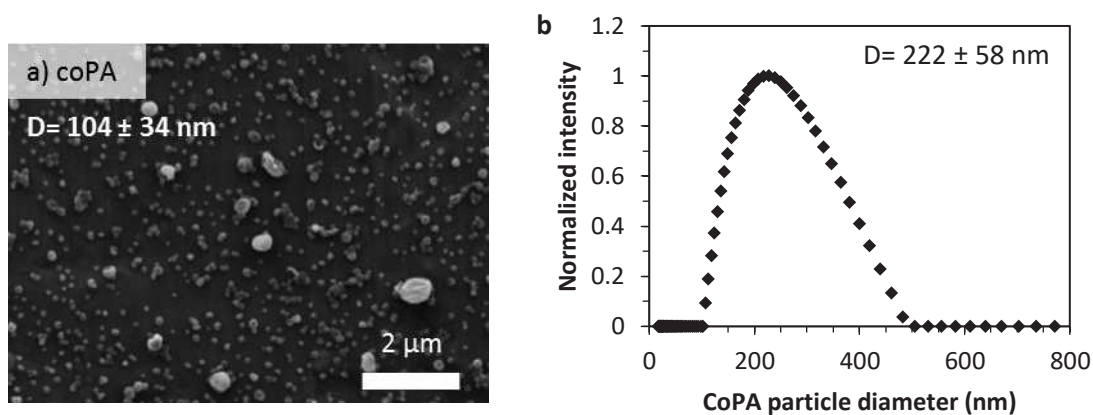


**Figure A5.1.** a) SEM image of dried coPA particles and their mean diameter. b) Distribution of the diameter of coPA particles measured by DLS.

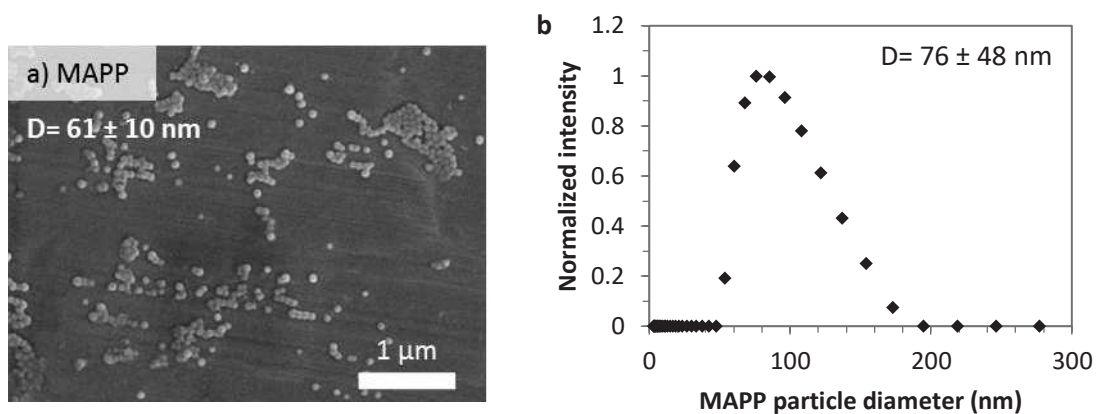


**Figure A5.2.** a) SEM image of dried MAPP particles and their mean diameter. b) Distribution of the diameter of MAPP particles measured by DLS.

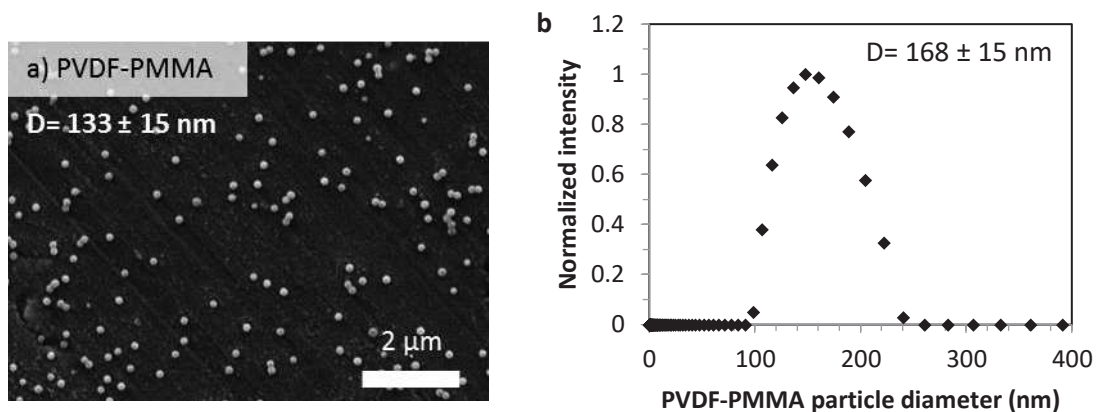


**Figure A5.3.** a) SEM image of dried PVDF-PMMA particles and their mean diameter. b) Distribution of the diameter of PVDF-PMMA particles measured by DLS.

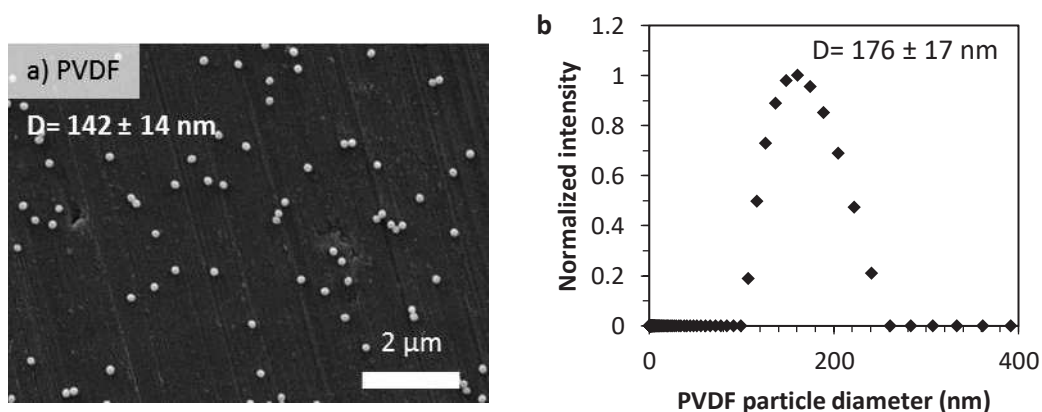


**Figure A5.4.** a) SEM image of dried PVDF particles and their mean diameter. b) Distribution of the diameter of PVDF particles measured by DLS.



Particle	Diameter measured by SEM	Diameter measured by DLS
coPA	104 ± 34 nm	222 ± 58 nm
MAPP	61 ± 10 nm	76 ± 48 nm
PVDF-PMMA	133 ± 15 nm	168 ± 15 nm
PVDF	142 ± 14 nm	176 ± 17 nm

**Table A5.1.** Particle diameters measured by SEM and by DLS.

The mean hydrodynamic diameter of all particles in suspensions was found to be higher than the mean diameter of dried particles. The difference between both values might lie in the fact that particles can unfold and spread out in water leading to higher diameters. The values given in Chapter 3 are the diameters measured by SEM (because particles are dried) in order to compare them to the diameters of particles measured in fibers (which are also dried).

## Glass transition temperatures and melting points

A differential scanning calorimetry apparatus (TA Q200) has been used to determine glass transition temperatures and melting points of polymers. Particles were dried before analysis. Spectra are given below in Figure A5.3 and A5.4. Only the first heating ramp is displayed as this ramp mimics the ramp undergone by electrospun mats during curing in Figure A5.3 and the heating rate is 3°C/min. For Figure A5.5, the heating rate is 10°C/min and the cooling rate 5°C/min. The glass transition temperatures and melting points are gathered in Table A5.2.

	Melting point
PVA	190°C
coPA	110 °C
MAPP*	155°C
PVDF-PMMA	94°C**
PVDF	148°C

**Table A5.2.** Glass transition temperatures and melting points of utilized polymers.

\* A first fusion is observed around 30°C. This fusion could not be explained.

\*\* The melting temperature given for PVDF-PMMA might also just be a relaxation temperature as no crystallization is observed in the cooling ramp (and consequently no fusion on the second heating ramp). The fact that no crystallization was observed might be related to the speed of the cooling ramp which might be too high.

Glass transition temperatures of polymers composing particles could not be determined by DSC. One could consider performing dynamic mechanical analysis (DMA) to calculate them. According to the literature, glass transition temperatures ( $T_g$ ) of amorphous polypropylene is around  $-13^\circ\text{C}$ , the  $T_g$  of PMMA is approximately  $105^\circ\text{C}$  and the  $T_g$  of PVDF is close to  $-40^\circ\text{C}$  (Brandrup, Johannes, Edmund Heinz Immergut, and Eric A. Grulke. Polymer Handbook, 4th Edition. Wiley, 2004.).

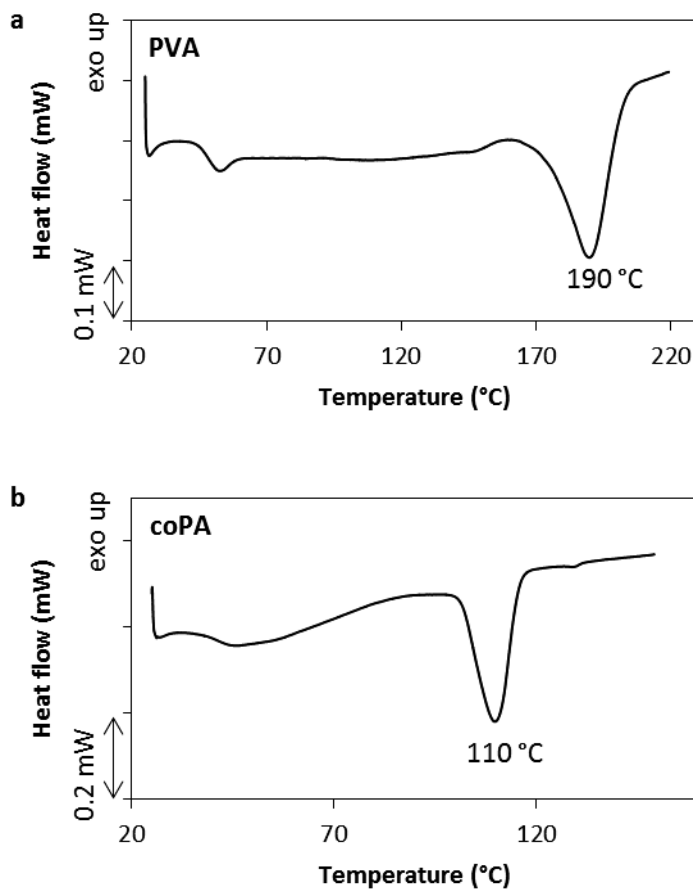


**Figure A5.5.** DSC spectra of a) PVA and b) coPA.

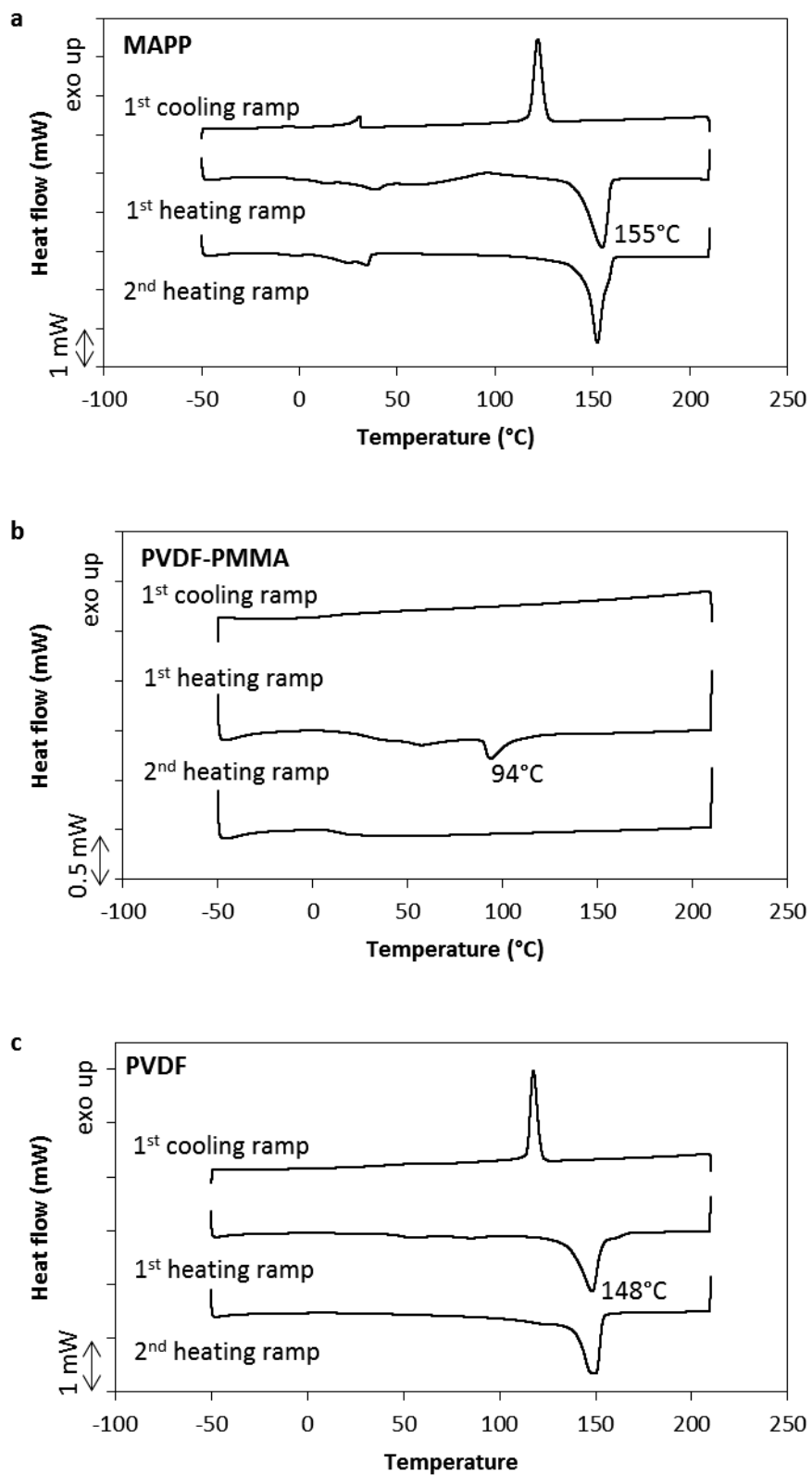
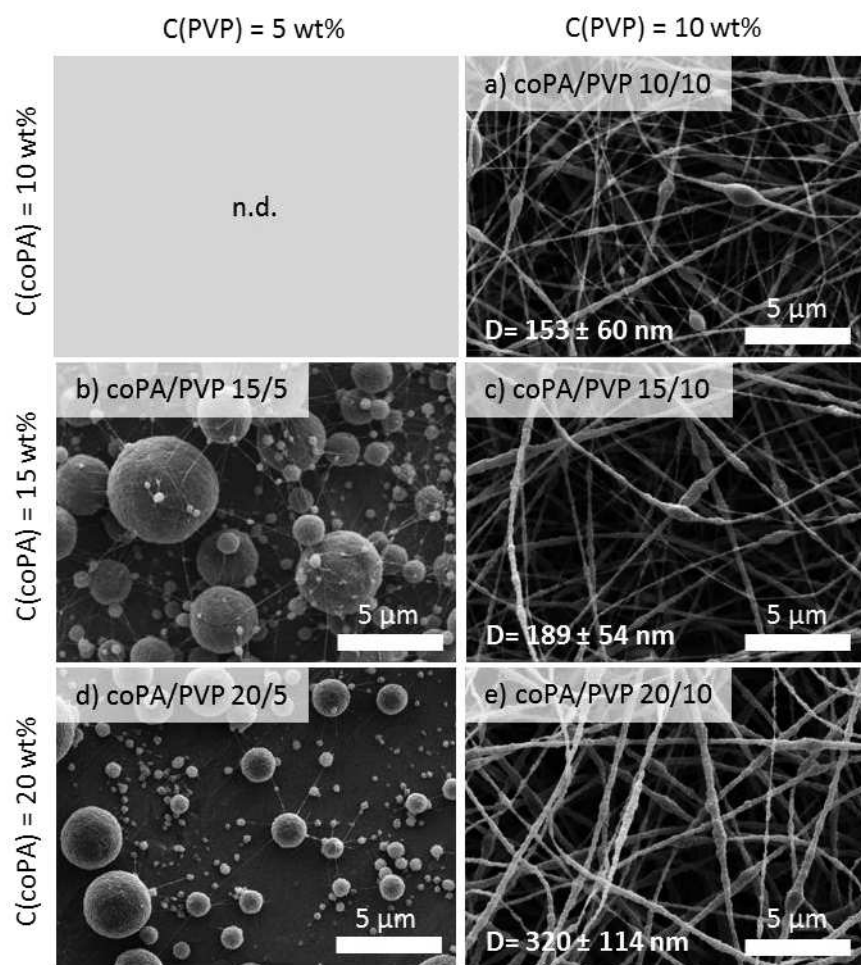


Figure A5.6. DSC spectra of a) MAPP, b) PVDF-PMMA and c) PVDF.

## Appendix 6:

# ELECTROSPINNING OF coPA WITH OTHER TEMPLATE POLYMERS

Two other template polymers were investigated: polyvinylpyrrolidone ( $M_w = 1\,300\,000$  g/mol) (PVP) purchased from Sigma-Aldrich and polyvinyl alcohol Gohsenhol (EG-05PW,  $M_w$  between 10 000 and 25 000 g/mol) (PVA<sub>G</sub>) purchased from the Nippon Synthetic Chemical Industries Co., Ltd. Suspensions were prepared with deionized water. Template polymers were chosen as they are water-soluble and as their transition temperatures (glass transition temperature of 182°C for PVP and melting point of 197°C for PVA<sub>G</sub> determined by DSC) are above the melting point of the dried co-polyamide particles (110°C). PVP were already used in the fabrication of core/shell fibers in Appendix 4. Its high molar mass would suggest that only a small amount of PVP in the blends would be sufficient to fabricate continuous and regular fibers. Besides, it was thought that thanks to the low molar mass of PVA<sub>G</sub>, the washing step would be more efficient.



**Figure A6.1.** SEM images of coPA/PVP electrospinning fibers a) 10/10, b) 15/5, c) 15/10, d) 20/5 and e) 20/10 wt%. n.d.: not done.

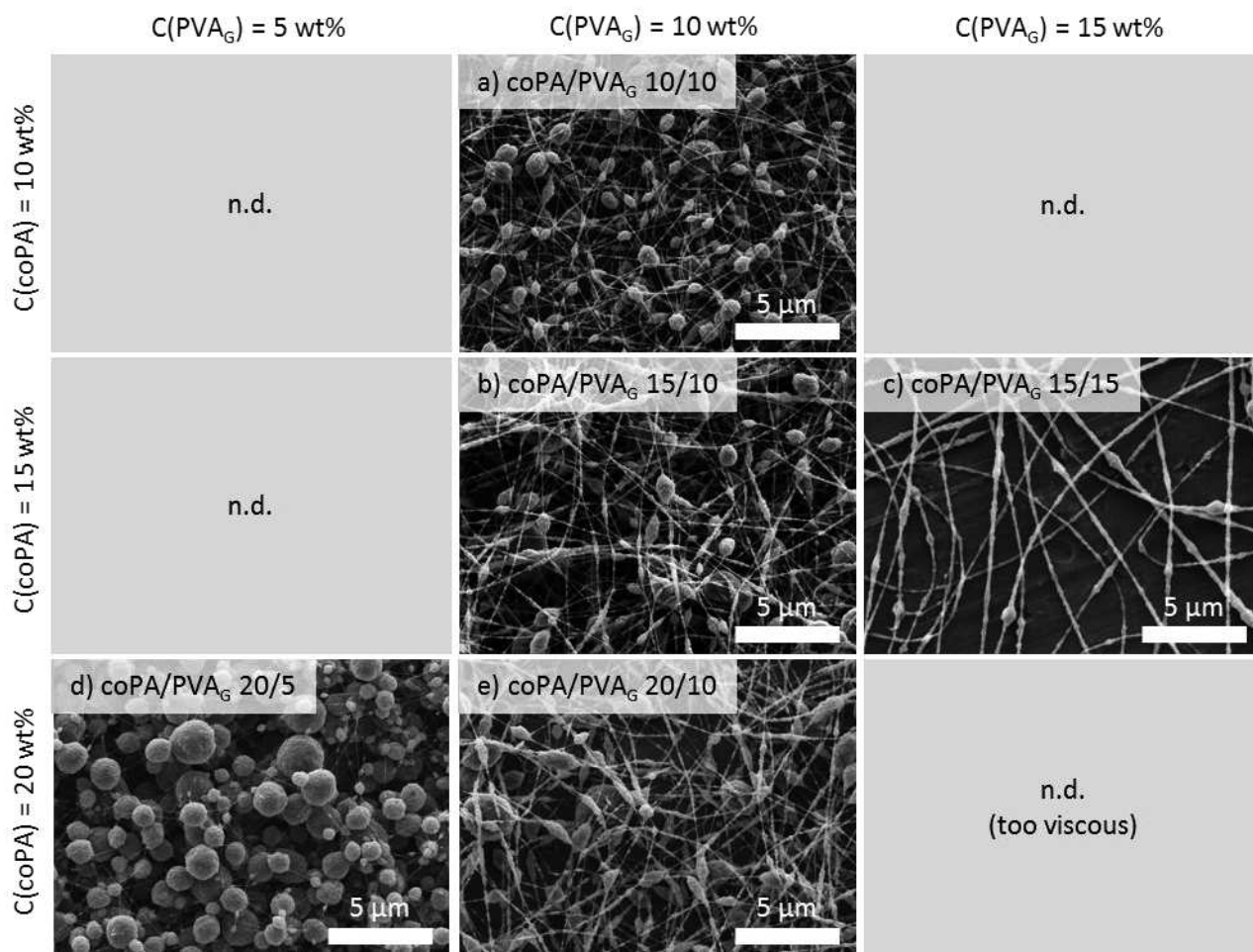


**Figure A6.2.** SEM images of coPA/PVA<sub>G</sub> electrospinning fibers a) 10/10, b) 15/10, c) 15/15, d) 20/5 and e) 20/10 wt%. n.d.: not done.

Continuous and regular fibers were not fabricated for the coPA/PVP ratio 20/5 wt% (Figure A6.1d), as it was the case for the coPA/PVA blend detailed in Chapter 3. Even if PVP has a higher molar mass ( $M_w = 1\,300\,000 \text{ g/mol}$ ) than that of PVA ( $M_w = 130\,000 \text{ g/mol}$ ), a coPA/PVP ratio of 20/10 (meaning a PVP concentration of 10 wt% for a concentration in solid particles of 20 wt%) was required to obtain continuous fibers (Figure A6.1e). The template polymer concentration is higher here for the same amount of coPA particles. PVP was not further used as, in order to wash efficiently mats, a low template polymer concentration is required.

The molar mass of PVA<sub>G</sub> is too low to enable entanglements in the blends unless coPA/PVA<sub>G</sub> concentration is raised to 15/15 wt% (Figure A6.2c). Beads were formed for the ratio 20/5 (Figure A6.2d). Bead-on-string fibers were fabricated for the ratios 10/10, 15/10 and 20/10 (Figure A6.2a,b,e). For the ratio 15/15 regular fibers with almost no beads were produced. However, at 15/15 wt%, the productivity is low as the blend is viscous.



# Appendix 7:

## ELECTROSPINNING, CURING AND WASHING OF MAPP/PVA, PVDF-PMMA/PVA AND PVDF/PVA MATS

The fabrication of mats in three steps (electrospinning, curing and washing) composed of regular and continuous fibers from a blend of particles and PVA is described here. Three aqueous suspensions are used: MAPP, PVDF-PMMA and PVDF. For the electrospinning step, the mass concentration of particles in blends was fixed at 20 wt%. PVA concentration was investigated for each blend to determine the lowest concentration of PVA enabling the formation of fibers. The fabrication of regular and continuous fibers with the lowest PVA content is essential to wash mats efficiently after the curing step. For the curing and the washing step, the aim was to cure mats at a temperature sufficiently high so that they can be washed without altering their fibrous structure. Optimal particles/PVA ratios as well as curing temperatures are gathered in Table A7.1.

### MAPP/PVA mats

**Electrospinning:** The optimal ratio allowing the fabrication of continuous and regular fibers with the lowest PVA content is 20/5 wt% MAPP/PVA (Figure A7.1).

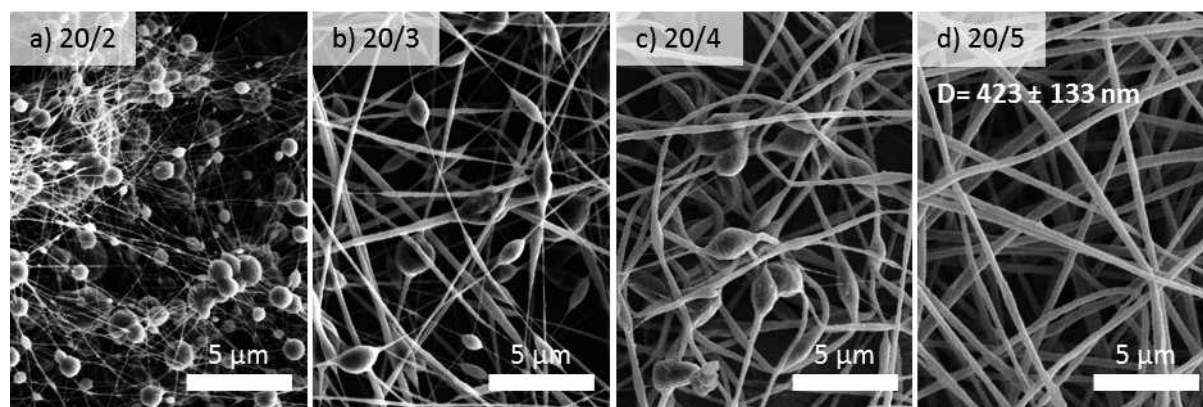


**Figure A7.1.** SEM images of MAPP/PVA electrospinning fibers with MAPP/PVA ratio a) 20/2, b) 20/3, c) 20/4 and d) 20/5 wt%.

**Curing and washing:** MAPP/PVA 20/5 wt% mats were cured at 130°C, 150°C and 170°C and washed (Figure A7.2). Curing temperatures were chosen in coherence with the melting point of MAPP particles (155°C). It can be seen that the structure of mats is still fibrous after curing for the three temperatures and that the higher the temperature, the more bonded fibers are. After curing at 170°C and washing, fibers are all stuck

together and the mean fiber diameter consequently increases. It was chosen to cure MAPP/PVA mats at 150°C so that fibers could bond together at junction points and to preserve the fibrous structure.

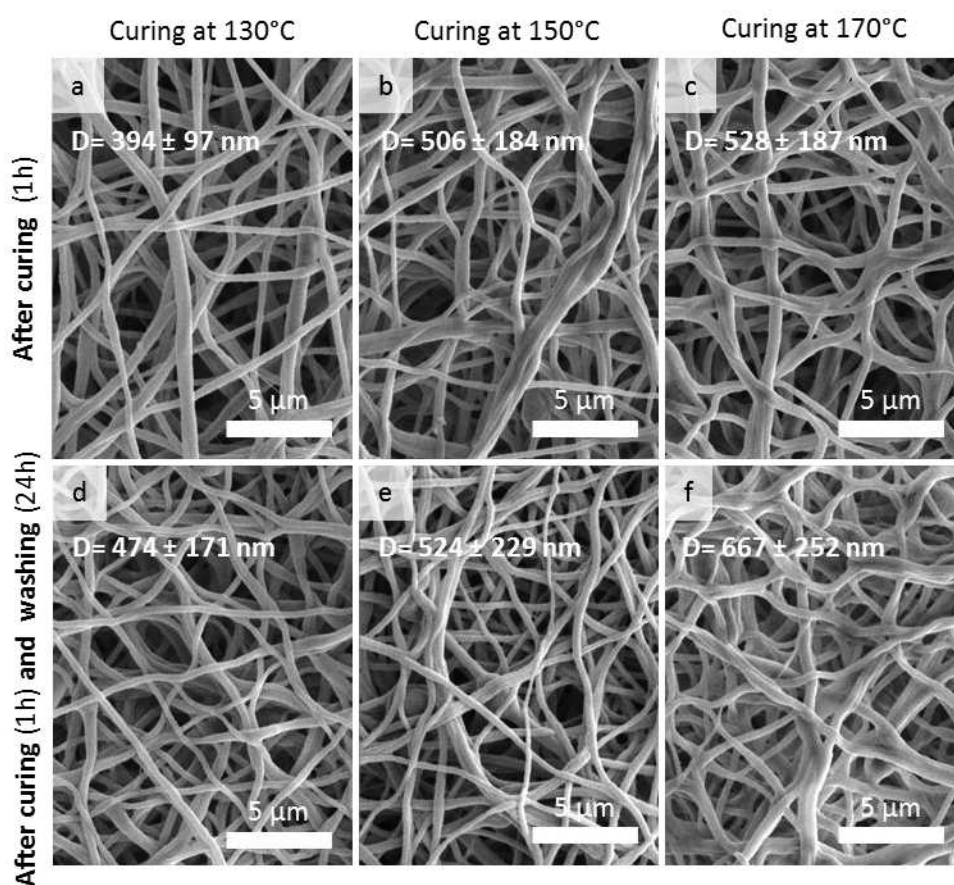


**Figure A7.2.** SEM images of 20/5 wt% MAPP/PVA electrospinning fibers a) after curing at 130°C and d) washing; b) after curing at 150°C and e) washing; and c) after curing at 170°C and f) washing.

## PVDF-PMMA/PVA mats

**Electrospinning:** Continuous and regular fibers were fabricated when the concentration in PVA was 5 wt%.

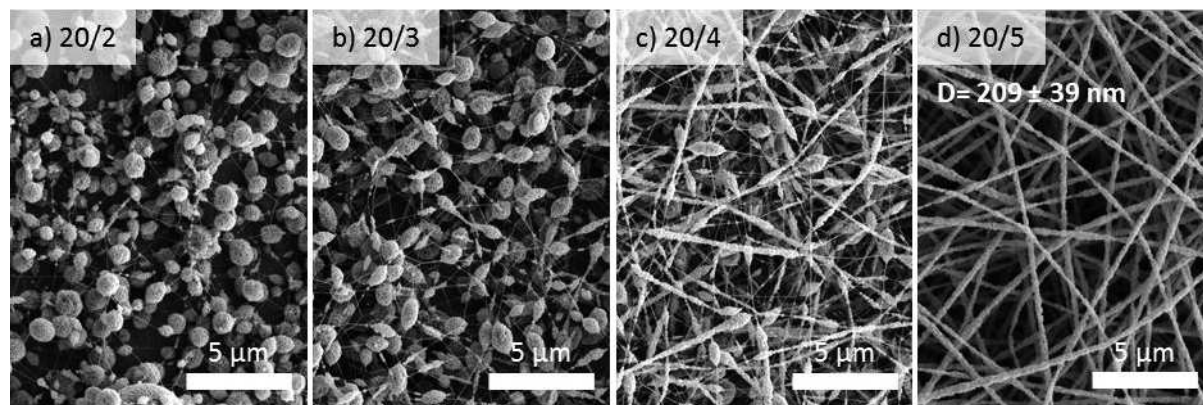


**Figure A7.3.** SEM images of PVDF-PMMA/PVA electrospinning fibers with PVDF-PMMA/PVA ratio a) 20/2, b) 20/3, c) 20/4 and d) 20/5 wt%.



**Curing and washing:** Curing and washing steps were performed with mats containing a PVDF-PMMA/PVA ratio of 20/5 wt%. Mats were cured at 80, 100, 120 and 140°C as the transition temperature of PVDF-PMMA is 94°C. Mats were destroyed during the washing step when cured at 80°C (Figure A7.4a,e). Mats cured at 100°C resisted the washing step but lots of fibers were broken (Figure A7.4b,f). Curing at 140°C led to the formation of a film (Figure A7.4d,h). Mats cured at 120°C and washed are still fibrous after the post-treatments (Figure A7.4c,g).

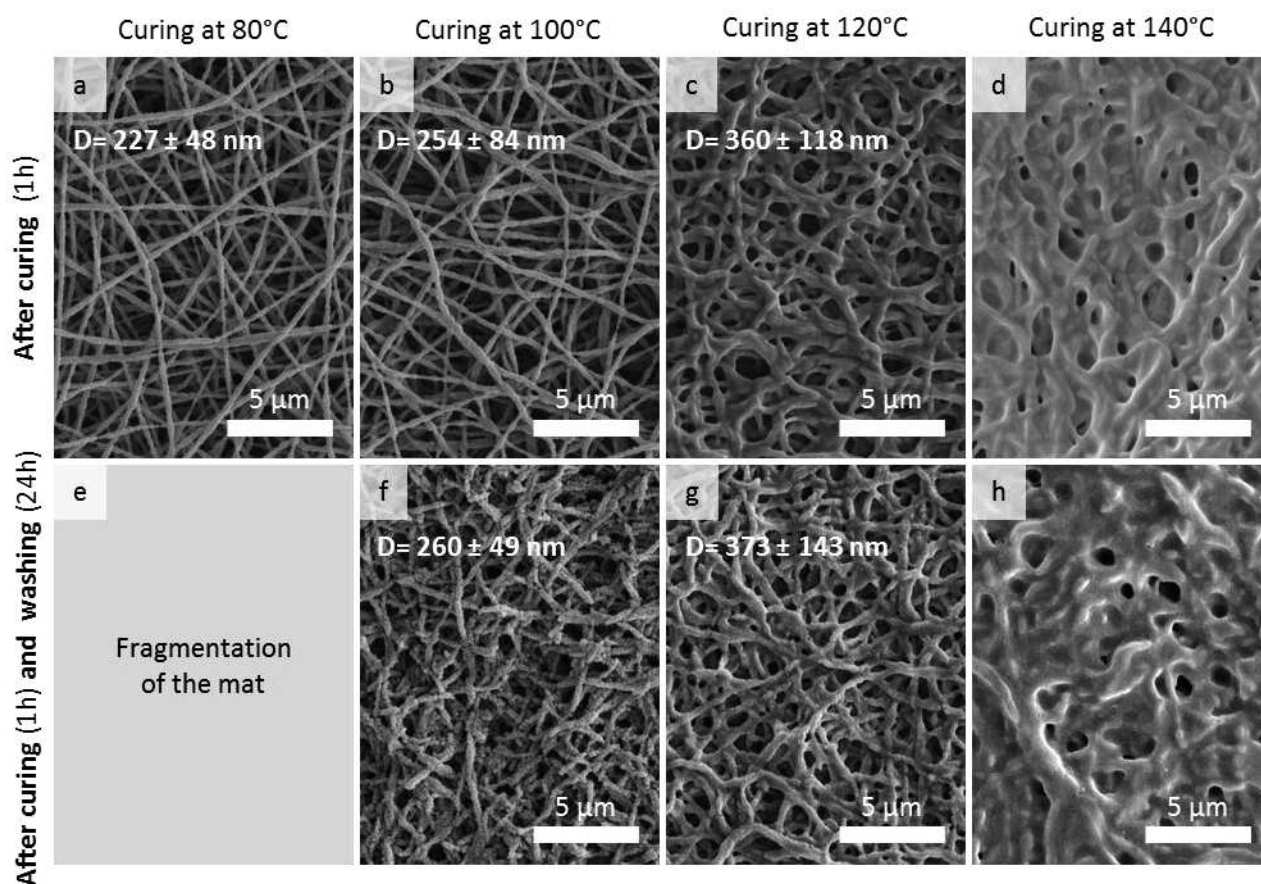


**Figure A7.4.** SEM images of 20/5 wt% PVDF-PMMA/PVA electrospinning fibers a) after curing at 80°C and e) washing; b) after curing at 100°C and f) washing; c) after curing at 120°C and g) washing; and d) after curing at 140°C and h) washing.

## PVDF/PVA mats

**Electrospinning:** It was not possible to electrospin fibers with the ratio PVDF/PVA 20/5 wt% (Figure A7.4a). PVA content had to be increase up to 8 wt% (Figure A7.4c). With increasing PVA content, the mean fiber diameter increased from 261 ± 64 nm for the ratio 20/8 wt% to 304 ± 69 nm for the ratio 20/10 wt%.

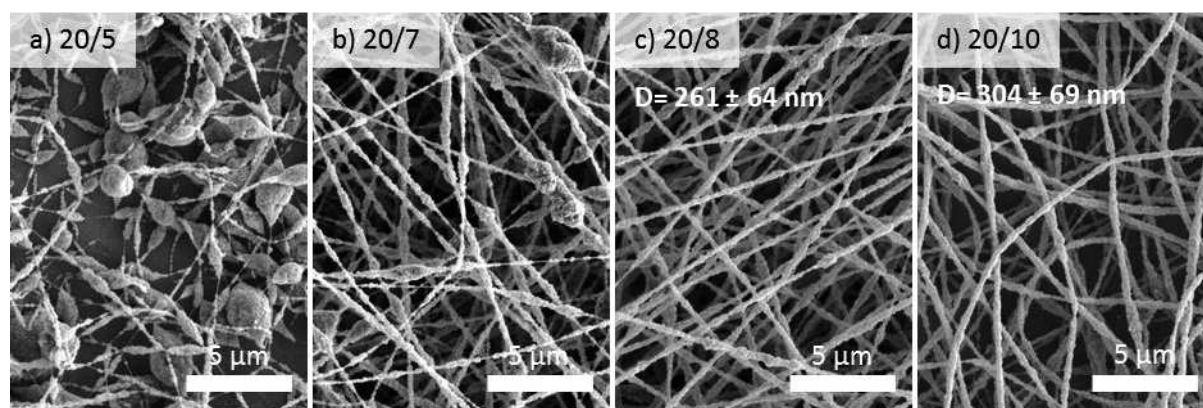


**Figure A7.5.** SEM images of PVDF /PVA electrospinning fibers with PVDF /PVA ratio a) 20/5, b) 20/7, c) 20/8 and d) 20/10 wt%.

**Curing and washing:** Curing and washing steps were performed with mats containing a PVDF/PVA ratio of 20/8 wt%. Mats resisted the washing step only when they were cured for 1h at 200°C (Figure A7.6). Interestingly, the optimal curing temperature was above the melting point of PVDF (148°C) and above that of PVA (190°C).

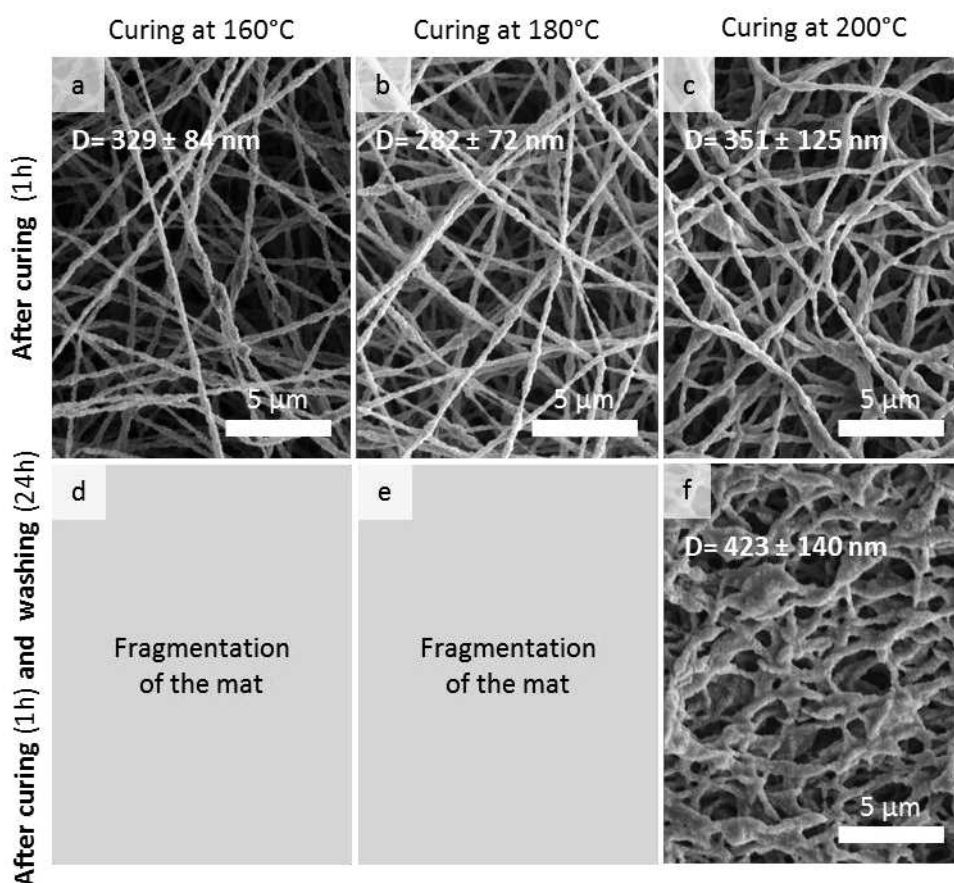


**Figure A7.6.** SEM images of 20/8 wt% PVDF /PVA electrospinning fibers a) after curing at 160°C and d) washing, b) after curing at 180°C and e) washing; and c) after curing at 200°C and f) washing.

<b>Particles/PVA</b>	<b>Ratio</b>	<b>Curing temperature (1h)</b>
MAPP/PVA	20/5	150 °C
PVDF-PMMA/PVA	20/5	120 °C
PVDF /PVA	20/8	200 °C

**Table A7.1.** Optimal particle/PVA ratios and curing temperature enabling the fabrication of fibrous mats.



# Appendix 8:

## POLYMER REMOVAL AFTER WASHING

### Measured by DSC

The washing of mats could hardly be followed by DSC. By DSC, a differential scanning calorimetry apparatus TA Q200 has been used and the heating rate was set at 3°C/min. It could be noticed that the peak corresponding to the melting point of PVA at 190°C disappears after washing proving at 22°C and at 50°C that some PVA was eliminated as it is showed in Figure A8.1 in the case of coPA/ PVA mats. Nevertheless, variations are rather slight as the peak before washing is already small. It can, in the end, only be concluded from these characterization that some PVA can be eliminated during the washing step. When not written, the washing step was performed at 22°C.

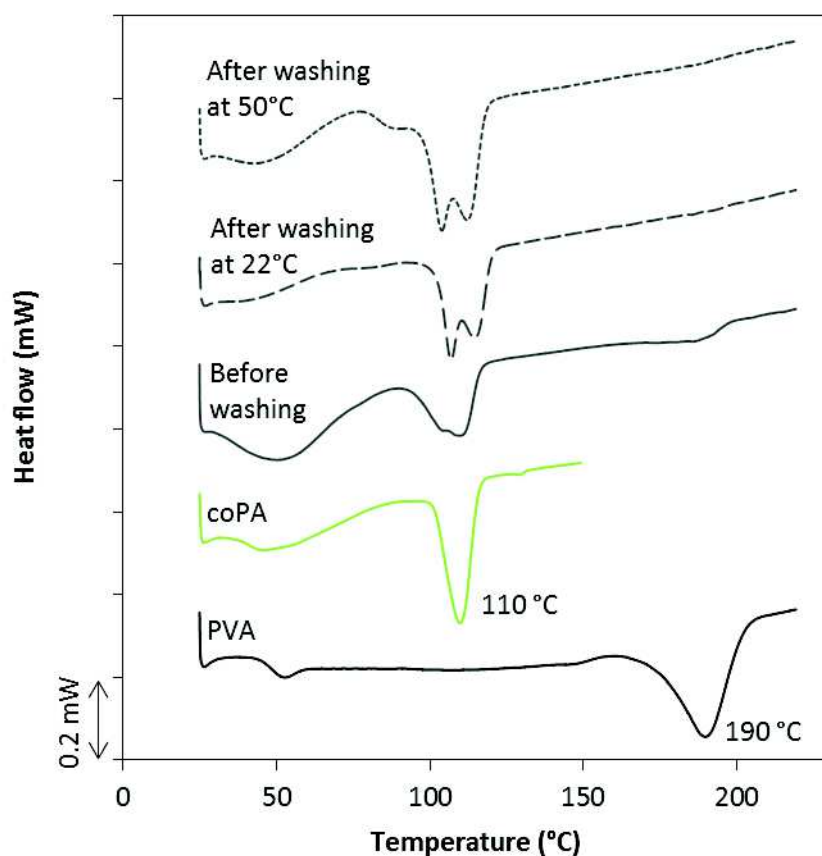


**Figure A8.1.** DSC thermograms of PVA (black line), coPA (light green line), coPA/PVA mat before washing (dark green line), coPA/PVA mat after washing at 22°C (dotted dark green line with long dots) and coPA/PVA mat after washing at 50°C (dotted dark green line with short dots).

## Measured by IR

The infrared analysis was performed on a Nicolet 380 Fourier-transform infrared spectrometer (Thermo Electron Corporation) equipped with ATR Smart Omni Sampler. Infrared spectra were collected from 4000-400  $\text{cm}^{-1}$ . By IR, the characteristic absorption bands of PVA (O-H stret at 3304  $\text{cm}^{-1}$ , CH<sub>2</sub> stret at 2909  $\text{cm}^{-1}$  and C=O stret at 1732  $\text{cm}^{-1}$ ) are quite always masked by the characteristic absorption bands of the polymer constituting the suspensions, so that comparisons between IR spectra before and after washing are arduous. This is the case of coPA (characteristic absorption bands: N-H stret at 3300  $\text{cm}^{-1}$ , CH<sub>2</sub> stret at 2918  $\text{cm}^{-1}$ , C=O stret at 1636  $\text{cm}^{-1}$  and N-H bend at 1541  $\text{cm}^{-1}$ ) (Figure A7.2) and MAPP (characteristic absorption bands: CH<sub>3</sub> stret at 2918  $\text{cm}^{-1}$  and CH<sub>3</sub> and CH<sub>2</sub> bend at 1452 and 1376  $\text{cm}^{-1}$ ) (Figure A8.3). This is also the case of PVDF-PMMA (characteristic absorption bands: CH<sub>3</sub> stret of PMMA at 2956  $\text{cm}^{-1}$ , C=O stret of PMMA at 1724  $\text{cm}^{-1}$ , C-F of PVDF at 1398  $\text{cm}^{-1}$  and CF<sub>2</sub> of PVDF at 1176  $\text{cm}^{-1}$ ). Indeed, the peak of PMA<sub>M</sub> at 3304  $\text{cm}^{-1}$  was not considered for the analysis (even if it does not overlay the PVDF-PMMA spectrum) due to the fact that it corresponds to O-H stretching vibrations and is widely influenced by water absorption (Figure A8.4).

Differently, for PVDF (Figure A8.5) (characteristic absorption bands: C-F at 1400  $\text{cm}^{-1}$  and CF<sub>2</sub> at 1182  $\text{cm}^{-1}$ ), two peaks belonging to PVA (1732  $\text{cm}^{-1}$ ) and to PVDF (1182  $\text{cm}^{-1}$ ) which do not overlay were found. However, the peak at 1732  $\text{cm}^{-1}$  of PVA was too small to be analyzed (maximum of absorbance: 0.06).

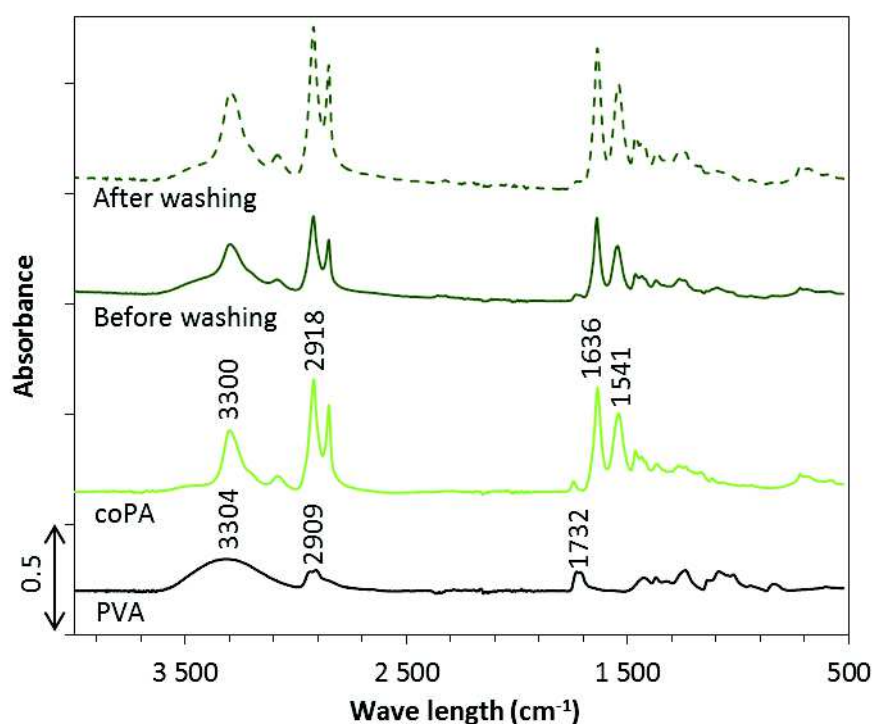


**Figure A8.2.** IR spectra of PVA (black line), coPA (light green line), coPA/PVA mat before washing (dark green line) and coPA/PVA mat after washing (dotted green line).

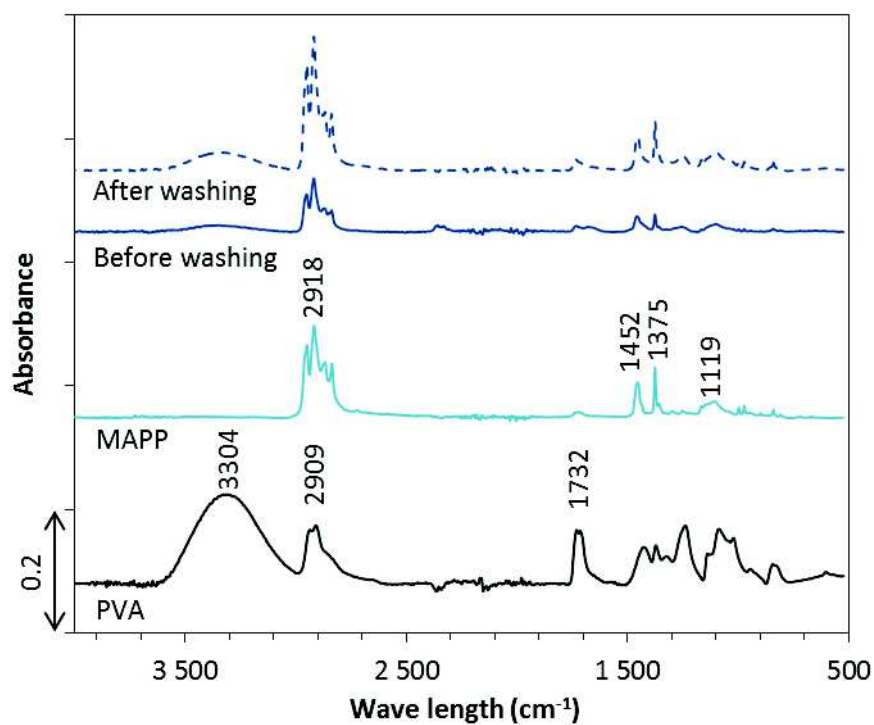


**Figure A8.3.** IR spectra of PVA (black line), MAPP (light blue line), MAPP/PVA mat before washing (dark blue line) and MAPP/PVA mat after washing (dotted dark blue line).

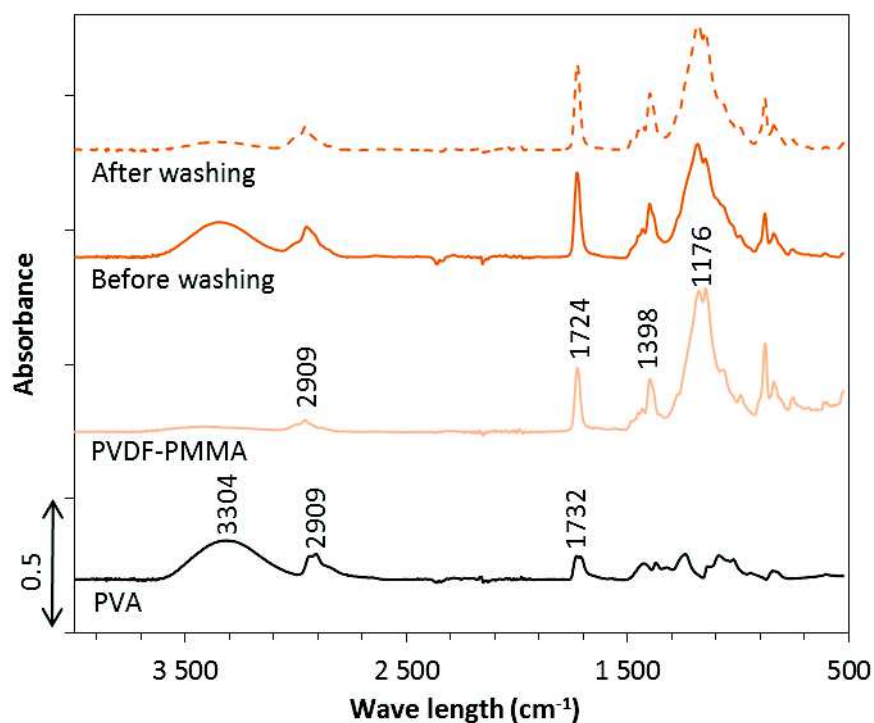


**Figure A8.4.** IR spectra of PVA (black line), PVDF-PMMA (light orange line), PVDF-PMMA/PVA mat before washing (dark orange line) and PVDF-PMMA/PVA mat after washing (dotted dark orange line).

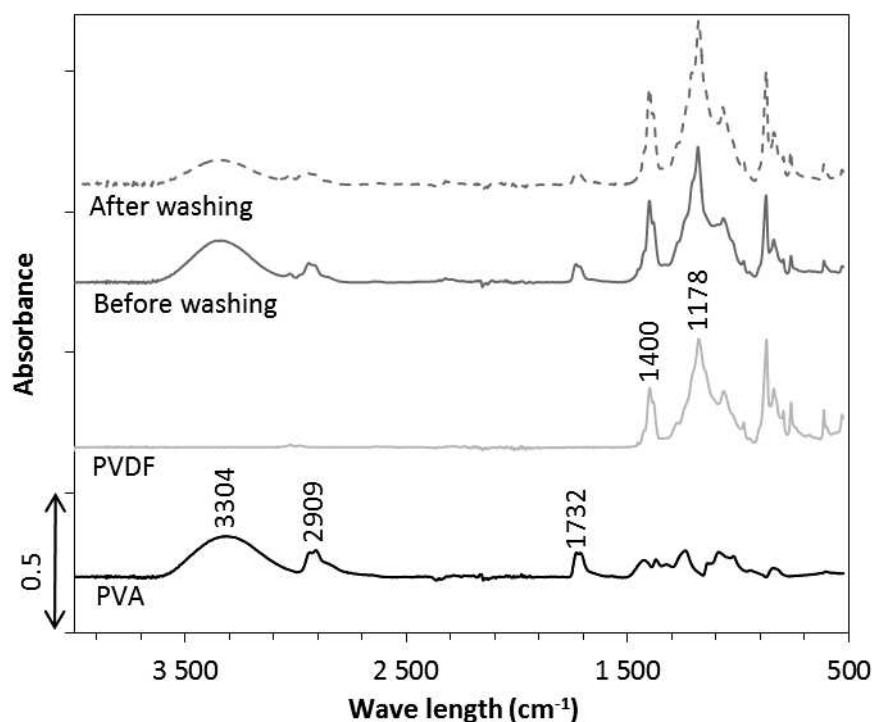


**Figure A8.5.** IR spectra of PVA (black line), PVDF (light grey line), PVDF/PVA mat before washing (dark grey line) and PVDF/PVA mat after washing (dotted dark grey line).

## Measured by weighing mats

PVA removal could also be followed by weighing mats before and after the washing step. Mats were dried overnight under vacuum before weighing them. Their initial masses were approximately of  $0.1 \pm 0.4$  nm. Nevertheless, this method implies an important assumption: it assumes that the different in weight before and after washing is only due to PVA removal and that no particles can also be eliminated during the washing step. By making this assumption, it could be inferred that half of the PVA content is removed during the washing step from MAPP/PVA mats. The entire amount of PVA is removed from PVDF-PMMA/PVA mats. Only 33 wt% of the initial PVA content is removed from PVDF/PVA mats. Measures have been repeated twice (with two different mats) and gave very close results (Figure A8.6). If some particles are also eliminated during the washing step, these values, representing the amount of PVA that was washed, are maxima.

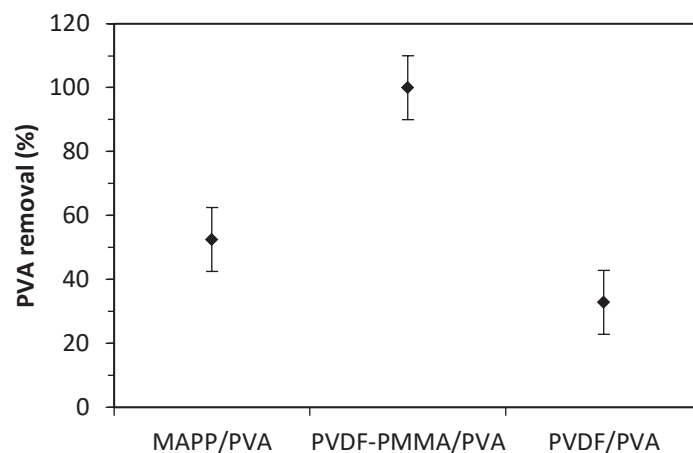


**Figure A8.6.** PVA removal (in wt%) after washing in MAPP/PVA, PVDF-PMMA/PVA and PVDF/PVA mats.

This method allowed calculating particles/PVA ratios in mats before and after washing (Figure A8.7).

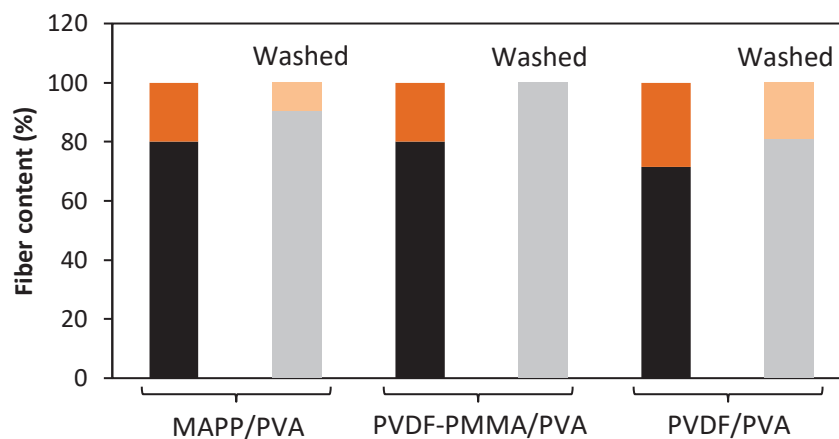


**Figure A8.7.** Particles (black)/PVA (orange) ratios before (dark colors) and after (light colors) washing in MAPP/PVA, PVDF-PMMA/PVA and PVDF/PVA mats.



# Appendix 9:

## STRESS–STRAIN CURVES

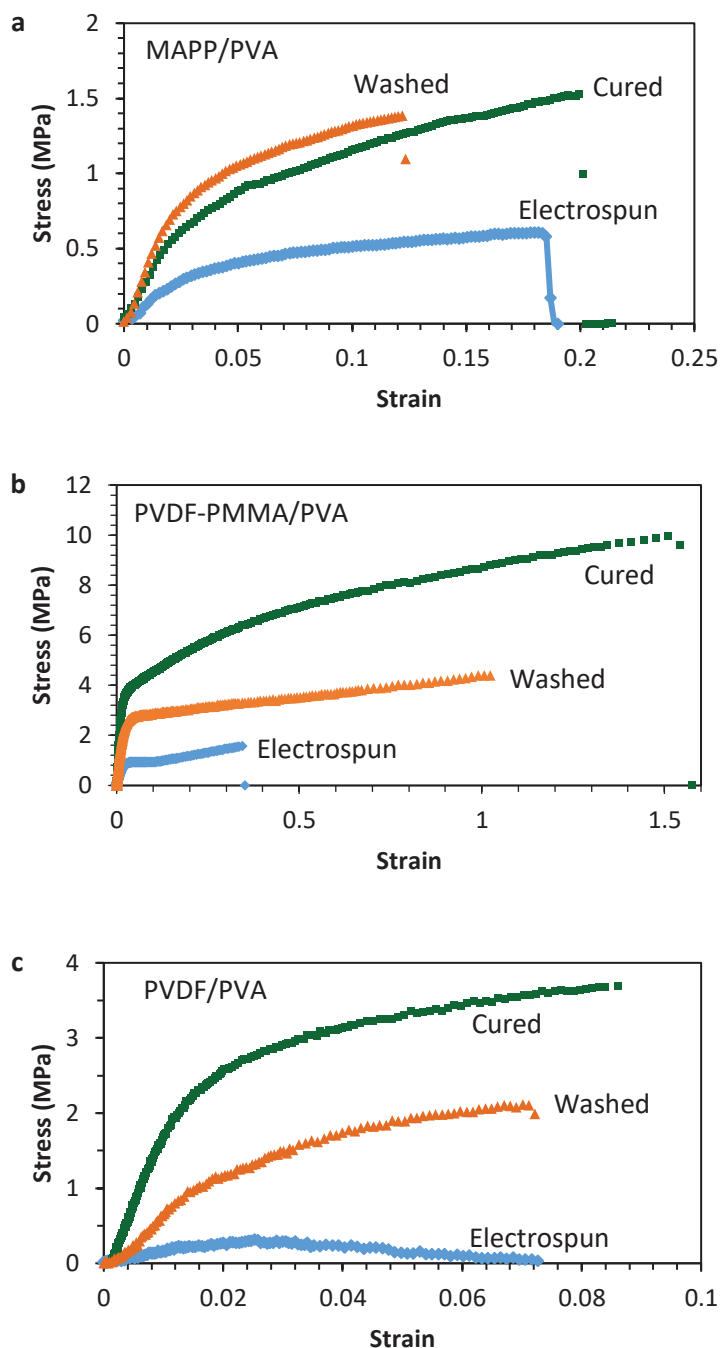


**Figure A9.1.** Stress-strain curves of a) MAPP/PVA mats, b) PVDF-PMMA/PVA mats and c) PVDF/PVA mats after electrospinning (blue), curing (dark green) and washing (orange)

# Appendix 10:

## CHARACTERIZATION OF FILTRATION SUSPENSIONS AND PERMEABILITY OF MATS

### **Size of silica suspensions**

The diameter of silica particles was calculated by Dynamic light scattering (DLS) and observed by Scanning Electron Microscopy (SEM, VEGA 3, TESCAN). DLS apparatus is equipped with an ALV CGS-3 goniometer system and a He-Ne laser (wavelength=633 nm). All experiments were performed at a scattering angle of 90°. The three suspensions at disposal contain respectively silica particles with diameter 1  $\mu\text{m}$  ( $1.06 \pm 0.06 \mu\text{m}$ ), 0.4  $\mu\text{m}$  ( $0.39 \pm 0.10 \mu\text{m}$ ) and 0.1  $\mu\text{m}$  ( $0.14 \pm 0.04 \mu\text{m}$ ). The distribution of silica particles was found to be tight and no big aggregates were registered meaning that silica particles were well-dispersed in water.

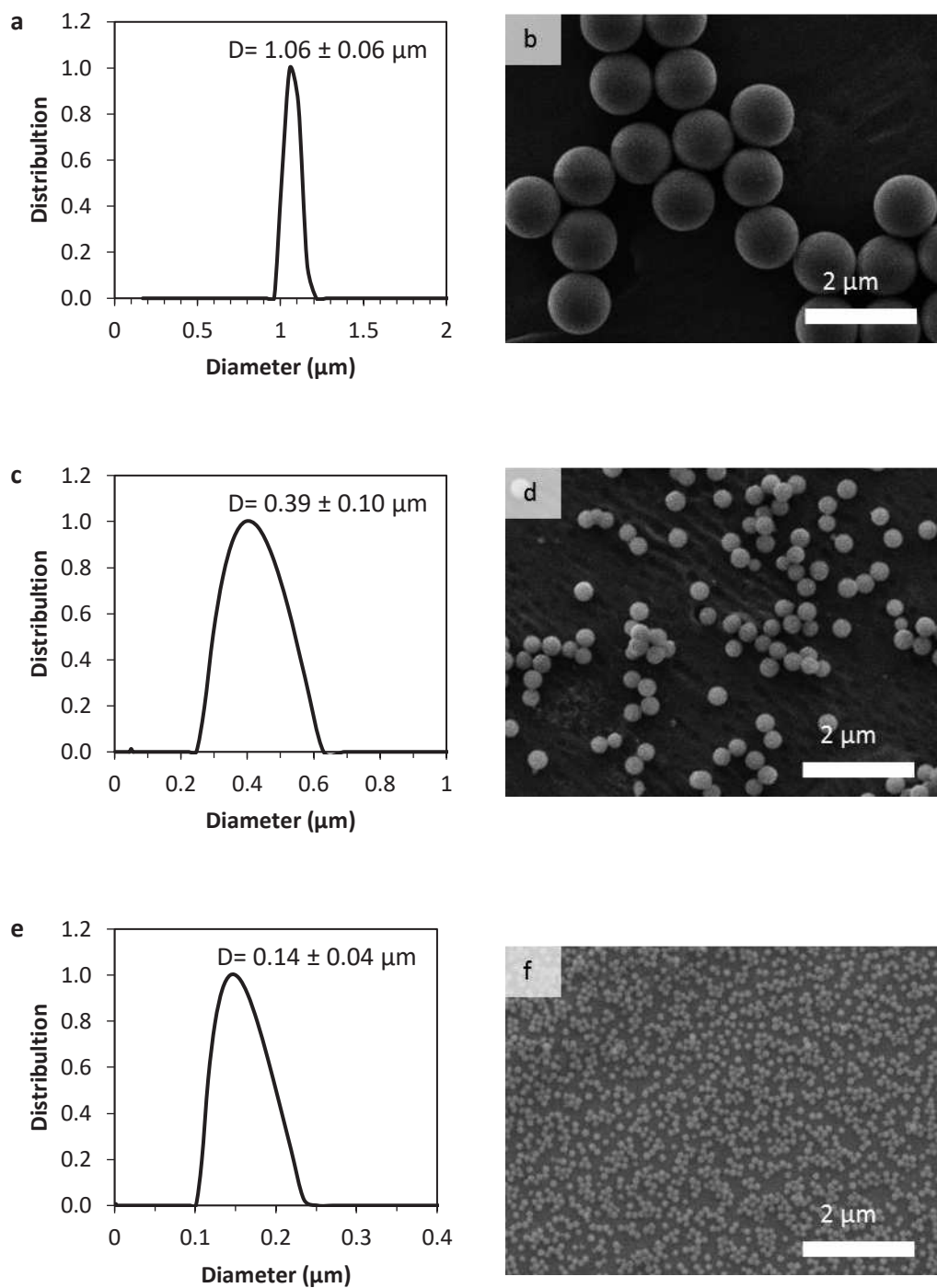


**Figure A10.1.** Particle diameter distribution measured by DLS (links) and SEM images (right) of silica suspensions with diameters a-b)  $1 \mu\text{m}$ , c-d)  $0.4 \mu\text{m}$  and e-f)  $0.1 \mu\text{m}$ .

## Calibration curves

Calibration curves were registered by UV-VIS spectrometry at a wave length of 450 nm (UV-2600 from Shimadzu).

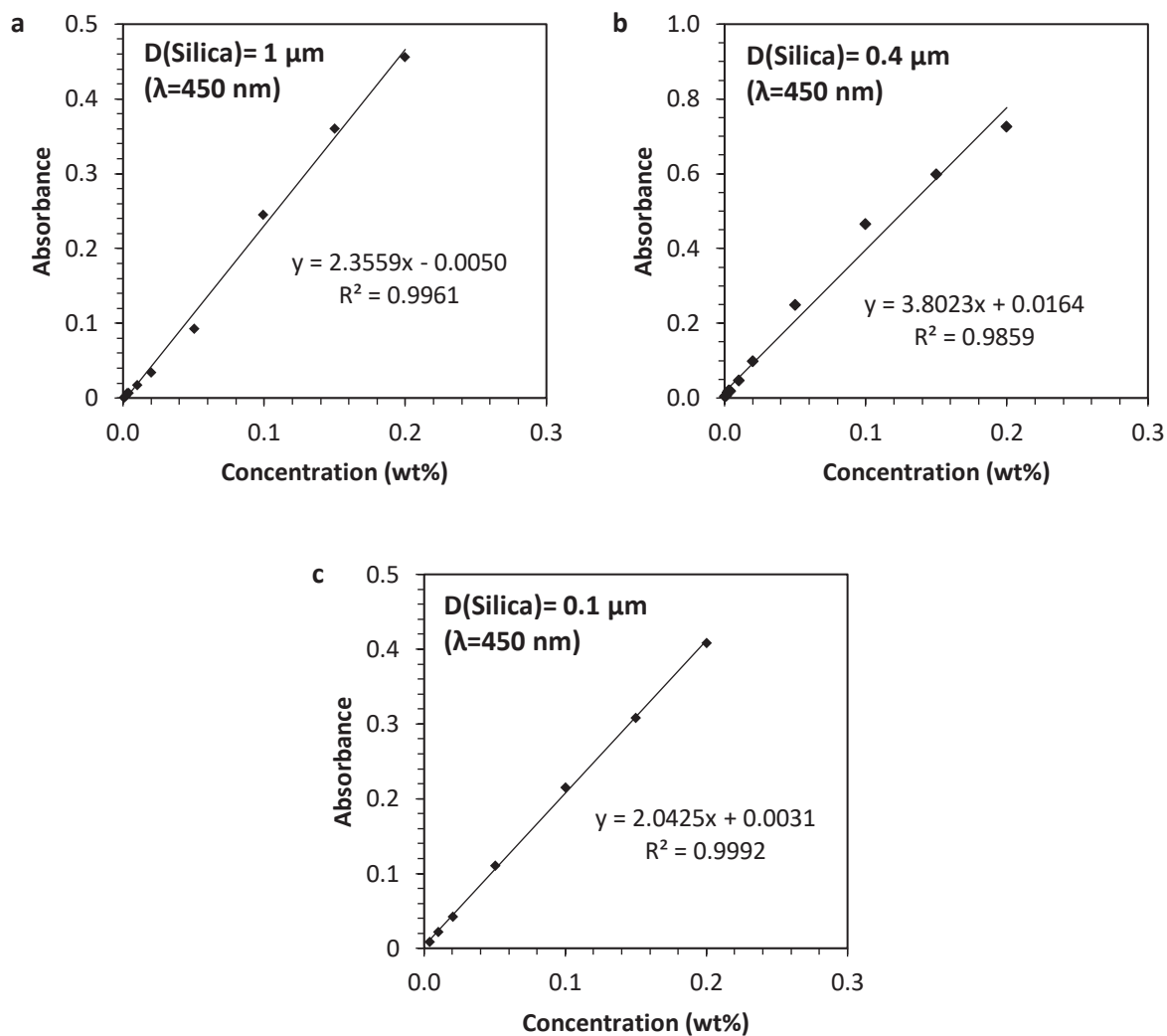


**Figure A10.2.** Absorbance as a function of the silica concentration. a)  $D(\text{Silica}) = 1 \mu\text{m}$ , b)  $D(\text{Silica}) = 0.4 \mu\text{m}$  and c)  $D(\text{Silica}) = 0.1 \mu\text{m}$ .

## Pictures of solutions before and after filtration

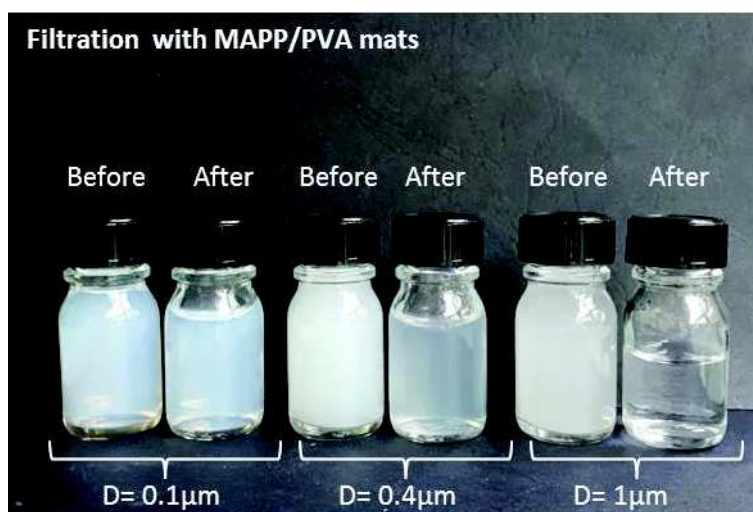


**Figure A10.3.** Pictures of solutions before and after filtration of silica particles having for mean diameters 0.1  $\mu\text{m}$ , 0.4  $\mu\text{m}$  and 1  $\mu\text{m}$  filtrated with MAPP/PVA mats.

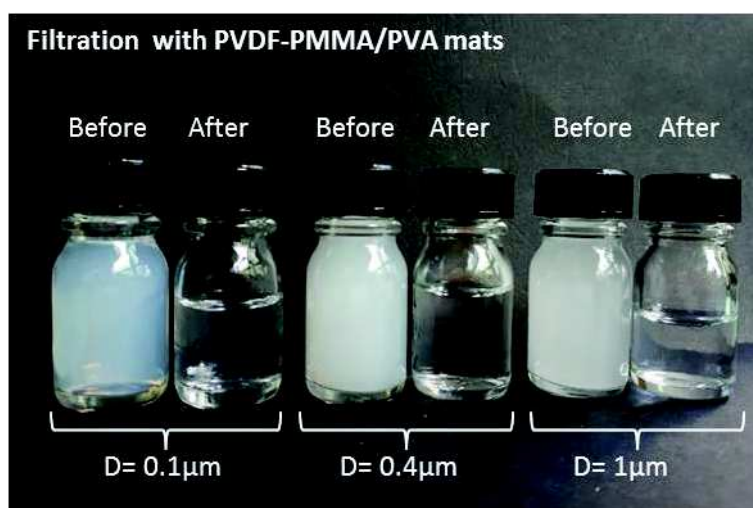


**Figure A10.4.** Pictures of solutions before and after filtration of silica particles having for mean diameters 0.1  $\mu\text{m}$ , 0.4  $\mu\text{m}$  and 1  $\mu\text{m}$  filtrated with PVDF-PMMA/PVA mats.

## Permeability

Liquid permeability was measured at the IFTS (Institut de la Filtration et des Techniques Séparatives (Fr) - International Filter Testing Services (En)). Values were deduced from the slope of the water flux as a function of the pressure graphs (Figure A10.5). Experiments were repeated twice. Mats had a thickness of  $28 \pm 9 \mu\text{m}$ .

Slopes were taken at the origin when necessary, as permeability can decrease with an increase of the water flux due to mat compaction leading to a reduction of the pore size and of pore connectivity [1-3].



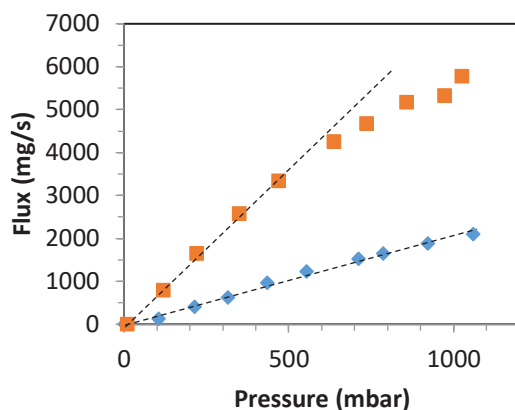


**Figure A10.5.** Water flux as a function of the pressure for MAPP/PVA mats (orange squares) and for PVDF-PMMA/PVA (blue diamonds).

Mat	Water permeability ( $\times 10^4$ L/h/m <sup>2</sup> /bar)
MAPP/PVA	$18 \pm 2$
PVDF-PMMA/PVA	$2.4 \pm 0.1$

**Table A10.1.** Water permeability of MAPP/PVA and PVDF-PMMA/PVA mats.

## References

- [1] Homaeigohar, S. Sh, K. Buhr, and K. Ebert. "Polyethersulfone Electrospun Nanofibrous Composite Membrane for Liquid Filtration." *Journal of Membrane Science* 365, no. 1–2 (December 1, 2010): 68–77. <https://doi.org/10.1016/j.memsci.2010.08.041>.
- [2] Huang, Liwei, Seetha S. Manickam, and Jeffrey R. McCutcheon. "Increasing Strength of Electrospun Nanofiber Membranes for Water Filtration Using Solvent Vapor." *Journal of Membrane Science* 436 (June 1, 2013): 213–20. <https://doi.org/10.1016/j.memsci.2012.12.037>.
- [3] Huang, Liwei, Jason T. Arena, Seetha S. Manickam, Xiaoqiang Jiang, Brian G. Willis, and Jeffrey R. McCutcheon. "Improved Mechanical Properties and Hydrophilicity of Electrospun Nanofiber Membranes for Filtration Applications by Dopamine Modification." *Journal of Membrane Science* 460 (June 15, 2014): 241–49. <https://doi.org/10.1016/j.memsci.2014.01.045>.

# Appendix 11:

## ESTIMATION OF HYDRODYNAMIC DIAMETERS $D_{TA}$ OF TA AGGREGATES FROM DLS MEASUREMENTS

Hydrodynamic diameters  $D_{TA}$  of TA aggregates were calculated from DLS measurements and the following equations:

Scattering vector  $q$ :

$$q = \frac{4\pi n}{\lambda} \sin\left(\frac{\theta}{2}\right)$$

With  $n$  the refractive index of the solvent,  $\lambda = 633$  nm is the wavelength of the used laser and  $\theta$  the used scattering angle.

Diffusion coefficient:

$$D = \frac{1}{2\tau q^2}$$

With  $\tau$  the characteristic time of the fast mode obtained from DLS measurements. They were obtained from the field correlation functions which were fitted with the stretched exponential functions having one to three relaxation modes. These functions fit well empirically the autocorrelation functions [2].

The diameter  $D_{TA}$  of TA aggregates are estimated from:

$$D_{TA} = \frac{2k_B T}{6\pi\eta D}$$

With  $k_B = 1.38 \times 10^{-23}$  m<sup>2</sup>.kg.s<sup>-2</sup>.K<sup>-1</sup> the Boltzmann constant,  $T = 298$  K the temperature and  $\eta$  the viscosity of the solvent.

The following parameters were measured to calculate  $D_{TA}$ :

$C_{TA}$ (wt%)	$\tau$ in water (ms)	$\tau$ in water/ethanol 37.5/62.5 wt% (ms)
2	$1.91 \times 10^{-2}$	$3.53 \times 10^{-2}$
10	$4.89 \times 10^{-2}$	$1.30 \times 10^{-1}$
35	$1.0 \times 10^{-1}$	$2.03 \times 10^{-1}$

Solvent	Water	Water/ethanol 37.5/62.5 wt%
$n$	1.332	1.36
$\eta$ (mPa.s)	0.89	2.22

## Reference

- [1] J. Brandrup, E.H. Immergut, E.A. Grulke, Polymer Handbook, 4th Edition, Wiley, 2004.
- [2] G. Nisato, P. Hébraud, J.-P. Munch, S.J. Candau, Diffusing-wave-spectroscopy investigation of latex particle motion in polymer gels, Phys. Rev. E. 61 (2000) 2879–2887. doi:10.1103/PhysRevE.61.2879.

# Appendix 12:

## SUMMARY IN FRENCH

La fabrication de membranes nanofibreuses pour la filtration de liquides via des stratégies plus respectueuses de l'environnement, ou pour ainsi dire plus « vertes », est aujourd'hui un souci majeur tant d'un point de vue écologique que pour la sécurité du personnel des usines de production. Les travaux ont donc consisté à développer des membranes nanofibreuses par un procédé d'électrospinning plus « vert » pour la microfiltration de liquides. Pour pouvoir prétendre à être des membranes de microfiltration liquide, les membranes doivent être composées de fibres fines et régulières afin que les pores soient petits (taille des pores entre 0,1  $\mu\text{m}$  et 10  $\mu\text{m}$ ), réguliers et interconnectés. Le procédé d'électrospinning permet de fabriquer des membranes répondant à ces critères. L'électrospinning est un procédé qui permet, à partir d'une solution de polymère, d'obtenir des membranes non-tissées poreuses dont le diamètre des fibres est compris entre 50 nm et quelques micromètres en fonction des paramètres du procédé et des matériaux. Grâce à la finesse et à la régularité des fibres produites, les membranes ont une taille de pore très petite, du même ordre de grandeur que le diamètre des fibres, tout en présentant une porosité élevée supérieure à 80%, ce qui les différencie des membranes de filtration commerciales dont la porosité n'avoisine pas 40%. La fabrication de membranes de filtration liquide par un électrospinning plus « vert » pourrait même, par conséquent, permettre d'accroître les débits de filtration tout en respectant davantage l'environnement.

Afin de mener à bien le projet, deux voies ont été explorées : la fabrication par électrospinning d'un matériau bio-sourcé et l'étude de la mise en œuvre par électrospinning en voie aqueuse. Ainsi, la première partie de la thèse, s'inscrivant dans le projet CLARIFIL financé par le fond unique interministériel (FUI), porte sur la mise en forme par électrospinning du polyamide 11, un polymère bio-sourcé, recyclable et déjà utilisé dans des applications liées à l'alimentaire (**Chapitre 2**). La deuxième partie de la thèse s'attache, quant à elle, à fabriquer les membranes de filtration par électrospinning en solution aqueuse pour s'affranchir des vapeurs souvent toxiques des solvants utilisés pendant le procédé (**Chapitre 3**). Dans ce cadre, deux stratégies ont été approfondies : (i) l'électrospinning de suspensions aqueuses de polymères hydrophobes et (ii) l'électrospinning d'une molécule bio-sourcée, l'acide tannique, par l'exploitation des interactions supramoléculaires présentes dans la solution mise en œuvre. Enfin, un émetteur multi-jets a été développé dans une dernière partie afin de produire des membranes suffisamment grandes pour pouvoir être utilisées dans les appareils de filtration membranaire standards (**Chapitre 4**). En effet, l'électrospinning est un procédé dont les cadences de production sont faibles et, de plus, un solvant toxique est souvent requis. Il est de ce fait encore peu utilisé industriellement. En mettant au point de nouvelles voies d'électrospinning qui permettent

un meilleur rendement de production et qui évite de recourir à des solvants toxiques, l'industrialisation du procédé d'électrospinning devient économiquement viable.

#### ELECTROSPINNING DE POLYAMIDE 11

Il a été choisi d'élaborer des membranes d'électrospinning en polyamide 11 (PA11) pour des applications de filtration liquide car celui-ci est un polymère bio-sourcé. L'objectif est de fabriquer, conformément au cahier des charges du projet CLARIFIL, des membranes de filtration liquide ayant des pores dont la taille est comprise entre 0,2 et 0,8  $\mu\text{m}$ . Sachant que le diamètre des pores d'une membrane non-tissée est directement relié au diamètre des fibres qui la constitue, un des objectifs est de pouvoir produire des nanofibres dont le diamètre est le plus faible possible. Avec cet objectif, trois paramètres majoritaires ont été mis en avant : la composition du solvant, l'humidité et la concentration en polymère. De plus, l'effet de la distribution de la masse molaire sur le diamètre des nanofibres a aussi été étudié en travaillant sur des formulations à base de PA11 de masse molaire différente. L'apport de PA11 de haute masse molaire permet d'assurer la continuité de la nanofibre produite par électrospinning alors que l'introduction dans la formulation de PA11 de faible masse molaire permet d'augmenter la concentration massique en polymère sans pour autant augmenter significativement le diamètre des nanofibres. L'électrospinning de fibres fines à partir de solutions concentrées permet donc de garantir le maintien d'une productivité élevée. Grâce à cette méthode, des membranes constituées de fibres ayant pour diamètre moyen 100 nm ont été produites à partir d'une solution concentrée à 13 wt% en PA11 (Figure 1.a). Sans cette stratégie, les fibres continues les plus fines (178 nm) pouvant être fabriquées l'ont été avec une solution concentrée à 6 wt% en PA11. De plus, grâce à cette stratégie, les membranes constituées de fibres de diamètre moyen 100 nm présentent une taille moyenne de pore de  $0,37 \pm 0,01 \mu\text{m}$ , une valeur comprise entre l'intervalle  $[0,2 \mu\text{m} ; 0,8 \mu\text{m}]$  spécifié par le cahier des charges du projet. La stratégie consistant à jouer sur la distribution en masse molaire pour réduire le diamètre des fibres tout en augmentant la productivité peut être utilisée avec tout type de polymères.

#### ELECTROSPINNING EN VOIE AQUEUSE

Contrairement à la méthode d'électrospinning développée avec le PA11 qui nécessite l'emploi de solvants tels que l'acide formique et le dichlorométhane, nous avons développé des stratégies d'électrospinning de solutions aqueuses dans une perspective écologique évitant de recourir à l'utilisation de solvants toxiques et polluants. Deux voies ont été explorées. La première est basée sur l'électrospinning de suspensions aqueuses de polymères non hydrosolubles. La seconde voie a consisté à explorer la possibilité de mettre en œuvre une molécule non-polymérique et fortement hydrosoluble, l'acide tannique, en exploitant les interactions supramoléculaires pouvant contribuer à la fibrillation lors de l'électrospinning.



### **Electrospinning de suspensions aqueuses**

Nous avons étudié l'électrospinning de suspensions aqueuses de différents polymères non hydrosolubles : le polyamide, le polypropylène, le poly(fluorure de vinylidène) (PVDF) et le polyméthacrylate de méthyle (PMMA). Un polymère hydrosoluble a été rajouté à la suspension mise en œuvre afin d'assurer la formation de la nanofibre pendant l'électrospinning sans rupture du jet. Dans une deuxième étape, un traitement thermique est appliqué à la membrane au-dessus de la température de fusion du polymère constitutif de la suspension et en-dessous de celle du polymère hydrosoluble. Ce traitement thermique a pour objectif de fusionner les particules entre elles sans détruire la structure fibreuse. L'influence des conditions du traitement thermique ainsi que de la composition de la formulation d'électrospinning sur les propriétés morphologiques et mécaniques des membranes ont été étudiés par la suite. Les résultats obtenus avec les suspensions PVDF-PMMA (Figure 1.b) sont très prometteurs puisque les membranes obtenues présentent une élongation à la rupture d'environ 80%. De plus, des essais de filtration ont été réalisés avec des particules de silice de tailles 0.1  $\mu\text{m}$ , 0.4  $\mu\text{m}$  et 1  $\mu\text{m}$ . Les membranes composées des suspensions de PVDF-PMMA ont pu filtrer ces particules avec des efficacités de  $95 \pm 4\%$  pour les particules de 0.1  $\mu\text{m}$  et de plus de 99% pour les particules de 0.4 et 1  $\mu\text{m}$ . Les membranes réalisées sont donc en conclusions adaptées pour des applications de microfiltration liquide.

### **Electrospinning d'acide tannique et sans polymère par auto-assemblage supramoléculaire**

Généralement, les membranes d'électrospinning sont fabriquées à partir d'une solution de polymère de haute masse molaire. Dans ce cas, la solution doit comporter suffisamment d'enchevêtrements entre les chaînes de polymère pour que le jet de solution ne se rompe pas lors du procédé et se dépose sous la forme d'une nanofibre continue et régulière sur le collecteur. Dans de rares cas, il a été montré que des molécules non-polymériques peuvent également être électrospinnées sans polymère. Au cours de nos travaux, nous avons démontré que cette situation est aussi le cas de l'acide tannique. Il a été mis en évidence que cette molécule, solubilisée dans un mélange eau-éthanol ainsi que dans de l'eau pure peut former des fibres par électrospinning. La formation d'agrégats d'acide tannique en solution a été mis en évidence par rhéologie, diffusion dynamique de la lumière et au cryo-TEM. Au-dessus d'une concentration critique, ces agrégats forment un réseau interconnecté supramoléculaire assez fort pour permettre l'électrospinning d'une nanofibre continue et régulière. La membrane résultante est mécaniquement stable et peut être manipulée. En outre, contrairement aux autres petites molécules pouvant être électrospinnées sans polymère, les membranes d'acide tannique peuvent être réticulées efficacement dans l'eau par réaction oxydante avec du périodate de sodium ou, mieux encore, avec du Fe III grâce à la combinaison d'une réaction oxydante et la formation de complexes de coordination (Figure 1.c). La stratégie d'électrospinning et de réticulation proposée est facile, peu coûteuse et utilise des solvants non toxiques ainsi qu'une molécule biocompatible et biofonctionnelle. De plus, en utilisant la capacité de l'acide tannique à se coordonner avec une grande variété de métaux, des membranes

hybrides intelligentes peuvent être envisagées pour diverses applications dans le domaine du biomédical, environnemental ainsi qu'en catalyse.

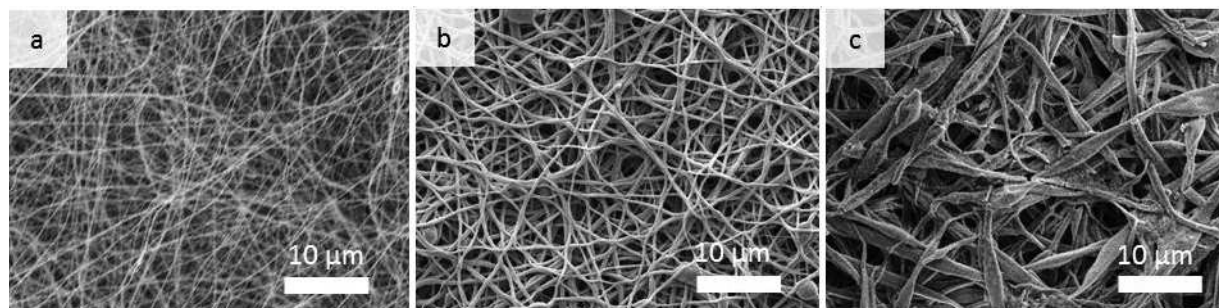


**Figure 1.** Membranes fabriquées au cours de la thèse par électrospinning. a) Membrane de polyamide 11. b) Membrane électrospinnée à partir d'une suspension aqueuse de PVDF-PMMA après traitement thermique et lavage. c) Membrane d'acide tannique après réticulation avec du nitrate de Fer III, lavage et stabilisation dans de l'eau pendant 1 semaine.

#### DEVELOPPEMENT ET OPTIMISATION D'UN EMETTEUR MULTI-JETS

Afin de produire des membranes suffisamment grandes pour pouvoir être caractérisées dans des appareils de filtration standards et que ces membranes aient une épaisseur constante sur toute leur surface, plusieurs émetteurs rotatifs multi-jets ont été développés: un émetteur multi-pointes, un émetteur multi-disques et un émetteur multi-CDs (Figure 2). Grâce à ces émetteurs, des solutions polymériques ainsi que des suspensions ont pu être électrospinnées. La répartition de l'épaisseur des mats sur le collecteur a été étudiée pour l'émetteur multi-pointes et pour l'émetteur multi-disques. Avec l'émetteur multi-pointes, des membranes d'épaisseur constante ont pu être fabriquées avec la condition que le collecteur doit être translaté selon le long de l'axe de rotation de l'émetteur sur au moins 8 cm ( $\pm 4$  cm). En revanche, avec l'émetteur multi-disques, la répartition du dépôt sur un collecteur plan est telle qu'il n'est pas possible de fabriquer des membranes d'épaisseur constante sur toutes leurs surfaces. Pour obtenir de telles membranes avec un émetteur multi-disques, il faudrait que le collecteur soit cylindrique et rotatif. La productivité, quant à elle, varie selon la solution d'électrospinning utilisée et selon les conditions d'électrospinning. En comparaison avec un électrospinning avec une aiguille, la productivité n'a pas été significativement augmentée avec une solution composée de PA11 dans un mélange acide formique et de dichlorométhane. Au contraire, pour une solution de PVA dans de l'eau à laquelle une faible proportion d'un tensio-actif a été ajoutée, la productivité a été augmentée par 35. Une étude sur l'impact de la géométrie des émetteurs sur les dépôts, sur les conditions d'électrospinning, ainsi que sur les interactions entre les jets a été commencée dans le but d'optimiser la géométrie des émetteurs. Trois paramètres ont été étudiés: la distance entre les rangées de pointes, la distance entre les pointes (pour l'émetteur multi-pointes) et la vitesse de rotation des émetteurs. La distance entre les pointes de l'émetteur multi-pointes et la distance entre les rangées des émetteurs multi-jets sont cruciales pour

optimiser la productivité. Si les distances sont trop petites, le champ électrique au niveau de chaque pointe et entre les rangées est perturbé et partiellement masqué par celui des pointes et des rangées voisines. Une réduction trop importante des distances conduit ainsi à une diminution de la productivité. La distance optimale est celle qui est la plus petite tout en assurant une perturbation minimale du champ électrique. D'autre part, la productivité augmente en multipliant le nombre de rangées, mais non linéairement puisque le champ électrique est différemment perturbé selon que les rangées soient situées à l'intérieur ou à l'extérieur de la ligne d'émetteurs multi-jets. En conclusion, cette étude permet de mieux comprendre comment la géométrie d'un émetteur multi-jets de type « rotatif » peut être optimisée afin de fabriquer des membranes d'épaisseur constante et pour garantir une productivité élevée. Cette étude doit être toutefois poursuivie. En outre, la conception de la zone d'alimentation de la solution doit également être optimisée afin de limiter l'évaporation à ce stade du procédé et afin que, par conséquent, la viscosité des solutions soit constante pendant toute la durée de la production.

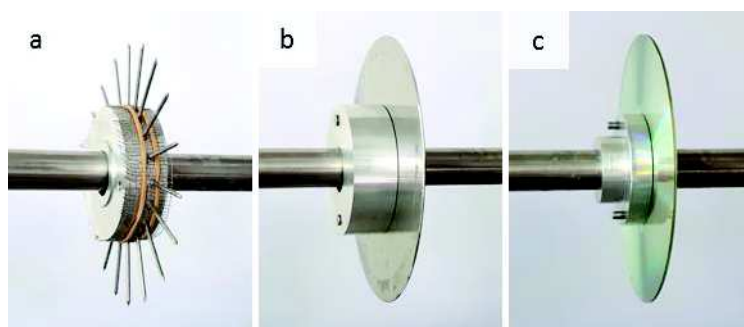


Figure 2. Émetteurs multi-jets (composés d'une seule rangée) développés et caractérisés au cours de la thèse : a) un émetteur multi-pointes, b) un émetteur multi-disques et c) un émetteur multi-CDs.

## CONCLUSION GENERALE

Ainsi, de nouvelles voies ont été étudiées pour que le procédé d'électrospinning soit plus « vert » afin de rendre davantage possible son industrialisation. Ces voies peuvent servir à fabriquer des membranes pour la filtration de liquides mais pourraient aussi être envisagées pour d'autres domaines d'applications.

La voie la plus prometteuse, car combinant le plus d'avantages « écologiques », est la voie utilisant une suspension de polymère puisque le procédé se déroule dans l'eau et que des membranes constituées de fibres fines et régulières ont pu être obtenues et caractérisées, notamment en filtration à une échelle expérimentale. De futures études pourraient maintenant s'attacher à filtrer toutes sortes de liquide grâce à ces membranes (de l'eau ou du vin par exemple). De plus, cette nouvelle voie pourrait être généralisée à d'autres domaines d'applications, être plus communément utilisée surtout industriellement et pourrait enfin être mise en place sur n'importe quelle machine d'électrospinning (appareils multi-jets inclus).

Dernièrement, cette « prometteuse » stratégie pourrait devenir encore plus « verte » en choisissant des suspensions dont le cycle de vie respecte encore plus l'environnement (i.e. en utilisant des suspensions biosourcées, recyclables et/ou biodégradables). De plus, les membranes de filtration liquides développées pourraient devenir plus efficaces en réduisant la taille des pores ainsi qu'il l'a été détaillé dans la thèse. Avec cet objectif, des suspensions plus fines pourraient être utilisées, de nouveaux polymères hydrosolubles pourraient être employés et une étude sur l'humidité pourraient être réalisée.

## Résumé

La fabrication de membranes nanofibreuses par un procédé d'électrospinning plus respectueux de l'environnement, ou plus « vert », est de nos jours un défi. L'électrospinning est un procédé qui permet, généralement à partir d'une solution de polymère, d'obtenir des membranes non-tissées dont le diamètre des fibres est compris entre 50 nm et quelques micromètres. Deux stratégies nouvelles ont été développées pour répondre à ce besoin croissant. La première consiste à fabriquer des membranes à partir de polymères bio-sourcés tandis que la deuxième vise à employer des solvants exclusivement aqueux. Cette deuxième stratégie permet de s'affranchir des vapeurs de solvants souvent toxiques utilisés au cours du procédé. Dans ce cadre, des membranes ont été fabriquées à partir de suspensions aqueuses de polymères non-hydrosolubles, d'une part, et à partir d'acide tannique, une molécule non-polymérique bio-sourcée en exploitant les interactions supramoléculaires. Ces stratégies plus « vertes » rendent moins dangereuse et moins coûteuse l'utilisation d'émetteurs multi-jets et permettent, de ce fait, une meilleure industrialisation du procédé d'électrospinning. Les membranes développées ont été fabriquées pour des applications de microfiltration liquide. En effet, les membranes d'électrospinning peuvent allier des tailles de pores submicroniques à des porosités supérieures à 80% contrairement aux membranes de microfiltration commerciales (porosité < 40%). La fabrication de membranes de filtration par un procédé d'électrospinning multi-jet « vert » permet ainsi d'accroître les débits de production et de filtration tout en respectant davantage l'environnement.

*Mots-clés : « Green » électrospinning, Nanofibres, Émetteur multi-jets, Filtration liquide*

## Abstract

The fabrication of nanofibrous mats by an environmentally friendly, or in other words by a "green", electrospinning process is nowadays a challenge. Electrospinning is a process allowing the fabrication, generally from a polymer solution, of nonwoven mats composed of fibers having diameters ranging between 50 nm and a few micrometers. Two new strategies have been developed to answer such a growing need. The first one consists in electrospinning bio-sourced polymers while the second one is based on the electrospinning of aqueous solutions exclusively. This second strategy allows avoiding toxic vapors coming from the evaporation of toxic solvents often used during the process. In this context, mats were electrospun from solutions composed of aqueous suspensions of water insoluble polymers, on one hand, and composed of tannic acid, a non-polymeric bio-based molecule exploiting supramolecular interactions. These new environmentally friendly strategies turn the electrospinning process in a less dangerous and less expensive one, and, as a result, ease the use of multi-jet setups and enable a better industrialization of the electrospinning process. Membranes have been developed for liquid microfiltration applications. As a matter of fact, electrospinning membranes can combine submicron pore sizes with porosities greater than 80% unlike commercial microfiltration membranes (porosity < 40%). The fabrication of liquid filtration membranes by a multi-jet "green" electrospinning process, thus, makes it possible to increase the production rates of electrospinning mats and filtration rates while respecting the environment.

*Keywords: « Green » electrospinning, Nanofibers, Multi-jet spinneret, Liquid filtration*